

STATUS OF THESIS

Title of thesis Enhanced Hydrogen Production in Integrated Catalytic Adsorption  
(ICA) Steam Gasification System Utilizing Palm Kernel Shell

I ZAKIR KHAN

hereby allow my thesis to be placed at the Information Resource Center (IRC) of Universiti Teknologi PETRONAS (UTP) with the following conditions:

1. The thesis becomes the property of UTP
2. The IRC of UTP may make copies of the thesis for academic purposes only.
3. This thesis is classified as

Confidential

Non-confidential

If this thesis is confidential, please state the reason:

Part of this research work is being filed for patent  
\_\_\_\_\_  
\_\_\_\_\_

The contents of the thesis will remain confidential for \_\_\_\_\_ years.

Remarks on disclosure:

\_\_\_\_\_  
\_\_\_\_\_  
\_\_\_\_\_

Endorsed by

\_\_\_\_\_  
Signature of Author

\_\_\_\_\_  
Signature of Supervisor

Assoc. Prof. Dr. Suzana Yusup

Permanent Address:  
House no. 443, Shahbaz Block  
Mustafa Town, Lahore, Pakistan

Date : \_\_\_\_\_

Date : \_\_\_\_\_

UNIVERSITI TEKNOLOGI PETRONAS

ENHANCED HYDROGEN PRODUCTION IN INTEGRATED CATALYTIC  
ADSORPTION (ICA) STEAM GASIFICATION SYSTEM UTILIZING PALM  
KERNEL SHELL

by

ZAKIR KHAN

The undersigned certify that they have read, and recommend to the Postgraduate Studies Programme for acceptance this thesis for the fulfilment of the requirements for the degree stated.

Signature:

---

Main Supervisor:

Assoc. Prof. Dr Suzana Yusup

---

Signature:

---

Co-Supervisor:

Dr. Murni Melati Ahmad

---

Signature:

---

Head of Department:

Assoc. Prof. Dr. Azmi Bustam @ Khalil

---

Date:

---

ENHANCED HYDROGEN PRODUCTION IN INTEGRATED CATALYTIC  
ADSORPTION (ICA) STEAM GASIFICATION SYSTEM UTILIZING PALM  
KERNEL SHELL

by

ZAKIR KHAN

A Thesis

Submitted to the Postgraduate Studies Programme

as a Requirement for the Degree of

DOCTOR OF PHILOSOPHY

DEPARTMENT OF CHEMICAL ENGINEERING

UNIVERSITI TEKNOLOGI PETRONAS

BANDAR SERI ISKANDAR,

PERAK

JULY 2013

DECLARATION OF THESIS

Title of thesis 

Enhanced Hydrogen Production in Integrated Catalytic Adsorption (ICA) Steam Gasification System Utilizing Palm Kernel Shell
---

I \_\_\_\_\_ ZAKIR KHAN \_\_\_\_\_

hereby declare that the thesis is based on my original work except for quotations and citations which have been duly acknowledged. I also declare that it has not been previously or concurrently submitted for any other degree at UTP or other institutions.

Witnessed by

\_\_\_\_\_  
Signature of Author

\_\_\_\_\_  
Signature of Supervisor

Permanent Address:  
House no. 443, Shahbaz Block  
Mustafa Town, Lahore, Pakistan  
Pakistan

Assoc. Prof. Dr. Suzana Yusup

Date : \_\_\_\_\_

Date : \_\_\_\_\_

## DEDICATION

*To my father*

*KHAN ZADIN (Late)*

## ACKNOWLEDGEMENTS

Alhamdulillah, all praises to The Almighty Allah for countless blessing and strength for completing this PhD work.

I would like to acknowledge Universiti Teknologi PETRONAS for the graduate assistance scheme and the financial support from the Petroleum Research Fund of PETRONAS.

I express my sincere gratitude to my supervisor, Assoc. Prof. Dr. Suzana Yusup, whose exceptional skills and scientific reasoning would always remain unparalleled. Her efforts to encourage me have not only been for this thesis but also to my life. I am grateful to her constant dedication and guidance for the completion of this work.

I owe my thanks to my co-supervisor, Dr. Murni Melati Ahmad, for her useful discussions in the modeling and simulation part. Her invaluable constructive comments and suggestions throughout this work have contributed to the success of this work.

I would like to express my deepest appreciation and thanks to member of Biohydrogen research group for the co-operation and assistance they offered.

I am very much grateful to my father Mr. Khan Zadin (Late) and my mother Ms. Merum Jana whose love and prayers have always been my greatest strength and inspiration.

I would like to thank my wife Qamer Zakir and my cute son Taimur Zakir for their encouragement and constant support throughout this work.

## ABSTRACT

Energy crises and serious environmental issues associated with fossil fuels urge for alternative, sustainable and renewable energy. Hydrogen has a potential to be a significant energy carrier in the future since it is a clean fuel. Hydrogen production from local biomass i.e. palm oil waste is an attractive option due to its abundance in the country. Biomass catalytic steam gasification and steam gasification with in-situ CO<sub>2</sub> adsorption processes show great potential for renewable hydrogen production. However, the quality and quantity of hydrogen rich gas with considerable tar inhibits the application of these processes in power generation and fuel cell.

The present study used catalyst and adsorbent in the system to enhance hydrogen production under steam gasification utilizing palm kernel shell as the feedstock. The design of fluidized bed gasifier was based on the hydrodynamic parameter such as minimum fluidization velocity to evaluate the diameter and height of the gasifier. In addition, design of experiments (DOE) was performed using Response Surface Methodology (RSM) in conjunction with Central Composite Rotatable Design (CCRD) in Expert Design-8 software. The range of process variables considered were; temperature of 600°C-750°C, steam to biomass ratio of 1.50-2.50 wt/wt, adsorbent to biomass ratio of 0.50-1.50 wt/wt, fluidization velocity of 0.15-0.26 m/s and biomass particle size of 0.355-2.00 mm.

The integrated catalytic adsorption (ICA) steam gasification produced maximum hydrogen yield of 150 g/kg biomass and was obtained at 750°C, steam/biomass ratio of 2.0 wt/wt, adsorbent to biomass ratio of 1.0 wt/wt, fluidization velocity of 0.21 m/s with catalyst to biomass ratio of 0.10 wt/wt. But maximum hydrogen composition of 84 vol% was observed at low temperature of 675°C while high temperature (750°C) decreased hydrogen composition to 67 vol% in the product gas due to reverse carbonation reaction. The comparative study with literature showed that the ICA steam gasification system was able to provide better composition and hydrogen yield in the product gas.

## ABSTRAK

Krisis tenaga dan isu alam sekitar yang serius berkaitan dengan bahan bakar fosil menggalakkan perkembangan tenaga alternatif, mampan dan boleh diperbaharui. Hidrogen mempunyai potensi untuk menjadi pembawa tenaga yang berkesan untuk masa depan memandangkan ia sumber tenaga yang bersih. Penghasilan hidrogen daripada biojisim tempatan seperti buangan minyak sawit adalah pilihan yang sangat menarik kerana ia kedapatan sangat banyak di negara ini. Pengegasan wap biojisim berpemangkin dan proses pengegasan wap bersama penjerap CO<sub>2</sub> menunjukkan potensi besar dalam penghasilan hidrogen diperbaharui. Walaubagaimanapun, kualiti dan kuantiti gas yang kaya dengan hidrogen dan kandungan tar yang berpatutan merencat aplikasi proses ini untuk penjanaan tenaga dan sel tenaga.

Kajian ini menggunakan pemangkin dan penjerap di dalam sistem untuk menggalakkan penghasilan hidrogen ketika pengegasan berwap menggunakan isirong kelapa sawit sebagai bahan mentah. Rekabentuk pengegas lapisan terbendalir adalah berdasarkan parameter hidrodinamik seperti halaju minuman bendalir untuk menilai lebar dan tinggi pengegas. Tambahan pula, rekabentuk eksperimen (DOE) telah dijalankan menggunakan (RSM) bersama dengan reka bentuk pusat putaran komposit berdasarkan pelbagai pemboleh ubah proses (CCRD) menggunakan perisian Expert Design-8. Julat proses pemboleh ubah yang telah digunakan ialah; suhu 600°C-750°C, nisbah wap kepada biojisim 1.50-2.50 wt/wt, nisbah penjerap kepada biojisim 0.50-1.50 wt/wt, halaju bendalir 0.15-0.26 m/s dan saiz zarah biojisim 0.355-2.0 mm.

Sistem pengegasan ICA menghasilkan gas hidrogen maksimum bagi 150 g/kg biojisim adalah pada 750°C, nisbah stim kepada biojisim adalah 2.0 wt/wt, nisbah penjerap kepada biojisim adalah 1.0 wt/wt, halaju bendalir adalah 0.21 m/s dengan nisbah pemangkin kepada biojisim ialah 0.1 wt/wt. Tetapi, komposisi hidrogen maksimum sebanyak 84 vol% telah didapati pada suhu yang rendah iaitu 675°C manakala pada suhu yang tinggi (750°C) telah mengurangkan komposisi hidrogen kepada 67 vol% di dalam produk gas kerana tindak balas pengkarbonatan terbalik.

Kajian perbandingan dengan kajian-kajian sebelum ini telah menunjukkan bahawa sistem pengegasan berwap ICA mampu untuk menghasilkan gas yang mempunyai kandungan dan komposisi hidrogen yang lebih baik.

In compliance with the terms of the Copyright Act 1987 and the IP Policy of the university, the copyright of this thesis has been reassigned by the author to the legal entity of the university,

Institute of Technology PETRONAS Sdn Bhd.

Due acknowledgement shall always be made of the use of any material contained in, or derived from, this thesis.

© Zakir Khan 2013

Institute of Technology PETRONAS Sdn Bhd

All rights reserved.

## TABLE OF CONTENT

ABSTRACT.....	vii
ABSTRAK.....	viii
LIST OF FIGURES .....	xviii
LIST OF TABLES .....	xxiv
CHAPTER 1 INTRODUCTION .....	1
1.1 Current Energy Scenario .....	1
1.2 Hydrogen as Alternative Fuel.....	3
1.3 Hydrogen from Renewable Resources .....	3
1.4 Biomass as a Source of Renewable Hydrogen.....	4
1.5 Hydrogen from Biomass: Environmental Impact and CO <sub>2</sub> Reduction .....	4
1.6 Challenges of Present Gasification Technologies for Hydrogen Production...	4
1.7 Problem Statement .....	5
1.8 Research Objectives .....	6
1.9 Thesis Scope and Outline .....	6
1.10 Chapter Summary .....	8
CHAPTER 2 LITERATURE REVIEW .....	9
2.1 Introduction .....	9
2.2 Biomass Resources .....	9
2.3 Hydrogen Production from Biomass .....	11
2.3.1 Hydrogen Production through Thermal Conversion of Biomass .....	11
2.3.2 Hydrogen Production from Bio-Chemical Conversion .....	13
2.4 Feed Characteristics .....	13
2.4.1 Biomass Properties .....	14
2.4.2 Biomass Selection for Gasification Process .....	16
2.5 Catalyst for Biomass Steam Gasification.....	18
2.5.1 Nickel Based Catalysts .....	19
2.5.2 Dolomite, Olivine and Metal Catalysts .....	20
2.6 Adsorbent for In-situ CO <sub>2</sub> Capturing in Biomass Gasification.....	20
2.7 Conceptual Process Design Approach .....	22
2.7.1 Initial Input Information of Process.....	23

2.7.2 Process Design: Batch versus Continuous.....	23
2.7.3 Process Input-Output Structure.....	24
2.7.4 Reactor Type.....	24
2.7.5 Separation System .....	24
2.7.6 Heating and Cooling System .....	25
2.7.7 Process Design of Biomass Gasification .....	25
2.8 Biomass Gasification.....	26
2.8.1 Biomass Gasification: Mechanism and Reactions.....	27
2.8.1.1 Drying .....	27
2.8.1.2 Devolatilization.....	27
2.8.1.3 Combustion .....	27
2.8.1.4 Gasification/Reforming.....	28
2.8.1.5 Reactions.....	28
2.8.1.6 Hydrogen Yield and Conversion Efficiencies .....	29
2.8.2 Recent Advancement in Biomass Gasification for Hydrogen Production .....	30
2.8.2.1 Fixed Bed Gasifier .....	32
2.8.2.2 Fluidized Bed Gasifier .....	32
2.8.2.3 Comparison between Fixed Bed and Fluidized Bed Gasifier ..	33
2.8.2.4 Biomass Steam Gasification .....	34
2.8.2.5 Biomass Catalytic Steam Gasification.....	35
2.8.2.6 Biomass Steam Gasification with In-situ CO <sub>2</sub> Adsorbent .....	36
2.8.2.7 Gasification of Palm Kernel Shell .....	38
2.9 Effect of Process Variables on Hydrogen Production.....	39
2.9.1 Effect of Temperature.....	39
2.9.2 Effect of Steam to Biomass Ratio.....	42
2.9.3 Effect of Adsorbent to Biomass Ratio .....	43
2.9.4 Effect of Fluidization Velocity .....	44
2.9.5 Effect of Biomass Particle Size .....	45
2.10 Kinetic Study of Biomass Steam Gasification for Hydrogen Production ....	46
2.10.1 Kinetic Modeling .....	46
2.10.2 Equilibrium Modeling .....	48
2.10.3 Kinetic Modeling with In-situ CO <sub>2</sub> Adsorption.....	49

2.10.4 Comparison between Kinetic and Equilibrium Model .....	50
2.10.5 Determination of Kinetic Parameters .....	51
2.11 Process Optimization Study using Design of Experiments .....	52
2.11.1 Response Surface Methodology (RSM) .....	53
2.11.2 Central Composite Rotatable Design (CCRD) .....	53
2.11.3 Model Fitting and Statistical Analysis .....	54
2.11.4 Optimization of Hydrogen Production .....	55
2.12 Chapter Summary .....	55
CHAPTER 3 MATERIALS AND METHODS .....	57
3.1 Introduction .....	57
3.2 Material Preparation .....	58
3.2.1 Feedstock Selection and Preparation .....	58
3.2.1.1 Moisture Content .....	58
3.2.1.2 Determination of Particle and Bulk Density .....	59
3.2.2 Biomass Characterization .....	59
3.2.2.1 Ultimate Analysis .....	59
3.2.2.2 Proximate Analysis .....	59
3.2.2.3 Calorific Value .....	60
3.2.3 Bed Material Preparation .....	61
3.3 Bed Material and Catalyst Characterization .....	61
3.3.1 X-ray Fluorescence (XRF) Analysis .....	61
3.3.2 X-ray Diffraction (XRD) Analysis .....	62
3.3.3 Scanning Electron Microscopy (SEM) Analysis .....	62
3.3.4 Physisorption Analysis .....	62
3.4 Process Design of ICA Steam Gasification .....	62
3.5 Fluidized Bed Reactor Design and Operational Profiles .....	65
3.5.1 Design Specification .....	65
3.5.1.1 Feedstock Specification .....	65
3.5.1.2 Choice of Gasification Medium .....	65
3.5.1.3 Product Gas Specification .....	66
3.5.2 Calculation of Internal Diameter of Gasifier .....	66
3.5.2.1 Hydrodynamics Study .....	66
3.5.2.2 Steam Load .....	69

3.5.3 Calculation of Height of Gasifier .....	70
3.5.3.1 Transport Disengaging Height (TDH) .....	71
3.5.3.2 Maximum Bubble Diameter Calculation .....	72
3.5.3.3 Bed Height .....	72
3.5.4 Distributor Plate Design .....	72
3.5.5 Fluidized Bed Reactor Geometry .....	75
3.5.6 Temperature and Pressure Drop Profiles .....	75
3.5.6.1 Temperature Profiles .....	75
3.5.6.2 Pressure Drop Profiles .....	76
3.6 ICA Steam Gasification System .....	76
3.6.1 Fluidized Bed Reactor Configuration .....	77
3.6.2 Biomass Feeding System .....	79
3.6.3 Steam Generation System .....	80
3.6.4 Gas Cleaning System .....	81
3.6.5 Gas Analyzing System .....	83
3.6.5.1 Online Sampling and Gas Conditioning .....	83
3.6.5.2 Calibration of Gas Chromatography (GC) .....	84
3.6.6 Gas Supply System .....	84
3.6.7 Experimental Operating Conditions .....	85
3.6.8 Gasifier Operational Problems and Remedy .....	86
3.6.8.1 Downstream Clogging .....	86
3.6.8.2 Presence of Moisture in Gas Analyzing System .....	87
3.6.8.3 Remedy of Operational Problems .....	88
3.7 Design of Experiments (DOE) .....	89
3.8 Performance Parameters .....	89
3.8.1 Product Gas Composition and Concentration .....	90
3.8.2 Hydrogen Yield .....	90
3.8.3 Gasification and Carbon Conversion Efficiency .....	90
3.8.4 Selectivity .....	91
3.8.5 Product Gas Heating Values .....	91
3.8.6 Product Gas Flow Rate .....	91
3.8.7 Amount of Char .....	92
3.8.8 Mass and Energy Balance .....	92

3.8.9 Heat and Mass Transfer Coefficients in Fluidized Bed.....	94
3.9 Kinetic Modeling.....	98
3.10 Chapter Summary.....	101
CHAPTER 4 RESULTS AND DISCUSSIONS .....	103
4.1 Introduction .....	103
4.2 Biomass Characterization.....	104
4.2.1 Particle and Bulk Density .....	104
4.2.2 Ultimate and Proximate Analysis .....	105
4.2.3 Calorific Value.....	106
4.3 Bed Material and Catalyst Characterization.....	106
4.3.1 Particle and Bulk Density of Bed Material.....	106
4.3.2 X-ray Fluorescence (XRF) Analysis .....	107
4.3.3 X-ray Diffraction (XRD) Analysis .....	108
4.3.4 Scanning Electron Microscopy (SEM) Analysis.....	109
4.3.5 Physisorption Analysis .....	109
4.4 Gasifier Operation and Performance .....	113
4.4.1 Temperature Profiles in Fluidized Bed Gasifier.....	113
4.4.2 Pressure Drop Profiles .....	115
4.4.2.1 Pressure Drop in Fluidized Bed Gasifier .....	115
4.4.2.2 Pressure Drop versus Velocity Diagram.....	116
4.4.3 Heat and Mass Transfer Coefficients .....	117
4.4.4 Design of Experiments Array .....	119
4.5 Parametric Analysis of Influential Variables .....	125
4.5.1 Effect of Reactor Temperature .....	125
4.5.1.1 Gas and Char Yield.....	125
4.5.1.2 Hydrogen Yield.....	127
4.5.1.3 Product Gas Composition .....	128
4.5.1.4 Gasification and Carbon Conversion Efficiency .....	131
4.5.1.5 Selectivity .....	132
4.5.1.6 Product Gas Heating Values .....	133
4.5.1.7 Energy Balance .....	134
4.5.2 Effect of Steam to Biomass Ratio.....	136
4.5.2.1 Gas and Char Yield.....	136

4.5.2.2 Hydrogen Yield.....	138
4.5.2.3 Product Gas Composition .....	140
4.5.2.4 Gasification and Carbon Conversion Efficiency .....	142
4.5.2.5 Selectivity .....	144
4.5.2.6 Product Gas Heating Values .....	145
4.5.2.7 Energy Balance .....	146
4.5.3 Effect of Adsorbent to Biomass Ratio .....	148
4.5.3.1 Gas and Char Yield.....	148
4.5.3.2 Hydrogen Yield.....	149
4.5.3.3 Product Gas Composition .....	150
4.5.3.4 Gasification and Carbon Conversion Efficiency .....	152
4.5.3.5 Selectivity .....	153
4.5.3.6 Product Gas Heating Values .....	153
4.5.3.7 Energy Balance .....	154
4.5.4 Effect of Fluidization Velocity .....	156
4.5.4.1 Gas and Char Yield.....	157
4.5.4.2 Hydrogen Yield.....	158
4.5.4.3 Product Gas Composition .....	159
4.5.4.4 Gasification and Carbon Conversion Efficiency .....	161
4.5.4.5 Selectivity .....	162
4.5.4.6 Product Gas Heating Values .....	163
4.5.4.7 Energy Balance .....	164
4.5.5 Effect of Biomass Particle Size .....	166
4.5.5.1 Gas and Char Yield.....	166
4.5.5.2 Hydrogen Yield.....	167
4.5.5.3 Product Gas Composition .....	168
4.5.5.4 Gasification and Carbon Conversion Efficiency .....	170
4.5.5.5 Selectivity .....	171
4.5.5.6 Product Gas Heating Values .....	172
4.5.5.7 Energy Balance .....	172
4.6 Optimization Study of Parameter Influence on ICA Steam Gasification ....	174
4.6.1 Analysis of Variance (ANOVA) .....	175
4.6.2 Predicted versus Actual Response .....	180

4.6.3 Three Dimensional (3D) Surface Plots.....	181
4.6.3.1 Hydrogen Composition.....	182
4.6.3.2 Hydrogen Yield.....	190
4.6.4 Optimization of Hydrogen Composition and Yield.....	198
4.6.5 Reproducibility of Experimental Results.....	198
4.7 Determination of Kinetic and Thermodynamic Parameters.....	199
4.8 Chapter Summary .....	205
CHAPTER 5 CONCLUSIONS AND RECOMMENDATIONS .....	209
5.1 Conclusions .....	209
5.2 Recommendations .....	211
REFERENCES .....	212
LIST OF PUBLICATION .....	233
APPENDIX A.....	241
APPENDIX B .....	247

## LIST OF FIGURES

Figure 2.1: Biomass production worldwide [18] .....	10
Figure 2.2: Biomass waste distribution in Malaysia [19] .....	10
Figure 2.3: Oil palm waste distribution in Malaysia [20] .....	11
Figure 2.4: Van Krevelen diagram for classification of various solid fuels [40] .....	16
Figure 2.5: C-H-O ternary diagram for biomass gasification process [38] .....	17
Figure 2.6: Biomass gasification process [75] .....	27
Figure 2.7: Types of gasifier [97, 98] .....	33
Figure 2.8: The equilibrium CO <sub>2</sub> partial pressure as a function of temperature [53] ..	41
Figure 2.9: CaO conversion characteristics at 0.1 atm CO <sub>2</sub> partial pressure [86] .....	41
Figure 3.1: Flow chart for overall research methodology .....	57
Figure 3.2: Block diagram of ICA steam gasification system .....	63
Figure 3.3: Process flow diagram of ICA steam gasification system .....	64
Figure 3.4: Fluidized bed reactor diameter estimation .....	67
Figure 3.5: Geldart classification of particles [171] .....	67
Figure 3.6: Transport disengaging height ( <i>TDH</i> ) in fluidized bed reactor [171] .....	71
Figure 3.7: Temperature and differential pressure indicators in fluidized bed gasifier .....	76
Figure 3.8: Fluidized bed gasifier .....	78
Figure 3.9: Biomass feeding system .....	79
Figure 3.10: Steam generation system .....	80
Figure 3.11: Cyclone solid separator .....	81
Figure 3.12: Gas cleaning system .....	82
Figure 3.13: Blockage in ICA gasification system a) check valve and b) piping .....	87
Figure 3.14: Moisture accumulation in a) tubing and b) sample flow meter associated with gas analyzing system .....	88
Figure 3.15: Energy balance of ICA steam gasification system .....	93
Figure 3.16: Flow chart of kinetic model using error minimization approach .....	100
Figure 4.1: X-ray diffraction analysis of Quicklime .....	108
Figure 4.2: X-ray diffraction analysis of Ni catalyst .....	108
Figure 4.3: Surface image of Quicklime .....	109

Figure 4.4: Quicklime pore size distribution .....	110
Figure 4.5: Ni catalyst pore size distribution .....	111
Figure 4.6: Adsorption isotherm for Quicklime .....	112
Figure 4.7: Adsorption isotherm for Ni powder .....	112
Figure 4.8: Temperature variation in the bed at 600°C, 675°C and 750°C .....	114
Figure 4.9: Axial temperature profiles in the fluidized bed gasifier.....	114
Figure 4.10: Pressure drop profiles of fluidized bed gasifier.....	115
Figure 4.11: Pressure drop versus velocity diagram.....	116
Figure 4.12: Bed Nusselt number ( $Nu_{bed}$ ) and Sherwood number ( $Sh_{bed}$ ) versus particle Reynolds number ( $Re_p$ ).....	118
Figure 4.13: Effect of temperature on gas yield .....	126
Figure 4.14: Effect of temperature on char yield.....	126
Figure 4.15: Effect of temperature on hydrogen yield.....	128
Figure 4.16: Effect of temperature on product gas composition .....	129
Figure 4.17: Comparative study of product gas composition .....	130
Figure 4.18: Effect of temperature on gasification and carbon conversion efficiency .....	131
Figure 4.19: Effect of temperature on selectivity .....	132
Figure 4.20: Effect of temperature on product gas heating values .....	133
Figure 4.21: Energy balance over gasifier at 600°C .....	135
Figure 4.22: Energy balance over gasifier at 750°C .....	135
Figure 4.23: Effect of steam to biomass ratio on gas yield.....	138
Figure 4.24: Effect of steam to biomass ratio on char yield .....	138
Figure 4.25: Effect of steam to biomass ratio on hydrogen yield.....	139
Figure 4.26: Effect of steam to biomass ratio on product gas composition.....	141
Figure 4.27: comparative study of product gas composition.....	142
Figure 4.28: Effect of steam to biomass ratio on gasification and carbon conversion efficiency .....	143
Figure 4.29: Effect of steam to biomass ratio on selectivity.....	144
Figure 4.30: Effect of steam to biomass ratio on product gas heating values .....	145
Figure 4.31: Energy balance over gasifier at steam to biomass ratio of 1.5 .....	146
Figure 4.32: Energy balance over gasifier at steam to biomass ratio of 2.5 .....	147
Figure 4.33: Effect of adsorbent to biomass ratio on gas yield .....	148

Figure 4.34: Effect of adsorbent to biomass ratio on char yield .....	149
Figure 4.35: Effect of adsorbent to biomass ratio on hydrogen yield.....	149
Figure 4.36: Effect of adsorbent to biomass ratio on product gas composition .....	151
Figure 4.37: Comparative study of product gas composition .....	151
Figure 4.38: Effect of adsorbent to biomass ratio on gasification and carbon conversion efficiency .....	152
Figure 4.39: Effect of adsorbent to biomass ratio on selectivity .....	153
Figure 4.40: Effect of adsorbent to biomass ratio on product gas heating values .....	154
Figure 4.41: Energy balance over gasifier at adsorbent to biomass ratio of 0.5.....	155
Figure 4.42: Energy balance over gasifier at adsorbent to biomass ratio of 1.5.....	155
Figure 4.43: Effect of fluidization velocity on gas yield .....	157
Figure 4.44: Effect of fluidization velocity on char yield.....	157
Figure 4.45: Effect of fluidization velocity on hydrogen yield .....	159
Figure 4.46: Effect of fluidization velocity on product gas composition .....	160
Figure 4.47: Comparative study of product gas composition .....	161
Figure 4.48: Effect of fluidization velocity on gasification and carbon conversion efficiency .....	162
Figure 4.49: Effect of fluidization velocity on selectivity .....	163
Figure 4.50: Effect of fluidization velocity on product gas heating values .....	164
Figure 4.51: Energy balance over gasifier at fluidization velocity of 0.15 m/s.....	165
Figure 4.52: Energy balance over gasifier at fluidization velocity of 0.26 m/s.....	165
Figure 4.53: Effect of biomass particle size on product gas composition .....	169
Figure 4.54: Comparative study of product gas composition .....	169
Figure 4.55: Energy balance over gasifier for biomass particle size of 0.355-0.50 mm .....	173
Figure 4.56: Energy balance over gasifier for biomass particle size of 1.0-2.0 mm .	174
Figure 4.57: Predicted versus actual hydrogen composition ( $Y_1$ ) .....	180
Figure 4.58: Predicted versus actual hydrogen yield ( $Y_2$ ) .....	181
Figure 4.59: Effect of temperature and steam to biomass ratio on hydrogen composition based on adsorbent to biomass ratio of 1.0 wt/wt, biomass particle size of 1000-2000 $\mu\text{m}$ and fluidization velocity of 0.21 m/s....	182
Figure 4.60: Effect of temperature and fluidization velocity on hydrogen composition based on steam to biomass ratio of 2.0 wt/wt, adsorbent to biomass ratio	

of 1.0 wt/wt, catalyst to biomass ratio of 0.1 wt/wt and biomass particle size of 1000-2000 $\mu\text{m}$ .....	183
Figure 4.61: Effect of temperature and adsorbent to biomass ratio on hydrogen composition at steam to biomass ratio of 2.0 wt/wt, fluidization velocity of 0.21 m/s, catalyst to biomass ratio of 0.1 wt/wt and biomass particle size of 1000-2000 $\mu\text{m}$ .....	184
Figure 4.62: Effect of temperature and biomass particle size on hydrogen composition based on steam to biomass ratio of 2.0 wt/wt, adsorbent to biomass ratio of 1.0 wt/wt, catalyst to biomass ratio of 0.1 wt/wt and fluidization velocity of 0.21 m/s .....	185
Figure 4.63: Effect of steam to biomass ratio and fluidization velocity on hydrogen composition at 675°C, adsorbent to biomass of 1.0 wt/wt, catalyst to biomass ratio of 0.1 wt/wt and biomass particle size of 1000-2000 $\mu\text{m}$ .....	186
Figure 4.64: Effect of steam to biomass ratio and adsorbent to biomass ratio on hydrogen composition at 675°C, fluidization velocity of 0.21 m/s, catalyst to biomass ratio of 0.10 wt/wt, and biomass particle size of 1000-2000 $\mu\text{m}$ .....	186
Figure 4.65: Effect of steam to biomass ratio and biomass particle size on hydrogen composition at 675°C, adsorbent to biomass ratio of 0.1 wt/wt, catalyst to biomass ratio of 0.1 wt/wt and fluidization velocity of 0.21 m/s .....	187
Figure 4.66: Effect of fluidization velocity and adsorbent to biomass ratio on hydrogen composition at 675°C, steam to biomass ratio of 2.0 wt/wt, catalyst to biomass ratio of 0.1 wt/wt and biomass particle size of 1000-2000 $\mu\text{m}$ .....	188
Figure 4.67: Effect of fluidization velocity and biomass particle size on hydrogen composition at 675°C, steam to biomass ratio 2.0 wt/wt, catalyst to biomass ratio of 0.1 wt/wt and adsorbent to biomass ratio of 1.0 wt/wt .....	189
Figure 4.68: Effect of adsorbent to biomass ratio and biomass particle size on hydrogen composition based on temperature of 675°C, steam to biomass ratio 2.0 wt/wt, catalyst to biomass ratio of 0.1 wt/wt and fluidization velocity of 0.21 m/s .....	189

Figure 4.69: Effect of temperature and steam to biomass ratio on hydrogen yield based on fluidization velocity of 0.21 m/s, adsorbent to biomass ratio of 1.0 wt/wt, catalyst to biomass ratio of 0.1 wt/wt and biomass particle size of 1000-2000 $\mu\text{m}$ .....	190
Figure 4.70: Effect of temperature and fluidization velocity on hydrogen yield based on steam to biomass ratio of 2.0 wt/wt, adsorbent to biomass ratio of 1.0 wt/wt, catalyst to biomass ratio of 0.1 wt/wt and biomass particle size of 1000-2000 $\mu\text{m}$ .....	192
Figure 4.71: Effect of temperature and adsorbent to biomass ratio on hydrogen yield at steam to biomass ratio of 2.0 wt/wt, fluidization velocity of 0.21 m/s, catalyst to biomass ratio of 0.1 wt/wt and biomass particle size of 1000-2000 $\mu\text{m}$ .....	192
Figure 4.72: Effect of temperature and biomass particle size on hydrogen composition based on steam to biomass ratio of 2.0 wt/wt, adsorbent to biomass ratio of 1.0 wt/wt, catalyst to biomass ratio of 0.1 wt/wt and fluidization velocity of 0.21 m/s .....	193
Figure 4.73: Effect of steam to biomass ratio and fluidization velocity on hydrogen yield at 675°C, adsorbent to biomass ratio of 1.0 wt/wt, catalyst to biomass ratio of 0.1 wt/wt and biomass particle size of 1000-2000 $\mu\text{m}$	194
Figure 4.74: Effect of steam to biomass ratio and adsorbent to biomass ratio on hydrogen yield at 675°C, fluidization velocity of 0.21 m/s, catalyst to biomass ratio of 0.1 wt/wt and biomass particle size of 1000-2000 $\mu\text{m}$	194
Figure 4.75: Effect of steam to biomass ratio and biomass particle size on hydrogen composition at 675°C, adsorbent to biomass ratio of 1.0 wt/wt, catalyst to biomass ratio of 0.1 wt/wt and fluidization velocity of 0.21 m/s .....	195
Figure 4.76: Effect of adsorbent to biomass ratio and fluidization velocity on hydrogen yield based on 675°C, steam to biomass ratio of 2.0 wt/wt, catalyst to biomass ratio of 0.1 wt/wt and biomass particle size of 1000-2000 $\mu\text{m}$ .....	196
Figure 4.77: Effect of biomass particle size and fluidization velocity on hydrogen yield at 675°C, steam to biomass ratio of 2.0 wt/wt, catalyst to biomass ratio of 0.1 wt/wt and adsorbent to biomass ratio of 1.0 wt/wt .....	197

Figure 4.78: Effect of biomass particle size and adsorbent to biomass ratio on hydrogen yield at 675°C, steam to biomass ratio of 2.0 wt/wt, catalyst to biomass ratio of 0.1 wt/wt and fluidization velocity of 0.21 m/s .....	197
Figure 4.79: Effect of temperature on product gas composition; modeling (—) and experiment (■) .....	200
Figure 4.80: Effect of steam to biomass ratio on product gas composition; modelling .....	201
Figure 4.81: Effect of adsorbent to biomass ratio on product gas composition; modeling (—) and experiment (■) .....	202
Figure 4.82: Effect of reactor temperature on the equilibrium of water gas shift reaction .....	205

## LIST OF TABLES

Table 2.1: Ranking of Malaysian agricultural biomass for gasification [41] .....	18
Table 2.2: Comparison of fixed bed and fluidized bed gasifier [23] .....	34
Table 3.1: Quicklime properties .....	69
Table 3.2: Steam properties at bed temperature of 750°C and 1 atm .....	69
Table 3.3: Input design parameter for distributor plate design .....	74
Table 3.4: Configuration of fluidized bed gasifier .....	75
Table 3.5: Fluidized bed gasifier system configuration .....	78
Table 3.6: Specification of biomass feeding system .....	80
Table 3.7: Specification of steam generation system .....	81
Table 3.8: Cyclone specification .....	82
Table 3.9: Specification of water scrubber and water separator .....	83
Table 3.10: Standard gas calibration for gas analyzers .....	84
Table 3.11: Fluidized bed gasifier operating conditions .....	86
Table 3.12: Process variables range for central composite rotatable design (CCRD) .....	89
Table 3.13: Parameters and constants for energy balance [4, 84] .....	94
Table 3.14: Data for thermal conductivity calculation [187] .....	97
Table 3.15: Basic data for calculation of heat and mass transfer coefficients .....	97
Table 3.16: Reactions schemes for kinetic parameter determination [81, 85, 106] .....	98
Table 4.1: Palm kernel shell properties .....	104
Table 4.2: Ultimate analysis of palm kernel shell (dry ash free) .....	105
Table 4.3: Proximate analysis of palm kernel shell (dry basis) .....	105
Table 4.4: Heating values of palm kernel shell .....	106
Table 4.5: Quicklime properties .....	106
Table 4.6: X-ray fluorescence analysis of Quicklime .....	107
Table 4.7: X-ray fluorescence analysis of Ni catalyst .....	107
Table 4.8: Surface properties of Quicklime and Ni catalyst .....	110
Table 4.9: Physical properties of Quicklime (adsorbent) and Ni catalyst .....	113
Table 4.10: Heat and mass transfer coefficients .....	117
Table 4.11: Comparative study of heat and mass transfer coefficients .....	117
Table 4.12: Experimental design for ICA steam gasification .....	120

Table 4.13: Effect of temperature .....	121
Table 4.14: Effect of steam to biomass ratio .....	121
Table 4.15: Effect of fluidization velocity .....	122
Table 4.16: Effect of adsorbent to biomass ratio .....	122
Table 4.17: Effect of biomass particle size .....	123
Table 4.18: Experimental run representing central points .....	123
Table 4.19: Factorial points in design of experiment .....	124
Table 4.20: Gasification energy requirement with respect to reactor temperature ....	136
Table 4.21: Gasification energy requirement with respect to steam to biomass ratio	147
Table 4.22: Gasification energy requirement with respect to adsorbent to biomass ratio.....	156
Table 4.23: Gasification energy requirement with respect to fluidization velocity...	166
Table 4.24: Effect of biomass particle size on gas and char yield.....	167
Table 4.25: Effect of biomass particle size on hydrogen yield.....	168
Table 4.26: Effect of biomass particle size on gasification and carbon conversion efficiency .....	171
Table 4.27: Effect of biomass particle size on selectivity .....	171
Table 4.28: Effect of biomass particle size on product gas heating values .....	172
Table 4.29: Gasification energy requirement with respect to biomass particle size..	174
Table 4.30: Experimental operating conditions and associated output responses .....	176
Table 4.31: Analysis of variance (ANOVA) on hydrogen composition .....	177
Table 4.32: Coefficient of determination on hydrogen composition response ( $Y_1$ )..	178
Table 4.33: Analysis of variance (ANOVA) on hydrogen yield .....	179
Table 4.34: Coefficient of determination on hydrogen yield response ( $Y_2$ ).....	179
Table 4.35: The optimum parameter selected to maximize $H_2$ composition and yield .....	198
Table 4.36: Results of confirmation runs for hydrogen composition and yield .....	199
Table 4.37: Comparison of experimental values with modeling for hydrogen composition and yield.....	199
Table 4.38: Evaluated kinetic parameters .....	200
Table 4.39: Mean error of product gas composition with temperature.....	201
Table 4.40: Mean error of product gas composition with steam to biomass ratio.....	202

Table 4.41: Mean error of product gas composition with adsorbent to biomass ratio  
.....203

Table 4.42: Effect of temperature on equilibrium constant and Gibbs free energy...204

## LIST OF ABBREVIATIONS AND SYMBOLS

### ABBREVIATIONS

AER	Absorption enhanced reforming
ANOVA	Analysis of variance
ASAP	Accelerated surface area and porosimetry
ASTM	American society for testing and materials
BEA	Beta zeolite
BET	Brunauer-Emett-Teller
BJH	Barret-Joyner-Halenda
BWGSR	Biological water gas shift reaction
CCRD	Central composite rotatable design
CGR	Char gasification reaction
DFB	Dual fluidized bed
DOE	Design of experiments
EFB	Empty fruit bunch
FC	Fixed carbon, wt%
FCCD	Face centred composite design
FIC	Flow indicator controller
FICFB	Fast inter circulating fluidized bed
GC	Gas chromatography
GEMENI	Gibbs Energy Minimization
HCW	Hot compressed water
HSC	Enthalpy (H), entropy (S) and heat capacity (C)
HT	High temperature, K
HYPR-RING	Hydrogen production by reaction integrated novel gasification
ICA	Integrated catalytic adsorption
ID	Internal diameter, m
IR	Infrared
IUPAC	International Union of Pure and Applied Chemistry
LT	Low temperature, K
MRSS	Mean value of residual sum squared (RSS)

Mtoe	Million tonnes of oil equivalent
MW	Megawatt
NLP	Nonlinear programming
PDI	Pressure differential indicator
PI	Pressure indicator
PKS	Palm kernel shell
RM	Malaysian Ringgit
RSM	Response surface methodology
RSS	Residual sum squared
SCADA	Supervisory control and data acquisition
SCWG	Supercritical water gasification
SEHP	Sorption-enhance hydrogen production
SESR	Sorption enhanced steam reforming
SEM	Scanning electron microscopy
SEWGS	Sorbent enhanced water gas shift
SMR	Steam methane reforming
TDH	Transport disengaging height, m
TI	Temperature indicator
TCD	Thermal conductive detector
UN	United Nation
WGSR	Water gas shift reaction
XRD	X-ray diffraction
XRF	X-ray fluorescence
3D	Three dimensional
2D	Two dimensional

## SYMBOLS

$a_2$	Constant to determine thermal conductivity of a single gas component
A	Adsorbent
A	Bed cross sectional area, m <sup>2</sup>
Adj-R <sup>2</sup>	Adjusted coefficient of determination (regression constant)
$A_i$	Frequency factor or pre-exponential factor, 1/s
$A_{or}$	Area of an orifice, m <sup>2</sup>

$b_2$	Constant to determine thermal conductivity of a single gas component
$B$	Biomass
$c_2$	Constant to determine thermal conductivity of a single gas component
$C_A$	Concentration of component A, mol/m <sup>3</sup>
$C_{dor}$	Drag coefficient across orifice
$C_p$	Specific heat capacity at constant pressure, kJ/kg
$d_b$	Diameter of bed particle, m
$D$	Bed diameter, m
$D_{b0}$	Initial bubble diameter, m
$D_{bio}$	Biomass particle size, mm
$D_{bm}$	Maximum bubble diameter, m
$D_{bmean}$	Mean bubble diameter, m
$D_c$	Molecular diffusion coefficient, m <sup>2</sup> /s
$E_i$	Activation energy of component $i$ , kJ/mol
$g$	Acceleration due to gravity, m/s <sup>2</sup>
$h_{bed}$	Heat transfer coefficient in the bed, kW/m <sup>2</sup> .K
$H_i$	Enthalpy of component $i$ , kW
$H_{f(i)}$	Heat of formation of component $i$ , J/mol
$HHV$	Higher heating value, MJ/kg
$k_{bed}$	Mass transfer coefficient in the bed, m/s
$k_g$	Thermal conductivity of gas mixture, kW/m.K
$k_{gi}$	Thermal conductivity of gas component $i$ , kW/m.K
$k_i$	Arrhenius constant (kinetic constant), 1/s
$K_{bc}$	Mass interchange coefficient between bubble and cloud, 1/s
$LHV$	Lower heating value, MJ/kg
$m_i$	Mass flow rate of component $i$ , g/h
$mol_i$	Mole of component $i$ , mol
$n_i$	Mole flow rate of gas component $i$ , mol/h
$N_d$	Total number of orifices in distributor plate/area of the distributor plate, 1/m <sup>2</sup>
$N_i$	Mole fraction of component $i$
$N_{or}$	Number of orifices in distributor plate
$Nu_{bed}$	Nusselt number (dimensionless)

$p$	Actual pressure of adsorbing gas, bar
$p_0$	Vapor pressure of adsorbing gas, bar
$P$	Pressure, kPa
$Q$	Volumetric flow rate at superficial gas velocity ( $U$ ), m <sup>3</sup> /h
$Q_{Ext}$	External energy, kW
$Q_{steam}$	Energy associated with steam, kW
$Q_{mf}$	Volumetric flow rate at minimum fluidization velocity ( $U_{mf}$ ), m <sup>3</sup> /h
$r_i$	Rate of reaction of component $i$ , mol/m <sup>3</sup> .s
$R^2$	Coefficient of determination (regression constant)
$R$	Universal gas constant, 8.314 kPa.m <sup>3</sup> /kmol.K
$R_c$	Distributor pressure drop/bed pressure drop
$Re$	Reynolds number (dimensionless)
$R_i$	Volumetric rate of component $i$ , mol/m <sup>3</sup> .s
$S$	Steam
$Sc$	Schmidt number (dimensionless)
$Sh_{bed}$	Sherwood number based on fluidized bed mass transfer coefficient
$Sh^*$	Particle Sherwood number based on local mass transfer coefficient for a single particle in the bed
$S_{CGR}$	Theoretical steam required for char gasification reaction, m <sup>3</sup> /h
$S_{SMR}$	Theoretical steam required for steam methane reforming, m <sup>3</sup> /h
$S_{WGSR}$	Theoretical steam required for water gas shift reaction, m <sup>3</sup> /h
$S_{Total}$	Total theoretical steam required for gasification, m <sup>3</sup> /h
$T$	Temperature, K
$U$	Gas superficial velocity (gas fluidization velocity), m/s
$U_{mf}$	Minimum fluidization velocity, m/s
$U_{or}$	Gas velocity through orifice, m/s
$y$	Fraction of inert or non adsorbing component
$Y_1$	Output response of hydrogen composition, vol%
$Y_2$	Output response of hydrogen yield, g/kg biomass
$y_{exp}$	Volume fraction generated by experiment
$y_{mod}$	Volume fraction generated by model
$Z$	Bed height, m

## GREEK SYMBOLS

$\delta$	Volume fraction of bubble in the bed
$\varepsilon$	Bed voidage at gas superficial velocity
$\varepsilon_{mf}$	Bed voidage at minimum fluidization velocity
$\Delta H_i$	Change in enthalpy of component $i$ , kW
$\Delta P_b$	Pressure drop across the bed, mbar
$\Delta P_d$	Pressure drop across the distributor plate, mbar
$\rho_b$	Bed particle density, kg/m <sup>3</sup>
$\rho_f$	Fluidizing gas density, kg/m <sup>3</sup>
$\eta_{cc}$	Carbon conversion efficiency, %
$\eta_d$	Adsorption efficiency for mass transfer, %
$\eta_g$	Gasification efficiency, %
$\gamma_b$	Fraction of solid in the bubble
$\mu$	Fluidizing gas viscosity, Pa.s
$\phi_b$	Sphericity of bed particle



## CHAPTER 1

### INTRODUCTION

#### **1.1 Current Energy Scenario**

The continuing growth in world population brings rapid development in industrialization which consumes half of the world total energy produced. This increases the overall world energy demand particularly in developing countries which consumes about 95% of the world increase particularly in the industrial sector. Moreover, from 2007 to 2035, the total energy demand increases by about 84% for developing countries as compared to 49% for developed countries [1]. In the current scenario, the world energy is mainly dependent on fossil fuel, which contributes 81.1% of world energy production. The world energy production is not increasing at the same pace as energy consumption due to limited fossil fuel reserves. In 2010, the world energy consumption was reported to be 12852 Mtoe (million tonnes of oil equivalent) as compared to the energy production of 12845 Mtoe [2]. Therefore, the future availability of the energy from fossil fuel will be a severe problem. High energy demand will raise the energy prices. The global economic recession from 2007-2009 was a recent example based on the consequences of world energy production and consumption scenario.

Apart from the finite reserves, fossil fuel energy dependency causes numerous environmental problems such as green house effect, ozone layer depletion, acid rain and other pollutions. More seriously, the carbon dioxide released by fossil fuel contributes 84% of greenhouse gas emissions released to the atmosphere [3]. According to International Energy Outlook 2010, it was estimated that the world energy-related carbon dioxide emission was 29.7 billion metric tonnes in 2007 which would be expected to increase to 42.2 billion metric tonnes in 2035 [1]. This high amount of CO<sub>2</sub> released would result in global warming which may affect forests

activities, food production and give problems to the ecosystem as well as to human health. These severe conditions will end up with world starvation and other social problems. Due to associated problems with fossil fuel, the search for alternative clean, sustainable and environmental friendly energy sources should be intensified.

Malaysia is a country of vast renewable and non-renewable sources of energy. The country energy demand mainly depends on non-renewable sources comprising of oil and gas. Up to 2005, non-renewable sources (oil, natural gas and coal) contributed about 87.9% of country energy demand while renewable sources (hydropower and biomass) shared only 12.1% [4]. Due to fast growing economy, the country energy demand is expected to be 18000 MW by the year 2010 [5]. Moreover, unwanted greenhouse gas emissions and other serious environmental issues associated with the transportation sector have become a great concern to the future of the country development. As part of the UN Convention on Climate Change and Kyoto Protocol, Malaysia has to take steps to reduce greenhouse gas emissions. More recently, in Copenhagen Climate Change Summit 2009, Malaysian Prime Minister has showed commitment to reduce carbon dioxide emission. The Prime Minister has also announced RM 1.5 billion in 2010 national budget for green technology development in the country [6]. The country needs to have abundant clean energy to maintain its journey towards achieving developed country status.

Malaysia has revised its energy policy from fourth-fuel to fifth-fuel under 8<sup>th</sup> Malaysian plan (2001-2005) in 1999. Renewable energy was considered the fifth fuel in the energy mix. In 2003, biomass was the only renewable source contributed about 1.1% in the energy mix. It was expected that about 5% of country's electricity would be generated from renewable sources by 2005 [7]. Moreover, according to the 9<sup>th</sup> Malaysian Plan (2006-2010), energy from renewable sources was expected to contribute about 300 MW in fuel mixture by 2010 [6]. According to 10<sup>th</sup> Malaysian plan (2011-2015), renewable energy is expected to contribute about 985 MW makes 5.5% of Malaysian total energy mix [8].

## **1.2 Hydrogen as Alternative Fuel**

Hydrogen contributes an economical and has wide application in the development of current energy requirements. Hydrogen may contribute significantly to clean energy for power generation, industrial, commercial and transportation sectors. Hydrogen combustion provides 2.8 and 4 times more energy content (per kilogram) as compared to gasoline and coal [9]. In addition, it is a clean fuel as the combustion of hydrogen produces only water as by-product. The application of hydrogen as a fuel in combustion engine and fuel cell for power generation has received favourable attraction [10]. Being a clean energy carrier with high energy content, hydrogen can contribute considerable energy in the near future without adding greenhouse gas to the environment.

## **1.3 Hydrogen from Renewable Resources**

Currently, 96% of hydrogen comes from non renewable resources such as fossil fuel. So far, steam methane reforming (SMR) is one of the well established methods to produce hydrogen that contributes 48% of world hydrogen production. Beside SMR, naphtha reforming and coal gasification gives 18% and 30% of worldwide hydrogen production, respectively. Almost 4% hydrogen comes from electrolysis using solar energy [11].

Recent development on renewable resources shows great potential to produce renewable hydrogen. These renewable resources mainly comprised of biomass and electrolysis. Electrolysis is a process of splitting water into hydrogen and oxygen using electrical current. Different sources of energy like solar and wind can be utilized to produce electrical current to split water.

Based on these findings, it is concluded that the hydrogen economy is fully dependent on finite fossil fuel reserves which is neither renewable nor sustainable. If hydrogen has to become a basic source of power generation as well as transportation fuel, it is necessary to search for novel resources and processes to meet continuous

increase in hydrogen demand. Secondly, it will help to lessen the dependency on fossil fuel.

#### **1.4 Biomass as a Source of Renewable Hydrogen**

Biomass is the fourth largest source of energy after coal, natural gas and oil fulfilled 15% of world primary energy demand and accounting for 38% of primary energy consumption in developing countries [12]. It is considered the largest and most important renewable source exist on earth and can be used in a variety of ways to produce different types of energy and chemical feedstocks.

#### **1.5 Hydrogen from Biomass: Environmental Impact and CO<sub>2</sub> Reduction**

Biomass is one of most promising source among renewable resources to produce abundant, clean and renewable hydrogen. Hydrogen from biomass provides a renewable and sustainable way of production as compared to conventional fossil fuel and may avoid the cost of getting rid of wastes especially industrial and solid wastes from the environment [13]. Naturally, biomass is CO<sub>2</sub> neutral if the life cycle is sustained. Furthermore, biomass contains low sulphur and nitrogen content and has very low tendency to produce SO<sub>x</sub> and NO<sub>x</sub>. Both these components and CO<sub>2</sub> in the atmosphere are responsible for acid rain which has harmful effect on aquatic animal life, plant and infrastructure.

#### **1.6 Challenges of Present Gasification Technologies for Hydrogen Production**

Tremendous efforts have been made to develop advance biomass gasification technologies in the last couple of decades. The present biomass gasification technologies are based on the coal gasification processes but slightly different to coal gasification due to high volatile matter and low temperature operation. The coal gasification technologies are used for heat and power generation purposes for more

than three decades. These processes are mostly operated at high pressure and temperature, and produce hydrogen by up to 45 vol% in the product gas [14].

The development of the existing biomass gasification technologies is to switch into hydrogen production technologies which are restricted by several problems. Tar (high hydrocarbons) and char particles in the exiting gas from the gasifier restrict the technology to be commercialized. Tar gives mechanical problem to downstream processing and causes clogging at colder parts of the gasification unit [15]. Char particles reduce the operation life of the catalyst inside the gasifier [16]. The reduction of these two components is based on the gasifier specifications and type of fuel. The hydrogen content and purity in the product gas generated from the conventional biomass gasification is not sufficient for direct utilization in fuel cell ( $H_2$  vol% >99.99). The conventional gasification process produces 40-50 vol% hydrogen in the product gas [17]. High reactor temperature in typical biomass gasification processes is another problem which does not produce an economical operation for commercial purposes.

Without any doubt, biomass gasification is an excellent choice for renewable hydrogen production. It's not only a renewable way to produce hydrogen but also very useful to deal with large amount of biomass wastes including municipal and solid waste which is difficult to dispose. However, great efforts are required to achieve successful commercial application of biomass gasification technology for hydrogen production. The present challenges for renewable hydrogen from biomass gasification thus need special attention.

### **1.7 Problem Statement**

Biomass steam gasification has gained more attention as compared to other thermal conversion processes. However, biomass steam gasification processes still need considerable efforts to be commercialized. The quality and quantity of hydrogen rich gas with considerable amount of tar inhibits the application of technology in power generation and fuel cell. The current biomass steam gasification technology needs better process design and reactor configuration to enhance hydrogen content

with minimum tar in the product gas. Beside, tremendous efforts from researchers via introduction of catalyst and CO<sub>2</sub> adsorption in the process, the subject area needs further improvement to produce vast amount of renewable hydrogen utilizing biomass as the feedstock.

## **1.8 Research Objectives**

To address the present challenges in biomass gasification technology, the present study investigates the in-situ catalytic and adsorption steam gasification system utilizing local oil palm waste to improve the hydrogen content in the product gas. The following measurable objectives are considered in the present study.

- To develop an alternative process that enhances hydrogen production through utilization of in-situ catalytic and adsorption process.
- To design optimum fluidized bed reactor configuration for the enhancement of biohydrogen production.
- To evaluate the performance of the gasification system for enhance hydrogen production under the effect of temperature, steam to biomass ratio, adsorbent to biomass ratio, fluidization velocity and biomass particle size.
- To determine the kinetic parameters through kinetic modeling of simultaneous reactions in in-situ catalytic and adsorption process.

## **1.9 Thesis Scope and Outline**

The scope of the present PhD work is to enhance the hydrogen yield in the product gas in the presence of in-situ catalyst and adsorbent in fluidized bed reactor. To achieve this, the following measurable goals are set.

- The overall process design is carried out using hierarchical approach. This approach divides the overall process into main gasification reactor system, solid separator system, water cooling and separator units.
- The design of fluidized bed reactor is conducted by combining the hydrodynamics and reaction based calculation based on the properties of CO<sub>2</sub>

adsorbent as a bed material (adsorbent) and steam as gasification agent. Hydrodynamics calculations give minimum fluidization velocity which is then adjusted with total steam required for the reactions to calculate the reactor internal diameter (ID). Reactor height is then calculated using transport disengaging height (TDH) based on the maximum bubble diameter determined.

- Material preparation and characterization of commercial Quicklime and Ni catalyst are considered. Quicklime is used due to its high CaO content (>90 wt%) for CO<sub>2</sub> adsorption in the reactor. Characterization techniques i.e. x-ray fluorescence (XRF), x-ray diffraction (XRD), scanning electron microscopy (SEM) and pysisorption analysis are carried out to determine the composition, pore size and surface morphology of the Quicklime and Ni catalyst.
- The effect of different process variables such as temperature, steam to biomass ratio, adsorbent to biomass ratio, fluidization velocity and biomass particle size are studied on hydrogen content in the product gas in the fluidized bed gasifier. Temperature is varied from 600-750°C where higher gasification temperature is unfavourable for CO<sub>2</sub> adsorption reaction (carbonation reaction based on CaO). High fluidization velocity, ranging from 3-5 times of minimum fluidization velocity, is considered to assure high mass and heat transfer coefficients in the reactor. Steam to biomass and adsorbent to biomass ratio are in the range of 1.5-2.5 wt/wt and 0.5-1.5 wt/wt, respectively. Two biomass particle sizes i.e. 0.355-0.5 mm and 1.0-2.0 mm are studied.
- The reaction kinetic model is presented to determine the kinetic parameters i.e. activation energy and frequency factor for the main reactions; char gasification, water gas shift, steam methane reforming, methanation, boudouard and CO<sub>2</sub> adsorption. The kinetic parameters are computed by minimizing the difference between predicted and experimental results using least squared error minimization approach in MATLAB.
- Process optimization study is carried out based on the two output response variables i.e. hydrogen composition and hydrogen yield in Design Expert-8 software.

## 1.10 Chapter Summary

This thesis consists of five chapters. The coverage of each chapter is given in the following paragraphs.

- Chapter 1 provides insight of the subject, background and current issues related to the work. It further explains the problem statement, research objectives and scope of the proposed study.
- Chapter 2 introduces the literature survey related to the experimental work and basic concept of the associated terms. This chapter also includes the insight of kinetic modeling and their related literature based on different modeling approach. Furthermore, the process optimization, definition of important terms and related literature is also needed.
- Chapter 3 comprises of methodology related to the material preparation and characterization, experimental work and kinetic modeling presented in the study. It further provides the related experimental procedure and information about the main equipments participating in the experimental study. The equations and formulas to define the important process performance parameters are also provided in the chapter.
- Chapter 4 provides results and discussions. The material characterization, experimental and modeling results are presented and explained based on the different arguments and theories. These results are then compared with related work published in the literature.
- Chapter 5 summarizes all the findings and conclusions in the present study and provides the future recommendations for the related work.

The anticipation of the present study is to contribute valuable work in the field of renewable hydrogen production from biomass steam gasification with in-situ catalytic and adsorption process. It is hoped that the findings and analysis provided in the present study will be used as a reference for the future work in the field of renewable hydrogen production from biomass gasification.

## CHAPTER 2

### LITERATURE REVIEW

#### **2.1 Introduction**

The present chapter reviews characteristics and properties of biomass suitable for biomass gasification processes to produce hydrogen rich gas. A detailed literature review is presented for parametric study, reaction kinetics and equilibrium modeling in biomass gasification, biomass steam gasification, biomass catalytic steam gasification and biomass gasification with in-situ CO<sub>2</sub> adsorbent. The kinetic parameters determination based on the product gas composition from the experimental work are also reviewed. Literature related to optimization approach for the experimental work is also discussed. At the end of each topic, research gaps are highlighted to point out the need of future work in the related field.

#### **2.2 Biomass Resources**

Asia has the highest potential of renewable hydrogen and other chemical feedstock production from biomass. As shown in Figure 2.1, Asia contributes 43.6% of worldwide biomass total resources of 1880 billion tonnes followed by Africa with 21.1% [18]. The developed countries contribute 23.3% of biomass resources worldwide.

As a tropical country involving in agricultural sectors, Malaysia has a variety of biomass wastes produced from oil palm, rice, sugarcane, wood industry and municipal solid waste as shown in Figure 2.2 [19]. Among these biomasses, oil palm contributes 85.5% of biomass wastes in the country while municipal solids waste standing second with 9.55%.

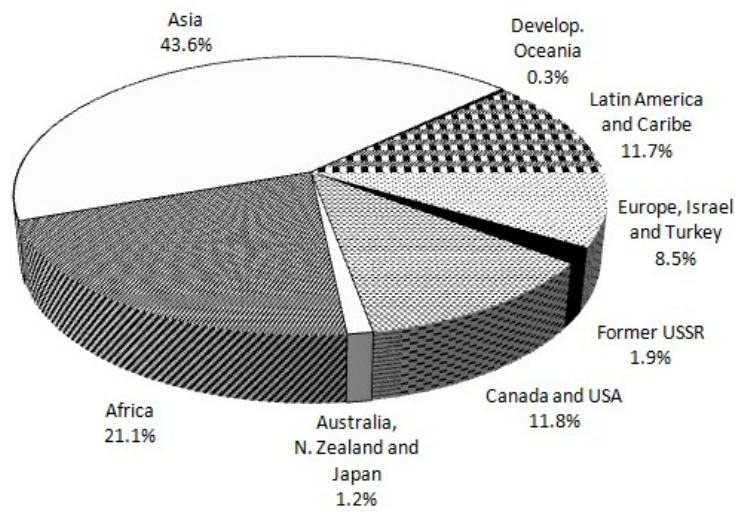


Figure 2.1: Biomass production worldwide [18]

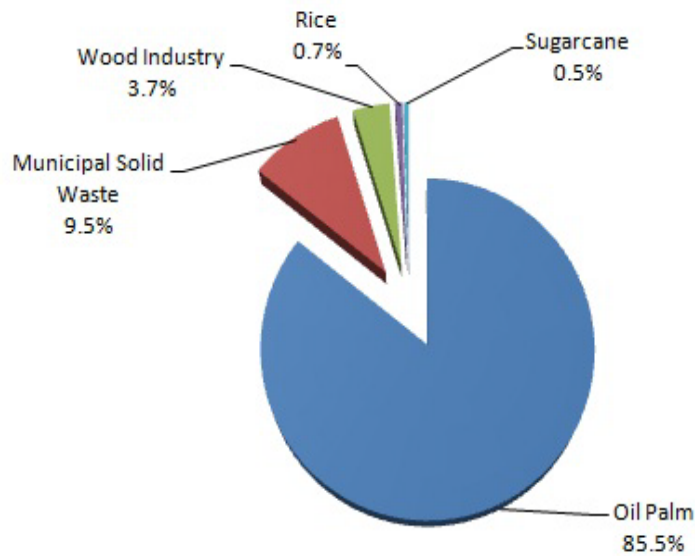


Figure 2.2: Biomass waste distribution in Malaysia [19]

Oil palm is the main resource for Southeast Asia particularly Malaysia and Indonesia, which collectively produces 87% of worldwide resources [19]. Biomass wastes produced from oil palm is derived from its plantation area (e.g. trunk and fronds), mill operation (e.g. empty fruit bunch (EFB), palm kernel shell (PKS) and mesocarp fibers). In 2008, total biomass wastes of 198.5 million tons were produced according to the distribution shown in Figure 2.3 [20]. It is noted that unlike other oil palm waste, oil palm trunk is obtained only during re-plantation of oil palm trees.

With the vast amount of biomass available in the country, the possibilities of hydrogen production from these sources are tremendous.

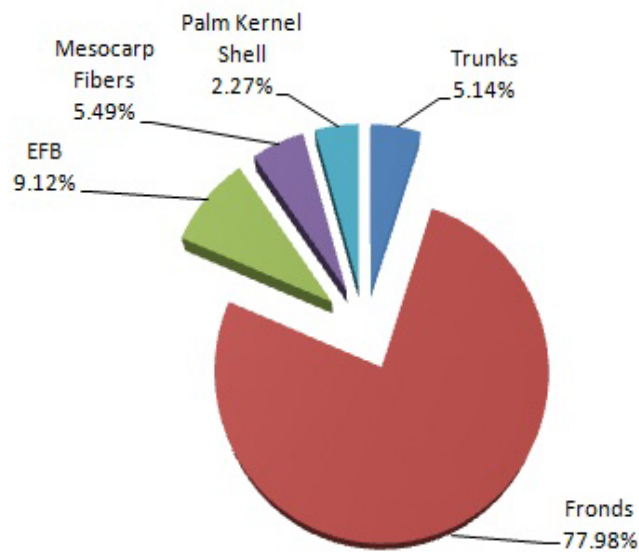


Figure 2.3: Oil palm waste distribution in Malaysia [20]

## 2.3 Hydrogen Production from Biomass

Hydrogen can be produced from biomass via thermal chemical conversion and biochemical chemical conversion processes. Each process has its own advantages and disadvantages.

### 2.3.1 Hydrogen Production through Thermal Conversion of Biomass

Thermochemical conversion processes include gasification, pyrolysis and supercritical water gasification (SCWG). Gasification is recognized as a potential technology to develop large scale hydrogen production system under the exploitation of vast biomass resources. Gasification is thermochemical conversion of solid biomass into gaseous product mainly consists of  $H_2$ ,  $CO$ ,  $CO_2$ ,  $CH_4$  and  $N_2$  by using air, oxygen and steam or in combination as the gasifying medium. The operating condition usually varies from  $800^{\circ}C$  to  $900^{\circ}C$  under atmospheric pressure. Steam gasification is being identified as a potential process to produce more and clean hydrogen [21]. Steam as a sole gasifying agent has numerous advantages over air

which dilutes the final product due to excess nitrogen, and pure oxygen is considered costly for small scale operation [22]. Typically, gasification process can accept biomass moisture content less than 35 wt%. Biomass gasification can be performed in fixed bed or fluidized bed reactor where the latter gives better performance in terms of high carbon conversion [23]. Problems associated with quality of gas due to tar and char impurities are the main challenges in the process. Tar in the product gas is one of the main problems associated with biomass gasification because it does create problems to the equipment and deactivate the downstream catalyst [24]. The use of catalyst in biomass steam gasification has gained a lot of interest in order to enhance reaction rate, lower reaction temperature and improve gas quality by reducing tar content in the product gas [25]. The catalyst activity in biomass steam gasification increases H<sub>2</sub> content up to more than 60 vol% in product gas [16]. Typical catalysts used in biomass steam gasification are alkali metal, dolomites and Ni based catalysts [26]. Recently, introduction of CO<sub>2</sub> adsorption in the process makes it more viable for commercial application. The presence of CO<sub>2</sub> adsorbent accelerates all the parallel reforming and gasification reaction towards H<sub>2</sub> production [27]. The typical hydrogen composition of 40 vol% (dry basis) is achieved in steam gasification which can be increased up to 75 vol% (dry basis) in the presence of CO<sub>2</sub> adsorbent [28].

Pyrolysis is thermal decomposition of biomass into liquid oil, solid charcoal, and gaseous products in the absence of air/oxygen at temperature range of 350°C to 525°C and pressure of 1-5 atm [29]. Pyrolysis is an endothermic reaction. Most pyrolysis processes are designed to produce bio-oil which is the basis of several other processes accounting for different chemical feedstocks. Hydrogen can be produced directly from fast or flash pyrolysis at high temperature, high heating rate and longer residence time of gaseous phase in the reactor [30]. The catalyst application in pyrolysis is helpful to enhance product yield and to improve product gas quality. Catalysts such as inorganic salts, chlorides, carbonates and chromates have the ability to enhance pyrolysis reaction rate. Some metal oxides such as Ni-based [31], K<sub>2</sub>CO<sub>3</sub> and Na<sub>2</sub>CO<sub>3</sub> also exhibit some catalytic effect for pyrolysis [32].

Supercritical water gasification (SCWG) is preferred when biomass contains moisture more than 50 wt% which contributes to high cost of moisture removal in

conventional gasification process [4]. The liquid and gas phase have similar properties when water is treated at its critical point (temperature higher than 374°C, pressure of 220 atm). The gaseous products comprises of H<sub>2</sub>, CO, CO<sub>2</sub> and CH<sub>4</sub>. This approach gives gasification conversion of almost 100% and hydrogen composition of 50 vol% in the product gas [29].

### **2.3.2 Hydrogen Production from Bio-Chemical Conversion**

Bio-chemical processes can be classified into biological water gas shift reaction (BWGSR) and fermentation which is further divided into dark fermentation and photo fermentation. BWGSR is relatively new technology for bio-hydrogen production. Some photo-heterotrophic bacteria are capable of performing CO oxidation into H<sub>2</sub> and CO<sub>2</sub> in the dark at ambient temperature and pressure [12]. These bacterial take CO as single carbon source and generate adenosine triphosphate, which couples with CO oxidation and result in reduction of H<sup>+</sup> to H<sub>2</sub>. As reaction occurs at ambient conditions, thermodynamic favors forward reaction to produce H<sub>2</sub> [9].

Fermentation by micro-organisms can be divided into dark fermentation (anaerobic) and photo-fermentation. Photo fermentation uses non sulphur bacteria under nitrogen environment in the presence of nitrogenase catalyst and solar energy. The final product mainly consists of H<sub>2</sub> and CO<sub>2</sub> [12]. Dark fermentation uses carbohydrates rich biomass waste in the presence of anaerobic bacteria in the dark. The final product mainly consists of H<sub>2</sub> and CO<sub>2</sub> along with lesser amount of CO, CH<sub>4</sub> and H<sub>2</sub>S [33].

### **2.4 Feed Characteristics**

Biomass as feedstock can be characterized based on different criterion, but generally it can be divided into four main types [34]:

- woody plants
- herbaceous plants/grasses,
- aquatic plants
- manures

Biomass is composed of cellulose, hemicellulose and lignin. The usual proportions for plant biomass (wt%) vary as 40-50% cellulose, 20-60% hemicellulose and 10-25% lignin [35]. Beside, animal manures contain 14-27% cellulose, 12-21% hemicellulose and 6-13% lignin [36]. Cellulose is long polymer chain with an average molecular weight of 100,000. It is represented by general molecular formula of  $C_6H_{10}O_5$ . Cellulose has strong crystalline structure which is resistive to hydrolysis.

Hemicellulose compares to cellulose has amorphous structure with little strength. It is a mixture of polysaccharides which is entirely consisted of sugars. Generally, hemicellulose can be represented by  $C_5H_8O_n$  with molecular weight of higher than 30,000. Hemicellulose can easily be hydrolyzed and soluble in weak acids and bases [37]. Lignin is a group of high molecular weight of amorphous related compound. Lignin behaves as cementing medium for cellulose fibers to keep adjacent cells together. It is highly insoluble even in sulfuric acid [37].

#### **2.4.1 Biomass Properties**

The properties of biomass determine its route for energy conversion. Typically, the main properties of biomass are [34].

- moisture content
  - intrinsic
  - extrinsic
- calorific value (heating value)
- proportions of volatiles matter and fixed carbon
- ash content
- alkali metal content
- lignin to cellulose ratio

Based on the above biomass properties, the first five are important for dry biomass conversion process whereas the first and the last properties are of interest for wet biomass conversion process [34]. The lignin to cellulose ratio is critical in wet biomass conversion due to low degradability of lignin via hydrolysis/enzymatic system which reduces the overall yield of the process.

Among the moisture content, the intrinsic property remains in biomass and prevailing weather does not affect this amount of moisture. The extrinsic moisture content is affected by the weather and is influenced by the surroundings and humidity. High moisture content biomass such as herbaceous plant i.e. sugarcane is more suitable for biological and SCWG processes. On the other hand, biomass with lower moisture content such as wood chip is more suitable for chemical conversion processes i.e. pyrolysis, combustion and gasification. Moisture content in biomass thermal conversion processes is critical to avoid an additional energy penalty in removal of excess moisture.

The calorific value or heating value of the sample represents the energy content that is released when samples are combusted under air atmosphere [34]. It can be measured as energy released per unit mass for solids, MJ/kg, for liquids, MJ/l and for gases, it is expressed as MJ/Nm<sup>3</sup>. The calorific value is further divided into lower heating value (LHV<sub>gas</sub>) and higher heating value (HHV<sub>gas</sub>). The LHV<sub>gas</sub> refers to the energy content without taking into account the latent heat of water vapors present in the gaseous product when sample is burned in air. Conversely, the HHV<sub>gas</sub> defines the total energy content with the latent heat of water vapors in the product gas. Thus HHV<sub>gas</sub> is higher than LHV<sub>gas</sub> due to difference in latent heat of water vapors [38].

The volatiles matter or volatiles content present in biomass is mass released as gas when heating biomass in inert atmosphere at high temperature of 950°C for 7 min [38]. The mass remaining after removing volatiles, excluding ash and moisture content is fixed carbon (FC). The ash content or ash residual is the solid residue after complete burning of biomass. The primary constituent of ash is Si, Al, Ca, K, Na, Mg and Ti (titanium). The alkali metals content Na, K, Mg and Ca present in biomass are important for thermal conversion processes. The alkali metals react with Si present in ash generates a sticky liquid phase which creates operational problem in the downstream equipments and pipes [34].

Biomass analysis that includes moisture content, volatiles matter, fixed carbon and ash is known as proximate analysis. Proximate analysis helps to choose a suitable gasifier for biomass thermochemical conversion processes. Typically, biomass with low volatiles matter is more suitable for partial oxidation gasification [39]. The

ultimate or elemental analysis of biomass includes; carbon (C), hydrogen (H) and oxygen (O) with small amount of N and S. Biomass ultimate and proximate properties are imperative tools for selection of the fuel in the gasification processes. Furthermore, these analyses are also helpful to choose a suitable energy conversion route to an individual biomass.

The atomic ratio is important classification of the fuel to understand product gas heating values. The atomic ratio in the fuel is based on the hydrogen, carbon and oxygen content. These ratios are represented as O:C and H:C values and can be explained by the help of van Krevelen diagram (Figure 2.4). Biomass with higher O:C and H:C ratios has low heating values (or energy content) [40]. Higher oxygen and hydrogen proportion reduces the energy content due to low energy associated with carbon-oxygen and carbon-hydrogen bonds, than in carbon-carbon bonds.

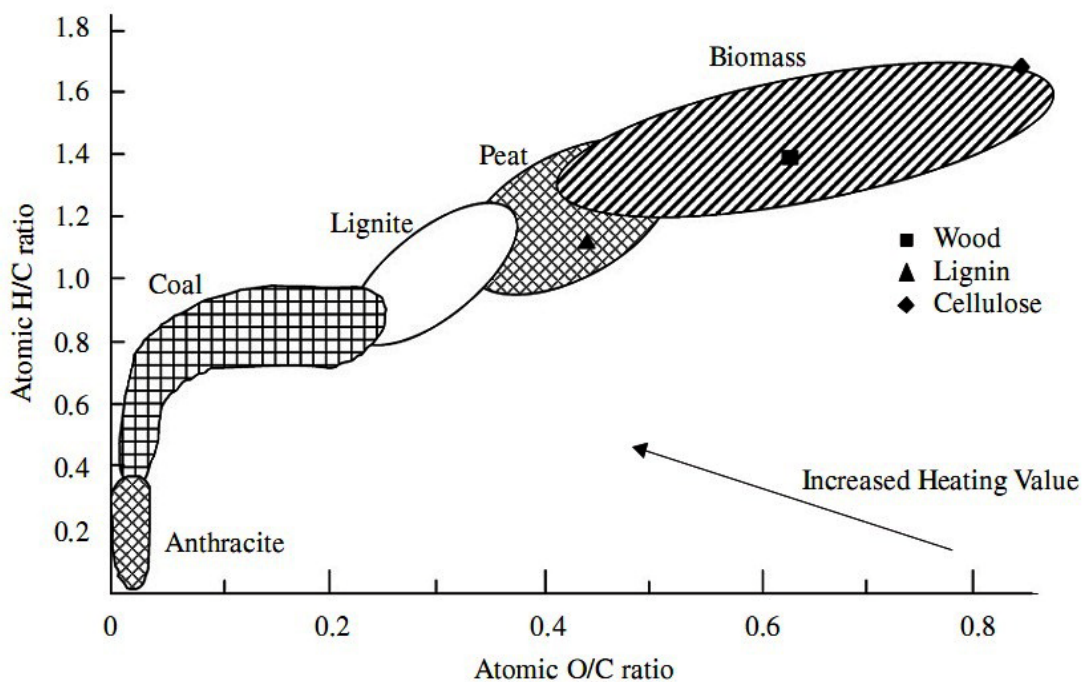


Figure 2.4: Van Krevelen diagram for classification of various solid fuels [40]

### 2.4.2 Biomass Selection for Gasification Process

To illustrate the selection of biomass for gasification processes, carbon-hydrogen-oxygen (C-H-O) diagram known as ternary diagram is considered. Ternary diagram

has triangular shape with C, H and O on each corner as shown in Figure 2.5. Slow pyrolysis (P) inclined towards carbon corner and thus produces more solid char. Fast pyrolysis (F) is moving towards hydrogen and moving away from oxygen corner shows high liquid product i.e.  $C_2H_4$ . Gasification with oxygen produces more  $CO_2$  and CO gases. Steam gasification (S) is moving away from carbon corner and moves towards hydrogen as gaseous product. The diagram clearly shows that the biomass with steam gasification is able to produce more hydrogen, less CO,  $CO_2$  and  $CH_4$ .

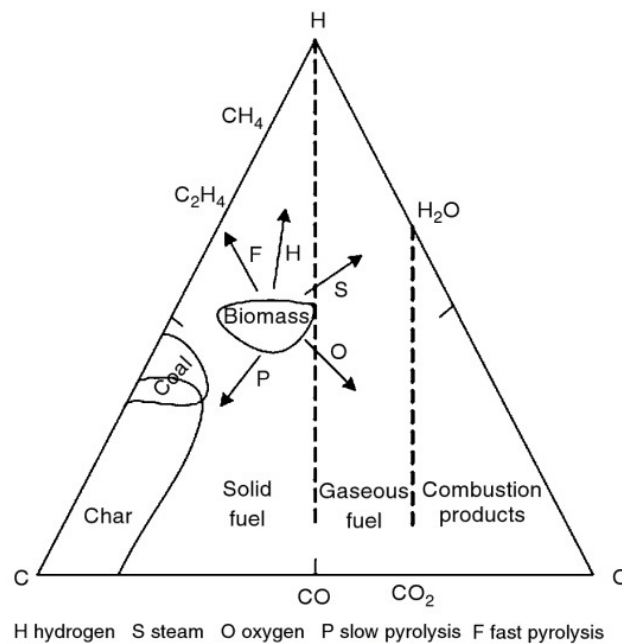


Figure 2.5: C-H-O ternary diagram for biomass gasification process [38]

Abdullah and Yusup [41] studied the screening of Malaysian biomass through aggregated matrix for hydrogen production via gasification. The study was carried out based on the biomass properties i.e. calorific value, moisture content, fixed carbon, volatile matter and ash content. The biomass was sorted based on the scoring from most preferred to least preferred. The results showed that three biomass, palm kernel shell, sawdust and coconut shell have the highest potential to be the feedstock for hydrogen production via gasification (Table 2.1). The three biomass samples have high calorific value, fixed carbon, volatiles matter, and low O:C and H:C ratios, ash and moisture content. Based on these properties, palm kernel shell, sawdust, and coconut shell are able to produce hydrogen with high calorific value, high combustion efficiency and avoid problems such as slugging, bridging and rusting which can lead

to additional operational cost [41]. Amongst the oil palm waste in Malaysia for hydrogen production, palm kernel shell can provide better choice for hydrogen production via gasification process due to high proportion of fixed carbon, volatile matter, and low content of ash and moisture [41].

Table 2.1: Ranking of Malaysian agricultural biomass for gasification [41]

Biomass	Characteristics					
	Calorific value	O:C and H:C ratio	Moisture content	Ash	Fixed carbon and volatiles	Total score
Empty fruit bunch	2	2	0	1	3	8
Mesocarp fibre	2	2	1	1	3	9
Palm kernel shell	3	2	2	2	3	12
Oil palm fronds	2	2	0	2	3	9
Rubber seed kernel	2	2	2	1	3	10
Sawdust	3	2	2	2	3	12
Sugarcane residue	2	2	0	2	3	9
Rice husk	2	2	2	0	3	9
Paddy straw	2	1	3	0	3	9
Coconut fibre	2	2	2	1	3	10
Coconut shell	3	2	2	2	3	12

## 2.5 Catalyst for Biomass Steam Gasification

The catalyst application in biomass steam gasification has proven to be effective to enhance hydrogen yield and to reduce tar content in the product gas. The catalyst can be used either as bed catalyst or downstream catalyst, and exploited by many research studies [17, 42-44]. The utilization of in-bed catalyst is more preferred due to the reduce cost for downstream equipment as compared to the downstream catalyst. The catalyst in biomass gasification should capable to enhance the desired product i.e.

hydrogen, effective in tar removing, should be able to be regenerated, should be capable to resist the deactivation, sintering and fouling, ease of regeneration and should be strong and inexpensive. The catalyst can be divided into nickel based catalysts, olivine, dolomite and metal catalysts [26].

### **2.5.1 Nickel Based Catalysts**

Nickel (Ni) is the most widely used catalyst in steam reforming and dry reforming industry. There is a large number of works reported on the application of these commercial catalysts in biomass gasification [26]. At temperature above 740°C, in steam methane reforming, the use of Ni catalyst generates high hydrogen and carbon monoxide, and reduces high hydrocarbon and methane concentration in the product gas. Furthermore, commercial reforming Ni catalyst shows 8-10 times more reactivity than calcined dolomite [45].

However, several deactivation mechanisms in biomass gasification have been identified using Ni based catalyst. These problems include; poisoning of the catalyst by sulfur, chlorine and alkali metals present as an intrinsic material in the biomass, sintering of Ni particles, coke formation on the surface of catalyst due to char deposition, and catalyst attrition [46]. Several studies [16, 42, 47, 48] are available on the effectiveness and problems occurring with Ni based catalyst in biomass gasification for hydrogen production.

Aznar et al. [42] studied the effectiveness of steam reforming using R67 (Ni/Mg/Al<sub>2</sub>O<sub>3</sub>) catalyst. The catalyst performance was studied in the downstream reformer reactor at a temperature of 720-760°C. A tar conversion of 99.95% was successfully achieved, and tar and methane content in the product gas was lowered below 5 mg/Nm<sup>3</sup>. However, the catalyst faced deactivation due to excess tar coming from primary reactor (fluidized bed gasifier) with operational life of a few hours. The main reason of deactivation was coke formation from tar cracking reaction. Maximum hydrogen content at the exit of the downstream reformer was reported to be 54 vol%. To cope with coking resistance and maximizing hydrogen content, few works [47, 48] have been reported on impregnate Ni catalyst with dolomite and olivine.

### **2.5.2 Dolomite, Olivine and Metal Catalysts**

Dolomite is a magnesium ore with chemical formula of  $MgCO_3 \cdot CaCO_3$ . Dolomite has received much attention in biomass gasification because it is cheap and disposable. Furthermore, some studies [25, 43] showed that the dolomite has excellent capabilities of reducing tar content in the product gas. Wei et al. [43] studied the activity of limestone, olivine and dolomite as catalysts at 750-850°C in free fall reactor with a short residence time. They concluded that even with short residence time, dolomite increased  $H_2$  yield to 45 mol%, and reduced tar content up to 10 g/kg biomass. Hu et al. [25] tested steam gasification with apricot as the feedstock and olivine and dolomite as the downstream catalyst for hydrogen rich gas production in fixed bed reactor. The study showed that the calcined catalyst had good activity as compared to the natural catalyst. The calcined olivine catalyst had much better mechanical strength after calcinations reaction whereas calcined dolomite became fragile after calcination. However, dolomite produced higher  $H_2$  yield compared to olivine.

The alkali metals are highly reactive metals. These metals exist in biomass in lesser extent in the form of ash specially Na and K. However, the major drawbacks of these ash based catalysts are their loss in activity due to agglomeration inside the gasifier. Sutton et al. [26] reviewed alkali metals and reported several disadvantages of using these metals directly into the gasifier which creates problems of disposing, increasing mass of char inside the reactor and exhibiting difficulties to recover the expansive catalysts. Lee et al. [49] observed that the addition of  $N_2CO_3$  to rice straw in steam catalytic gasification over Ni catalyst enhanced the production of permanent gases. Furthermore, the activity of the tested alkali metals based on formation of permanent gases follows the reactivity order as  $Na \geq K > Cs > Li$ .

### **2.6 Adsorbent for In-situ $CO_2$ Capturing in Biomass Gasification**

$CO_2$  separation from other light gases is a topic of great concern due to serious environmental issues related to the rising  $CO_2$  concentration in the atmosphere. Since the time of industrial revolution, the  $CO_2$  concentration in atmosphere has increased

to 35% of its current level of 380 ppm and it will be still rising if the sources of CO<sub>2</sub> generation remained unchecked [50].

Based on the separation of CO<sub>2</sub> in industrial application, CO<sub>2</sub> capturing system can be divided into post combustion and pre-combustion or in-situ CO<sub>2</sub> capturing system. Post combustion refers to coal gasification system where downstream equipment is installed to capture CO<sub>2</sub> from the product gas. Pre-combustion finds its application in steam methane reforming and biomass gasification process to remove CO<sub>2</sub> from the product gas. For steam methane reforming, carbon is eliminated from methane prior injection to the reformer. In utilizing biomass as the feed stock for syngas and hydrogen production, in-situ CO<sub>2</sub> separation technology becomes more valuable for the large scale application. In biomass gasification process, water gas shift reaction and CO<sub>2</sub> capturing reaction takes place simultaneously. This complex reactions system involves suitable reaction conditions under which various reactions can be carried out. This process condition allows limited material application in in-situ CO<sub>2</sub> biomass gasification. Florin and Harris [21] suggested the following properties for CO<sub>2</sub> adsorbent in biomass gasification system.

- The adsorbent must be highly reactive within temperature range of 550-750°C.
- The adsorbent decomposition or calcination temperature should be greater than gasification temperature, but not too high than 1000°C to avoid the energy penalties in regeneration step.
- The adsorbent particles should be well resistive to attrition, deterioration and sintering problem at gasification temperature.
- The adsorbent particles should be robust and regenerative.
- The adsorbent should be resistive to the by-products of biomass gasification i.e. organic matter.

CaO based adsorbent is significant due to low cost, abundant and can be produced from naturally occurring rocks including limestone, dolomite and calcium hydroxides [21]. A number of attempts have been carried out to produce efficient CO<sub>2</sub> adsorbent material for biomass gasification. Initially, a number of synthetic oxides based adsorbent have been developed for high temperature (550-770°C) CO<sub>2</sub> capture including Li<sub>2</sub>ZrO<sub>3</sub> [51] and Na<sub>2</sub>ZrO<sub>3</sub> [52] showed good capturing capabilities but

proved to be expensive. Additionally, for Lithium (Li) based sorbents to be more economical compared to natural occurring limestone, it should be remained effective for 10,000 reactions cycles [21].

Naturally occurring metal oxides which are abundant in natural rocks proved to be low cost CO<sub>2</sub> adsorbent. However, calcination temperature of these metals carbonates i.e. MgCO<sub>3</sub> (385°C), ZnCO<sub>3</sub> (340°C) and MnCO<sub>3</sub> (440°C) are lower which makes them not suitable for in-situ CO<sub>2</sub> capture in biomass gasification [21]. Among these metal oxides, decomposition temperature for CaCO<sub>3</sub> is 800°C which makes CaO more suitable as a sorbent [53]. Besides, CaO is also extracted from different other sources i.e. eggshell [54] and cockle shell [55] in the form of CaCO<sub>3</sub> which is further calcined and used as a CaO for CO<sub>2</sub> adsorption.

The effectiveness of CaO as CO<sub>2</sub> adsorbent and bed material produced from limestone and calcium hydroxide have been studied extensively. Xu et al. [56] reported that the in-situ CaO reduced the CO<sub>2</sub> level to less than 10 vol% in the product gas at a temperature less than 727°C. It was further reported that the addition of CaO increased the product gas heating value. Fang et al. [41] reported the activity of limestone in fluidized bed reactor and concluded that calcined limestone captured CO<sub>2</sub> with high efficiency but its capacity decreased with successive carbonation/calcination reactions cycles. For calcium hydroxide, Guoxin et al. [57] observed not only good adsorption capacity of calcium hydroxide but also significantly enhanced hydrogen yield. In conclusion, high amount of CaO generated by different natural rock shows good CO<sub>2</sub> adsorption capacity for biomass gasification processes.

## **2.7 Conceptual Process Design Approach**

Conceptual process design is an imperative tool to define the procedures for the evaluation of the new technologies. Because of this technique, it is easy to give the detail process design in short time by a single personnel than the conventional procedure in which process design takes long time and engages several manpower

[58]. For biomass conversion technologies, a number of process designs were evaluated for hydrogen, syngas and methanol production [59].

A process design can be done in a variety of different approaches [60]. Based on hierarchal approach, Douglas et al. [61, 62] divided the complex process design problem into six smaller levels which is much simple to handle. Thus, this provides an easy and time saving approach with fewer efforts to be done for systematic design of complex processes. These six levels will be the focus of discussions in the present work. This procedure is adopted by various researchers for renewable energy production system of biomass gasification process [58, 63].

### **2.7.1 Initial Input Information of Process**

At the start of process design, initial information of raw materials i.e. availability, catalyst, product purity and process reactions should be worked out. The availability of raw material is an important parameter which actually defines the location and scale of the process [58].

Furthermore, the biomass collection and transporting charges is one of the important criteria for the process to be economical. Without this, the main aim of cheap biomass availability will be no longer valid. Biomass gasification processes that utilize catalyst and CO<sub>2</sub> adsorbent require similar strategy on the availability of catalyst and adsorbent. In addition, this level of design helps to define the selection of gasifying agent (air, steam or O<sub>2</sub>) for hydrogen production from biomass gasification.

### **2.7.2 Process Design: Batch versus Continuous**

In the second stage of process design, the mode of the process needs to be defined either batch or continuous. For low volume generating biofuels processes, batch mode can be used while for high volume processes such as hydrogen production from biomass gasification, continues mode is most preferred [58].

### **2.7.3 Process Input-Output Structure**

This stage of the process defines purification system, recycle, purge stream, number of product stream and most important design variables that can bring low cost product possibilities. In most of the biomass gasification technologies, the purification step is the most important due to tar content which restricts the technology from being commercialized. This step brings some additional cost to the process in the form of tar treatment by in-bed catalyst or downstream catalyst in the downstream reactors [26].

### **2.7.4 Reactor Type**

At present level, reactor type and associated recycle streams are defined and added to the process flow sheet. However, the reactor system is only selected here but detail reactor design is not considered in this level. In case of equilibrium reactions, one of the reactant is considered in excess to increase product conversion. However, this excess amount of reactant adds additional heating in the reactor and brings additional cost to the process. For example, biomass gasification technologies with steam as gasifying agent, prefer excess steam to increase hydrogen content but there is a penalty of additional cost of heating in the reactor [64]. Moreover, heating and condensation of the steam reduces the thermal efficiency of the process [65]. Thus amount of this excess reactant should be optimized at the time of deciding operating conditions for the process. Added to the reactor type, more parameters i.e. catalyst type, reactor size, operating conditions (temperature and pressure), phase (homogeneous and heterogeneous) and feed conditions are defined at this stage of process design [66].

### **2.7.5 Separation System**

After the reactor, the separation system is considered to remove vapors, liquid and solid phase from the product gas exiting from the reactor. Typically, biomass gasification technologies include cyclone system to remove solid particles from the product gas stream [67]. In these technologies, the main problem is tar concentration in product gas which requires intense cleaning system in downstream, and introduces

large cost and often defines the feasibility of the whole process. Thus, the design of effective separation system is an important step in the development of biofuels processes that is economically feasible [68]. The additional condensation system needs to be provided to remove water vapors from the product gas. This type of arrangement is used in biomass steam gasification to remove water from the product gas before gas enters the gas analyzing system [42].

### **2.7.6 Heating and Cooling System**

Biofuels systems need considerable attention to cope with the vital cost of heat required to generate energy. Specially, processes operating at high temperature such as combustion and gasification require heat integration for optimum operating conditions. Biomass gasification processes using steam need more attention due to excess heating requirement inside the reactor. Moreover, excess steam leaving the reactor at relatively high temperature which needs heat exchanger to be used to utilize the heat of steam leaving the system. Upadhye et al. [58] proposed that the heat required for decanter and flash column in hemicellulose conversion process could be obtained from the heat carried by the product stream of gasification process.

In conclusion, biomass renewable energy technologies for hydrogen production and syngas generation will be attractive if the system operates with lower production cost. Proper selection of the reactor is important to maximize the process efficiency. Additionally, reduction of utilities cost is also important for upgrading the technology to the commercial scale.

### **2.7.7 Process Design of Biomass Gasification**

Vast literature is reported on the conceptual process design of biomass gasification processes for hydrogen production. Corella et al. [69] developed air gasification system utilizing wood as the feedstock for hydrogen rich gas production. The process comprised of fluidized bed reactor followed by hot filter as a solid separator, guard bed reactor and catalytic reactor utilizing commercial reformer catalyst. The final product gas comprised of 24 vol% H<sub>2</sub>, 27 vol% CO, 8 vol% CO<sub>2</sub>

and 4 vol% CH<sub>4</sub> based on wet basis. Zhang et al. [70] proposed a complex process design to convert switchgrass into hydrogen rich gas through pilot scale air gasification system. The process mainly consisted of fluidized bed gasifier followed by guard bed reactor utilizing dolomite as the bed material to remove trace contaminants and reduce tar content in the product gas. The product gas then passed through the steam reformer utilizing NiO as catalyst followed by low and high temperature water gas shift reactors. The final product gas comprised of 27 vol% H<sub>2</sub>, 27 vol% CO<sub>2</sub> and 2 vol% CH<sub>4</sub> with no CO present. Zabaniotou et al. [71] proposed process design of a bench scale gasification system utilizing agro biomass feedstock. The system comprised of a fluidized bed reactor followed by cyclone separator to remove solids from the product gas. No data of product gas composition was reported for the system.

Based on the literature, it can be concluded that most of the biomass gasification processes presented for hydrogen production have complex system which contains a number of downstream equipments. These downstream equipments raise the overall hydrogen production cost which does not make renewable biomass as a competitive source for hydrogen production.

## **2.8 Biomass Gasification**

Gasification is an attractive thermal conversion process and has higher process efficiency as compared to combustion [72]. Among thermal conversion processes, biomass gasification has been recognized as one of the potential process to produce hydrogen rich gas [15]. Hydrogen production via biomass gasification is a complex process that is influenced by a number of factors; feedstock composition, moisture content, reactor temperature and pressure, amount of oxidant present, gasifier design and mode of gas-solid contact [73]. Kumar et al. [74] reviewed that high temperature, high steam to biomass ratio, equivalence ratio and type of catalyst enhanced hydrogen content in the product gas. However, to understand the effect of all the parameters on hydrogen production from biomass gasification, basic chemistry of all the reactions inside the gasifier needs to be considered.

### 2.8.1 Biomass Gasification: Mechanism and Reactions

Biomass steam gasification is a complex process comprising of several decomposition steps. The basic process steps are shown in Figure 2.6.

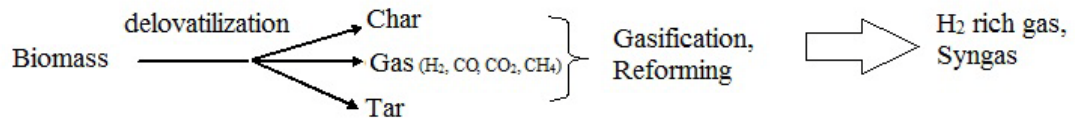


Figure 2.6: Biomass gasification process [75]

#### 2.8.1.1 Drying

Drying is the initial step of biomass gasification inside the gasifier. Once biomass enters the gasifier, it is heated up and drying takes place through water evaporation up to 200°C [76]. Gasification process accepts biomass with moisture content less than 50 wt% to avoid energy penalty in removing excess water in the drying step [6].

#### 2.8.1.2 Devolatilization

Devolatilization is the first thermal decomposition step in biomass gasification. This step occurs slowly at less than 300°C and instantaneously accelerates up to 700°C [77]. Devolatilization process releases water vapors, organic liquids, permanent gases ( $H_2$ ,  $CO$ ,  $CO_2$  and  $CH_4$ ) and char as a solid carbon of biomass.

#### 2.8.1.3 Combustion

Reaction of oxygen with char (solid carbon) is considered to be one of the most important combustion reactions. The products of combustion are mainly  $CO_2$  and  $H_2O$ . Moreover, combustion is an exothermic reaction and provides thermal energy to endothermic gasification reactions in the system.

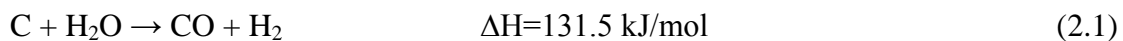
#### 2.8.1.4 Gasification/Reforming

Gasification/reforming include endothermic reactions which utilizes heat generated from combustion reaction. Gasification products mainly consists of H<sub>2</sub>, CO, CO<sub>2</sub> and CH<sub>4</sub> [77]. The important reactions involved in gasification/reforming are discussed in detail in the following section.

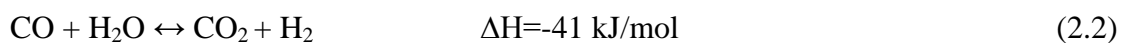
#### 2.8.1.5 Reactions

The type of main reactions involved in gasification/reforming depend on the gasifying agent i.e. air, pure oxygen, steam or in combination. Moreover, the product gas composition also depends on the type of gasifying agent used for gasification. Steam as a sole gasifying agent is more significant because it gives product gas with relatively high hydrogen content. Additionally, it provides product gas of high heating values, and less char and tar content in the product gas due to steam reforming reactions [78]. The following important reactions are considered in biomass steam gasification [79-81]:

Char gasification reaction



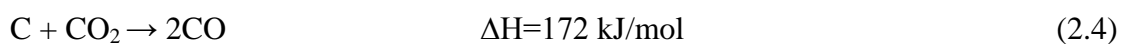
Water gas shift reaction



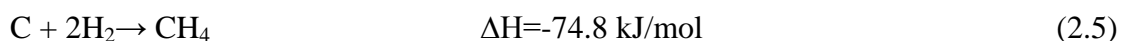
Steam methane reforming



Boudouard reaction



Methanation reaction



Char gasification reaction (Equation 2.1), steam methane reforming (Equation 2.3) and boudouard reaction (Equation 2.4) are endothermic reactions and favor formation of products at high temperature. Water gas shift reaction (Equation 2.2) and methanation reaction (Equation 2.5) are exothermic reactions and low temperature favors generation of the products. However, Walawender et al. [82] reported the

activity of forward water gas shift reaction at temperature above 700°C. They further proposed that the forward reaction was due to the excess steam which increased H<sub>2</sub> content and reduced CO concentration in the product gas as the temperature increased. Similar observation was also reported by Franco et al. [83].

#### 2.8.1.6 Hydrogen Yield and Conversion Efficiencies

Several performance parameters are defined for biomass gasification process for hydrogen production. Yield and conversion efficiencies are most common and important to evaluate the performance of the gasification system. Generally, yield is defined as mass or moles of a product divided by mass or moles of reactant feed [84]. For hydrogen production, most common definition of yield can be written as mass of hydrogen produced over mass of biomass feed [85] which are used by various biomass gasification studies [15, 86]:

$$\text{Hydrogen yield} = \frac{\text{Mass of hydrogen produced (g)}}{\text{Mass of biomass feed (kg)}} \quad (2.6)$$

Kelly-Yong et al. [87] introduced hydrogen yield % for the hot compressed water (HCW) gasification system:

$$\text{Hydrogen yield (\%)} = \frac{\text{Mass of hydrogen produced (kg)}}{\text{Mass of hydrogen in biomass feed (kg)}} \times 100 \quad (2.7)$$

However, the representation is based on hydrogen content in biomass feed. Biomass is mainly consisted of carbon, hydrogen and oxygen. Carbon content in biomass contributes to hydrogen production via char gasification reaction (Equation 2.1) in biomass gasification processes [79, 88]. It is important to consider carbon content to evaluate hydrogen yield in biomass gasification system. Therefore, Equation 2.6 is more appropriate to determine hydrogen yield.

Conversion efficiencies are measure of system performance to convert solid lignocelluloses biomass into gaseous product. Gasification and carbon conversion efficiencies are commonly used to evaluate the system performance. Mahishi et al. [89] reported following definition of carbon conversion efficiency ( $\eta_{cc}$ ):

$$\eta_{cc} (\%) = \frac{\text{Moles of carbon containing gases produced (CO, CH}_4, \text{CO)}}{\text{Moles of total carbon in biomass}} \times 100 \quad (2.8)$$

Similar definitions were reported by Hanaoka et al. [90] for biomass steam gasification with in-situ CO<sub>2</sub> adsorption and Detournay et al. [91] in terms of gasification rate for biomass steam gasification.

Limited literature is available to define the gasification efficiency ( $\eta_g$ ) in biomass gasification process. Kelly-Yong et al. [87] introduced the gasification efficiency according to Equation 2.9. Detournay et al. [91] reported similar equation in terms of gasification ratio:

$$\eta_g (\%) = \frac{\text{Mass of total gas produced (H}_2, \text{CO, CO}_2, \text{CH}_4)(\text{kg})}{\text{Mass of biomass feed (kg)}} \times 100 \quad (2.9)$$

### 2.8.2 Recent Advancement in Biomass Gasification for Hydrogen Production

Gasification technologies offer the opportunities to convert lignocelluloses biomass into clean fuels i.e. hydrogen or synthesis gas (mixture of CO and H<sub>2</sub>). The application of biomass gasification to produce hydrogen is a potential way to implement cleaner application such as fuel cell. Biomass gasification is usually added up by steam and catalyst to improve the product gas composition towards hydrogen rich gas production. More recently, the addition of in-situ CO<sub>2</sub> adsorbent in gasification process makes biomass as a negative CO<sub>2</sub> emitter. Over last couples of decades, considerable efforts have been made to develop biomass gasification processes more attractive to produce hydrogen and syngas for clean fuel application. Aznar et al. [92] investigated the steam-O<sub>2</sub> gasification of biomass and claimed that the hydrogen content of 73 vol% was achieved by using a secondary reforming reactor after fluidized bed gasifier and steam methane reformer. The CO shift reactor was divided into low temperature (LT) and high temperature (HT) shift reactions. Lahijani et al. [93] studied the oil palm empty fruit bunch and saw dust air gasification in pilot scale fluidized bed gasifier to produce syngas. Carbon conversion efficiency of 93% and 85% were reported for empty fruit bunch and sawdust, respectively. However, the operation was affected by agglomeration in the case where empty fruit bunch was subjected to high temperature.

A few studies have been reported for biomass gasification with in-situ CO<sub>2</sub> adsorption. Marquard et al. [27] studied Absorption Enhanced Reforming (AER) for biomass steam gasification with CO<sub>2</sub> capturing in a Fast Inter Circulating Fluidized Bed (FICFB) with internal regeneration system. The system consisted of separate gasification and combustion processes in internally connected fluidized bed reactors. The combustion process used air for regenerating the bed material for gasification process. In this way, the adsorbent material was circulated between the two reactors. The system generated H<sub>2</sub> content of more than 70 mol% in the product gas. Hanaoka et al. [90] introduced a special type of reactor to study the CO<sub>2</sub> adsorption in biomass gasification at high pressure. The reactor was a Tammann tube made of Al<sub>2</sub>O<sub>3</sub> with volume of 0.5×10<sup>4</sup> m<sup>3</sup> and was placed in an autoclave. Wei et al. [94] investigated biomass gasification with CaO as in-situ CO<sub>2</sub> adsorbent in a External Circulating Concurrent Moving Bed (ECCMB) system that was based on similar concept as FICFB. Gasification and combustion processes took place in separate fluidized reactors that were connected internally to circulate the bed materials and char particles. The H<sub>2</sub> composition in the product gas was 60-70 mol%. Koppatz et al. [95] studied the 8 MW Dual Fluidized Bed (DFB) reactor constructed in Guessing, Austria for biomass steam gasification in the presence of CaO. The DFB reactor comprised of gasification and combustion chambers within the same fluidized bed reactor. Steam was introduced into the gasification chamber while air was provided in the combustion chamber. The range of operating temperature for gasification and the combustion processes were 600-700°C and 800-900°C, respectively. The maximum H<sub>2</sub> composition observed was 50 vol%. Pfeifer et al. [96] compared dual fluidized bed steam gasification with and without CO<sub>2</sub> selective transport. The maximum hydrogen content of 75 vol% was reported for CO<sub>2</sub> adsorption process (CO<sub>2</sub> transport) as compared to 40 vol% for dual fluidized bed reactor (without CO<sub>2</sub> transport). Han et al. [86] studied the effect of different process variables; gasification temperature, steam to carbon ratio and adsorbent to carbon ratio. All parameters tested were favorable to enhance hydrogen content in the product gas. It was found that the results were different from those reported in fixed bed reactor which was mainly due to the type of the reactor used. In fixed bed reactor [37], the decrease in hydrogen yield was observed by varying the steam to biomass ratio from 0.83 to 1.58 due to decrease in temperature by excess steam in the reactor. Furthermore, no significant changed was

observed in H<sub>2</sub> composition by varying adsorbent to biomass ratio from 1.0 to 2.0 which was due to long reaction time considered in fixed bed reactor. This long reaction time allowed thermodynamic equilibrium of biomass steam gasification with in-situ CO<sub>2</sub> adsorbent and offered no significance increased in H<sub>2</sub> composition by varying the adsorbent to biomass ratio from 1.0 to 2.0.

Type of gasifier influences the process efficiency and product gas composition. A wide range of gasifier configuration has been developed till date. The gasifier type can be divided into two groups i.e. fixed bed and fluidized bed [97]. The following paragraphs describe the types of gasifier and resulting product gas composition from the gasifier.

#### *2.8.2.1 Fixed Bed Gasifier*

Fixed-bed gasifiers are the oldest, simplest in their operation and construction, and most common reactors for syngas production. Fixed bed can be divided into updraft and downdraft (Figure 2.7). In updraft gasifier, biomass is introduced from the top whereas gasifying agent is injected from the bottom where combustion takes place. In this type of contacting mode, the product gas exits at the top which is the cooler part of the reactor, and thus product gas carries large amount of tar. In downdraft gasifier, biomass and the product gas exiting from the bottom at high temperature (800°C). This type of design produces less tar due to high exit temperature. Typical gas composition by volume are CO (10-15%), H<sub>2</sub> (15-20%), CH<sub>4</sub> (3-5%), CO<sub>2</sub> (10-15%) reported in fixed bed gasifier operations [97].

#### *2.8.2.2 Fluidized Bed Gasifier*

Fluidized bed gasifier has been proven to be the best for combustion and gasification processes with their high flexibility and efficiency. Fluidized bed gasifier is an excellent choice for biomass gasification and has number of advantages over conventional gasifier. It accepts wide variety of biomass, produces high carbon conversion rates and gives uniform temperature distribution in the gasifier [23]. These

types of gasifier accept small feed size compared to the fixed bed gasifier, and capable of handling higher and lower quality fuels [97].

Fluidized bed gasifier is divided into two main classes; bubbling fluidized bed and circulating fluidized bed. In bubbling fluidized bed, gasifying agent passes through the bottom and fluidize the solid inert bed material. This fluidized bed gives uniform temperature distribution throughout the bed. In circulating fluidized bed gasifier, hot inert bed material is circulated between the reactor and cyclone. This circulation helps to remove ash from the system whereas remaining bed material and char particle are recycled to the gasifier as shown in Figure 2.7.

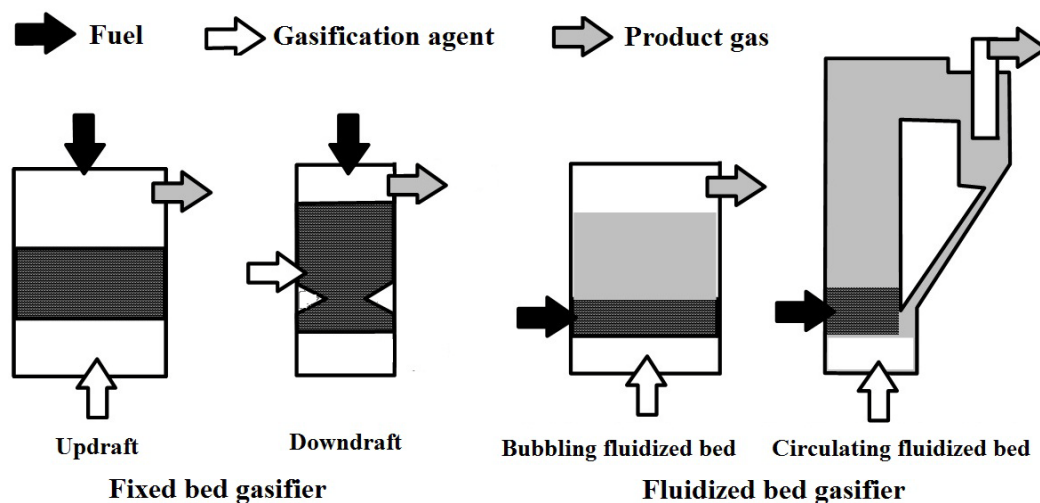


Figure 2.7: Types of gasifier [97, 98]

### 2.8.2.3 Comparison between Fixed Bed and Fluidized Bed Gasifier

Significant comparison between fixed bed and fluidized bed gasifier is shown in Table 2.2. Fluidized bed has good temperature distribution provides good mass and heat transfer between gas and solid phases. The main disadvantage of fixed bed gasifier is uneven temperature distribution which requires long time to heat up, low specific capacity and low potential for scale up.

Based on biomass steam gasification with in-situ CO<sub>2</sub> capture, the application of fluidized bed gasifier is capable to provide high hydrogen yield due to homogeneous

temperature distribution, and high heat and mass transfer between gas and solid phases. Limited studies were carried out in fixed bed reactor to investigate the adsorbent reactivity. However, a previous study [37] reported that the excess steam in fixed bed reactor decreased the hydrogen yield. Excess steam reduced the gasification temperature thus reduced the hydrogen content in the product gas. This effect is significantly reduced in fluidized bed reactor due to high heat transfer coefficients where wide range of steam to biomass ratio can be used without reducing bed temperature.

Table 2.2: Comparison of fixed bed and fluidized bed gasifier [23]

Fixed bed gasifier	Fluidized bed gasifier
(-) Higher investment cost (10%)	(+) Lower investment cost
(-) Hot spot in exothermic reaction	(+) Homogeneous temperature distribution
(-) Agglomeration problem of the feedstock	(+) No fine agglomeration
(-) Need uniform particle size	(+) Broad particle size distribution
(+) Can accept large particle size (up to 100 mm)	(-) Limited particle size (up to 50 mm)
(+) Nearly tar free gas (downdraft gasifier)	(-) High tar content in the gas
(+) High carbon conversion efficiency	(+) High carbon conversion efficiency

(+) advantages (-) disadvantages

#### 2.8.2.4 Biomass Steam Gasification

Biomass steam gasification uses pure steam as compared to other gasification processes which usually utilizes pure air/oxygen or in combination with steam. Potentially, biomass steam gasification has gained high reputation due to hydrogen rich gas production [21].

Steam generates more hydrogen content as compared to air and O<sub>2</sub> as gasification agents. Gil et al. [99] compared the effect of different gasifying agents i.e. air, pure

steam and steam-O<sub>2</sub> mixture on hydrogen yield and concluded that the steam gasification produced 5 times more hydrogen content than air gasification in fluidized bed gasifier. In addition, Ahmed and Gupta et al. [100] observed high hydrogen yield in steam gasification than pyrolysis. It was also reported that the gasification process had an advantage over pyrolysis due to char gasification reaction in the presence of steam.

Many researchers found the significance of water gas shift reaction in biomass steam gasification. This significance is due to the attainment of equilibrium of water gas shift reaction even at short residence time [25]. Franco et al. [83] argued that the water gas shift is more dominant reaction than char gasification (Equation 2.1), steam reforming (Equation 2.3), boudouard reaction (Equation 2.4) and methanation (Equation 2.5) in biomass steam gasification. The study presented by Herguido et al. [101] concluded that the water gas shift reaction attained the equilibrium at high temperature of 750°C and enhanced hydrogen content in the product gas.

#### *2.8.2.5 Biomass Catalytic Steam Gasification*

A number of studies have been carried out to investigate the effect of different types of catalyst on biomass steam gasification. In addition, use of in-bed catalyst and downstream catalyst were also studied in order to elaborate the effectiveness of catalyst location.

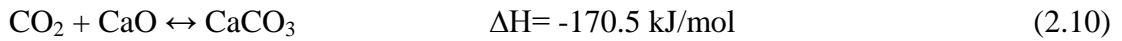
Different catalysts such as Ni, calcined dolomite and limestone have been studied as in-bed as well in the downstream. However, some studies reported the deactivation of Ni as in-bed catalyst for biomass steam gasification [102]. The study further elaborated that the inherent sulfur content present in biomass acted as a poison to the catalyst. To avoid Ni deactivation, Corella et al. [17] used commercial Ni catalyst in downstream reformer reactor followed by two shift reactors for hydrogen production. The study achieved 90% carbon monoxide conversion to hydrogen via water gas shift reaction with hydrogen yield of 140 g/kg biomass. However, such complex system brings additional cost of downstream equipments to the biomass steam gasification system for hydrogen production. Xiao et al. [44] studied two Ni-based catalysts i.e.

Ni/Al<sub>2</sub>O<sub>3</sub> and Ni-loaded brown char in the freeboard of fluidized bed reactor. The authors found that the Ni-loaded brown char provided better resistance against coking with minimum tar content of 2 Nm<sup>3</sup>/kg.

Many researchers have studied the application of natural rock i.e. dolomite, limestone magnacites and calcite as a catalyst in biomass steam gasification for hydrogen production. Such materials are cheap and easy to dispose after use. Delgado et al. [103] used calcined dolomite, limestone and magnacites as downstream catalyst in a fixed bed reactor for cleaning hot gas from fluidized bed gasifier. No serious catalyst deactivation occurred and tar concentration was found to be 48 g/Nm<sup>3</sup> at temperature higher than 800°C. In different study, calcined dolomite as the catalyst was found to enhance hydrogen yield and concentration. Low methane and carbon monoxide concentrations were reported due to the high activity of dolomite catalyst for steam methane reforming and water gas shift reaction.

#### *2.8.2.6 Biomass Steam Gasification with In-situ CO<sub>2</sub> Adsorbent*

Biomass steam gasification with in-situ CO<sub>2</sub> adsorbent makes the process more viable for commercial application. The process commonly known as absorption enhance reforming (AER) or sorption-enhance hydrogen production (SEHP) [57]. The presence of CO<sub>2</sub> adsorbent accelerates all the parallel reforming and gasification reactions toward H<sub>2</sub> production [27]. Furthermore, CO<sub>2</sub> adsorption process is an exothermic reaction thus it provides heat for endothermic gasification reactions and reduces overall energy requirement for the process in the gasifier [27, 104]. Addition of CO<sub>2</sub> adsorbent allows the gasification process to take place at a temperature less than 800°C [27, 56, 90, 104]. Typical hydrogen composition of 40 vol% (dry basis) is achieved in conventional biomass gasification which can be increased to 75 vol% (dry basis) in the presence of CO<sub>2</sub> adsorbent [105]. Previous studies showed that even at low gasification temperature, the tar concentration in the product gas was considerably reduced to a minimum level of 1.5 g/Nm<sup>3</sup> [27]. The CaO adsorbent material indicates tremendous ability towards tar cracking in product gas [17, 103]. The following CO<sub>2</sub> adsorption reaction assists in removing CO<sub>2</sub> in the product gas in biomass steam gasification using in-situ CO<sub>2</sub> adsorbent [106].



The concept of CO<sub>2</sub> capturing process with solid CaO is not new. In 1868, DuMotay and Marechal used lime to produce hydrogen rich gas from steam reforming of hydrocarbons [105]. Later on, Curran et al. [21] developed “CO<sub>2</sub> acceptor process” to produce hydrogen from steam gasification of lignite coal. Sun et al. [107], Gupta and Fan [108] considered CaO to separate CO<sub>2</sub> from coal combustion flue gases. Lin et al. [109] proposed “HYPR-RING” (Hydrogen production by reaction integrated novel gasification) at a very high pressure of 3-12 MPa and at temperature of 600-700°C. The hydrogen concentration produced was higher than 80 vol% (dry basis). For steam methane reforming, Hildenbrand et al. [110] introduced “sorbent enhanced steam reforming (SESR)” using dolomite as a in-situ CO<sub>2</sub> capture for hydrogen production. For synthesis gas, Lee et al. [111] proposed “sorbent enhanced water gas shift (SEWGS)” which was combined with water gas shift to capture CO<sub>2</sub> simultaneously. In addition, several studies were performed to investigate the in situ CO<sub>2</sub> adsorption in biomass steam gasification process to produce hydrogen rich gas.

The application of in-situ CO<sub>2</sub> adsorption in biomass gasification process lowers down the gasification temperature to less than 800°C. The biomass steam gasification with in-situ CO<sub>2</sub> adsorbent process is capable to produce high hydrogen composition with minimum tar content even at low gasification temperature. Marquard et al. [27] observed more than 75 vol% hydrogen concentration in the product gas in in-situ CO<sub>2</sub> capture in fluidized bed gasifier at temperature of 650°C. Similarly, Hanaoka et al. [90] conducted steam gasification in the presence of CaO as CO<sub>2</sub> adsorbent in a pressurized reactor. The maximum hydrogen content of 83 vol% with no CO<sub>2</sub> content in product gas was reported at 6 atm and 700°C. Han et al. [86] studied CaO sorbent enhanced gasification in fluidized bed gasifier. The best temperature range for carbonation reaction was found to be 489-770°C for hydrogen production. Moreover, it was also reported that the water gas shift reaction moved towards product side due to lower partial pressure of CO<sub>2</sub> in the system within the said temperature range. The maximum hydrogen concentration and yield predicted were 62 vol% and 72 g/kg of biomass, respectively, at 740°C.

The application of CO<sub>2</sub> adsorbent in biomass steam gasification brings numerous advantages over conventional biomass gasification. It is possible to operate biomass steam gasification process at lower temperature (500-750°C) which enhances the overall energy efficiency of the process. The previous study [27] showed that even at temperature range of 600-750°C, the tar concentration in the product gas was considerably reduced to a minimum level (1.5 g/Nm<sup>3</sup>). The adsorbent material especially CaO-based indicates tremendous ability towards tar cracking [17, 103]. Moreover, Guoxin and Hao [57] showed that CaO played dual role of catalyst and sorbent that enhanced H<sub>2</sub> production.

#### *2.8.2.7 Gasification of Palm Kernel Shell*

Palm oil waste is considered to be a source of renewable hydrogen especially in Malaysia and Indonesia which produces huge amount of oil palm wastes. Empty fruit bunch, palm kernel shell, fronds, trunks and mesocarp fibers are most abundant oil palm wastes that need to be exploited for renewable hydrogen production. So far, most of biomass gasification studies have been carried out using empty fruit bunch as the feedstocks [88, 93, 112-115]. Very few works have been carried out to study hydrogen production from palm kernel shell (PKS) as the feedstock for gasification process.

For air gasification process, high temperature produces hydrogen rich gas utilizing oil palm waste. Studies reported by Ghani et al. [116] and Moghadam et al. [117] reported hydrogen composition of 67 vol% and 40 vol% at 900°C and 1000°C, respectively.

On the other hand, steam catalytic gasification gives better performance in terms of high hydrogen composition and low tar content at relatively lower temperature than air gasification. Li et al. [15] and Mohamad et al. [118] investigated the steam gasification of oil palm wastes at temperature range of 700°C to 800°C, and reported 54 vol% and 70 vol% hydrogen using Ni-based catalyst. In addition, study reported by Li et al. [15] observed minimum tar content of 2.11 g/Nm<sup>3</sup> using the tri-metallic

catalyst. Moreover, it was observed that the high temperature favored hydrogen yield but it reduced lower heating value of the product gas.

Based on the literature, most of the works have been done for palm kernel shell under air gasification which usually operates at high temperatures as compared to the steam gasification process with in-situ CO<sub>2</sub> adsorbent. Furthermore, even at high temperature, air gasification does not able to produce high hydrogen content in the product gas. In the present study, ICA steam gasification utilizing PKS may contribute high hydrogen content with minimum CO<sub>2</sub> in the product gas.

## **2.9 Effect of Process Variables on Hydrogen Production**

Generally, it is important to determine the important process parameters that affect the hydrogen composition and yield in the gasification process. Present discussions consider the most significant parameters and their optimum range in steam, catalytic and in situ CO<sub>2</sub> biomass gasification processes that are capable to enhance hydrogen content in the product gas.

### **2.9.1 Effect of Temperature**

Temperature is considered to be the most important parameter that influences the product gas composition. By increasing temperature, biomass conversion into gaseous product is increased. This statement can be supported by the existence of endothermic reactions i.e. char gasification, steam methane reforming and boudouard reaction in biomass steam gasification. As temperature increases, char gasification reaction moves towards product side and generates CO and H<sub>2</sub>. Furthermore, tar cracking and reforming are endothermic reactions and enhance gas yield at high temperature [119]. By choosing suitable reactor temperature for enhancing hydrogen production, Florin and Harris [21] proposed that there must be a balance between kinetic and thermodynamic limitations among exothermic and endothermic reactions taking part in steam gasification process. They further stated that the suitable selection of reactor

temperature requires a balance between maximum available hydrogen yield and conversion of char to gas.

For steam gasification, Boating et al. [120] studied the effect of temperature over the range of 700-800°C in fluidized bed gasifier for rice hull. The total gas yield in the product gas increased with increasing temperature. However, decreased in carbon monoxide over the temperature range was reported due to reactivity of water gas shift reaction. Similar observations were also observed by Wei et al. [43] over a temperature range of 750-850°C. Furthermore, they reported decrease in tar and char yield with increasing temperature. This decrease in tar and char yield was observed due to the endothermic nature of tar cracking, reforming and char gasification reactions.

In catalytic steam gasification, Xiao et al. [121] observed increase of hydrogen composition, yield and carbon conversion efficiency with increasing temperature using Ni-Al<sub>2</sub>O<sub>3</sub> catalyst in fluidized bed gasifier. However, in biomass steam gasification with in-situ CO<sub>2</sub> capturing, carbonation reaction with metal oxide (CaO) affects the reactor temperature due to the limitation of the reverse carbonation reaction (reverse reaction, Equation 2.10). Xu et al. [56] studied the limitation of gasification reactor temperature with in-situ CO<sub>2</sub> adsorbent in atmospheric fluidized bed reactor and observed that the temperature should not be higher than 700°C to get maximum hydrogen content in the product gas. They further noticed that the decreased of hydrogen and CO<sub>2</sub> content in the product gas at temperature higher than 800°C was due to the decomposition reaction of CaCO<sub>3</sub>.

The optimum operating temperature for in-situ CO<sub>2</sub> adsorption based on the partial pressure of CO<sub>2</sub> in the system have been discussed by many researchers. Florin and Harris [53] explained the reaction between CO<sub>2</sub> and CaO based on the partial pressure of CO<sub>2</sub> against reactor temperature as shown in Figure 2.8. The driving force for CO<sub>2</sub> to be captured is the difference between the partial pressure of the CO<sub>2</sub> in the product gas and equilibrium partial pressure of CO<sub>2</sub>. According to the observation, low temperature favors effective CO<sub>2</sub> capturing via CaO adsorbent. In order to keep the effectiveness of CO<sub>2</sub> capturing at high temperature, high pressure process needs to be considered. Han et al. [86] investigated the CaO conversion to CaCO<sub>3</sub> at CO<sub>2</sub>

partial pressure of 0.1 atm (0.1 bar) in temperature range of 100-900°C (Figure 2.9). The study showed three stages with rise in temperature; slow carbonation, fast carbonation and CaCO<sub>3</sub> calcination. The favorable temperature for effective CO<sub>2</sub> capturing was in the range of 480-770°C (at CO<sub>2</sub> partial pressure of 0.1 atm).

It can be concluded that the biomass steam gasification with in-situ CO<sub>2</sub> adsorbent needs to be operated at lower temperature (500-770°C) for enrich hydrogen gas production in atmospheric fluidized bed gasifier.

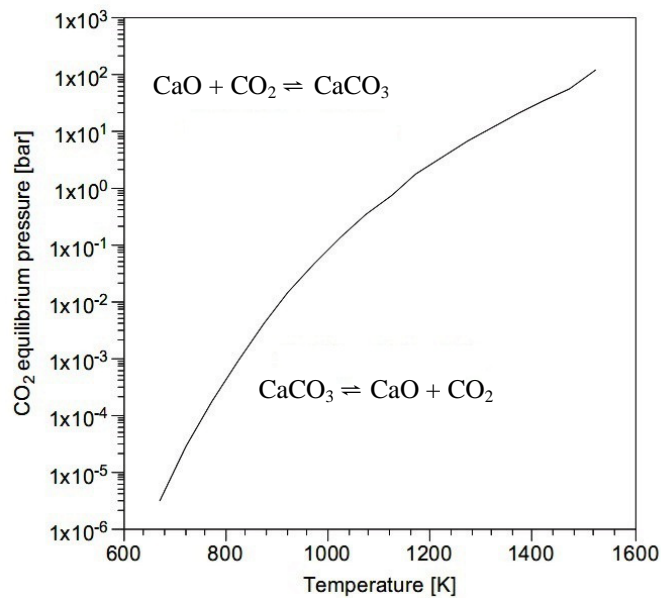


Figure 2.8: The equilibrium CO<sub>2</sub> partial pressure as a function of temperature [53]

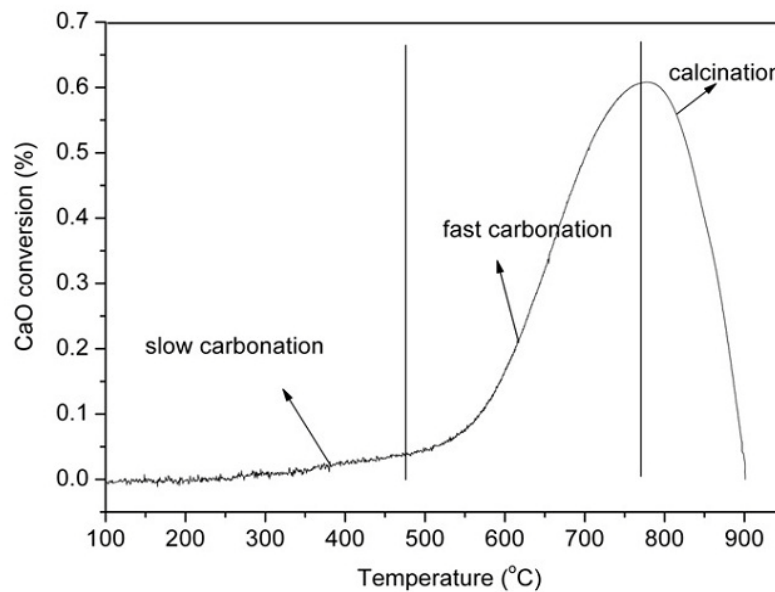


Figure 2.9: CaO conversion characteristics at 0.1 atm CO<sub>2</sub> partial pressure [86]

### 2.9.2 Effect of Steam to Biomass Ratio

For steam gasification, by increasing amount of steam eventually increases the hydrogen content via char gasification, water gas shift reaction and steam methane reforming. Furthermore, steam also enhances the hydrocarbon reactions to produce good quality hydrogen rich gas.

The influence of steam to biomass ration on biomass steam gasification has been reported by many researchers. Herguido et al. [101] and Turn et al. [122] both observed an increase in hydrogen and carbon dioxide composition, and decreased in carbon monoxide, methane and high hydrocarbons in fluidized bed gasifier. This observation explained high activity of water gas shift reaction, methane steam reforming and tar cracking reaction under excess steam. Moreover, amount of char decreased with increasing steam was due to high activity of char gasification reaction [101]. However, the rate of hydrogen increased was slower at high steam to biomass ratio (higher than 2.0).

For catalytic steam gasification, Xiao et al. [44] observed similar results at varying steam to carbon ratio of 0 to 3.0 (mol/mol) as presented by Herguido et al. [101] for steam gasification. Garcia et al. [123] noticed positive effect of increasing steam to biomass ratio on the Ni-Al catalyst operation life. Moreover, influence of steam to biomass ratio was more dominant in the range of 0 to 1.5 wt/wt.

The effect of steam to biomass ratio in biomass gasification with in-situ CO<sub>2</sub> adsorbent is studied by several researchers. Acharya et al. [37] reported continuous decrease in total gas and hydrogen yield by increasing steam to biomass ratio at 670°C. The authors further suggested that the excess steam in fixed bed reactor lowered down the reactor temperature which reduced overall gas yield in the process. Conversely, effect of steam to biomass ratio behaves differently in fluidized bed. Han et al. [86] studied the steam to biomass (carbon) ratio of 1.2-2.18 (mol/mol) at 740°C in fluidized bed gasifier. The hydrogen composition and yield increased with increasing steam to biomass ratio. However, highest increased in hydrogen concentration was observed at steam to biomass ratio of 1.7 (mol/mol) while slow increase was reported at higher steam to biomass ratio.

High steam feed rate to the gasifier is expected to increase overall hydrogen content in the product gas. Nevertheless, there is a significant waste of energy associated with excess steam that lowers the thermal efficiency of the gasification process [65]. For this, steam to biomass ratio may need significant attention to be optimized. Based on previous studies [44, 101], the optimum value may range from 1.0 to 2.0 wt/wt.

### **2.9.3 Effect of Adsorbent to Biomass Ratio**

The introduction of in situ CO<sub>2</sub> adsorbent in biomass steam gasification provides more viable way to produce hydrogen [21, 27, 56]. The addition of CO<sub>2</sub> adsorbent in biomass steam gasification almost doubles the hydrogen yield in the product gas. Weerachanchai et al. [106] observed almost 66% increase in hydrogen content at 650°C when compared the results with and without CaO in steam gasification of larch wood in fluidized bed gasifier. Similarly, Xu et al. [56] reported 78% (based on vol%) increase in hydrogen composition in product gas at operating temperature of 722°C. Few works have been reported the effect of adsorbent to biomass ratio on hydrogen production. Initially, Acharya et al. [37] varied the adsorbent to biomass ratio of 0.0-2.0 (wt/wt) to investigate the product gas composition at 670°C. The hydrogen content increased up to 54% at 0.0 to 1.0 (wt/wt) of adsorbent to biomass ratio while only 9% increase was observed by varying the ratio from 1.0-2.0 (wt/wt). In fluidized bed gasifier, Han et al. [86] studied variation in product gas composition in fluidized bed gasifier at adsorbent to biomass (carbon) ratio (mol/mol) of 0.0-2.0 at 740°C. The hydrogen content was continuously increased and became almost double as compared to the absence of CaO. This constant increased in hydrogen content was due to the large surface area provided by CO<sub>2</sub> adsorbent in the case of high adsorbent to biomass ratio.

In conclusion, the optimum value of the adsorbent to biomass ratio reported [37] was 1.0 in fixed bed reactor as no significant change was observed by further increase in the ratio. However, in fluidized bed reactor, adsorbent to biomass ratio higher than unity helped to reduce significant CO<sub>2</sub> content and enhanced hydrogen composition in the product gas [86].

#### 2.9.4 Effect of Fluidization Velocity

The fluidization velocity or gas superficial velocity is an important parameter to ensure stable fluidization inside the bed. In the bubbling fluidized bed, any excess of gas velocity that exceeds the minimum fluidization velocity passes through in the form of bubbles [38]. Initially, Raman et al. [124] studied the effect of fluidization velocity in the range of 0.31 to 0.37 m/s on feedlot manure gasification in fluidized bed gasifier. They found that the tested range of gas velocities had no effect on product gas composition, yield and gas heating values. Corella et al. [125] studied the steam gasification of sawdust in a fluidized bed with downstream vessels. The effect of fluidizing velocity was conducted in the order of 2-5 times of minimum fluidization velocity which was 0.1-0.25 m/s. At velocity of 0.12 m/s, it was found that the char was segregated in the upper part of the bed. At velocity range of 0.15-0.21 m/s, no influence on product gas distribution, char and tar yield was observed. Later on, Shen et al. [78] conducted experiments to study biomass mixing in two dimensional fluidized bed gasifier. The results showed that there was high degree of biomass mixing found in vertical direction of the bed whereas relatively limited mixing was observed in the horizontal directions. Additionally, at low gas velocity, more uniform distribution was found in the bottom of the bed as compared to the top of the bed. Conversely, at high gas velocity, biomass distribution increased at the top of the bed whereas the distribution decreased in the bottom region.

For oil palm wastes, Ghani et al. [116] investigated the effect of fluidization velocity for oil palm kernel shell and coconut shell on hydrogen production in air gasified fluidize bed reactor. For palm kernel shell, the hydrogen content in the product was constantly increased in the range of 2.0-3.3 m/s whereas no effect was observed for coconut shell in the range of 2.2-2.8 m/s. For both biomass wastes, the CO<sub>2</sub> content increased with rising gas velocity due to rapid exothermic reaction in the presence of large amount of air available for the combustion reaction.

Based on the discussion made, the fluidization velocity has different affect depending upon gasifying agent. In addition, it also depends on type of feed to be gasified. However, these reported works [78, 116, 124, 125] were based on the inert

bed materials and further investigation is necessary for the beds containing reactive material such as CaO.

### **2.9.5 Effect of Biomass Particle Size**

It is a well known fact that the product gas composition and yield depends on the heating rate of biomass particles. High heating rates help to produce high amount of light gases with low tar and char [126]. Small particle has large surface area and therefore exhibits faster heating rates. So it can be expected that the particle size may affect the final product gas composition and yield.

The effect of biomass particle size on product gas composition, hydrogen yield and gas yield is studied by the previous researchers in biomass gasification. Rapagna et al. [102] observed that the lower biomass particle size (0.3 mm) produced more hydrogen and gas yield as compared to the large particle size (1.0 mm) at temperature range of 600-750°C in fluidized bed gasifier. However, the authors found no significance effect of biomass particle size at high temperature (800°C) due to high heating rates which reduced overall heat transfer resistance in large particles. Guo et al. [127] found that the particle size of less than 1.0 mm exhibited reaction kinetics as the controlling step for biomass decomposition. For large particles, the decomposition was actually controlled by the reaction kinetics and heat transfer thus produced lower conversion rate. Similar observations were reported by Li et al. [15] for steam catalytic gasification and Mohammed et al. [113] for air gasification using oil palm waste as the feedstock. In addition, Mohammed et al. [113] found that the larger biomass particle size exhibited high temperature gradient between the core and its surface which resulted in low gas yield and high char yield in the fluidized bed gasification system.

In conclusion, particle size has a measurable effect on the product gas composition. Smaller biomass particles produce more hydrogen and carbon dioxide than methane and carbon monoxide in the product gas for biomass gasification. It would be interesting to observe the effect of particle size on product gas distribution

in in-situ catalyst and adsorbent steam gasification utilizing palm kernel shell which is not reported to date.

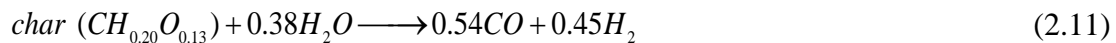
## 2.10 Kinetic Study of Biomass Steam Gasification for Hydrogen Production

Biomass gasification is a mixture of complex reactions. Numerous models are available to simulate biomass gasification reactions. These models are based on the different aspects of the process such as kinetic, equilibrium and hydrodynamics of different type of reactors [76]. The modeling approaches for biomass gasification can be divided into kinetic modeling and equilibrium modeling [128].

### 2.10.1 Kinetic Modeling

A kinetic model predicts the product gas composition and gas yield based on reaction kinetics of main reactions involved in the process. At given operating conditions, kinetic model is capable to predict product gas profiles and overall gasification efficiency of the process. Several kinetic models have been reported for biomass gasification using mixture of air and steam as gasifying agent.

Corella and Sanz [129] developed a reaction kinetic model considering pyrolysis and gasification processes in circulating fluidized bed reactor. The kinetic parameters used were both from their own kinetic experiments and published equations from the literature [130-132]. The model considered several reactions; fast pyrolysis, oxidation, char gasification, water gas shift, steam methane reforming and tar reforming. The char gasification reaction is represented by:



The kinetic constants for char gasification was taken from literature [130] as represented by:

$$r_{char} = k_{char} C_{char} C_{H_2O} \quad k_c = 2.0 \times 10^5 \exp\left(\frac{-6000}{T}\right) \quad (2.12)$$

Lü et al. [133] produced air-steam gasification model in fluidized bed reactor assuming instantaneous devolatilization, steady state condition and uniform temperature inside the reactor. The effect of temperature and equivalence ratio (ER) were studied on product gas composition considering oxidation reaction of char and carbon monoxide, char gasification, methanation reaction, boudouard reaction, water gas shift and steam methane reforming reactions, given by:



The kinetic parameters were taken from the literature [134-136]. The model was validated with experimental data based on published work for pine sawdust gasification. The equilibrium constant for water gas shift reaction was taken from literature [135]:

$$K_w = \frac{k_4}{k_5} = 0.0265 \times \exp\left(\frac{3955.7}{T}\right) \quad (2.21)$$

Very limited literature is available for the kinetic modeling using pure steam as gasification agent. Ji et al. [137] considered kinetic model for biomass steam gasification. The fluidized bed gasifier along with downstream steam methane reformer and H<sub>2</sub> membrane water gas shift reactor were considered for hydrogen rich gas production and high CO<sub>2</sub> generation. Nine reactions had been considered in all reactors. The rate of reactions for all reactions was solved using kinetics data from the literature [132, 138, 139]. Furthermore, the model was validated by experimental data

adopted from the literature [101]. The rate of water shift reaction was selected from literature [139] as given:

$$r_w = 2.78 \times 10^6 \exp\left(\frac{-1510}{T}\right) \left(y_{CO} y_{H_2O} - \frac{y_{CO_2} y_{H_2}}{K_{eq}}\right) C_{mol}^2 \quad K_{eq} = 0.0265 \times 10^5 \exp\left(\frac{3968}{T}\right) \quad (2.22)$$

The effect of temperature and steam/biomass ratio had been studied on hydrogen purity and yield. The hydrogen purity was predicted to be more than 60 mol% at 750°C and steam/biomass ratio of 3.0. Lower heating value of the product gas decreased by raising the temperature and steam/biomass ratio due to increased in hydrogen composition in the product gas. Salaices [140] investigated the reaction kinetic model for catalytic steam gasification of biomass in fluidized bed reactor using surrogates as model compounds. The kinetics model was based on the coherent reaction engineering approach. The reaction rates were based on the dominant reactions i.e. water gas shift (WGS), steam reforming (SR) and dry methane reforming (DRM), and reactions like methanation and boudouard were neglected. The rate of each species was calculated by:

$$r_i = \sum r_{ij} = r_{WRG} + r_{SR} + r_{DRM} \quad (2.23)$$

MATLAB was used as a tool to solve the kinetic model. The effect of temperature and steam/biomass ratio was investigated on hydrogen content in the product gas.

### 2.10.2 Equilibrium Modeling

Equilibrium models are based on reactions equilibrium which provides the highest amount of hydrogen in the product gas. Though chemical equilibrium may not be reached in the actual gasifier, this approach gives maximum achievable gas yield and composition with reasonable predictions.

Extensive studies have been carried out to investigate the biomass gasification using equilibrium model approach. Shen et al. [141] proposed equilibrium model for interconnected fluidized bed system for hydrogen production via steam gasification using straw biomass. The main reactions considered in the gasifier were char gasification, boudouard, methanation, water gas shift and steam reforming. The model was developed in ASPEN PLUS software under steady state condition with inert ash

in the system. Li and Suzuki [142] studied hydrogen rich gas from biomass using pyrolysis and steam gasification. The concept was based on pyrolysis reactor connected with a gas reactor which was further connected with oil cracker and gasifier. A thermodynamic model was presented to investigate the effect of temperature and steam/biomass ratio on product gas composition using Gibbs free energy minimization approach. Detournay et al. [91] studied the biomass steam gasification with reactive and inert bed material using equilibrium model in fluidized bed gasifier. The bed materials considered were silica sand, alumina and alumina impregnated with Ni. The equilibrium model calculation was simulated in HSC chemistry 5.1 software based on Gibbs Energy MINimization (GEMINI code). The results showed that the equilibrium was far away from the experimental results obtained for inert bed material i.e. sand. On the other hand, results with reactive bed material (alumina/Ni) allowed the system to reach equilibrium.

### **2.10.3 Kinetic Modeling with In-situ CO<sub>2</sub> Adsorption**

Limited studies have been conducted on the modeling and simulation of hydrogen production via biomass steam gasification with in-situ CO<sub>2</sub> capture. Florin and Harris [53] developed a thermodynamic equilibrium model to investigate the effect of fundamental process parameters such as temperature, steam to biomass ratio, adsorbent to biomass ratio and pressure on the hydrogen production from methyl cellulose using concept of gasification and combustion steps in separate reactors. The model was simulated in software package FactSage 5.4.1(EQULB Module) using Gibbs free energy minimization. Maximum hydrogen composition of 83 mol% was predicted at atmospheric pressure, steam to biomass ratio of 1.5 (mol/mol) and adsorbent to biomass ratio of 0.9 (mol/mol). The model prediction was also compared and validated with experimental work taken from the literature [101]. The model results showed that the H<sub>2</sub> composition was increased to 20% by using CaO as an adsorbent compared to the conventional steam gasification process. Pröll and Hofbauer [143] presented thermodynamic equilibrium model for hydrogen rich gas production by selective CO<sub>2</sub> transport in dual fluidized bed system. The CaO/CaCO<sub>3</sub> system was used as bed material for selective CO<sub>2</sub> transport from gasification to the

combustion reactor by carbonation and calcination reactions. The equilibrium model equations were simulated in steady state simulation software (IPSE-pro). The developed model showed that the selective CO<sub>2</sub> transport resulted in high hydrogen content in product gas. Lower temperature gasification helped to increase energy conversion efficiency. Mahishi et al. [104] developed an equilibrium model for biomass steam gasification using CaO as an adsorbent in ASPEN PLUS. Ethanol was taken as the model compound for the steam gasification using Gibbs free energy minimization approach. The model results showed that the CaO had the potential to increase almost 19% hydrogen composition than the conventional gasification process. Additionally, it was found that the sorbent-enhanced gasification not only increased the yield of hydrogen but also lowered down the hydrogen production cost.

Very limited kinetic models have been reported for biomass steam gasification with in-situ CO<sub>2</sub> adsorbent utilizing oil palm wastes. Inayat et al. [85] developed reaction kinetic model for oil palm empty fruit bunch (EFB) to produce hydrogen using sum squared technique in MATLAB. The CO<sub>2</sub> adsorbent reaction along with water gas shift, steam methane reforming, char gasification, methanation and boudouard reactions were considered to simulate the process. The reaction kinetics was taken from the literature [129-132, 144, 145]. The general rate equation is represented:

$$r_i = k_i C_A C_B \quad (2.24)$$

And rate equation for water gas shift was selected from literature [130] as given by:

$$r_{wgs} = k_{wgs} \left( C_{CO} C_{H_2O} + \frac{C_{CO_2} C_{H_2}}{K_w} \right) \quad (2.25)$$

K<sub>w</sub> is the equilibrium constant for water gas shift reaction. The developed kinetic model was used to investigate the effect of temperature and steam to biomass ratio on hydrogen composition, yield and efficiency.

#### 2.10.4 Comparison between Kinetic and Equilibrium Model

Generally, equilibrium models are the best option when the kinetics of the system are unknown in which basic assumption is made related to thermodynamic equilibrium of the system. The disadvantage of this kind of model is the

overestimation of hydrogen and carbon monoxide and underestimation of carbon dioxide concentration [128]. Moreover, Puig-Arnavat et al. [146] discussed that the equilibrium models are reasonable tools for preliminary results, but not feasible for accurate results. The kinetic model gives more accurate predictions as compared to the thermodynamic equilibrium models [147]. Altafini et al. [148] argued that the thermodynamic equilibrium never takes place in the gasification temperature higher than 800°C. The kinetic models are found to be more accurate in estimating product gas compositions at lower temperature range [76].

### 2.10.5 Determination of Kinetic Parameters

The determination of kinetic parameters from experimental data using modeling approach has been presented in few studies [140, 149, 150]. Wang and Kinoshita [150] presented kinetic model for O<sub>2</sub>-steam biomass gasification. The kinetic parameters are computed by minimizing the difference between predicted and experimental results using computer program (SCoP) as given in Equation 2.26 for four main reactions i.e. char gasification (CG), boudouard (B), methanation (M) and methane reforming (MR):

$$\text{Min}(k_{CG}, k_B, k_M, k_{MR}) = \text{Min} \sum_{j=1}^m \sum_{i=1}^N (x_{\text{mod}ij} - x_{\text{exp},ij}) \quad (2.26)$$

The residence time, temperature, pressure, equivalence ratio and moisture had been investigated on the product gas composition. The experimental data was taken from their previous work on O<sub>2</sub>-steam gasification utilizing sawdust as the feedstock [151]. Salaices [140] developed kinetic parameters for catalytic steam gasification. The kinetic constant ( $\vec{k}$ ) for three main reaction; water gas shift, methane reforming and steam reforming were evaluated using their own experimental data by minimizing least squares objective function defined as sum of the squared of the residuals (SSR) between experimental ( $\vec{y}$ ) and modeling ( $\hat{y}$ ) values via optimization toolbox of MATLAB:

$$SSR = \sum_{i=1}^{N_{\text{exp}}} \sum_{j=1}^N \left[ \hat{y} - \vec{y}(t_i, \vec{k}) \right]^T \left[ \hat{y} - \vec{y}(t_i, \vec{k}) \right] \quad (2.27)$$

$N_{\text{exp}}$  represents total number of experiments.

For oil palm wastes, Inayat et al. [149] evaluated kinetic parameters such as activation energy and pre-exponential factor for steam gasification with in-situ CO<sub>2</sub> adsorbent utilizing empty fruit bunch as the feedstock. The kinetic parameters were computed by minimizing the difference between predicted ( $y_m$ ) and experimental ( $y_e$ ) results using least squared error minimization approach in MATLAB represented by Equation 2.28. The experimental data was taken from the literature [15].

$$\text{Residual sum squared (RSS)} = \sum_{i=1}^N \left( \frac{y_e - y_m}{y_e} \right)^2 \quad (2.28)$$

It is concluded that the most of the kinetic models are reported for conventional biomass gasification. On the other hand, equilibrium models are carried out for biomass steam gasification with in-situ CO<sub>2</sub> adsorbent. In addition, only one reaction kinetic model was reported [85, 149] for biomass steam gasification with in-situ CO<sub>2</sub> adsorbent using experimental data [149] and kinetic parameters [85] from the literature. It would be interesting to carry out the kinetic model for biomass steam gasification with in-situ catalyst and adsorbent for kinetic parameters determination using own experimental data.

## 2.11 Process Optimization Study using Design of Experiments

The statistical design of experiments has gained much interest in chemical engineering processes. Experimental designs are performed based on the empirical relationship; in terms of a mathematical model, between one or more measured output responses and a number of input variables [152]. Experimental design and mathematical modelling are important mathematical tools used to optimize a process. Traditional methods of optimization involved changing one independent variable while fixing the others at a certain level [153]. These techniques are developed to allow maximum process information with minimum number of experiments [154]. Experimental design techniques are usually based on empirical model in order to evaluate experimental data and provide optimum process conditions.

### **2.11.1 Response Surface Methodology (RSM)**

Response surface methodology (RSM) is a useful statistical tool for experimental design along with multiple regression analysis to measure the effect of two or more independent variables on dependent variables. The main advantage of RSM is that it requires less number of experimental runs to generate information necessary for a statistically acceptable result. It helps researchers to generate models, assess the effects of several factors and establish optimum conditions for the desired output response variables [155].

RSM is an experimental modelling approach to relate various operating variables and response variables. It provides a systematic experimental strategy for generating and optimizing an empirical model. Therefore, RSM is a collection of mathematical and statistical events that are helpful to model and analyse the problems in which the response is affected by the operating variables. The response surface technique has been extensively used in practical engineering design problems that need to be optimized [156]. This method initiated for the science disciplines in which physical experiments are performed to search the unknown relations for a system between a set of input variables and output variables. RSM is often used in the optimization of industrial processes [157], and is used as basis for developing design of experiments in the present study.

RSM is widely used for optimization studies for biomass gasification. Kelly-Yong et al. [87] conducted optimization study of hydrogen yield from hot compressed water (HCW) gasification of oil palm waste using RSM. In addition, Sahu et al. [158] conducted response surface methodology for the optimization of activated carbon production. Satonsaowapak et al. [159] studied gasifier system identification for biomass power plants using RSM.

### **2.11.2 Central Composite Rotatable Design (CCRD)**

Statistical approaches are commonly used in experimental design to optimize and relate several parameters simultaneously. Generally, these approaches are full factorial, partial factorial and central composite rotatable design (CCRD). A full

factorial design requires at least three levels of individual variables to provide the response model. This technique gives high number of experiments to execute to get the optimization of the desired responses. The second technique, partial factorial design gives less number of experiments than full factorial design. Nevertheless, this technique is applicable in cases where some of the process variables already know to show no effect [160]. Central composite rotatable design gives more information than the three factorial design, requires less experimental runs and has shown considerably good optimization to most of the steady state processes [161].

### **2.11.3 Model Fitting and Statistical Analysis**

In order to test the significance of the experimental data for a particular model; test for regression model, the individual model coefficients and lack of fit are performed in analysis of variance (ANOVA) [162]. The ANOVA provides statistical results that enable researchers to evaluate the suitability of the models [163].

In general, significance of model can be checked using factors that can be ranked based on the F -value or p-value (also known prob. > F). The larger the magnitude of F-value and correspondingly smaller the p-value, the more significant is the corresponding coefficient. The p -values are used as a tool to check the significance of each of the coefficients. For a confidence level of 95 % of variability of responses, p-value should be less than 0.05. For lack of fit, p-values higher than 0.05 shows insignificant contribution of the variables to a particular model.

Similarly, approach of significant and insignificant of individual variables and interaction of two or more variables for a particular response can be explained based on p-values [164]. The interaction of two or more variables can also be explained by 2D or 3D graphs. The 2D graph is also known as contour plot [154].

The precision of the regression model is checked by determination coefficient ( $R^2$ ). But  $R^2$  increases as the number of variables increase, so Adj- $R^2$  is introduced as an additional variable in the model. The high values of these two coefficients show the good relation between independent variables [164].

#### **2.11.4 Optimization of Hydrogen Production**

Several optimization studies have been carried out for hydrogen production [165, 166]. Kelly-yong et al. [87] used response surface methodology with CCRD for optimization of syngas production from hot compressed water using oil palm waste as the feedstock. Fermoso et al. [155] applied face centred composite design (FCCD) based on RSM to assess the combined effect of several operating variables on hydrogen rich gas production in high pressure coal gasification. The response variables were; hydrogen, carbon monoxide, syngas composition, H<sub>2</sub>/CO ratio and carbon conversion efficiency. The results showed that the gasification temperature was the most influential variable. Kusworo et al. [154] used design of experiments to optimize the hydrogen production from partial oxidation of methane using NiO-CoO/MgO as a catalyst. Full factorial design and RSM coupled with central composite design (CCD) was used to optimize the process. In conclusion, optimization study for hydrogen production in ICA steam gasification using design of experiment approach is still lacking.

#### **2.12 Chapter Summary**

Biomass characteristics and its properties as fuel to generate optimum hydrogen are reviewed. Based on the review on different biomass properties, it can be concluded that the palm kernel shell has great potential as feedstock for hydrogen production based on its high volatiles matter, carbon content, and low ash and moisture content. Furthermore, palm kernel shell has the potential to produce hydrogen rich gas with higher calorific values which can improve process efficiency.

Availability of effective catalyst and CO<sub>2</sub> adsorbent are then discussed. Amongst the catalysts used in biomass gasification processes, Ni showed great potential to produce high hydrogen content in the product gas. Different adsorbent have then discussed based on their, cost, calcination temperature (reverse reaction), physical strength and lifetime in the gasification process. CaO from natural rocks shows better performance to be used as in-situ CO<sub>2</sub> adsorbent. However, source of direct CaO is encouraged due to time and energy require for calcination of CaCO<sub>3</sub> to produce CaO.

It is concluded that the most of the works have been done for palm kernel shell under air gasification which usually operated at high temperature as compared to the steam gasification process with in-situ CO<sub>2</sub> adsorbent. Even at high temperature, air gasification is not able to produce high hydrogen content in the product gas. Thus, the present study utilizes the palm kernel shell steam gasification with in-situ catalyst and adsorbent in fluidized bed gasifier. This process has great potential to enhance hydrogen yield and reduce CO<sub>2</sub> content in the product gas.

Different process variables i.e. temperature, steam to biomass ratio, adsorbent to biomass ratio, fluidization velocity and biomass particle size have been tested only for steam catalytic gasification and steam gasification with in-situ CO<sub>2</sub> adsorbent. It would be interesting to see the effect of all these process variables on the performance of in-situ catalyst and adsorbent system for hydrogen production. In addition, based on the review, optimal ranges of these process variables are discussed for palm kernel shell in-situ catalyst and adsorbent steam gasification system.

Kinetic models for the biomass gasification are then reviewed. It is concluded that the kinetic model for in-situ catalyst and adsorbent system using palm kernel shell is not reported to date. Kinetic parameters determination based on product gas composition is then reviewed and discussed.

Process optimization study is presented using design of experiments. Important terminologies are defined and reviewed. It is found that the lack of optimization study on hydrogen production from biomass gasification with in-situ catalyst and adsorbent exists. Moreover, optimization study would help to select the optimum steam to biomass ratio which is critical due to high energy associated with heating and condensation of excess steam in the process. The current work focused to fill in the identified research gaps.

CHAPTER 3  
MATERIALS AND METHODS

**3.1 Introduction**

This chapter describes overall research methodology and procedures involved in the present study. The overall research methodology is shown in Figure 3.1.

The first part involves feedstock and bed material (Quicklime) preparation to required size for physical characterization, and gasification in fluidized bed gasifier. Proximate analysis, ultimate analysis and calorific value are determined. Quicklime and Ni catalyst are then characterized through different techniques i.e. X-ray fluorescence, X-ray diffraction, scanning electron microscopy and physisorption analysis.

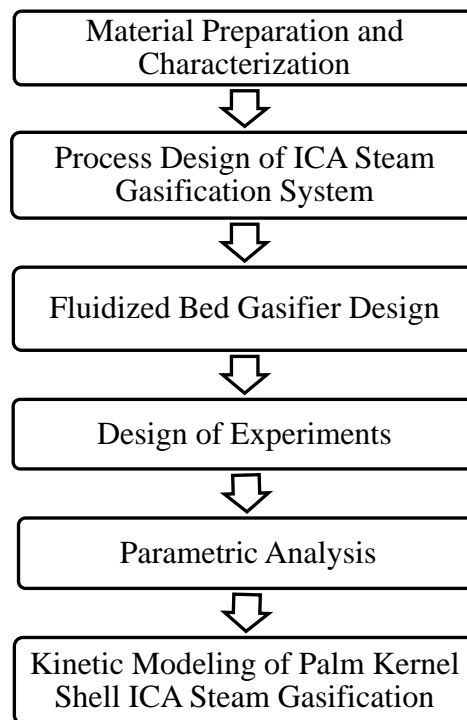


Figure 3.1: Flow chart for overall research methodology

## 3.2 Material Preparation

The materials involved in the present study were palm kernel shell, Quicklime and Ni catalyst. Quicklime was used as bed material as well as for CO<sub>2</sub> capture in the process. Quicklime sample contained CaO higher than 90 wt%. The particle size of Quicklime (as received) was in the range of 16-25 mm. Ni powder was used as the catalyst. The particle diameter of Ni catalyst was in the range of ~10 µm and purity of the sample was > 99.5 wt%. The PKS, diameter range of 0.1-4 mm, was supplied by My 4-Seasons International Sdn. Bhd, Selangor, Malaysia. Quicklime was obtained from Universal Lime Sdn. Bhd. Ni catalyst was purchased from Merck chemicals.

### 3.2.1 Feedstock Selection and Preparation

Palm kernel shell was selected as the feedstock for hydrogen production via ICA steam gasification in the present study. Palm kernel shell can enhance hydrogen production via gasification process due to its abundance and physical properties i.e. high proportion of fixed carbon, volatile matter, and low ash and moisture content [41].

#### 3.2.1.1 Moisture Content

Palm kernel shell was subjected to excess moisture removal before sieving. The fresh biomass was dried under the sunlight for 2-4 hours. This process eased the sieving process where fine particles agglomerated in the presence of excess moisture in the sample. PKS was sieved using CISA BA 300N (Cedaceria Industries) into particle size of 0.355-0.500 mm, 0.71-1.0 mm and 1.0-2.0 mm. PKS was then stored in plastic bags and kept in air tight containers.

Moisture content of the sample was measured using Mettler Toledo HR 83 moisture analyzer. The moisture content of PKS obtained was 9.61 wt% ±0.26. This moisture content was defined under the proximate analysis along with ash and volatiles content present in the biomass (Section 3.2.2.2).

### *3.2.1.2 Determination of Particle and Bulk Density*

The particle density of palm kernel shell was evaluated in Ultrapycnometer 1000, Quantachrome Corporation. The analysis was performed at temperature of 30°C. The particle diameter range was 0.500-0.700 mm while weight of the sample recorded was 5.19 g.

ASTM (American Society for Testing and Materials) 1895 B standard procedure was followed to determine the bulk density of PKS. A known mass of the PKS was poured in funnel which provided the volume of the sample. The weight per unit of volume gave the bulk density of the PKS.

## **3.2.2 Biomass Characterization**

PKS was sieved to a diameter range of 0.150-0.250 mm. This size was selected as most of the ASTM procedure requires particle size of less than 0.250 mm in diameter [41]. This particle size was considered to avoid mass and heat transfer resistance inside the particle [167, 168]. The sample was then dried at 100°C for 24 hours in oven until the weight of the sample become constant. These samples were then stored in air tight bottles.

### *3.2.2.1 Ultimate Analysis*

The ultimate or elemental analysis of PKS was performed in LECO CHNS 932 elemental analyzer. A standard sample of approximately 2 mg was put in the silver capsule and analyzed. The furnace temperature was maintained at 1000°C.

### *3.2.2.2 Proximate Analysis*

The volatile matter, ash content, and fixed carbon were determined based on dry basis. For ash content, ASTM D-3175-01 procedure was used to evaluate the ash content in the biomass. In the present study, 1.0 g of palm kernel shell was put in a furnace and heated up to 250°C at heating rate of 10 °C/min, and hold for 30 min at

this temperature. It was then heated to 575°C at 10 °C/min. The temperature was kept constant for twelve hours to assure complete burning of carbon present in the sample. The sample was then cooled and weighed.

Volatile matter was determined by following ASTM E-872 procedure. The sample of 1.0 g dried PKS was kept in the covered crucible to avoid contact with air during devolatilization process. This covered crucible was then placed in the furnace and heated up to 950°C at 100 °C/min and kept for 7 min at this temperature. The crucible was then cooled and weighed. Fixed carbon was determined by subtracting the sum of volatiles matter and ash content in the biomass based on the dry basis as represented:

$$\text{Fixed carbon (wt\%)} = 100 - \text{Volatile matter (wt\%)} - \text{Ash content (wt\%)} \quad (3.1)$$

### 3.2.2.3 Calorific Value

The calorific value of PKS was determined in IKA C5000 oxygen bomb calorimeter. The ASTM E711-87 procedure was considered to determine the calorific value. A sample weight of 0.3055 g was placed in the crucible which was then put in the decomposition vessel (stainless steel vessel). Pure oxygen (99.98%) was used as oxidant. The sample was then ignited through a cotton thread connected with ignition wire in the decomposition vessel and burned. The temperature and pressure inside the vessel were raised up to 1000°C and 200 bars, respectively. In these conditions, all organic matter was burned and oxidized. As water remained in the product gas as vapors, the calorific value referred to higher heating value (*HHV*) which was then converted to lower heating value (*LHV*) of the sample using Equation 3.2 [169]. The *LHV* and *HHV* were measured in kJ/kg (dry basis).

$$\text{LHV} = \text{HHV} - 2441.8(9 \times H) \quad (3.2)$$

*H* is hydrogen content (dry basis) in PKS and constant 9 shows that the water forms in the combustion is 9 times of the hydrogen content. The heat of vaporization of water is 2441.8 kJ/kg [170].

### **3.2.3 Bed Material Preparation**

Quicklime commonly known as calcium oxide was used as a bed material and as well as a source of CaO. Its function was to adsorb the CO<sub>2</sub> in the product gas. The Quicklime was grinded in Pulverise HE 25, Fritsch. The grinded material was then sieved in CISA BA 300N (Cedaceria Industries) to a particle size of 0.150-0.250 mm.

The particle density of Quicklime was estimated in Ultrapycnometer 1000, Quantachrome Corporation. The analysis was performed at temperature of 30°C. The diameter range of 0.150-0.250 mm was considered while weight of sample was 4.68±0.001 g.

The Quicklime bulk density was determined by following ASTM 1895 B procedure. A known mass of the sample was poured in the funnel which gave the volume of the sample. The weight per unit of volume determined the bulk density of the Quicklime.

### **3.3 Bed Material and Catalyst Characterization**

Material characterization is an important part of a research study to evaluate chemical and physical properties, and structure characteristics of the material used. The chemical composition and surface morphology of commercial Quicklime and Ni catalyst were determined using different characterization techniques such as X-ray fluorescence (XRF), X-ray diffraction (XRD), scanning electron microscopy (SEM) and Physisorption analysis.

#### **3.3.1 X-ray Fluorescence (XRF) Analysis**

The aim of XRF characterization was to determine the chemical composition of the commercial Quicklime and Ni catalyst. The Bruker AXS XRF S4 Pioneer was utilized to analyze the composition of Quicklime and Ni catalyst in the diameter range of 0.150-0.250 mm and 10 µm, respectively. The weight of the sample was 20 g.

### **3.3.2 X-ray Diffraction (XRD) Analysis**

In the present study, the XRD analysis of Quicklime and Ni catalyst was carried out using Bruker d8 Advance. The main objective was to investigate the different compound present and structure of the sample based on its crystal morphology.

### **3.3.3 Scanning Electron Microscopy (SEM) Analysis**

SEM analysis was used to observe the surface images of the samples. The surface morphology of quicklime and Ni catalyst samples was studied using scanning electron microscopy Oxford LEO 1430.

### **3.3.4 Physisorption Analysis**

This technique was used to study the characteristics of material pores and to determine if it is microporous, mesoporous and macroporous. These properties were size, volume and surface area of the pores. In the present study, pore size and surface area were characterized by Brunauer- Emmett-Taylor (BET) method while surface volume was measured using Barrett-Joyner-Halenda (BJH) method.

The analysis was conducted in accelerated surface area and porosimetry analyzer (Micromeritics ASAP 2020). Sample weight of  $0.1444 \pm 0.0001$  g was used. Prior to the analysis, sample was degassed at  $250^{\circ}\text{C}$  for 4 hrs. The analysis was carried out based on the measured content of liquid  $\text{N}_2$  adsorbed and desorbed at its boiling conditions ( $-196^{\circ}\text{C}$  and 1 atm). The total gas quantity adsorbed or desorbed was then recorded at standard temperature and pressure ( $0^{\circ}\text{C}$  and 1 atm).

## **3.4 Process Design of ICA Steam Gasification**

Process design development is an imperative tool to understand the process fundamentals and its different components. Moreover, it provides basis for process block diagram and process flow diagram.

Based on the review of process design (Section 2.7), a process block diagram for ICA steam gasification utilizing PKS for H<sub>2</sub> production was generated as shown in Figure 3.2. The overall process consisted of gasification, gas cleaning, and cooling and separation systems. Furthermore, gasification system was assisted by PKS feeding and steam generation systems. Gas cleaning system separated fine particles from the product gas stream. Finally, the product gas passed through the water cooling system followed by the water separator to remove the water content from the product gas.

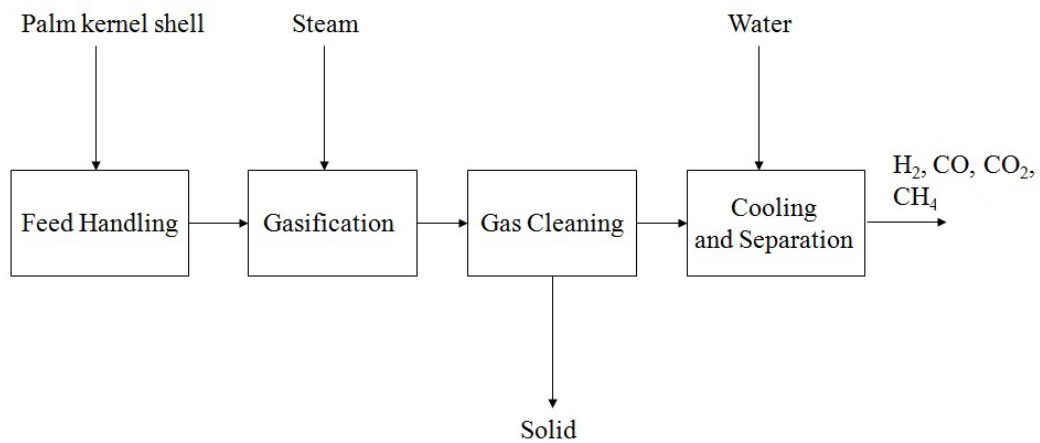


Figure 3.2: Block diagram of ICA steam gasification system

The process flow diagram was then generated from the block diagram of ICA steam gasification system as shown in Figure 3.3. The gasification unit consisted of fluidizing bed reactor. The selection of fluidized bed reactor was made based on its large scale application [59], homogeneous temperature distribution, good heat and mass transfer, and provides high carbon conversion efficiency [23]. The fluidized bed reactor was assisted with continuous biomass feeding and steam generation units. The screw type feeder has a compact design along with pressurized plug to feed the biomass into the gasifier. This type of feeder was widely used for biomass gasification processes under atmospheric pressure [59]. On the other hand, superheated steam was required to assist the gasification at high temperature (600-750°C) as a fluidizing agent as well as the reactant. Therefore, steam generation unit contained boiler unit which produced pressurized steam (6 bar<sub>g</sub>) at 120°C and further heating was performed in superheater to achieve superheated steam at 250-300°C prior injection to the fluidized bed reactor.

For separation of solid particles, cyclone was utilized at the exit of the fluidized bed gasifier. Solid fines removal took place at the exit of reactor to avoid tar condensation on the surface of gas cleaning equipment in downstream. The cyclone separated particles with the cut off diameter of less than 50  $\mu\text{m}$ . Additionally, a heating tape assisted the heating of the cyclone system to avoid tar condensation on the wall of the cyclone. The water scrubber was placed after the cyclone. This unit was used to cool down the product gas's temperature to 40°C prior injection to the gas analyzing system. Final moisture content in the product gas was removed in the separator. The product gas was then sent to the gas analyzing unit.

$\text{N}_2$  supply was provided to assist the biomass feeder to avoid any back flush from the gasifier. Moreover, it was also used in purging of gasification system to remove entrapped gases before the start of each experiment. Generally, air supply was provided to assist the smooth functioning of control valve. The detail of each individual unit is given in Section 3.6.

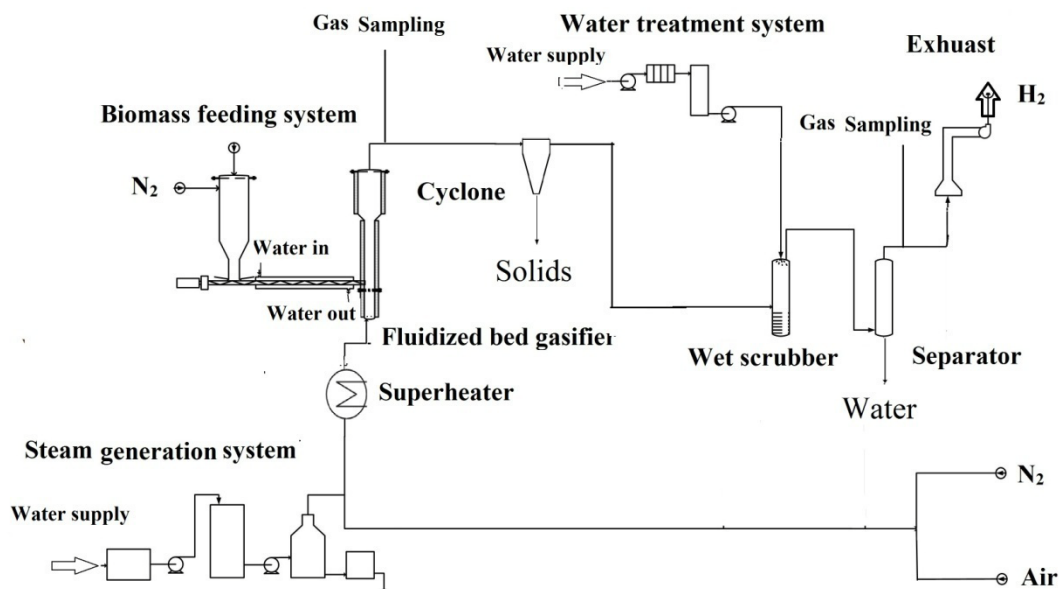


Figure 3.3: Process flow diagram of ICA steam gasification system

### **3.5 Fluidized Bed Reactor Design and Operational Profiles**

The selection of a reactor is an important step for biomass steam gasification in terms of flexibility of operation, product yield, and process efficiency. Fluidized bed gasifier is an excellent choice for biomass steam gasification and has a number of advantages over conventional gasifier.

#### **3.5.1 Design Specification**

The input parameters for design specification of the fluidized bed reactor comprised of feedstock properties, choice of gasifying medium and product gas quality. The choice of gasifying medium was made based on the quality of product gas i.e. hydrogen quality and heating value.

##### *3.5.1.1 Feedstock Specification*

The selection of PKS as a fuel in the present study was discussed in Sections 2.4.1 and 2.4.2. Physical properties of biomass have an important influence on the design of fluidized bed reactor. The PKS properties i.e. proximate and ultimate analyses were determined in Sections 3.2.2.1 and 3.2.2.2. The PKS and steam properties were used in fluidized bed reactor sizing to evaluate the reactor diameter (Section 3.5.2).

##### *3.5.1.2 Choice of Gasification Medium*

Steam was used as a gasification medium in the present study. The selection was made to produce hydrogen rich gas with good product gas heating value. However, steam as a gasifying agent will brought energy penalty if excess steam is used. The optimum steam to biomass ratio needs to be determined for economical operation.

### 3.5.1.3 Product Gas Specification

The product gas quality or specification influences gasification process efficiency and is important to define the goal of the proposed ICA steam gasification process. The following parameters were selected to provide guideline for application of final product gas.

- Hydrogen yield (hydrogen produced, g/kg biomass)  
This indicates that how efficient is the gasification system based on the quantity of the hydrogen produces per unit mass of biomass feed.
- Heating value (product gas with medium heating value)  
When steam is used as gasifying agent, the gasification process generates medium heating value quality gas. The ranking of the product gas heating values based on different gasifying medium is oxygen > steam > air.
- Production rate of the product gas (based on the volume flow rate, m<sup>3</sup>/h, or mass flow rate, g/hr).

## 3.5.2 Calculation of Internal Diameter of Gasifier

The internal diameter (ID) of fluidized bed gasifier was estimated by combining hydrodynamics and reactions based steam calculations as shown in Figure 3.4. The hydrodynamics calculation was based on the properties of the bed material and the total steam required for all the reaction involved in ICA steam gasification.

### 3.5.2.1 Hydrodynamics Study

Fluidized bed gasifier design calculation initially included hydrodynamics study. The study was evaluated to estimate the important parameter that influences the fluidization behaviour in the reactor. Currently, hydrodynamic parameter i.e. minimum fluidization velocity was considered in order to calculate reactor dimensions as shown in Figure 3.4. Minimum fluidization velocity was calculated based on the physical properties of the bed particle and steam used as gasifying agent. These properties consisted of particle diameter, particle density, bulk density and steam density.

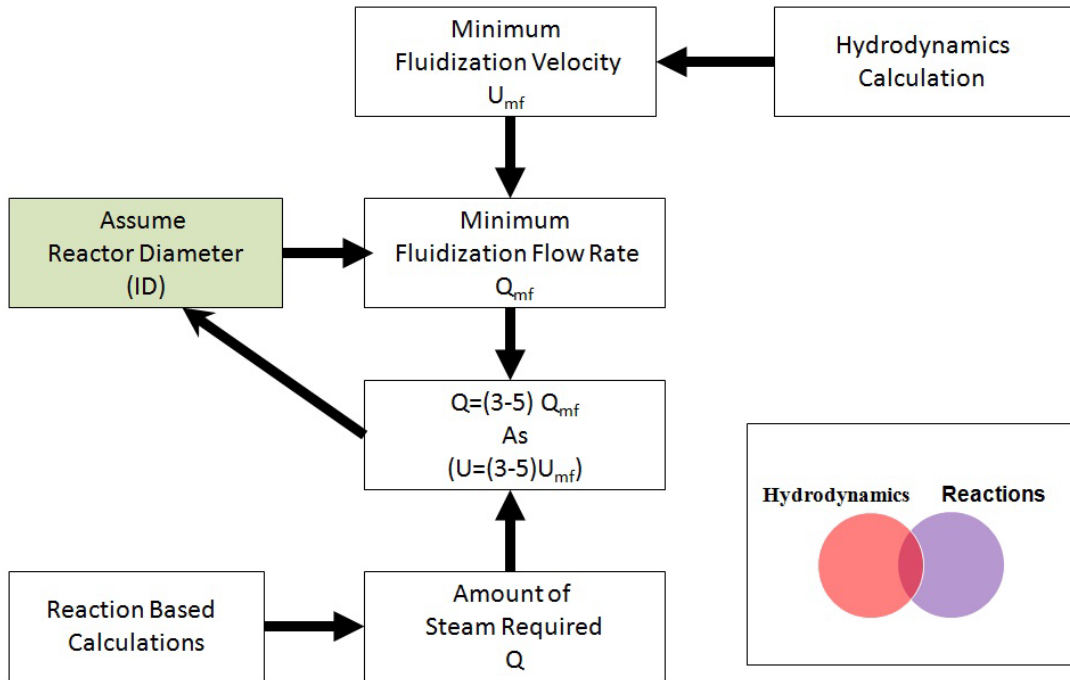


Figure 3.4: Fluidized bed reactor diameter estimation

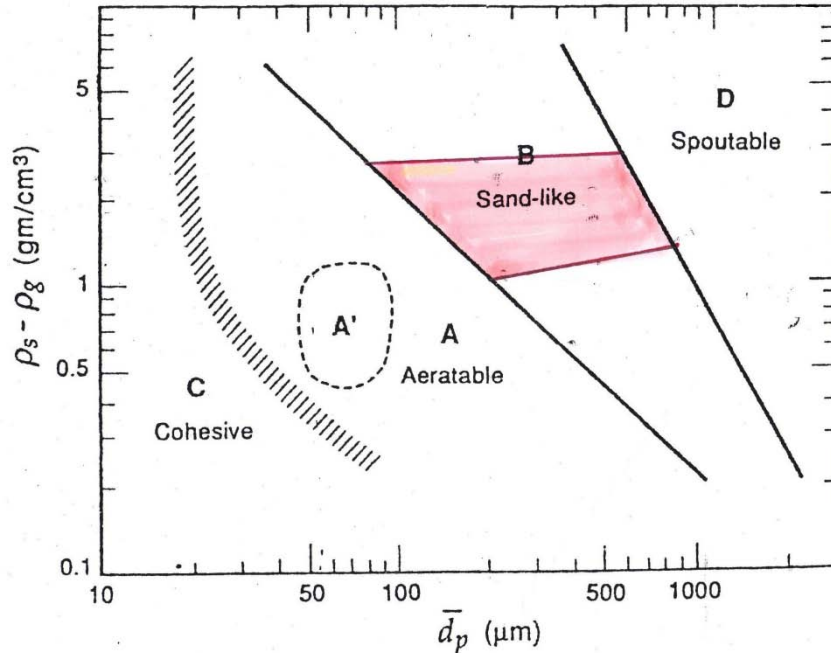


Figure 3.5: Geldart classification of particles [171]

Based on Geldart classification of particles, Group B are types of particles that possess good fluidization characteristics [77]. The region of the Geldart type particle

B is shown in Figure 3.5. The diameter range of particle type B is 40-500  $\mu\text{m}$  based on difference in density of bed particle and fluidizing gas i.e. 1400-4100  $\text{kg/m}^3$ . Thus, to achieve good fluidization region, particle diameter should be kept in the range of Geldart particle B type.

In present study, bed particles comprised of PKS and Quicklime (CaO). The CaO was assumed as continuum single bed particle for calculation of reactor dimensions i.e. only CaO mean particle diameter was considered. The properties of bed material are given in Table 3.1. Based on properties of the bed particles, these materials were well represented by the Geldart particle B (sand like).

The minimum fluidization velocity ( $U_{mf}$ ) is a basic design parameter to define fluidization conditions in the bed. The modified form of Ergun equation in the form of Archimedes number ( $Ar$ ) for pressure drop across fixed bed at minimum fluidization conditions was used to estimate  $U_{mf}$  [171]:

$$Ar = \frac{150(1-\varepsilon_{mf})}{\varphi_b^2(\varepsilon_{mf}^3)} \text{Re}_{mf} + \frac{1.75}{\varphi_b(\varepsilon_{mf}^3)} \text{Re}_{mf}^2 \quad (3.3)$$

where  $Ar$  is can be calculated as:

$$Ar = \frac{d_b^3 \rho_f (\rho_p - \rho_f) g}{\mu^2} \quad (3.4)$$

and Reynolds number at minimum fluidization condition is:

$$\text{Re}_{mf} = \frac{d_p \rho_f U_{mf}}{\mu} \quad (3.5)$$

where  $d_b$  and  $\rho_b$  are bed particle diameter (m) and density ( $\text{kg/m}^3$ ),  $\rho_f$  and  $\mu$  are viscosity (Pa.s) and density ( $\text{kg/m}^3$ ) of steam,  $g$  is acceleration due to gravity ( $\text{m/s}^2$ ),  $\varepsilon_{mf}$  is bed voidage at minimum fluidization velocity and  $\varphi_b$  is bed particle sphericity.

Bed voidage and sphericity must be known at minimum fluidization to estimate  $U_{mf}$  using Equations 3.3, 3.4 and 3.5. These basic equations give more reliable predictions of  $U_{mf}$  as compared to empirical expressions [171] and thus considered in the present work. The bed voidage at minimum fluidization velocity was calculated

from the following expressions [172]:

$$\varepsilon_{mf} = \frac{\rho_b}{\rho_p} - 1 \quad (3.6)$$

The sphericity for CaO was calculated from previous published work [106] using Equations 3.3-3.5 for known minimum fluidization velocity. The value determined was 0.43 which was in a good agreement with the value reported by Basu (2006) [77].

The properties of the steam i.e. density and viscosity were considered at the bed conditions of 750°C and 1 atm. The properties of steam are listed in Table 3.2.

Table 3.1: Quicklime properties

Bed Material	CaO
Mean particle diameter (mm)	0.250
Particle density (kg/m <sup>3</sup> )	3053
Bulk density (kg/m <sup>3</sup> )	1047
Bed voidage	0.69
Sphericity	0.43 [106]

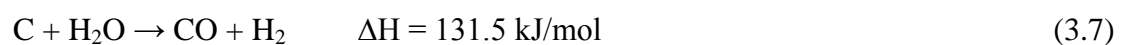
Table 3.2: Steam properties at bed temperature of 750°C and 1 atm

Fluidizing agent	Steam
Density (kg/m <sup>3</sup> )	0.22 [173]
Viscosity (Pa.s)	0.00004 [173]

### 3.5.2.2 Steam Load

The amount of steam was evaluated based on the gasification reactions that consume steam as the reactant. These reactions were char gasification, methane steam reforming and water gas shift as represented:

Char gasification reaction (CGR)



Steam methane reforming (SMR)



Water gas shift reaction (WGSR)



Moreover, the following scheme was considered to calculate the amount of steam required for the reactions involved:

- Char is produced by fixed carbon content of biomass in proximate analysis [174]. This char is expected to participate in the char gasification reaction (CGR) and thus can be estimated directly from the given biomass feed rate.
- The biomass devolatilization produces gases such as H<sub>2</sub>, CO, CO<sub>2</sub>, CH<sub>4</sub> and H<sub>2</sub>O [175]. However, to calculate the steam load, only CH<sub>4</sub> composition was considered. The amount of CH<sub>4</sub> released from biomass was estimated based on the proximate and ultimate analysis. The total elemental carbon content in biomass was 49.74 wt% which consisted of fixed carbon (C) and volatile matter (assumed to be CH<sub>4</sub> only). The remaining carbon portion in volatile matter was estimated by subtracting the fixed carbon from the total elemental carbon,
- It was assumed that the amount of steam available for water gas shift reaction was estimated from CO produced by char gasification and steam methane reforming reactions. The amount of CO in water gas shift reaction considered as a sum of CO generated from char gasification and steam methane reforming reactions. In short, the amount of steam required ( $S_{\text{total}}$ ) for gasification is presented by:

$$S_{\text{Total}} = S_{\text{CGR}} + S_{\text{SMR}} + S_{\text{WGSR}} \quad (3.10)$$

### 3.5.3 Calculation of Height of Gasifier

The height of the fluidized bed reactor was calculated based on transport disengaging height ( $TDH$ ), the height over which only fine particles are carried over (Figure 3.6). The overall equation of reactor height can be written as:

$$\text{Reactor height} = TDH + \text{Bed height} \quad (3.11)$$

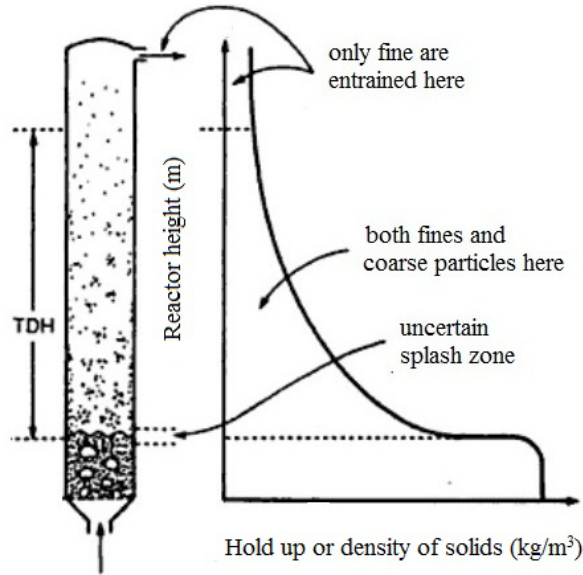


Figure 3.6: Transport disengaging height (*TDH*) in fluidized bed reactor [171]

### 3.5.3.1 Transport Disengaging Height (*TDH*)

The height from the bed surface to the top of disengaging zone is known as *TDH* as shown in Figure 3.6. Above this height, the rate of carryover of fine particles is constant. Moreover, the height at which gas exits from the fluidized bed reactor should be higher than *TDH* to avoid the entrainment of solid particles.

Several empirical expressions were used to determine *TDH* based on maximum bubble diameter. Among these, Horio empirical equation (1980) and Zenz graphical presentation (1958, 1983) are more reliable [172]. However, the graphical presentations are available for fine particles corresponding to Geldart particles A [171] whereas present study considered Geldart particles B. Horio et al. [172] equation for *TDH* was considered in the present which can be used for Geldart particles B:

$$TDH = 4.47 \times (D_{bm})^{0.5} \quad (3.12)$$

where  $D_{bm}$  is the maximum bubble diameter (m) on the surface of the bed.

### 3.5.3.2 Maximum Bubble Diameter Calculation

Maximum bubble diameter ( $D_{bm}$ ) is an important parameter to avoid slugging in bubbling fluidized bed reactor. The mass transfer rate between bubble and emulsion phases is an important parameter that influences overall reaction rate.

In present study, correlation (Equation 3.13) of Mori and Wen [128] was used to determine the  $D_{bm}$ . This correlation is valid for both Geldart types B and D particles classification:

$$D_{bm} = 0.652 \left[ A(U - U_{mf}) \right]^{2/5} \quad (3.13)$$

where  $U$  is superficial gas (steam) velocity (m/s) and  $A$  is the bed cross sectional area ( $m^2$ ). Maximum bubble diameter increases with increasing superficial velocity and bed height [77, 176].

### 3.5.3.3 Bed Height

For better fluidization condition in the bed, it is generally recommended that the ratio of bed height ( $Z$ ) to bed diameter ( $D$ ) varies between 1.0-2.0 [177]. In the present study, ratio of 1.0 was considered to facilitate good fluidization region and helped to keep the bubble size small enough to avoid slugging phenomena. Slugging occurs when the size of bubble is grown enough to reach the size of the bed diameter. At this stage, the bubble passes through the bed as a slug and fluidization conditions are not sustained in the reactor [172].

### 3.5.4 Distributor Plate Design

The distributor plate plays a vital role in the homogeneous fluidization condition all over the bed. It is important that the fluidized bed distributor is properly designed to ensure uniform distribution of gas flow. Better design approach of distributor plate for good fluidization represents a certain ratio between pressure drops across the bed

to distributor plate. A perforated plate type distributor was used due to its simplicity to fabricate, hole size modification and easy to clean.

Suitable distributor design is based on the pressure drop across the distributor to be equal to a fraction of pressure drop across the bed. Zuiderweg et al. [171] used rule of thumb to obtain pressure drop across the distributor. They considered 0.2-0.4 ratio for distributor pressure drop to the bed pressure drop. However, this approach gives a high pressure drop inside the reactor [171] and is not considered in present study. Qureshi et al. [178] developed an empirical relation for the ratio of distributor pressure drop to bed pressure drop  $R_c$ , and showed stable and unstable operation region of the distributor using following expression:

$$\frac{\text{Distributor pressure drop}}{\text{Bed pressure drop}} = R_c = 0.01 + 0.02 \times [1 - \exp(-\frac{0.5D}{Z})] \quad (3.14)$$

$D$  is the bed diameter (m) and  $Z$  is the bed height (m). The aspect ratio of the bed ( $D/Z$ ) was assumed as 1.0 to ensure stable operating region for the distributor [178]. Pressure drop across the bed at superficial velocity was then calculated from Equation 3.15 [171].

$$\Delta P_b = Z(1 - \varepsilon)(\rho_p - \rho_f) \quad (3.15)$$

where  $\varepsilon$  refers to bed voidage and  $Z$  is the bed height at gas superficial velocity. Bed voidage at superficial velocity can be considered as the bed voidage at minimum fluidization  $\varepsilon = \varepsilon_{mf}$ , because no change in pressure drop can be seen for Geldart B type particles if gas velocity rises over minimum fluidization velocity [172]. Distributor pressure drop was determined using Equation 3.14 which was further used to determine total number of orifices in perforated distributor plate (Table 3.3).

General design procedure [171] was followed to estimate the total number of orifices on triangular pitch for a plate of particular reactor internal diameter.

- Number of orifice ( $N_{or}$ ) in the distribution plate was determined using following expression:

$$N_{or} = \frac{A_{or} U_{or}}{Q_{mf}} \quad (3.16)$$

$Q_{mf}$ ,  $A_{or}$ ,  $U_{or}$  are minimum fluidization volumetric flow rate ( $m^3/h$ ), area of an orifice ( $m^2$ ) and gas velocity ( $m/s$ ) through orifice in the distributor plate. All these quantities were based on properties of fluidizing agent (density and viscosity).

- Velocity through orifices was calculated by:

$$U_{or} = C_{dor} \left( \frac{2\Delta P_d}{\rho_f} \right) \quad (3.17)$$

$\Delta P_d$  is the pressure drop (bar) across the distributor plate and was calculated based on the pressure in the bed as  $\Delta P_d = 0.089 \Delta P_b$  where 0.089 represents  $R_c$ . Constant  $C_{dor}$  is drag coefficient.

- Drag coefficient,  $C_{dor}$  (dimensionless), and vessel Reynolds number ( $Re(v)$ ) related as:

$$Re(v) = \frac{\rho_f U_{or} D}{\mu} \quad (3.18)$$

The total number of orifices in the distributor plate was then evaluated. The specification of the distributor plate is listed in the following section.

Table 3.3: Input design parameter for distributor plate design

Parameter	Value
Orifice diameter (m)	0.002
Minimum fluidization velocity (m/s)	0.051
Gas (steam) superficial velocity (m/s)	0.26
Gas (steam) density ( $kg/m^3$ )	0.22 [179]
Gas (steam) viscosity (Pa.s)	0.00004 [173]
Particle density ( $kg/m^3$ )	3053
Bed voidage $\left( 1 - \frac{\text{bulk density of bed particle}}{\text{particel density of bed particle}} \right)$	0.66
$D/Z$ $\left( \frac{\text{bed diameter}}{\text{bed height}} \right)$	1.0
$R_c$ $\left( \frac{\text{distributor pressure drop}}{\text{bed pressure drop}} \right)$	0.089

### 3.5.5 Fluidized Bed Reactor Geometry

The outputs of reactor design process are diameter and height of the fluidized bed reactor. The reactor dimensions evaluated in the design process are listed in Table 3.4. The freeboard is kept larger than the bed area size to reduce solid entrainment from the gasifier and provide longer residence time of product gas to enhance tar cracking [180]. The freeboard of the reactor is expanded up to a diameter of 0.19 m with height of 0.3 m.

Table 3.4: Configuration of fluidized bed gasifier

Parameters	Value
Reactor diameter (ID) (m)	0.15
Reactor height (m)	2.00
Bed height (m)	0.15
Freeboard diameter (m)	0.19
Freeboard height (m)	0.30
Number of orifices in the distribution plate	158

### 3.5.6 Temperature and Pressure Drop Profiles

#### 3.5.6.1 Temperature Profiles

Fluidized bed gasifier is equipped with three internal temperature indicators (TI) at different locations. These locations are; i) just below the distributor plate and 0.1 m from the bottom section, ii) located in the bed and 0.85 m from the bottom section and iii) situated in freeboard and 1.85 m from the bottom section. The three points located at different location in fluidized bed gasifier are shown in Figure 3.7. Temperature variation at these three or any of these locations needs to be monitored to avoid large variation of temperature within the reactor.

Temperature variation in the bed was studied at three different levels i.e. 600°C, 675°C and 750°C. Temperature profiles were plotted with respect to time for 60 min, the total time of gasification considered for all the experiments in the present study.

Each temperature reading was taken at 6 min intervals. The TI at different locations of fluidized bed gasifier is shown in Figure 3.7.

### 3.5.6.2 Pressure Drop Profiles

Initially, pressure drop variation was encountered with respect to time for each velocity i.e. 0.15 m/s ( $3U_{mf}$ ), 0.21 m/s ( $4U_{mf}$ ) and 0.26 m/s ( $5U_{mf}$ ). Velocity to pressure drop diagram was then generated at a given fluidization velocity. The average pressure drop during 60 min gasification operation was then plotted with respect to fluidization velocity. Velocity versus pressure drop diagram was studied to incorporate the pressure drop across fluidized bed gasifier. Pressure drop was measured through pressure differential indicator (PDI) between the points located below the distributor plate and in freeboard as shown in Figure 3.7.

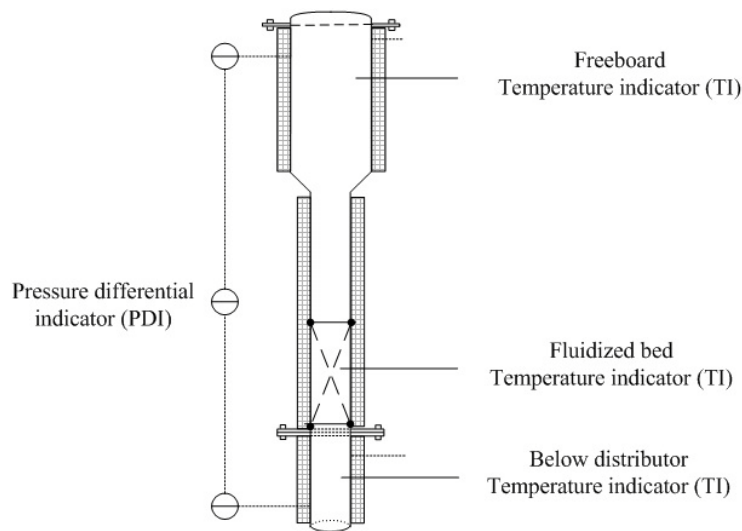


Figure 3.7: Temperature and differential pressure indicators in fluidized bed gasifier

## 3.6 ICA Steam Gasification System

The palm kernel shell ICA steam gasification system for hydrogen production mainly comprised of fluidized bed reactor, biomass feeding system and steam generation system. To the downstream of the fluidized bed gasifier, the product gas passed through the cyclone followed by the wet scrubber and water separator.

### 3.6.1 Fluidized Bed Reactor Configuration

The biomass gasification process takes place in fluidized bed gasifier (Figure 3.8) which contains bed material with steam as fluidizing agent. The superficial velocity of the fluidized bed is of several times of  $U_{mf}$ . Based on the different fluidization regions, the present study considered the bubbling fluidized bed region that incorporates gas superficial velocity of 3–5 times of  $U_{mf}$ . The  $U_{mf}$  was estimated based on the physical properties of bed material and superheated steam properties at the bed conditions of 750°C and 1 atm.

The location of biomass feeding point in the gasifier is an important criterion. It is beneficial for large system to feed biomass at the bottom near the distributor plate. This type of design is recommended to reduce tar and char content [125]. In the present study, the feeding point is 0.20 m above the distributor plate. The fluidized bed mainly comprised of three parts; region below the distributor plate called plenum, the main bed region above the distributor plate, and the top expanded zone known as the freeboard. The main bed section is the section where bed material is fluidized and the entire gasification reactions takes place. This region also contains the biomass feeding point. The main gasifier is equipped with three internal temperature indicators (TI) to monitor temperature at different locations as discussed in Section 3.5.6.1. The analyzing point consists of flow indicator (FI), pressure indicator (PI) and temperature indicator (TI). The analyzing point is located at the exit of the fluidized bed reactor to monitor change in process variables and product gas compositions. The pressure differential indicator is provided between the point below the distributor plate and in the free board section to monitor total pressure drop across the reactor.

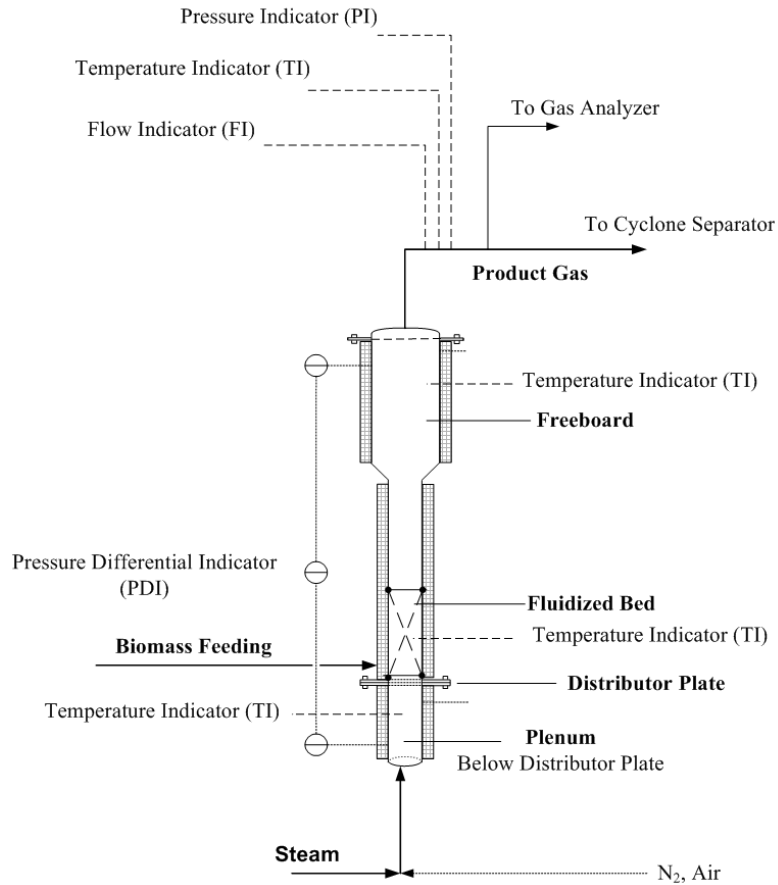


Figure 3.8: Fluidized bed gasifier

Table 3.5: Fluidized bed gasifier system configuration

Parameter	Value
Internal diameter (ID) (m)	0.15
Total height (m)	2.00
Freeboard height (m)	0.30
Freeboard ID (m)	0.19
Plenum height (m)	0.30
Distributor plate hole ID (m)	0.002
Feeding point location from the distributor (m)	0.20
Operating temperature (°C)	600-900
Preheat temperature of the steam (°C)	250-300
Operating pressure (bar <sub>g</sub> )	1-6

### 3.6.2 Biomass Feeding System

Constant and steady feeding of biomass is considered as main process challenge due to low bulk density and fibrous nature of biomass. The capacity of feeding system is 600–4500 g/hr with hopper storage capacity of 9500 g. The biomass feeding system is shown in Figure 3.9. The internal diameter of biomass hopper is 0.5 m and width to height ratio (aspect ratio) of 1.5. The biomass is first introduced into the hopper which is attached to the screw feeder to transfer the biomass from silo to the feeding vessel at continuous steady rate. The pressurized pneumatic feeder is used to feed biomass from hopper to fluidized bed gasifier up to a maximum pressure of 6 bar<sub>g</sub>. It consists of screw feeder and two feeding vessels. Biomass is transferred to the feeding Tube 1 from hopper by screw feeder and then the tube is closed, and pressurized by N<sub>2</sub> gas at 2-3 bar with flow rate of 5-6 m<sup>3</sup>/hr. During this time, biomass feeding is switched to Tube 2. The biomass in Tube 1 is transferred into the gasifier at a specified interval of time to achieve the desired biomass flow rates. The procedure is then switched to Tube 2 for continuous biomass feeding.

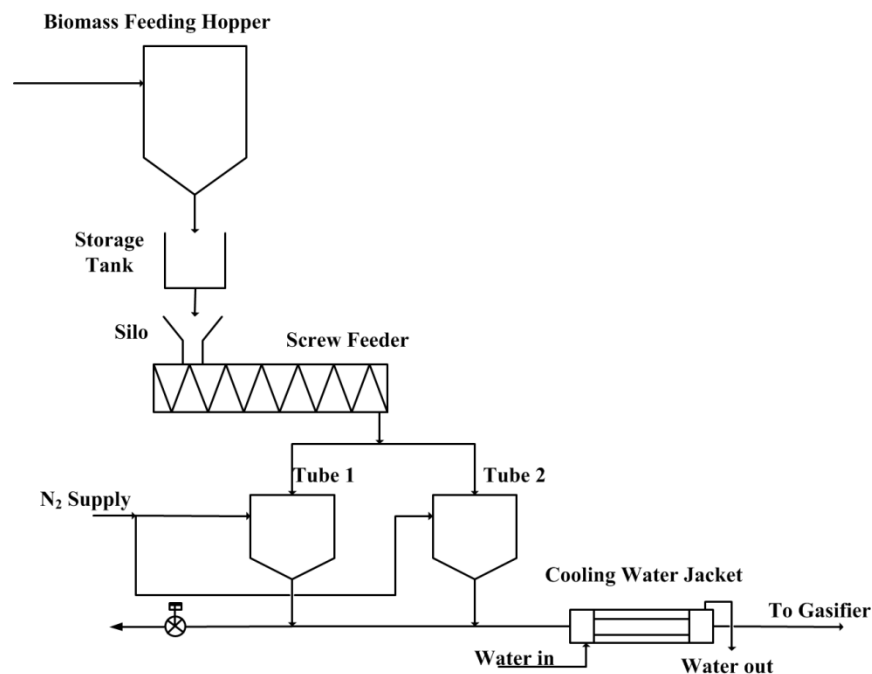


Figure 3.9: Biomass feeding system

The feeder tip carries the biomass into the gasifier and transfers the biomass completely into the fluidizing bed while preventing the bed material from back

flushing. Since the feeder tip is in contact with the gasifier, heat is built up at this location. Therefore, a cooling water jacket is placed along the transfer line between feeding tubes and the gasifier to remove any generated heat. The biomass feeding system specifications are given in Table 3.6.

Table 3.6: Specification of biomass feeding system

Parameter	Value
Hopper capacity (g)	$9500 \pm 100$
Screw feeder capacity (g/h)	$650-4500 \pm 6.5-45$
Feeder operating temperature ( $^{\circ}\text{C}$ )	$<100 \pm 5.0$

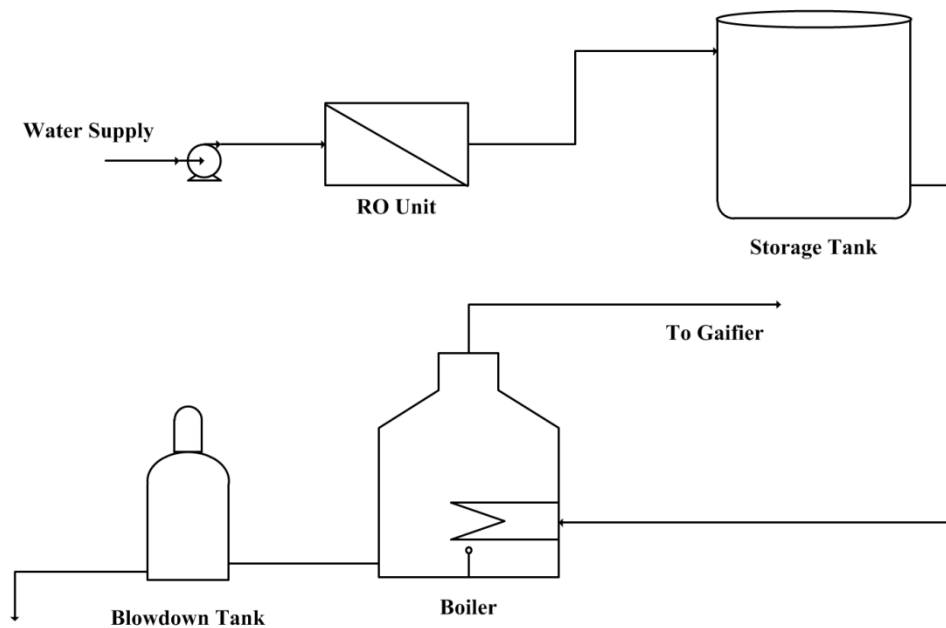


Figure 3.10: Steam generation system

### 3.6.3 Steam Generation System

The steam generation system provides superheated steam to the fluidized bed gasifier (Figure 3.10). The system consists of demineralize water treatment unit (RO) with storage tank, water pump and boiler unit with blowdown tank. The water supply to gasification system is treated by demineralization unit (RO) to remove unwanted minerals and ions. The boiler system has steam generating capacity of 8 kg/h at a temperature range of 100-150 $^{\circ}\text{C}$  up to a pressure of 6 bar<sub>g</sub>. The steam generated from

the boiler is further heated up to 250-300°C in the superheater prior injection to the fluidized bed reactor. The specification of steam generation system is given in Table 3.7.

Table 3.7: Specification of steam generation system

Parameter	Value
Water tank capacity (L)	200
Boiler operating temperature (°C)	100-150 ± 5-8
Boiler operating pressure (bar <sub>g</sub> )	6 ± 0.08
Boiler operating flow rate (g/h)	2000-8000 ± 30-80

### 3.6.4 Gas Cleaning System

The gas cleaning system consists of two stages. The first stage comprises of cyclone solid separator. The second stage contains a wet scrubber and water separator which separates water and some tar impurities from the product gas prior injection to the gas analyzing system.

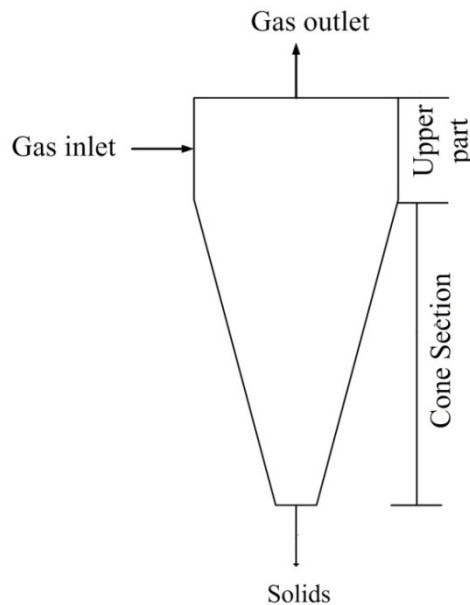


Figure 3.11: Cyclone solid separator

Generally, cyclone is applied to separate solid particles from the product gas exiting from the fluidized bed reactor as shown in Figure 3.11. The pressure drop of

the product gas is minimized after passing through the cyclone. The dust or solid particles to be separated mainly consists of fine ash, char and fine bed particles. The cyclone considered in the present study works on 98% cut off efficiency for 50  $\mu\text{m}$  size particles in product gas exiting from fluidized bed gasifier. The main specifications are given in Table 3.8.

Table 3.8: Cyclone specification

Parameter	Value
ID (upper part) (m)	0.15
Height (upper part) (m)	0.30
Height (cone section) (m)	0.45
Operating flow rate (maximum) ( $\text{m}^3/\text{hr}$ )	25
Cut off efficiency (based on 50 $\mu\text{m}$ particle size) (%)	98

The second stage of cleaning system is designed into two stages as shown in Figure 3.12. The first stage is a direct contact of water with product gas in water scrubber. The unwanted impurities in the product gas such as tar and solid particulates may remove from the product gas. Secondly, this process results in the condensation of the unreacted steam in the product gas. The product gas then passes through the water separator. Table 3.9 provides the specifications of water scrubber and water separator systems.

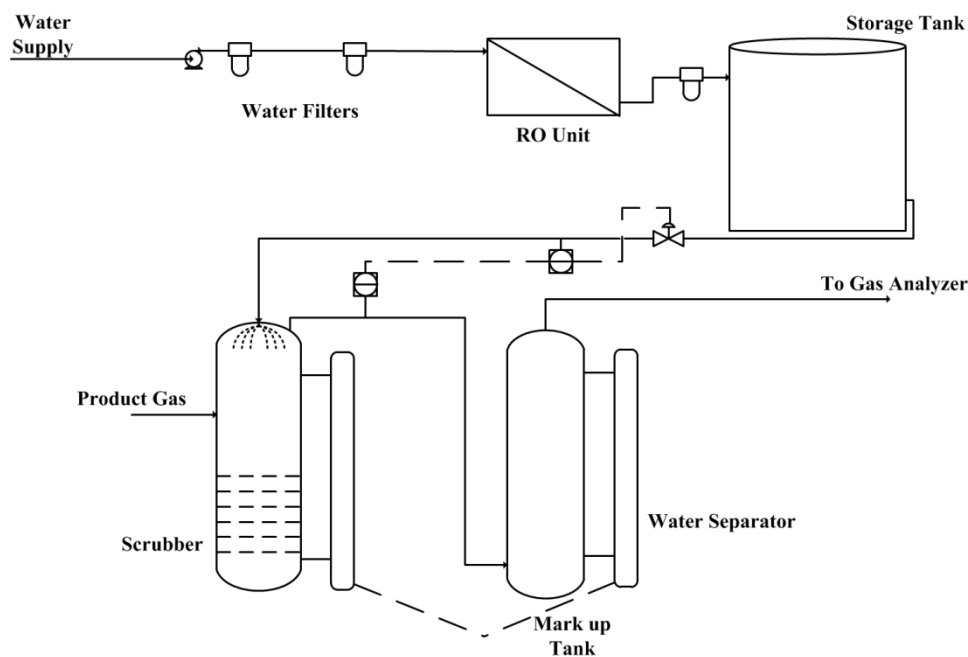


Figure 3.12: Gas cleaning system

Table 3.9: Specification of water scrubber and water separator

Equipment	Parameter	Value
Water scrubber	Inlet temperature (°C)	700-950
	Outlet gas temperature (°C)	≤ 40
	Operating pressure (bar)	1-6
	Pressure drop (bar)	< 0.5
Water separator	Temperature (°C)	40-50
	Pressure (bar)	1-6

### 3.6.5 Gas Analyzing System

#### 3.6.5.1 Online Sampling and Gas Conditioning

The gas analyzing system consists of four different gas analyzers based on the type of gas to be measured. The product gas i.e. CO<sub>2</sub>, CO, CH<sub>4</sub> and O<sub>2</sub> are analyzed based on Infrared (IR) type detector. Similar type of detector, Teledyne 7600, is used to measure NO and SO<sub>2</sub>. These analyzers have response time of less than 1 min. H<sub>2</sub> and N<sub>2</sub> are detected by Teledyne 4060 based on GC-TCD (Thermal Conductive Detector) type of detector and works on the response time of 6 min. Furthermore, Teledyne 2000XTC, a thermal conductivity type of detector, is used to detect H<sub>2</sub> with response time of less than 1 min. The gas analyzing system is equipped with sample flow meter and bypass flow meter to assure stable operation. The optimum flow of sample gas is 1 mL and it can be adjusted through probe. Argon (Ar) gas is used as a carrier gas for the system and its pressure is maintained at 9 psig.

High moisture content, tar and solid particulate are expected to be part of the product gas. Thus, the product gas stream is passed through wire mesh filter of less than 5 μm to eliminate fine solid particulate. Finally, moisture removal is carried out using water condenser before the gas injection to the gas analyzers. Due to high composition of unreacted steam in the product gas, nitrogen purging is used to remove excess moisture from the gas analyzing system before start of the experiment, and during the experiment if necessary.

### 3.6.5.2 Calibration of Gas Chromatography (GC)

To achieve better results from GC, calibration needs to be carried out. For this purpose, calibrations are performed for H<sub>2</sub>, CO, CO<sub>2</sub>, CH<sub>4</sub>, NO and SO<sub>2</sub> utilizing standard calibration gas cylinders with N<sub>2</sub> as the balance gas. Initially, zero calibration was initiated for the individual gas analyzers by introducing the N<sub>2</sub> flow. Once the minimum reading adjusted at zero for all the analyzers and individual gas component, gas analyzers further calibrated for maximum measurable gas composition (vol%). Difference between the set value and the measured value was referred to the uncertainty (accuracy) of the gas analyzer for individual gas component. Standard gas compositions and accuracy of individual gas components are given in Table 3.10.

Table 3.10: Standard gas calibration for gas analyzers

Gas	Standard Composition	Unit	Uncertainty ( $\pm$ %)
H <sub>2</sub>	70	vol %	0.14
CO	50	vol %	0.72
CO <sub>2</sub>	50	vol %	0.02
CH <sub>4</sub>	30	vol %	0.57
O <sub>2</sub>	21	vol %	0.05
NO	80	ppm	8.12
SO <sub>2</sub>	80	ppm	1.75
N <sub>2</sub>	Balance	vol %	-

### 3.6.6 Gas Supply System

The compressed air, N<sub>2</sub> and Ar gases are supplied to the gasification system. The compressed air was used for the instrumentation of control valve. N<sub>2</sub> gas was used to pressurize the biomass feeding system. It was also used to purge the reactor and gas analyzing system to remove any moisture and entrapped gases. Ar gas was used as carrier gas for gas analyzing system. Calibration gases i.e H<sub>2</sub>, CO<sub>2</sub>, CO, CH<sub>4</sub>, O<sub>2</sub>, NO and SO<sub>2</sub> were also included in gas supply system.

### 3.6.7 Experimental Operating Conditions

Effect of five parameters i.e. temperature, steam to biomass ratio, adsorbent to biomass ratio, fluidization velocity and biomass particle size are tested for hydrogen production. The range of these parameters is chosen based on the operating conditions for the gasification reactions to optimize hydrogen composition and yield in the product gas. Table 3.11 shows the experimental operating conditions for palm kernel shell ICA steam gasification. The steam flow rate is referred to gas superficial velocity that is 3-5 time of  $U_{mf}$ . Biomass flow rate was then adjusted for the same steam flow rates. The biomass steam gasification with in-situ CO<sub>2</sub> adsorbent process needs to be operated at lower temperature (500-770°C) for enrich hydrogen gas production at atmospheric condition in fluidized bed gasifier [86]. Similarly, palm kernel shell ICA steam gasification is considered to be operated at temperature range of 600-750°C. For steam to biomass ratio, the optimum value range is from 1.0 to 2.0 wt/wt [44, 101] where higher values may be studied to identify the dependent rate of hydrogen in the product gas. Steam to biomass ratio is varied from 1.5-2.5 (wt/wt). Adsorbent to biomass ratio is in the range of 0.5 -1.5 to reduce significant CO<sub>2</sub> and enhance hydrogen content in the product gas [86]. The operating range of fluidization velocity is 3-5 of  $U_{mf}$ . This operating range comes under the bubbling fluidization region [171]. Biomass particle size has measurable effect on the product gas composition. It is observed that the overall product gas yield, hydrogen composition and yield increase as the particle size decreases [102]. Due to this, small biomass particle size is considered which is in the range of 0.350-2.0 mm. Catalyst to biomass ratio is kept constant at 0.1 (wt/wt). Previous study of steam catalytic gasification [123] in bench scale fluidized bed gasifier showed that the ratio higher than 0.25 (wt/wt) at steam to biomass ratio of almost 2.0 had no significant effect on hydrogen yield.

Table 3.11: Fluidized bed gasifier operating conditions

Parameter	Value
Biomass flow rate (g/h)	1000-1800 $\pm$ 10-18
Steam flow rate (g/h)	2000-3500 $\pm$ 11-19
Temperature ( $^{\circ}$ C)	600-750 $\pm$ 5-8
Pressure (atm)	1 $\pm$ 0.002
Steam to biomass ratio (wt/wt)	1.5-2.5
Adsorbent to biomass ratio (wt/wt)	0.5-1.5
Catalyst to biomass ratio (wt/wt)	0.1
Bed material particle size (mm)	0.150-0.250
Minimum fluidization velocity (m/s)	0.051
Fluidization velocity (m/s)	3-5 $U_{mf}$
Biomass particle size (mm)	0.355-2.0

### 3.6.8 Gasifier Operational Problems and Remedy

The following section elaborates operational problems observed in ICA steam gasification utilizing palm kernel shell as the feedstock. It also highlights the appropriate remedy to the associated problems related to the gasification system.

#### 3.6.8.1 Downstream Clogging

The fluidized bed gasifier contained Quicklime as the bed material with size range of 0.150-0.250 mm. The superheated steam at 250-300 $^{\circ}$ C was injected from the bottom and fluidized the solid bed particles. In addition to the product gases, the stream exiting the fluidized bed reactor entrained excess steam, tar (high hydrocarbon), fine char particles and fine solid particles separated from the bed material due to attrition. Drastic decrease in temperature resulted in steam saturation and tar condensation in the mixture. In this situation, fine particles started to agglomerate and produce a paste like mixture which clogs the downstream pipe and equipment. A heating tape was provided with maximum temperature of 300-400 $^{\circ}$ C.

But due to the excess amount of steam in the product gas, the heating tape was not able to conserve sufficient heat at longer distance of pipe. In addition, blockage was observed in the downstream pipes and valves especially at the exit of the cyclone due to the formation of paste like mixture as shown in Figure 3.13.

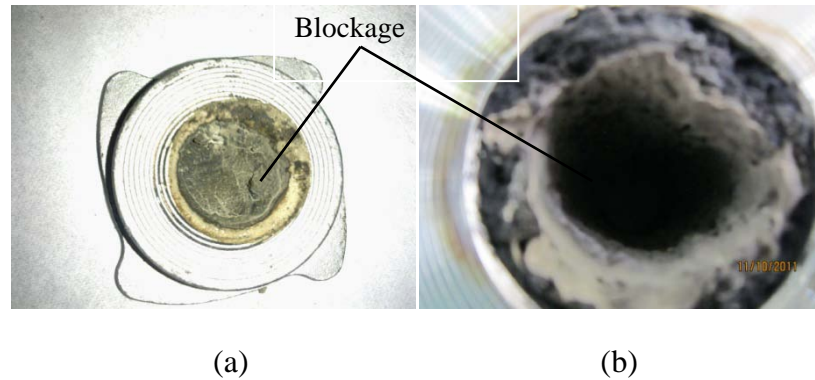


Figure 3.13: Blockage in ICA gasification system a) check valve and b) piping

#### 3.6.8.2 Presence of Moisture in Gas Analyzing System

Steam was a major portion of the product gas at the exit of the fluidized bed gasifier. After passing through the cleaning system (cyclone separator, water scrubber and water separator), the product gas was then injected to the gas analyzing system. In the gas analyzing system, the product gas passed through the small condenser which separates moisture content from the product gas stream. The efficiency of the condenser depends on the moisture present in the product gas. At high steam to biomass ratio, high amount of unreacted steam exits from the gasifier and contributes a major part of the product gas stream. The product gas still carried significant amount of moisture after passing through the cleaning system. This high amount of moisture content reduced the separation efficiency of the condenser. The moisture entered into the tubing system of analyzers as shown in Figure 4.14 (a) and then passed through sample flow meter as shown in Figure 4.14 (b) associated with gas analyzing system. This situation resulted in accumulation of moisture in the gas analyzing system.

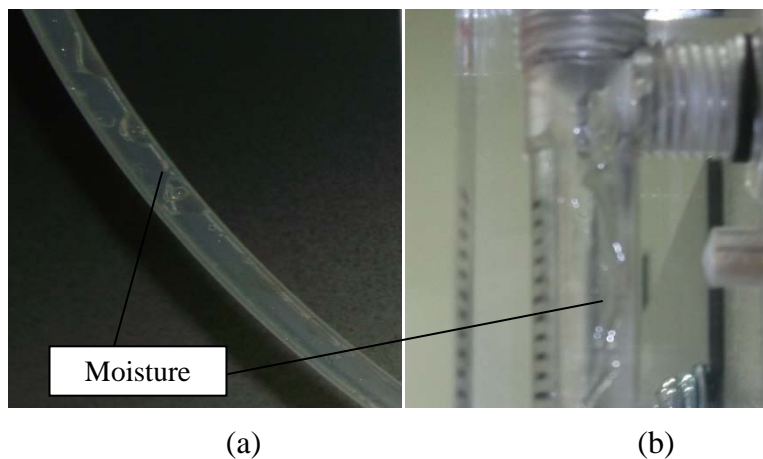


Figure 3.14: Moisture accumulation in a) tubing and b) sample flow meter associated with gas analyzing system

### 3.6.8.3 Remedy of Operational Problems

Two major problems were encountered during the ICA steam gasification utilizing palm kernel shell as the feedstock. First, the problem associated with clogging of the downstream pipe and valve was due to the temperature reduction at the exit of the fluidized bed gasifier which caused steam to be saturated and tar condensation on inner surface of the pipe. To avoid this situation, nitrogen was injected into the system just before start of the biomass feeding into the system. Nitrogen flow consumed heat from the reactor at high temperature i.e. 600-750°C and then passed through, and heated up the pipe and equipments in the downstream. This enhanced the efficiency of the heating tape which was able to maintain high temperature operation at 300-400°C. This procedure was followed for all the experiments to avoid blockage within the system. Second problem associated with moisture content present in gas analyzing system which could cause false reading of the product gas composition measured by the GC. This effect was eliminated by nitrogen purging before start of each experiment. N<sub>2</sub> carried away any residual moisture content and entrapped gases (H<sub>2</sub>, CO, CO<sub>2</sub> and CH<sub>4</sub>) present in gas analyzing system. Nitrogen purging was also used for a couple of minutes during the experiments to remove the moisture content. During this operation, the connection to

the main analyzers was opened and the moisture was drained before entering the gas analyzers.

### 3.7 Design of Experiments (DOE)

Design of experiments is a series of tests which is referred to study the influence of process variables on the output usually termed as response. In the present study, response surface methodology (RSM) was used to produce design of experiments. Among RSM, central composite rotatable design (CCRD) is the most popular [162]. The Expert Design-8 software was used to perform the design of experiments.

The present study considered five process variables; temperature, steam to biomass ratio, adsorbent to biomass ratio, fluidization velocity and biomass particle size. RSM was used to study the influence of these five process variables on output responses; hydrogen composition and yield in the product gas. The selection of each process variable range is provided in detail in Section 3.6.7. By considering these ranges, parameters and their factors along with level are given in Table 3.12. The levels are defined as minimum, middle or centre value and maximum value of the process variables.

Table 3.12: Process variables range for central composite rotatable design (CCRD)

Variables	Operating Range		
	Minimum	Centre point	Maximum
Temperature (°C)	600	675	750
Steam to biomass ratio (wt/wt)	1.5	2.0	2.5
Adsorbent to biomass ratio (wt/wt)	0.5	1.0	1.5
Fluidization velocity (m/s)	0.15	0.21	0.26
Biomass particle size (mm)	0.355	1.175	2.000

### 3.8 Performance Parameters

Performance parameters define the efficiency of a system. In the present study, important parameters such as product gas composition, concentration, flow rate,

hydrogen yield, gasification and carbon conversion efficiencies, and selectivity and product gas heating values are considered to evaluate the ICA steam gasification system.

### 3.8.1 Product Gas Composition and Concentration

Product gas composition is an important criterion to define the process output in terms of individual gas composition. The individual gas composition in the product gas can be defined as:

$$Vol\%(i) = \frac{\text{volume of gas}_{(i)} (m^3)}{\text{Total volume of product gas} (m^3)} \times 100 \quad (3.19)$$

The concentration (mol/m<sup>3</sup>) of individual gas in the product gas can be defined by following expression [84]:

$$Concentration_{(i)} = \frac{\text{moles of gas}_{(i)}}{\text{Total volume of product gas} (m^3)} \quad (3.20)$$

### 3.8.2 Hydrogen Yield

Hydrogen yield is an important parameter to be measured. It can be calculated as [85]:

$$\text{Hydrogen yield} = \frac{\text{Mass of hydrogen produced} (g)}{\text{Mass of biomass feed} (kg)} \quad (3.21)$$

### 3.8.3 Gasification and Carbon Conversion Efficiency

Gasification efficiency ( $\eta_g$ ) and carbon conversion efficiency ( $\eta_{cc}$ ) increase with temperature and can be determined using following expression [89, 181]:

$$\eta_g (\%) = \frac{\text{Mass of total gas produced} (H_2, CO, CO_2, CH_4) (kg)}{\text{Mass of biomass feed} (kg)} \times 100 \quad (3.22)$$

$$\eta_{cc} (\%) = \frac{\text{Moles of carbon containing gases produced} (CO, CH_4, CO)}{\text{Moles of total carbon in biomass}} \times 100 \quad (3.23)$$

### 3.8.4 Selectivity

The selectivity of the product gas in the ICA steam gasification was calculated based on the mol of hydrogen produced as the desired product to the moles of CO, CH<sub>4</sub>, CO<sub>2</sub> and char as the undesired product in the product gas [84]:

$$\text{Selectivity} = \frac{\text{Moles of } H_2 \text{ produced}}{\text{Moles of } CO, CH_4, CO_2 \text{ and Char produced}} \quad (3.24)$$

### 3.8.5 Product Gas Heating Values

Lower heating value (LHV<sub>gas</sub>) and higher heating values (HHV<sub>gas</sub>) are important parameters to be considered to assess the syngas quality for energy application. In the present study, LHV<sub>gas</sub> (MJ/Nm<sup>3</sup>) and HHV<sub>gas</sub> (MJ/Nm<sup>3</sup>) of product gas was determined using following expressions [182, 183]:

$$LHV_{gas} = (30 \times CO + 25.7 \times H_2 + 85.4 \times CH_4) \times 0.0042 \quad (3.25)$$

$$HHV_{gas} = (H_2 \times 30.52 + CO \times 30.18 + CH_4 \times 95) \times 0.0042 \quad (3.26)$$

### 3.8.6 Product Gas Flow Rate

The mass flow rate of a product gas component was determined from the total volumetric flow rate of the gases. In the present study, the volumetric flow rate of the product gas was calculated by multiplying the total volumetric gas flow rate with individual gas volume fraction present in the stream. The mass flow rates were then determined by multiplying volumetric flow rates with gas density at 25°C and 1 atm (product gas measuring conditions).

For steam calculation, inlet water mass flow rate was taken from the flow indicator controller (FIC) at the entrance of the fluidized bed reactor. Unreacted steam was calculated from the total volumetric gas flow rate at the exit of the reactor minus volumetric gas flow rate after the water separator. Biomass flow rate was directly taken from biomass flow indicator located at the biomass feeding system.

### 3.8.7 Amount of Char

The amount of char in the reactor was calculated from the combustion of solid residue after the gasification experiment. After completion of gasification experiment, biomass feed supply was stopped, steam flow was cut off and air was introduced into the reactor. Air was first introduced into the supeheater and then sent to the reactor. The amount of air introduced was in excess and calculated from the fixed carbon content of PKS. The amount of char was then calculated from Equation 3.27 based on CO<sub>2</sub> formation. This amount of char calculated comprised of char particles in the bed, and char sample deposited in the piping system and downstream equipments:



### 3.8.8 Mass and Energy Balance

Mass balance over fluidized bed gasifier was carried out for input stream i.e. biomass flow rate, steam flow rate, and output stream consisted of gas flow rate and solid residual remained after the experiment (Figure 3.15). The product gas included H<sub>2</sub>, CO, CO<sub>2</sub>, CO and unreacted steam exiting from the reactor. The solid residual in reactor that needs to be balanced consisted of char, ash, CaO and CaCO<sub>3</sub>. This solid residual was assumed to be comprised of ash, CaCO<sub>3</sub>, Ca(OH)<sub>2</sub> and unreacted CaO. Ash in the solid residual was separated and weighted. The remaining solid content was characterized using XRD technique to conform the compounds i.e. Ca(OH)<sub>2</sub>, CaCO<sub>3</sub> and CaO (Appendix B) at temperature of 600°C, 675°C and 750°C. The XRD analysis was carried out for fine solids obtained from cyclone separator. Tar content in the system was assumed to be negligible as shown by Appendix B. Tar sample was analyzed by GC-17A gas chromatography (Shimadzu) coupled with GCMS-QP 5050 (Shimadzu) with fused silica capillary column. Overall, mass balance over fluidized bed reactor is written as [184]:

$$\sum_{i=1}^N m_{in} = \sum_{e=1}^M m_{out} \quad (3.28)$$

where  $i$  and  $e$  are total components at the inlet and outlet streams.  $N$  and  $M$  are total number of components at the inlet and outlet stream. Mass balance was carried out

using eSankey 2.x software. Energy balance over fluidized bed gasifier is shown in Figure 3.14 and is carried out using following expression:

$$\sum_{input} (H_{PKS} + H_{H_2O} + Q_{Steam} + Q_{Ext}) = \sum_{output} (H_{H_2} + H_{CO} + H_{CO_2} + H_{CH_4} + H_{unsteam}) \quad (3.29)$$

$H$  represents the enthalpy of each component,  $Q_{Steam}$  is energy associated with steam and  $Q_{Ext}$  is heat provided to the reactor via external heaters. Generally,  $H$  is calculated based on the heat of formation or formation enthalpy represented as  $H_f$ . The enthalpy of each component is calculated by:

$$H_i = n_i \times (H_{f(i)} + \Delta H_i) \quad (3.30)$$

where  $n_i$  refers to the total number of moles flow rate associated with each component at the inlet and out streams. It was further elaborated in terms of specific capacity,  $C_p$ , along with initial temperature ( $T_1$ ) and final temperature ( $T_2$ ).  $\Delta H_i$  was then calculated using Equation 3.31. The values for  $H_f$  and  $C_p$  are given in Table 3.13.

$$\Delta H = \int_{T_1}^{T_2} C_p dT \quad (3.31)$$

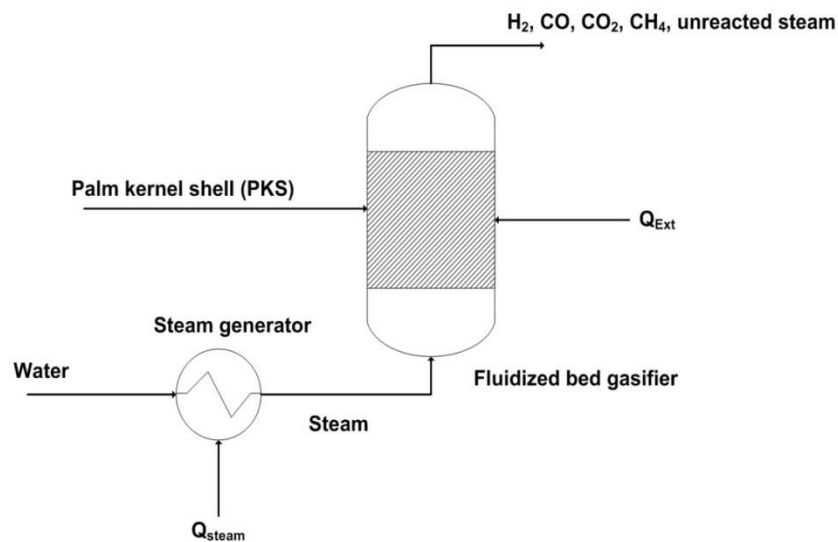


Figure 3.15: Energy balance of ICA steam gasification system

Table 3.13: Parameters and constants for energy balance [4, 84]

Component	$H_f, (\text{J}\cdot\text{mol}^{-1})$	$C_p(\text{J}\cdot\text{mol}^{-1}\cdot\text{K})$
Water	-241830	$72.43 + (10.39 \times 10^{-3})(T) - (1.50 \times 10^{-6})(T^2)$
Hydrogen	0	$27.01 + (3.51 \times 10^{-3})(T) + (0.69 \times 10^5)(T^{-2})$
Carbon monoxide	-110530	$28.07 + (4.63 \times 10^{-3})(T) - (0.26 \times 10^5)(T^{-2})$
Carbon dioxide	-393520	$45.37 + (8.69 \times 10^{-3})(T) - (9.62 \times 10^5)(T^{-2})$
Methane	-74870	$14.15 + (75.5 \times 10^{-3})(T) - (18 \times 10^{-6})(T^2)$
Calcium oxide	-635600	$41.84 + (2.03 \times 10^{-2})(T) - (4.52 \times 10^5)(T^{-2})$
Calcium carbonate	1206900	$82.34 + (4.975 \times 10^{-2})(T) - (12.87 \times 10^5)(T^{-2})$
PKS (Cellulose)	$LHV + H_{CO_2}^f + \frac{x}{2}(H_{H_2O}^f)$	$176.667 + (406.843 \times 10^{-3})(T) - (59.818 \times 10^5)(T^{-2}) - (151.538 \times 10^{-6})(T^2)$

### 3.8.9 Heat and Mass Transfer Coefficients in Fluidized Bed

Heat and mass transfer coefficients in the fluidized bed were evaluated to investigate the extent of heat and mass transfer in the bed. The fluidized bed gasifier operated in the bubbling region of fluidization and most of the fluidizing gas appears in the bed in the form of bubbles. Mass and heat transfer from the bubble to emulsion phase and vice a versa was evaluated. Therefore, bubbling bed model of Kunii and Levenspiel [171] was referred. This model assumed uniform bubble size and well distributed throughout the bed. Furthermore, special case of gas adsorbing bed particle was considered [171, 185] due to the active bed particle (Quicklime, CaO) used. The overall mass transfer coefficient in the bed,  $k_{bed}$ , is related to the dimensional Sherwood number,  $Sh_{bed}$ , by following expression [171]:

$$Sh_{bed} = \frac{k_{bed}d_b.y}{D_c} \quad (3.32)$$

where  $d_b$  refers to bed particle diameter (m),  $D_c$  shows diffusion coefficient ( $m^2/s$ ) and  $y$  represents fraction of inert or non adsorbing component.  $Sh_{bed}$  is calculated as [171]:

$$Sh_{bed} = \frac{\delta}{1-\varepsilon} \left[ \gamma_b (Sh^*) \eta_d + \frac{\phi_b d_b^2 y}{6D_c} K_{bc} \right] \quad (3.33)$$

where  $Sh^*$  is local or particle Sherwood number based on local mass transfer coefficient for the single particle in the bed,  $K_{bc}$  is mass interchange coefficient between bubble and cloud ( $s^{-1}$ ),  $\gamma_b$  is fraction of solid in bubble,  $\eta_d$  is adsorption efficiency for mass transfer,  $\varepsilon$  is bed voidage at superficial gas velocity,  $\phi_b$  is bed particle sphericity,  $\delta$  is volume fraction of bubble in the bed and  $D_c$  is molecular diffusion coefficient,  $m^2/s$ . The Equation 3.33 was used to estimate the  $Sh_{bed}$  based on the particle and fluidizing gas properties. Mass interchange from bubble to cloud (emulsion) is determined [171]:

$$K_{bc} = 4.5 \left( \frac{U_{mf}}{D_{bmean}} \right) + 5.85 \left( \frac{D_c^{0.50} g^{0.25}}{D_{bmean}^{1.25}} \right) \quad (3.34)$$

where  $U_{mf}$  is the minimum fluidization velocity (m/s),  $g$  is the acceleration due to gravity ( $m/s^2$ ), and  $D_{bmean}$  is the mean bubble diameter in the bed (m). Mean bubble diameter in the bed was calculated [186]:

$$D_{bmean} = D_{bm} - (D_{bm} - D_{bo}) \exp(-0.3Z / D) \quad (3.35)$$

where  $Z$  is height (m) of the bed. The mean bubble diameter was calculated at half of the bed height ( $Z/2$ ).  $D$  is the reactor diameter (m);  $D_{bm}$  and  $D_{bo}$  are the maximum and initial bubble diameter (m) and calculated by following expressions [186]:

$$D_{bm} = 0.652 \left[ A(U - U_{mf}) \right]^{2/5} \quad (3.36)$$

$$D_{bo} = 0.347 \left( A \frac{U - U_{mf}}{N_d} \right) \quad (3.37)$$

where  $A$  is the bed cross sectional area ( $m^2$ ) and  $N_d$  ( $m^{-2}$ ) is the hole density in the perforated distributor plate.  $Sh^*$  is determined based on the dimensional Schmidt number ( $Sc$ ) and particle Reynolds number ( $Re_p$ ) [171]:

$$Sh^* = 2 + 0.6(Re_p^{0.5} Sc^{0.3}) \quad (3.38)$$

$Re_p$  and  $Sc$  numbers are written as:

$$Re_p = \frac{\rho_f d_p U}{\mu} \quad (3.39)$$

$$Sc = \frac{\mu}{\rho_f D_c} \quad (3.40)$$

where  $\rho_f$  is gas density ( $kg/m^3$ ),  $\mu$  is gas viscosity ( $kg/m.s$ ) and  $U$  is gas superficial velocity ( $m/s$ ). The overall heat transfer coefficient in the bed,  $h_{bed}$ , was related to the dimensional Nusselt number ( $Nu_{bed}$ ) [171]:

$$Nu_{bed} = \frac{h_{bed} d_b}{k_g} \quad (3.41)$$

where  $h_{bed}$  shows the heat transfer coefficient ( $kW/m^2.K$ ) between the gas and bed of solid particles and  $k_g$  represents the thermal conductivity ( $kW/m.K$ ) of gas mixture.  $Nu_{bed}$  was explained by Kothari's relation [77] in the range of 0.1-100 for  $Re_p$  number as given by:

$$Nu_{bed} = 0.03 Re_p^{1.3} \quad (3.42)$$

Thermal conductivity of individual gases component,  $k_{gi}$ , was calculated as [186]:

$$k_{gi} = a_2 + b_2 T + C_2 T^2 \quad (3.43)$$

Thermal conductivity of gas mixture,  $k_g$ , was determined by:

$$k_g = \sum_{i=1}^N N_i k_{gi} \quad (3.44)$$

where  $N_i$  shows mole fraction of  $i$  gas in the mixture. Constants  $a_2$ ,  $b_2$ , and  $c_2$  are listed in Table 3.14. Basic data for calculation of heat and mass transfer is listed in Table 3.15.

Table 3.14: Data for thermal conductivity calculation [187]

Gas	$a_2$	$b_2$	$c_2$
H <sub>2</sub>	2.73	$2.32 \times 10^{-2}$	$-7.63 \times 10^{-6}$
CO <sub>2</sub>	$-8.09 \times 10^{-1}$	$6.03 \times 10^{-2}$	$-2.82 \times 10^{-5}$
CO	$-5.24 \times 10^{-1}$	$7.96 \times 10^{-2}$	$-7.82 \times 10^{-5}$
CH <sub>4</sub>	$2.97 \times 10^{-1}$	$3.71 \times 10^{-2}$	$1.22 \times 10^{-5}$
N <sub>2</sub>	$2.55 \times 10^{-2}$	$7.53 \times 10^{-2}$	$-6.52 \times 10^{-5}$
Steam	80.4	$4.00 \times 10^{-8}$	$-2.73 \times 10^{-7}$

Table 3.15: Basic data for calculation of heat and mass transfer coefficients

Parameters	Values
$U_{mf}$ (minimum fluidization velocity), (m/s)	0.051
$U$ (gas superficial velocity), (m/s)	0.26 ( $5U_{mf}$ )
$\gamma_b$ (fraction of solid in the bubble)	0.005 [171]
$\delta$ (volume fraction of the bubble in the bed), $\delta = \frac{U - U_{mf}}{U_b - U_{mf}}$ [171]	0.22
$U_b$ (bubble rising velocity), (m/s)	0.99
$\varepsilon$ (bed voidage at superficial gas velocity), ( $\varepsilon_{mf} = \varepsilon$ )	0.66
$\varphi_b$ (bed particle sphericity)	0.43 [106]
$k_g$ (Gas mixture thermal conductivity), ( $\text{kg/m}^3$ )	$3.45 \times 10^{-2}$
$N_d$ (Total number of orifices in distributor plate /area of the distributor plate), ( $1/\text{m}^2$ )	8962

### 3.9 Kinetic Modeling

The kinetic modeling approach was carried out by considering six reactions (Equations 2.1-2.5 in Section 2.8.1.5 and Equation 2.10 in Section 2.8.2.6) occurring in the gasification process. These reactions are presented in Table 3.16. Among these reactions, char gasification, methanation and boudouard reactions were modified by replacing C (carbon) in the chemical formula of PKS. This approach was adopted from the literature due to its applicability in biomass steam gasification with in-situ CO<sub>2</sub> adsorbent [85]. The chemical formula of PKS is C<sub>4.15</sub>H<sub>5.68</sub>O<sub>2.71</sub> derived from the ultimate analysis (Section 3.2.2.1) based on the mole of individual component.

Table 3.16: Reactions schemes for kinetic parameter determination [81, 85, 106]

No	Name	Reaction	ΔH (kJ/mol)
1	Char gasification	$C_{4.15}H_{6.13}O_{2.73} + 1.44H_2O \rightleftharpoons 4.25H_2 + 4.15CO$	131.5 <sup>a</sup>
2	Methanation	$C_{4.15}H_{6.13}O_{2.73} + 8.2H_2 \rightleftharpoons 4.15CH_4 + 2.71H_2O$	-74.8 <sup>a</sup>
3	Boudouard	$C_{4.15}H_{6.13}O_{2.73} + CO_2 \rightleftharpoons 2.25H_2 + 4.15CO + 0.56H_2O$	172 <sup>a</sup>
4	Methane reforming	$CH_4 + H_2O \rightleftharpoons CO + 3H_2$	206
5	Water gas shift	$CO + H_2O \rightleftharpoons CO_2 + H_2$	-41
6	Carbonation	$CO_2 + CaO \rightleftharpoons CaCO_3$	-170.5

<sup>a</sup> reaction enthalpy based on the reacting carbon in the biomass

The following assumptions were made for the kinetic model:

- The fluidized bed was under isothermal conditions, temperature distribution was homogeneous throughout the bed and operation was under atmospheric pressure [78, 129].
- All reactions took place at constant temperature and volume [78]. Thus, first order kinetics was assumed which was represented by the concentration of reacting species. Rate of reaction *i* of reactant A and B is represented by:

$$r_i \rightarrow k_i C_A C_B \quad (3.45)$$

Here  $k_i$  represented Arrhenius constant for each reaction (1/s) and is represented as:

$$k_i = A_i \exp \frac{E_i}{RT} \quad (3.46)$$

where  $A_i$  is the frequency factor or pre-exponential factor (1/s),  $E_i$  is activation energy (J/mol),  $R$  is the universal gas constant (J/mol.K) and  $T$  is the temperature (K).

- Tar formation in the product gas was negligible [133, 175].
- Biomass devolatilization was an instantaneous process [174].
- Hydrodynamic of fluidized bed gasifier was insensitive to the reactor performance [85]. This was considered due to the assumption of perfect mixing and uniform temperature distribution in the fluidized bed gasifier [146].
- Gaseous product mainly consisted of H<sub>2</sub>, CO, CO<sub>2</sub> and CH<sub>4</sub> [149].

The volumetric flow rate of individual gas component was defined by [129]:

$$R_{H_2} = 4.25r_1 - 8.2r_2 + 2.25r_3 + 3r_4 + r_5 + r'_5 \quad (3.47)$$

$$R_{CO} = 4.15r_1 + 4.15r_2 + r_4 - r_5 + r'_5 \quad (3.48)$$

$$R_{CO_2} = r_5 - r'_5 - r_6 - r_3 \quad (3.49)$$

$$R_{CH_4} = 4.15r_2 - r_4 \quad (3.50)$$

where  $r_5$  and  $r'_5$  are rate of forward and reverse water gas shift reactions. The numerical values multiplied with  $r_1$  to  $r_6$  in volumetric rate of the individual gas component (Equations 3.47-3.50) represents stoichiometric coefficients that appeared in reactions 1 to 6 (Table 3.16).

The kinetic parameter evaluation was carried out by minimizing the residual error between the model values ( $y_{mod}$ ) and the experimental values ( $y_{exp}$ ). The residual error was described by:

$$residual\ error = \sum_{i=1}^N \left( \frac{y_{exp} - y_{mod}}{y_{exp}} \right)^2 \quad (3.51)$$

Figure 3.15 shows the kinetic modeling approach used in the present study. The kinetic parameters determined were used as input variables to calculate the volumetric

rate of individual components (Equations 3.47-3.50) in the kinetic model [149]. The model results was then evaluated and compared with experimental data. The deviation between  $y_{mod}$  and  $y_{exp}$  was carried out using sum squared method [149]:

$$RSS = \sum_{i=1}^N \left( \frac{y_{exp} - y_{mod}}{y_{exp}} \right)^2 \quad (3.52)$$

$$MRSS = \frac{RSS}{N} \quad (3.53)$$

$$Mean\ error = \sqrt{MRSS} \quad (3.54)$$

where  $RSS$  is residual sum squared,  $MRSS$  is mean of  $RSS$  and  $N$  is the total number of points.

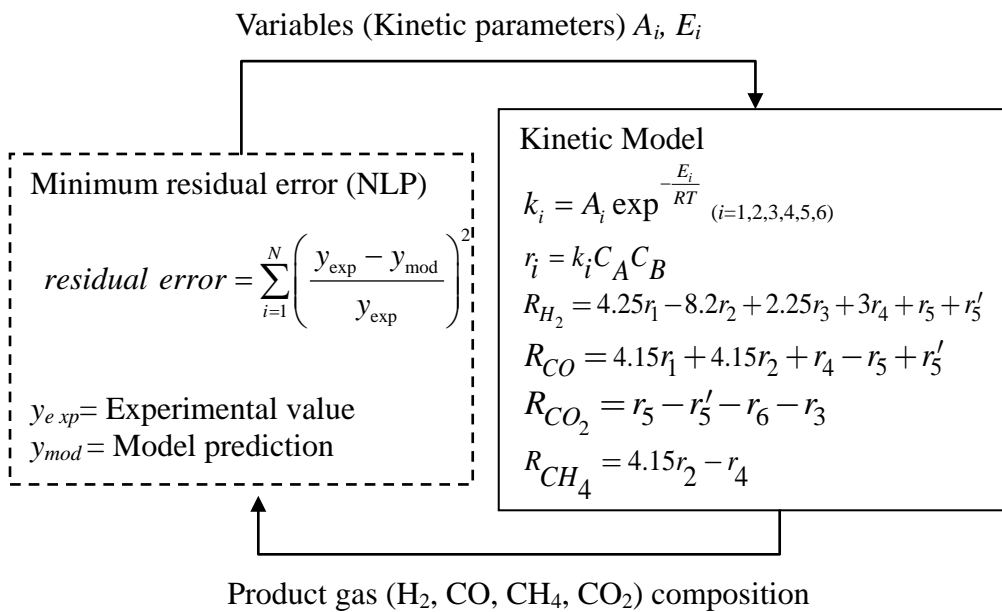


Figure 3.16: Flow chart of kinetic model using error minimization approach

The MATLAB *fmincon* function was used to carry out the nonlinear programming (NLP). Nonlinear programming is the technique used in the mathematics to solve a set of unknown variables based on the objective function to be minimized or maximized, where some of the nonlinear functions are present [188].

### 3.10 Chapter Summary

This chapter elaborates the step by step methods and procedures starting from material preparation to the design of experiments. Biomass characterization has provided the measurement of basic feedstock properties that are used as the starting step in fluidized bed reactor sizing. Furthermore, the physical properties of the bed material are measured which are important inputs to the bed hydrodynamics variable i.e. minimum fluidization velocity. The reactor diameter and height calculated are 0.15 m and 2.5 m, respectively, for ICA steam gasification system. The orifice type of distributor is proposed and designed. The chapter further highlights the basic units and their operation in the biomass gasification system. The experiments are designed based on specific range of process variables i.e. temperature (600-750°C), steam to biomass ratio (1.5-2.5 wt/wt), adsorbent to biomass ratio (0.5-1.5 wt/wt), fluidization velocity (0.15-0.26 m/s) and biomass particle size (0.355-2.0 mm). Kinetic model is then considered to evaluate the kinetic parameters i.e. frequency factor and activation energy using residual sum squared (*RSS*) technique.



## CHAPTER 4

### RESULTS AND DISCUSSIONS

#### 4.1 Introduction

This chapter presents and discusses the overall results produced. Material characterization is carried out for Quicklime (CaO) and Ni catalyst. These characterization techniques included x-ray fluorescence (XRF), x-ray diffraction (XRD), scanning electron spectroscopy (SEM) and physisorption analysis are used to evaluate the chemical composition, surface morphology and pore properties of the sample. Detail discussion is made and comparative study is provided with other commercial materials i.e. calcined limestone and Ni based catalyst.

Effect of different process variables such as temperature, steam to biomass ratio, adsorbent to biomass ratio, fluidization velocity and biomass particle size are studied on the performance of ICA steam gasification system. The range for the process variables studied are; 600-750°C, 1.5-2.5 wt/wt, 0.5-1.5 wt/wt and 0.355-2.0 mm for temperature, steam to biomass ratio, adsorbent to biomass ratio, fluidization velocity and biomass particle size, respectively. Process performance parameters such as product gas composition, hydrogen yield, gas and char yield, gasification and carbon conversion efficiencies, and product gas heating values are discussed. In addition mass and energy balance were carried out on overall process. At the end of the section, comparative study is made for all the performance parameters.

The optimization of experimental conditions for ICA steam gasification is carried out to evaluate the optimal process conditions using hydrogen composition and yield as the output responses. The study is done using Design Expert-8 software. Initially, the fitting of the experimental results using quadratic model is

checked via analysis of variance (ANOVA) based on correlation coefficients i.e. p-value and determination coefficient ( $R^2$ ). The analysis is also extended to the significant and nonsignificant process variables for output response based on p-value. Finally, the process conditions are optimized based on the hydrogen composition and yield. Kinetic modeling approach is used to determine the kinetic parameters for the main reactions involved in ICA steam gasification system. The kinetic parameters are evaluated by minimizing the difference (residual) between the experimental and theoretical data. The kinetic parameters are then used to generate the product gas profiles under the effect of temperature, steam to biomass ratio and adsorbent to biomass ratio and compared with the experimental results.

## 4.2 Biomass Characterization

The present section provides the results and discussions of properties of PKS utilized as the feedstock in ICA steam gasification. The properties i.e. ultimate and proximate analysis and calorific value are presented and discussed.

### 4.2.1 Particle and Bulk Density

Particle and bulk density of PKS is shown in Table 4.1. High particle density of  $3334 \pm 8.3 \text{ kg/m}^3$  shows that the palm kernel shell is a compact and hard waste as compared to other oil palm wastes i.e. empty fruit bunch which is fibrous in nature and posses low density. Due to high particle density, palm kernel shell offers good flowability characteristic in the biomass feeding system.

Table 4.1: Palm kernel shell properties

Parameter	Value ( $\text{kg/m}^3$ )
Particle density	$3334 \pm 8.3$
Bulk density	$606 \pm 4.6$

#### 4.2.2 Ultimate and Proximate Analysis

The ultimate analysis of PKS is listed in Table 4.2. The analysis shows high carbon content of  $49.74 \pm 1.45$  wt%. This high carbon content releases via devolatilization process in the form of solid char, high hydrocarbons i.e. tar and light gasses specially methane. Solid char and methane further reacts with steam through char gasification and methane reforming reactions produce hydrogen rich gas. Cracking and reforming of high hydrocarbons also contributes to the hydrogen production. In addition, low sulfure and nitrogen content may contribute to low  $\text{NO}_x$  and  $\text{SO}_x$  composition in the product help to promote PKS as the potential feedstock for hydrogen and power generation through gasification process. Based on proximate analysis in Table 4.3, low fixed carbon refers to low solid char content, inhibits the problem of handling large solid char via endothermic gasification reaction at high temperature. High volatiles matter and low fixed carbon may enable the operation of steam gasification process at low temperature ( $600\text{-}750^\circ\text{C}$ ). On the other hand, low ash content in PKS avoids agglomeration and slugging problems due to the formation of sticky liquid by the alkali and silica content present in the ash. This will save the additional cost of installing ash removal system in steam gasification processes utilizing PKS as the feedstock.

Table 4.2: Ultimate analysis of palm kernel shell (dry ash free)

Element	Composition (wt%)
C	$49.74 \pm 1.45$
H	$5.68 \pm 0.14$
N	$1.02 \pm 0.03$
S	$0.27 \pm 0.02$
O (by difference)	$43.36 \pm 1.46$

Table 4.3: Proximate analysis of palm kernel shell (dry basis)

Parameter	Composition (wt%)
Volatiles matter	$80.92 \pm 1.11$
Ash content	$4.31 \pm 0.11$
Fixed carbon (by difference )	$14.67 \pm 1.10$

### 4.2.3 Calorific Value

Calorific values i.e. *LHV* and *HHV* are shown in Table 4.4. The result shows good heating value for PKS. These good heating values are due to the low moisture content of 9.60 wt% present in PKS utilized in the present study. High moisture content needs additional energy to evaporate the excess moisture thus reduces the overall heating values of the biomass.

Table 4.4: Heating values of palm kernel shell

Parameter	Value (MJ/kg)
<i>HHV</i>	18.46 $\pm$ 0.64
<i>LHV</i>	17.22 $\pm$ 0.64

### 4.3 Bed Material and Catalyst Characterization

Material characterization was carried out for Quicklime (CaO) and Ni catalyst. The characterization techniques such as X-ray fluorescence (XRF), X-ray diffraction (XRD), Scanning electron microscopy (SEM) and Physisorption analysis were used to evaluate the chemical composition, surface morphology and pore properties of both Quicklime and Ni catalyst.

#### 4.3.1 Particle and Bulk Density of Bed Material

Particle and bulk density of Quicklime as the bed material is given in Table 4.5. The particle diameter of the sample was 0.150-0.250 mm. Based on the Geldart classifications of particles, particle density and diameter of quicklime sample falls under the classification of Geldart type B particles which shows good fluidization characteristics. This region refers to sand-like properties for the particles to be fluidized.

Table 4.5: Quicklime properties

Parameter	Value (kg/m <sup>3</sup> )
Particle density	3053 $\pm$ 3.10
Bulk density	1047 $\pm$ 2.60

### 4.3.2 X-ray Fluorescence (XRF) Analysis

The chemical composition of different compounds in Quicklime is listed and compared with that of CaO based limestone as shown in Table 4.6. The result shows that 93.32 wt% of CaO is present in the commercial Quicklime with 4.42 wt% MgO. Other compounds such as SiO<sub>2</sub>, Fe<sub>2</sub>O<sub>3</sub> and Al<sub>2</sub>O<sub>3</sub> contribute less than 1 wt%. Other metal oxides i.e. MnO, CuO, SrO and ZnO collectively contribute about 1 wt% of the sample composition. High amount of CaO offers good potential as CO<sub>2</sub> adsorbent via carbonation reaction. The amount of CaO exists in the XRF analysis of Quicklime is compared with most commonly used source of CaO such as calcined limestone. The comparison shows that the high CaO content in Quicklime is comparable to other existing source.

Table 4.6: X-ray fluorescence analysis of Quicklime

Components	Composition (wt %)	
	Quicklime	Calcined limestone [106]
CaO	93.32	99.26
MgO	4.24	0.37
SiO <sub>2</sub>	0.95	0.00
Fe <sub>2</sub> O <sub>3</sub>	0.23	0.00
Al <sub>2</sub> O <sub>3</sub>	0.18	0.36
Other metal oxides (MnO, CuO, SrO, ZnO)	1.0	-

Ni catalyst was analyzed using XRF analysis and the result is shown in Table 4.7. The sample contains maximum Ni content of 97.42 wt% which shows the purity of the commercial catalyst. Other compounds found in the sample are P<sub>2</sub>O<sub>5</sub> and Fe<sub>2</sub>O<sub>3</sub> which contribute about 2.20 wt% and 0.38 wt%, respectively.

Table 4.7: X-ray fluorescence analysis of Ni catalyst

Components	Composition (wt %)
Ni	97.42
Fe <sub>2</sub> O <sub>3</sub>	0.38
P <sub>2</sub> O <sub>5</sub>	2.20

### 4.3.3 X-ray Diffraction (XRD) Analysis

The XRD spectrum of commercial Quicklime is shown in Figure 4.1. The Quicklime spectra shows the existence of strong phase of CaO based on the presence of main peaks at  $32.3^\circ$ ,  $37.3^\circ$ ,  $53.9^\circ$ ,  $64.2^\circ$  and  $67.1^\circ$  at  $2\theta$ . These results verified the existence of CaO phase in commercial Quicklime sample. The CaO phase occurs at different points on  $2\theta$  scale and is consistent with XRD analysis of lime sample [189]. Furthermore, CaO phase is represented by narrow and sharp peaks which show high crystallinity of the CaO phase present in the sample [190]. Similar results are reported by Mohamed et al. [191] for commercial and synthesized CaO from cockle shell.

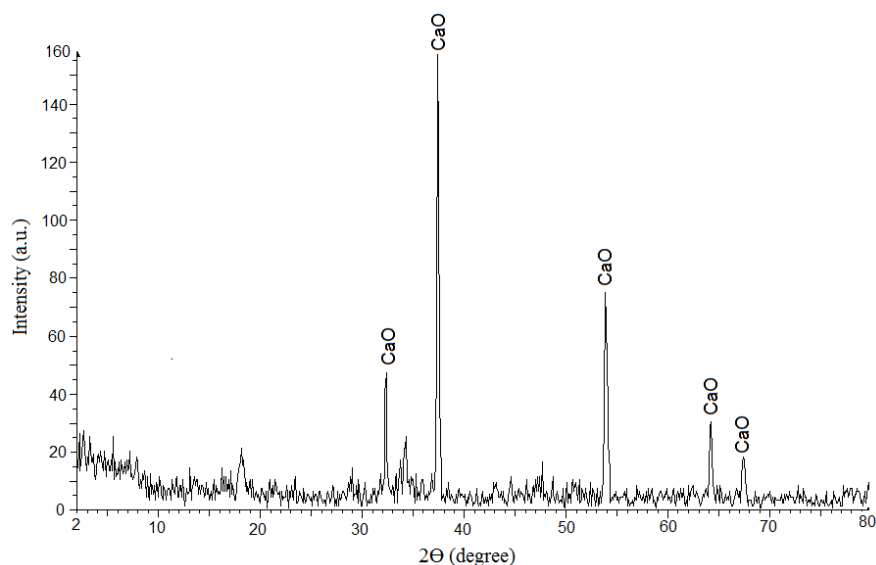


Figure 4.1: X-ray diffraction analysis of Quicklime

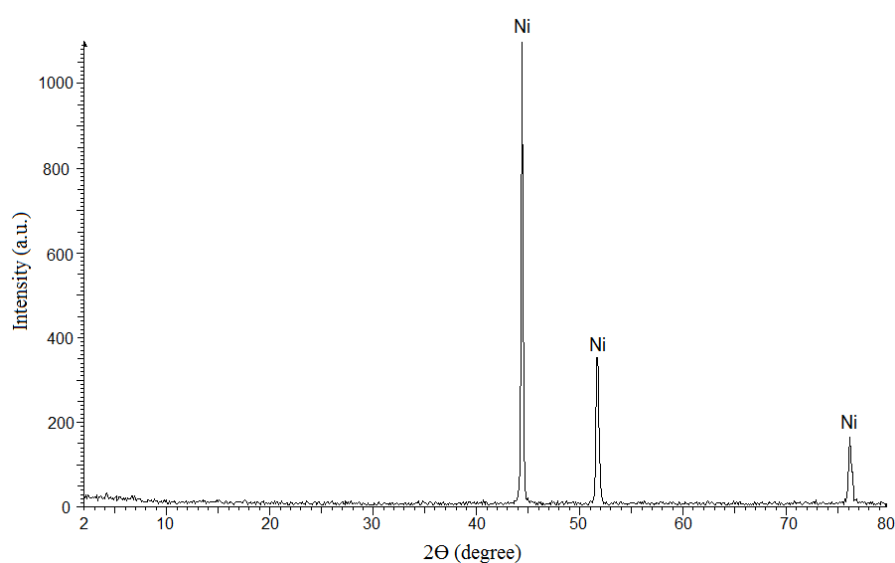


Figure 4.2: X-ray diffraction analysis of Ni catalyst

The XRD analysis of commercial Ni catalyst is shown in Figure 4.2. The main peaks appears at  $44.3^\circ$ ,  $51.8^\circ$  and  $76.1^\circ$  at  $2\theta$  show strong Ni phase which is consistent with the results reported by Therdthianwong et al. [192]. The narrow and sharp peaks in the sample clearly show the crystallinity of the Ni catalyst.

#### 4.3.4 Scanning Electron Microscopy (SEM) Analysis

SEM analysis was used to analyze the surface of Quicklime (CaO). Figure 4.3 shows the surface image of the commercial Quicklime at 3000 time magnification. The image shows that the quicklime sample represents grain like structure. Sun et al. [107] and Mohamed et al. [191] reported existence of grain like structure for calcined limestone and synthesized CaO from cockle shell, respectively. This indicates that the surface morphology of the Quicklime is similar to calcined limestone which is used as a source of CaO for CO<sub>2</sub> adsorption in biomass steam gasification process [106]. The grain like structure is similar to a sphere which exhibits high surface area thus may provides better CO<sub>2</sub> adsorption in the fluidized bed gasifier. This can be justified with a good BET surface area of the Quicklime as shown in Table 4.8.

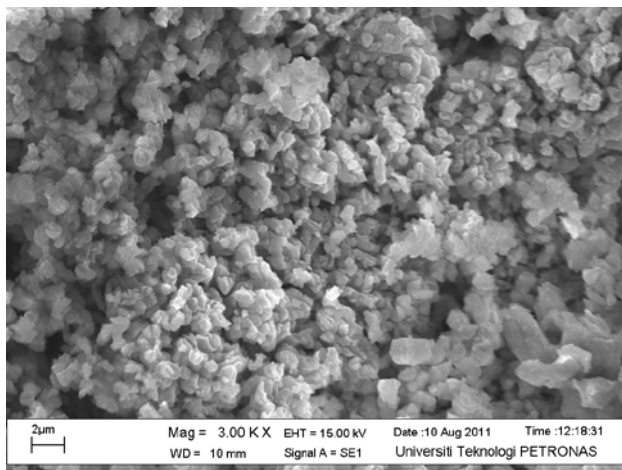


Figure 4.3: Surface image of Quicklime

#### 4.3.5 Physisorption Analysis

Physisorption analysis was performed to determine the pore properties of commercial Quicklime and Ni catalyst. The pore size of Quicklime and Ni catalyst is 16 nm and 6.2 nm, respectively, which falls under the characteristics of mesoporous

solid and mainly contributes to pore size range of 2-50 nm [193]. The BET surface area of Quicklime and Ni is shown in Table 4.8. The results show that the specific surface area of Quicklime adsorbent and Ni catalyst is 4.73 m<sup>2</sup>/g and 0.78 m<sup>2</sup>/g, respectively. The porosity fraction that is associated to macropores and mesopores are an important factor that controls the carbonation reaction. In addition, the mesoporous structured of CaO based sorbent favors high carbonation efficiency of 90% [194].

Table 4.8: Surface properties of Quicklime and Ni catalyst

Parameters	Quicklime	Ni
Mean pore size (nm)	16	6.2
Pore volume (Barret-Joyner-Halenda, BJH) (cm <sup>3</sup> /g)	0.019	0.0016
BET surface area (m <sup>2</sup> /g)	4.74	0.78

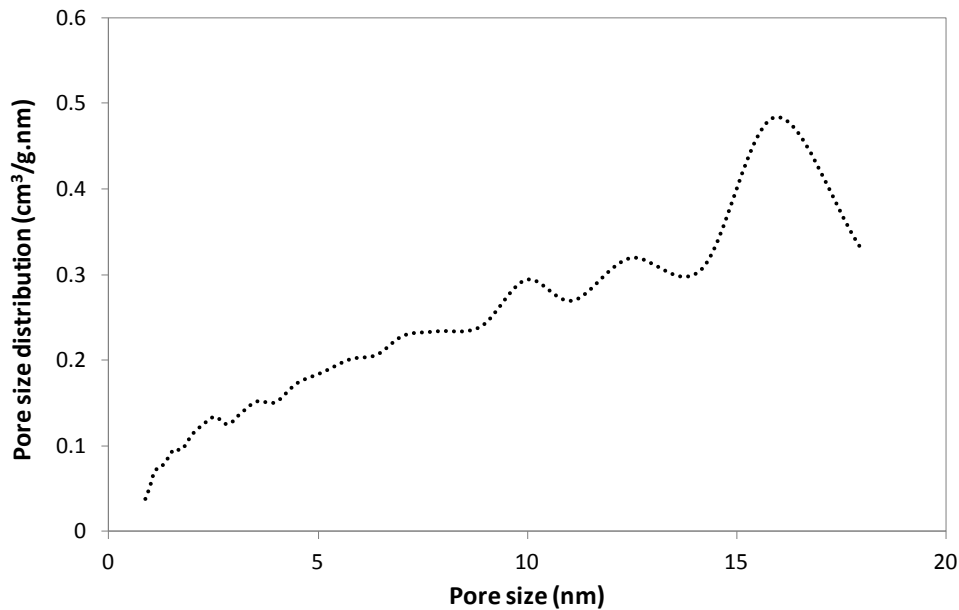


Figure 4.4: Quicklime pore size distribution

Figures 4.4 and 4.5 shows pore size distributions of Quicklime and Ni catalyst, respectively. The present analysis is based on the quantity of gas volume adsorbed at standard temperature and pressure (0°C and 1 atm) with respect to the ratio of actual gas pressure (p) to the vapor pressure (p<sub>0</sub>) of adsorbing gas. Both samples follow multimodal pore size distribution characteristics. The Quicklime and Ni catalyst pore size distribution observed in the range of 15-20 nm and 1-10 nm, respectively. This pore size distribution shows larger pore size of mesoporous type and can provide

large surface area for good CO<sub>2</sub> adsorption and catalytic activities in ICA steam gasification system.

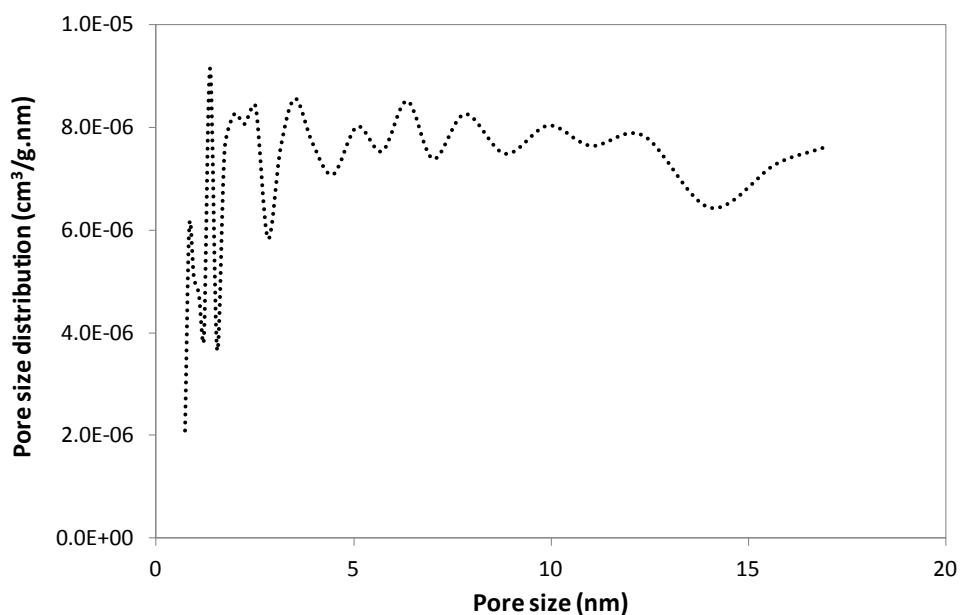


Figure 4.5: Ni catalyst pore size distribution

Figure 4.6 and Figure 4.7 shows the adsorption isotherm for Quicklime and Ni catalyst, respectively. The adsorption isotherms exhibit characteristics of type II according to the IUPAC (International Union of Pure Applied Chemistry) classification [195]. Type II indicates either non-porous or relatively large pores and shows monolayer-multilayer adsorption. This type of material i.e. Quicklime has hysteresis loop in its isotherm as observed by other researchers [191] for commercial and synthesized CaO. The hysteresis of isotherm is located near the region of saturation pressure. This type of isotherm suggested that the material is mesoporous and is justified by the mean pore size of 16 nm and 6.2 nm of Quicklime and Ni catalyst, respectively as shown in Table 4.4. Furthermore, Xu et al. [56] studied mesoporous CaO in in-situ CO<sub>2</sub> for coffee ground steam-O<sub>2</sub> gasification. The CaO captured 55% of CO<sub>2</sub> and increased hydrogen content up to 78% in the product gas (based on volume percent).

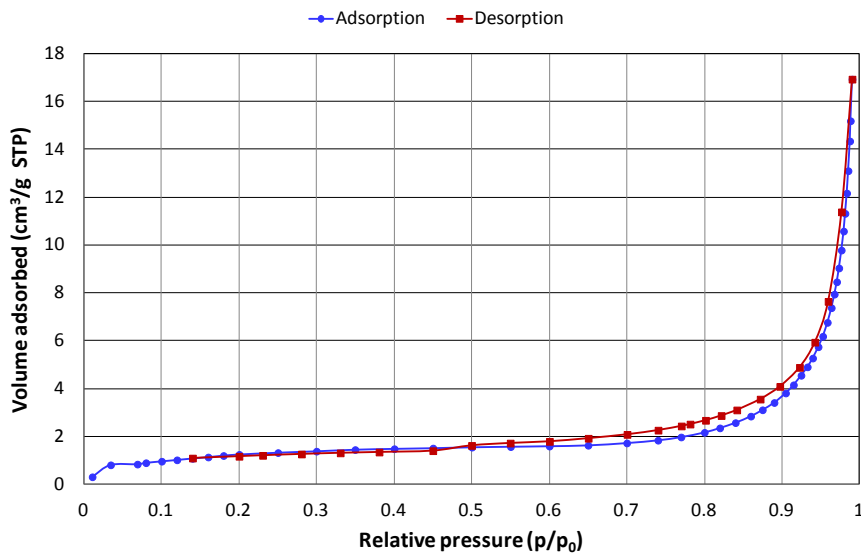


Figure 4.6: Adsorption isotherm for Quicklime

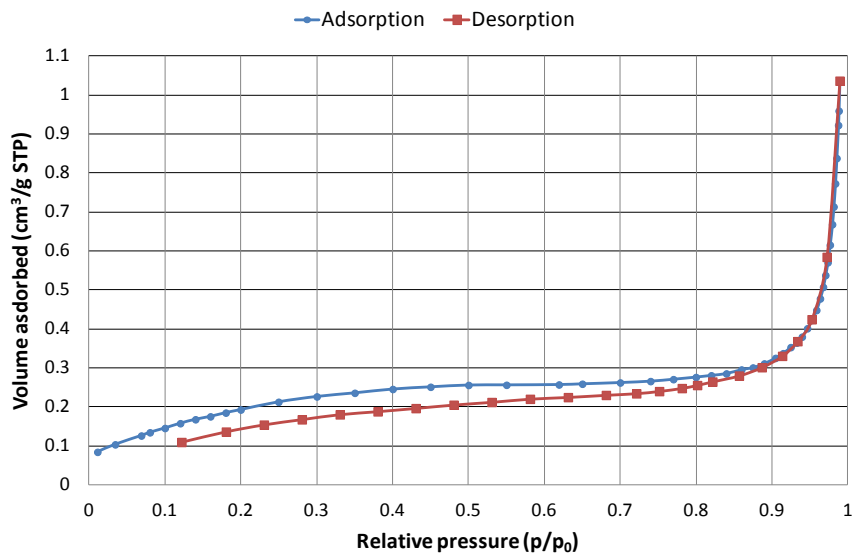


Figure 4.7: Adsorption isotherm for Ni powder

Table 4.9 provides the comparison of Quicklime (CaO) and Ni catalyst with that used in the literature for hydrogen production from biomass steam gasification process. The surface area of Quicklime sample is comparable with calcined limestone ( $5.86 \text{ m}^2/\text{g}$ ) [106] and CaO from calcium hydroxide ( $2\text{-}5 \text{ m}^2/\text{g}$ ) [56] which are widely used as  $\text{CO}_2$  adsorbent in biomass steam gasification. However, surface area of Ni catalyst is low as compared to other commercial catalyst [69]. This low surface area is due to the application of unsupported Ni catalyst in the present study whereas high surface area ( $2.7 \text{ m}^2/\text{g}$ ) is associated to the commercial Ni catalyst with  $\text{Al}_2\text{O}_3$  support.

Meanwhile, specific volume of the Quicklime and the Ni catalyst are 0.019 cm<sup>3</sup>/g and 0.0016 cm<sup>3</sup>/g, respectively.

Table 4.9: Physical properties of Quicklime (adsorbent) and Ni catalyst

Properties	Pore size (nm)	BET surface area (m <sup>2</sup> /g)	Pore volume (cm <sup>3</sup> /g)	Reference
Quicklime (source of CaO)	16	4.74	0.019	This study
	20	2-5	0.01	[56]
Ni catalyst	6.2	0.78	0.0016	This study
	-	0.44	-	[196]
	233	2.9	0.026	[69]*

\*Commercial Ni catalyst on Al<sub>2</sub>O<sub>3</sub> support

#### 4.4 Gasifier Operation and Performance

The following section describes the temperature profiles in the bed and temperature profiles in axial directions of the fluidized bed gasifier. Pressure drop fluctuation at different fluidization velocity and the average pressure drop in the system is drawn versus fluidizing velocity to generate velocity-pressure drop diagram.

##### 4.4.1 Temperature Profiles in Fluidized Bed Gasifier

Figure 4.8 shows the temperature profiles in the bed at 600°C, 675°C and 750°C for 60-minute duration. The analysis shows no significant temperature variation is observed in the bed for ICA steam gasification system. The result showed that the standard variations of ±5.0°C, ±5.8°C and ±6.0°C for 600°C 675°C and 750°C, respectively, are observed within the said operation time. This is due to the presence of carbonation reaction which is an exothermic reaction and produce heat supplement for the endothermic gasification reactions. Similar observations are reported by other researchers [197].

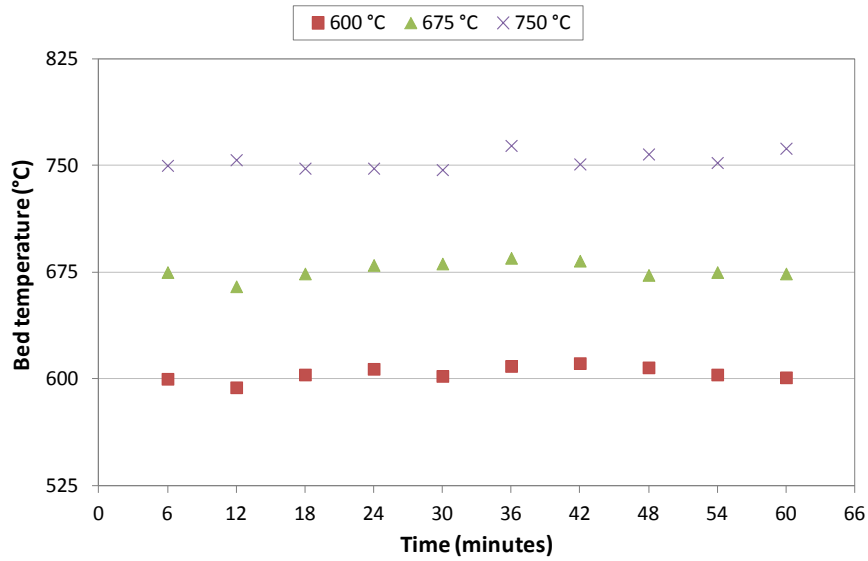


Figure 4.8: Temperature variation in the bed at 600°C, 675°C and 750°C

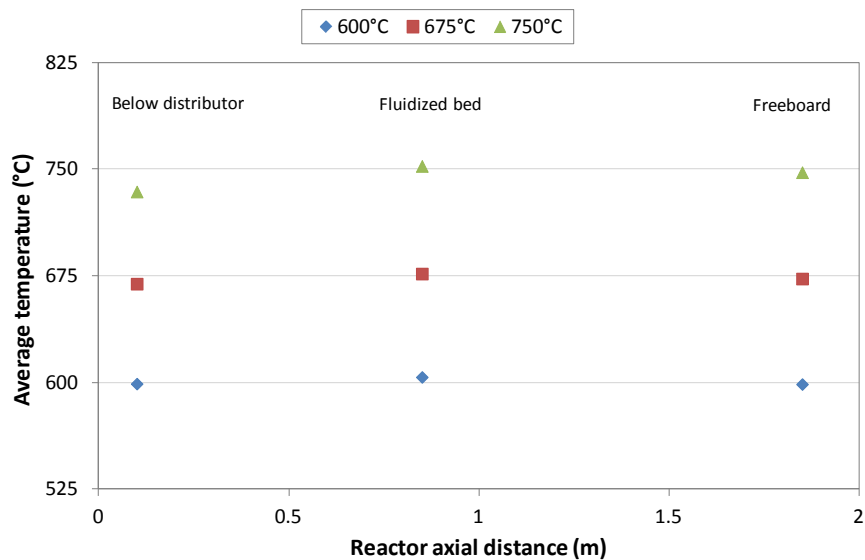


Figure 4.9: Axial temperature profiles in the fluidized bed gasifier

As discussed in Section 3.5.6.1, fluidized bed gasifier is equipped with three internal temperature indicators (TI) at different locations which are i) below the distributor plate, ii) in the bed and iii) in the freeboard section. Because of the different location in the fluidized bed gasifier, each point has different temperature variation although an attempt is made to keep the temperature constant throughout the fluidized bed reactor with the help of external heating system. To encounter these variations, an average temperature is measured over an operation time of 60 min with

respect to the axial distance of the reactor as shown in Figure 4.9. The results show that no significant variation is observed in the freeboard area. Conversely, amongst the three locations, significant variation is observed just below the distributor plate particularly at high temperature of 675°C and 750°C due to the influence of steam injection at this point which consume available energy. It should be noted that the steam is injected at 250-300°C which is lower than that of reactor temperature i.e. 600-750°C.

#### 4.4.2 Pressure Drop Profiles

##### 4.4.2.1 Pressure Drop in Fluidized Bed Gasifier

Figure 4.10 shows the pressure drop fluctuation with respect to time at different fluidization velocity i.e. 0.15 m/s, 0.21 m/s and 0.26 m/s which represents 3, 4 and 5 times of the fluidization velocity in the fluidized bed gasifier. Theoretical pressure drop is also shown for comparison.

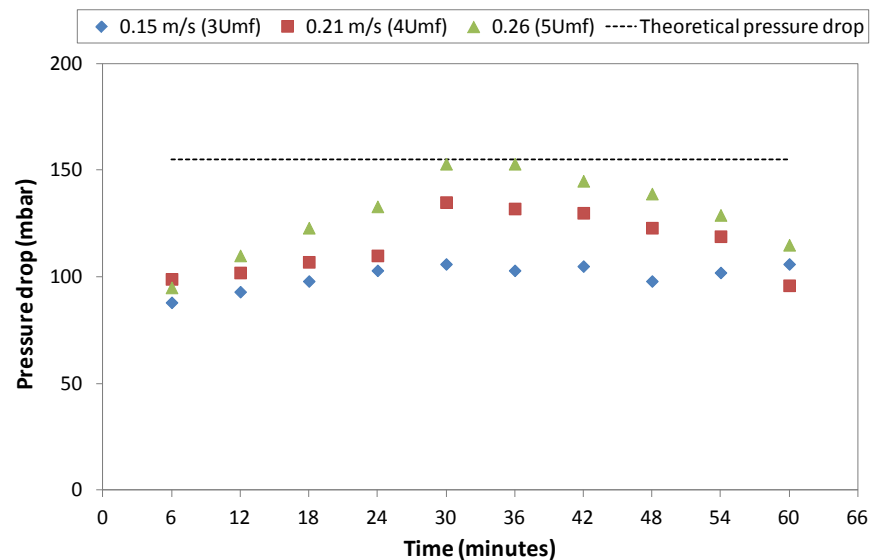


Figure 4.10: Pressure drop profiles of fluidized bed gasifier

Theoretical pressure drop was calculated using Equation 3.15 (Section 3.5.4) based on the diameter to height ratio of 1.0. The analysis shows that the pressure drop

fluctuation increases by increasing the fluidization velocity within operation time of 60 min. Maximum pressure drop is observed at high fluidization velocity. However, low fluidization velocity produces less pressure drop and shows less fluctuation in pressure drop as compared to high fluidization velocities i.e. 0.21 m/s and 0.26 m/s.

#### 4.4.2.2 Pressure Drop versus Velocity Diagram

Figure 4.11 describes the relationship of pressure drop to fluidization velocity in the fluidized bed gasifier. The pressure drop represents an average value over 60 min of operational time. The analysis shows that the average pressure drop observed is in the range of 75-129 mbar by varying fluidization velocity from 0.15-0.26 m/s. It shows that the pressure drop variation in the present study is not significant by varying fluidization velocity of 0.15-0.26 m/s for the ICA steam gasification system. The bed starts to expand at the onset of minimum fluidization velocity, and further increase in fluidization velocity does not show any significant increase in the pressure drop.

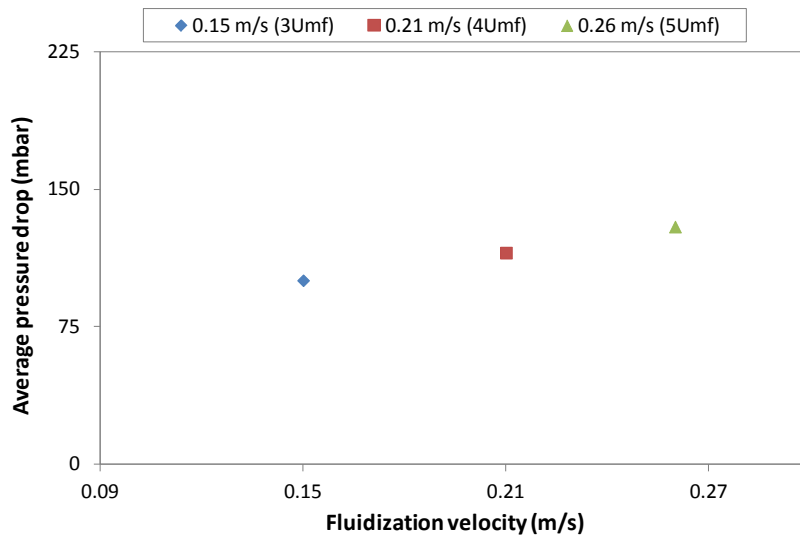


Figure 4.11: Pressure drop versus velocity diagram

#### 4.4.3 Heat and Mass Transfer Coefficients

The heat and mass transfer coefficients in the fluidized bed are determined based on the hydrodynamics parameters of the fluidized bed gasifier. The evaluated heat and mass transfer coefficients and other parameters are given in Table 4.10. The value of particle Reynolds number ( $Re_p$ ) is 0.36 which satisfies the Kothari's correlation ( $Nu_{bed} = 0.03Re_p^{1.3}$ ) criteria ( $0.1 < Re_p < 100$ ) for the corresponding bed Nusselt number ( $Nu_{bed}$ ) [77]. Moreover, lower value of  $Re_p$  corresponds to the region where  $Nu_{bed}$  and  $Sh_{bed}$  falls rapidly which is in agreement by the observation of other researchers [171]. Lower  $Re_p$  is due to lower superficial velocity based on the smaller particle size used (mean particle diameter of 250  $\mu\text{m}$ ) as the bed material. Lower  $Sh_{bed}$  and  $Nu_{bed}$  are also related to the smaller bed particle diameter [198].

Table 4.10: Heat and mass transfer coefficients

Parameter	Value
$k_{bed}$ (mass transfer coefficient in the bed), m/s	0.0063
$h_{bed}$ (heat transfer coefficient in the bed), kW/m <sup>2</sup> .K	1.10
$Sh_{bed}$ (bed Sherwood number)	0.0066
$Nu_{bed}$ (bed Nusselt number)	0.0067
$Re_p$ (Reynold number)	0.36

Table 4.11 provides the comparison of heat and mass transfer coefficients evaluated in the present study with that in the literature. In the case of mass transfer coefficient, comparative value in the literature is lower. It is important to note that mass transfer coefficient was determined in the literature [185] at ambient conditions while limited work [199] was carried out at higher temperature (500°C). On the other hand, high heat transfer coefficient of 1.10 kW/m<sup>2</sup>.K is predicted in current study as compared to 0.13 kW/m<sup>2</sup>.K which was experimentally determined at 700°C utilizing inert sand as the bed material.

Table 4.11: Comparative study of heat and mass transfer coefficients

Parameter	Present study	Literature
$k_{bed}$ (mass transfer coefficient in the bed), m/s	0.0063	0.0011 [198]
$h_{bed}$ (heat transfer coefficient in the bed), kW/m <sup>2</sup> .K	1.10	0.13 [200]

$Nu_{bed}$  and  $Sh_{bed}$  evaluated in present study is required to check if it fits to the experimental data within the fluidized bed region. For this purpose,  $Nu_{bed}$  and  $Sh_{bed}$  are plotted with respect to particle  $Re_p$  number as shown in Figure 4.12. The area between two lines (----) represents the experimental data reported by Kunii and Levenspiel [201] under fluidized bed region. Based on the correlation of  $Nu_{bed}$  and  $Sh_{bed}$ , it can be seen that the heat and mass transfer of the fluidized bed gasifier fall within the range of fluidized bed operation. The  $Nu_{bed}$  and  $Sh_{bed}$  values at lower part of the graph are due to low  $Re_p$ . At lower  $Re_p$ , Kunii and Levenspiel [171] explained that the heat transfer coefficient of gas-particle was lower than the heat transfer coefficient of a single isolated particle. Conversely, for large particles, they found that the heat transfer coefficients for large particle and single isolated particles were much closer as compared to the smaller particles.

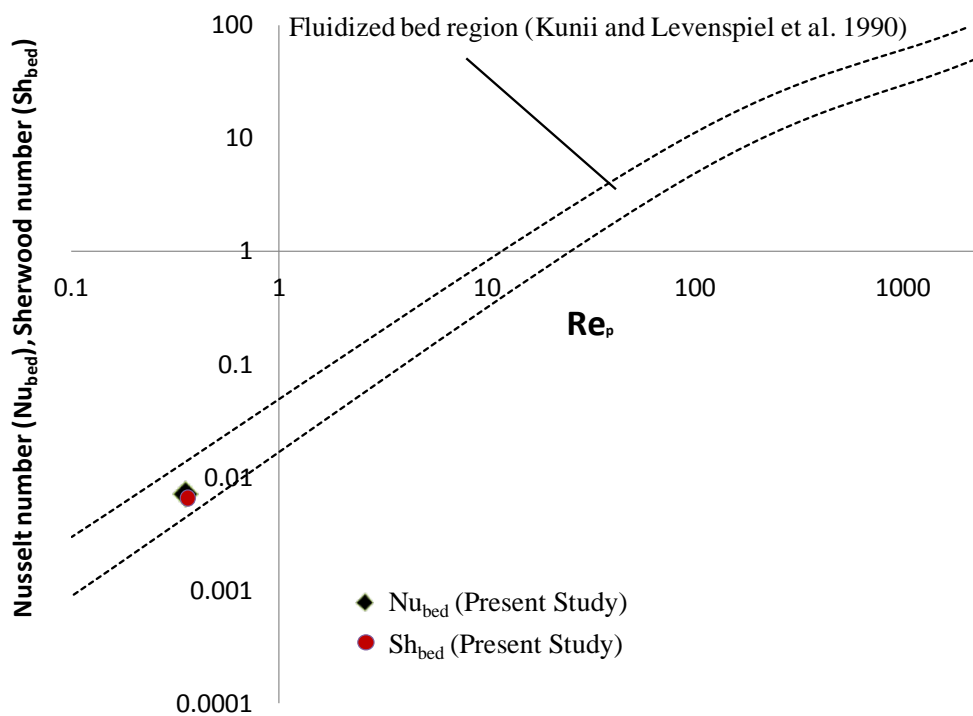


Figure 4.12: Bed Nusselt number ( $Nu_{bed}$ ) and Sherwood number ( $Sh_{bed}$ ) versus particle Reynolds number ( $Re_p$ )

#### 4.4.4 Design of Experiments Array

The design of experiment in present study was based on CCRD which represented 2 level factorial designs with five independent variables involved in ICA steam gasification process. Two level factorial with small CCRD design was used to minimize the total number of experimental runs for ICA steam gasification. Small CCRD design produced 26 experiments (Table 4.12). Total 26 experiments comprised of 11 factorial point, 10 axial points and 5 central points runs. The axial point shows minimum and maximum values for each independent variable i.e. temperature of 600-750°C, steam to biomass ratio of 1.50-2.50 wt/wt, adsorbent to biomass ratio of 0.50-1.50 wt/wt, fluidization velocity of 0.15-0.26 m/s and biomass particle size of 0.355-2.0 mm. The axial points are shown in Table 4.13-4.17 which represent the effect of different independent process variables. The centre points represent the middle value of each independent variables i.e. temperature of 675°C, adsorbent to biomass ratio of 1.0 wt/wt, steam to biomass ratio of 2.0 wt/wt, fluidization velocity of 0.21 m/s and biomass particle size of 1.0-2.0 mm. In all experimental runs, run 2 is the centre point. All the centre points are given in Table 4.18. These central points are also known as repeated runs or replicate which help to optimize the results based on the values of output responses. Moreover, central points provide independent estimate of experimental error. Experimental points generated within the axial and centre points are referred to factorial points i.e. temperature of 634°C and 716°C, steam to biomass ratio of 1.73 wt/wt and 2.27 wt/wt, fluidization velocity of 0.17 m/s and 0.24 m/s, adsorbent to biomass ratio of 0.73 wt/wt and 1.27 wt/wt, and biomass particle size of 0.71-1.0 mm and 1.0-2.0 mm. These factorial points are shown in Table 4.19. The axial points represent the effect of process variables up to 3 variable points as shown in Tables 4.13-4.17. The ratio of catalyst to biomass was fixed to 1.0 wt/wt for all experimental runs.

Table 4.12: Experimental design for ICA steam gasification

Run	Temperature (°C)	Mass flow rate (kg/h)				Steam/Biomass ratio	Fluidization velocity (m/s)	CaO/Biomass ratio	Biomass particle dia. (mm)
		Biomass	Steam	CaO	Catalyst				
1	716	1.320	2.280	1.680	0.135	1.730	0.170	1.270	1.000-2.000
2	675	1.350	2.670	1.350	0.135	2.000	0.210	1.000	1.000-2.000
3	634	1.320	2.280	0.960	0.135	1.730	0.170	0.730	0.710-1.000
4	675	0.980	1.960	0.980	0.100	2.000	0.150	1.000	1.000-2.000
5	634	1.350	3.070	0.980	0.135	2.270	0.240	0.730	1.000-2.000
6	675	1.350	2.670	1.350	0.135	2.000	0.210	1.000	1.000-2.000
7	600	1.350	2.670	1.350	0.135	2.000	0.210	1.000	1.000-2.000
8	750	1.350	2.670	1.350	0.135	2.000	0.210	1.000	1.000-2.000
9	716	1.780	3.070	1.290	0.180	1.730	0.240	0.730	1.000-2.000
10	716	1.000	2.280	1.280	0.100	2.270	0.170	1.270	0.700-1.000
12	675	1.350	2.670	1.350	0.135	2.000	0.210	1.000	1.000-2.000
13	716	1.780	3.070	2.260	0.180	1.730	0.240	1.270	0.710-1.000
14	675	1.690	3.390	1.690	0.170	2.000	0.260	1.000	1.000-2.000
15	675	1.350	2.670	1.350	0.135	2.000	0.210	1.000	1.000-2.000
16	675	1.350	2.670	2.000	0.135	2.000	0.210	1.500	1.000-2.000
17	675	1.350	2.670	0.670	0.135	2.000	0.210	0.500	1.000-2.000
18	716	1.000	2.280	0.730	0.100	2.270	0.170	0.730	1.000-2.000
19	675	1.350	2.670	1.350	0.135	2.000	0.210	1.000	0.355-0.500
20	675	1.780	2.670	1.780	0.180	1.500	0.210	1.000	1.000-2.000
21	634	1.000	2.280	1.280	0.100	2.270	0.170	1.270	1.000-2.000
22	634	1.350	3.070	1.720	0.135	2.270	0.240	1.270	1.000-2.000
23	634	1.780	3.070	2.260	0.180	1.730	0.240	1.270	1.000-2.000
24	675	1.070	2.670	1.070	0.110	2.500	0.210	1.000	1.000-2.000
25	675	1.350	2.670	1.350	0.135	2.000	0.210	1.000	1.000-2.000
26	716	1.350	3.070	0.980	0.135	2.270	0.240	0.730	0.710-1.000

Table 4.13: Effect of temperature

Run	Temperature (°C)	Mass flow rate (kg/h)				Steam/Biomass ratio	Fluidization velocity (m/s)	CaO/Biomass ratio	Biomass particle dia. (mm)
		Biomass	Steam	CaO	Catalyst				
7	600	1.350	2.670	0.135	0.135	2.000	0.210	1.000	1.000-2.000
2	675	1.350	2.670	0.135	0.135	2.000	0.210	1.000	1.000-2.000
8	750	1.350	2.670	0.135	0.135	2.000	0.210	1.000	1.000-2.000

Table 4.14: Effect of steam to biomass ratio

Run	Temperature (°C)	Mass flow rate (kg/h)				Steam/Biomass ratio	Fluidization velocity (m/s)	CaO/Biomass ratio	Biomass particle dia (mm)
		Biomass	Steam	CaO	Catalyst				
20	675	1.780	2.670	1.780	0.180	1.500	0.210	1.000	1.000-2.000
2	675	1.350	2.670	1.350	0.135	2.000	0.210	1.000	1.000-2.000
24	675	1.070	2.670	1.070	0.110	2.500	0.210	1.000	1.000-2.000

Table 4.15: Effect of fluidization velocity

Run	Temperature (°C)	Mass flow rate (kg/h)				Steam/Biomass ratio	Fluidization velocity (m/s)	CaO/Biomass ratio	Biomass particle dia. (mm)
		Biomass	Steam	CaO	Catalyst				
4	675	0.980	1.960	0.980	0.100	2.000	0.150	1.000	1.000-2.000
2	675	1.350	2.670	1.350	0.135	2.000	0.210	1.000	1.000-2.000
14	675	1.690	3.390	1.690	0.170	2.000	0.260	1.000	1.000-2.000

Table 4.16: Effect of adsorbent to biomass ratio

Run	Temperature (°C)	Mass flow rate (kg/h)				Steam/Biomass ratio	Fluidization velocity (m/s)	CaO/Biomass ratio	Biomass particle dia. (mm)
		Biomass	Steam	CaO	Catalyst				
17	675	1.350	2.670	0.670	0.135	2.000	0.210	0.500	1.000-2.000
2	675	1.350	2.670	1.350	0.135	2.000	0.210	1.000	1.000-2.000
16	675	1.350	2.670	2.000	0.135	2.000	0.210	1.500	1.000-2.000

Table 4.17: Effect of biomass particle size

Run	Temperature (°C)	Mass flow rate (kg/h)				Steam/Biomass ratio	Fluidization velocity (m/s)	CaO/Biomass ratio	Biomass particle dia. (mm)
		Biomass	Steam	CaO	Catalyst				
19	675	1.350	2.670	1.350	0.135	2.000	0.210	1.000	0.355-0.500
2	675	1.350	2.670	1.350	0.135	2.000	0.210	1.000	1.000-2.000
11	675	1.350	2.670	1.350	0.135	2.000	0.210	1.000	1.000-2.000*

\*Additional run due to same particle size

Table 4.18: Experimental run representing central points

Run	Temperature (°C)	Mass flow rate (kg/h)				Steam/Biomass ratio	Fluidization velocity (m/s)	CaO/Biomass ratio	Biomass particle dia. (mm)
		Biomass	Steam	CaO	Catalyst				
2	675	1.350	2.670	1.350	0.135	2.000	0.210	1.000	1.000-2.000
6	675	1.350	2.670	1.350	0.135	2.000	0.210	1.000	1.000-2.000
12	675	1.350	2.670	1.350	0.135	2.000	0.210	1.000	1.000-2.000
15	675	1.350	2.670	1.350	0.135	2.000	0.210	1.000	1.000-2.000
25	675	1.350	2.670	1.350	0.135	2.000	0.210	1.000	1.000-2.000

Table 4.19: Factorial points in design of experiment

Run	Temperature (°C)	Mass flow rate (kg/h)				Steam/Biomass ratio	Fluidization velocity (m/s)	CaO/Biomass ratio	Biomass particle dia. (mm)
		Biomass	Steam	CaO	Catalyst				
1	716	1.320	2.280	1.680	0.130	1.730	0.170	1.270	1.000-2.000
3	634	1.320	2.280	0.960	0.130	1.730	0.170	0.730	0.710-1.000
5	634	1.350	3.070	0.980	0.130	2.270	0.240	0.730	1.000-2.000
9	716	1.780	3.070	1.290	0.180	1.730	0.240	0.730	1.000-2.000
10	716	1.000	2.280	1.280	0.100	2.270	0.170	1.270	0.710-1.000
13	716	1.780	3.070	2.260	0.180	1.730	0.240	1.270	0.710-1.000
18	716	1.000	2.280	0.730	0.100	2.270	0.170	0.730	1.000-2.000
21	634	1.000	2.280	1.280	0.100	2.270	0.170	1.270	1.000-2.000
22	634	1.350	3.070	1.720	0.130	2.270	0.240	1.270	0.710-1.000
23	634	1.780	3.070	2.260	0.180	1.730	0.240	1.270	1.000-2.000
26	716	1.350	3.070	0.980	0.130	2.270	0.240	0.730	0.710-1.000

## 4.5 Parametric Analysis of Influential Variables

The effect of different process variables i.e. temperature, steam to biomass ratio, adsorbent to biomass ratio, fluidization velocity and biomass particle size on hydrogen composition, yield and other performance parameters are evaluated in the ICA steam gasification system.

### 4.5.1 Effect of Reactor Temperature

Temperature is considered as an important process variable that influences conversion of biomass to hydrogen rich gas. In the present study, effect of temperature is studied for char and gas yield, H<sub>2</sub> yield, product gas composition, gasification and carbon conversion efficiencies, and selectivity and product gas heating values.

#### 4.5.1.1 Gas and Char Yield

Figures 4.13 and 4.14 show the effect of temperature on total gas yield of gaseous product i.e. H<sub>2</sub>, CO, CO<sub>2</sub>, CH<sub>4</sub> and char yield. Overall, the gas yield varies from 0.50-2.7 m<sup>3</sup>/kg biomass at temperature range of 600-750°C. Conversely, char yield varies in the range of 32.89 g/kg biomass to 21 g/kg biomass at the said temperature range. Gas yield increases as the temperature increases but char yield decreases with increasing temperature due to the char gasification reaction which is an endothermic reaction and dominates at high temperature. Several factors influence the gas yield at high temperature which includes; i) high activity of endothermic reactions (steam methane reforming and char gasification and ii) tar cracking activities which mainly contribute to increase in gaseous product [37].

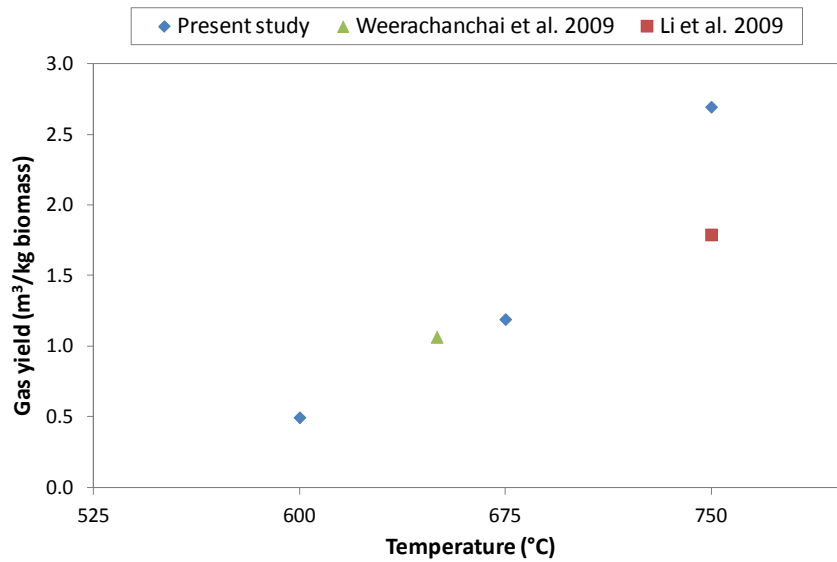


Figure 4.13: Effect of temperature on gas yield

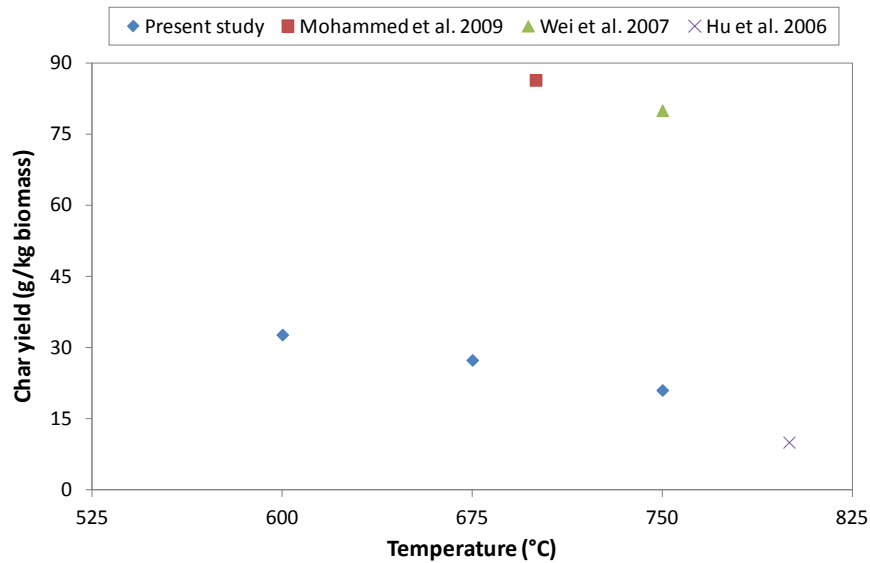


Figure 4.14: Effect of temperature on char yield

The gas and char yield observed are compared with that in the literature as shown in Figures 4.13 and 4.14. The results show that ICA steam gasification provides high gas yield as compared to oil palm waste catalyst steam gasification observed by Li et al. [15] in fixed bed gasifier along with solid cyclone separator, water cooler, final particle separator and gas dryer, and steam gasification with in-situ CO<sub>2</sub> adsorption reported by Weerachanchai et al. [106] utilizing wood chip as the feedstock in fluidized bed gasifier with tar and ice-cold trapping for downstream gas cleaning. Similarly, comparative study of char yield shows that the present study reported

lowest residual char as compared to the study reported by Mohammed et al. [182] using oil palm empty fruit bunch air gasification in fluidized bed gasifier with downstream water cooler and glass wool filter for solid separation, and steam gasification reported by Wei et al. [202] in free-fall reactor with downstream solid cyclone separator, tar trapper and glass wool filter utilizing pine saw dust as the fuel. However, study by Hu et al. [25] observed lowest char yield in catalytic steam gasification of apricot stone in free fall reactor at relatively high temperature of 800°C with downstream dolomite catalyst in the same reactor.

#### *4.5.1.2 Hydrogen Yield*

Figure 4.15 shows the effect of temperature on hydrogen yield. The yields produced are 31.8 g/kg biomass, 80.39 g/kg biomass and 150 g/kg biomass at 600°C, 675°C and 750°C, respectively. The hydrogen yield increases as temperature increases. At high temperature, biomass to gaseous conversion is high and the individual gas component flow rates are higher as compared to that at lower temperature. This can be verified from mass balance analysis (Appendix A). High temperature favors endothermic reaction i.e. methane reforming which forms three molecules of hydrogen for each methane molecule consumed. This can also be observed by lower methane concentration of 10.47 vol% at higher temperature as shown in Figure 4.16. Tar cracking is an endothermic reaction and contributes to an increase in hydrogen content in the product gas. Presence of CO<sub>2</sub> and high CO content resulted in lower composition of hydrogen content at higher temperature.

The increasing trends of hydrogen yield in ICA steam gasification with respect to temperature is also observed in biomass steam gasification [88, 203], biomass catalytic steam gasification [44, 121] and biomass steam gasification with CO<sub>2</sub> adsorbent [37, 86]. Temperature is the most significant process parameter that influences the hydrogen yield in biomass gasification processes.

Hydrogen yield reported in the present study is 150 g H<sub>2</sub>/kg biomass at 750°C as shown in Figure 4.15. The comparison is made with other studies reported in the literature. Study reported by Nipattummakul et al. [88] observed 97.14 g/kg biomass

of H<sub>2</sub> yield using only steam gasification of oil palm empty fruit bunches (EFB) in fixed bed reactor. Hydrogen yield reported by Weerachanchai et al. [106] was based on 85% steam and 15% N<sub>2</sub> as gasification medium at 650°C with in-situ CO<sub>2</sub> adsorbent in fluidized bed gasifier. Study reported by Hu et al. [25] produced hydrogen yield of 130.9 g/kg biomass at high temperature of 850°C in the fixed bed reactor with dolomite as the downstream catalyst. Overall, the present study provides better H<sub>2</sub> yield at low gasification temperature as compared to that reported in the literature.

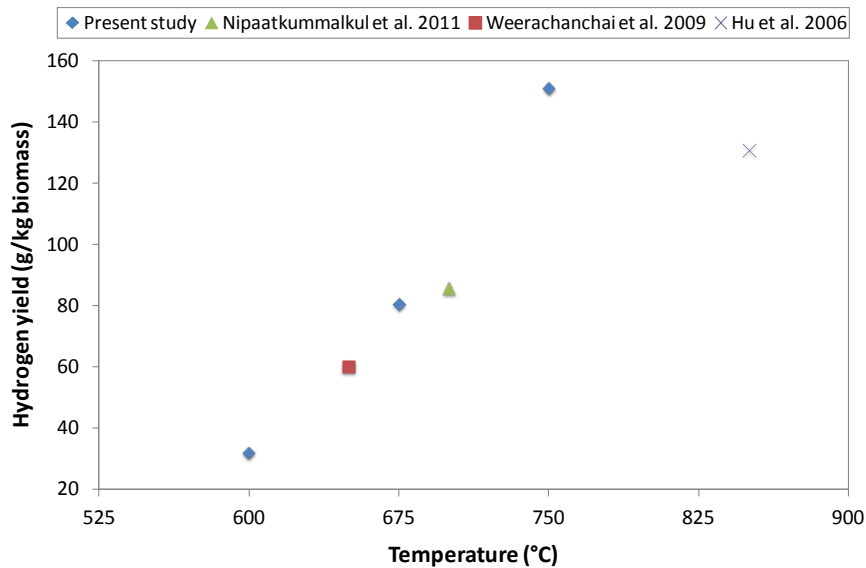


Figure 4.15: Effect of temperature on hydrogen yield

It is concluded that the hydrogen yield is highly dependent on the reactor temperature. Higher temperature (750°C) produces good quantity of hydrogen gas. However, high reactor temperature brings additional energy cost which needs to be optimized for ICA steam gasification system.

#### 4.5.1.3 Product Gas Composition

The product gas compositions at three different temperatures are shown in Figure 4.16. The hydrogen content increases as temperature increases from 600°C to 675°C and then decreases at 750°C. Conversely, carbon monoxide decreases as temperature increases from 600°C to 675°C. This change hydrogen and carbon monoxide content

may be due to high activity of water gas shift reaction in this temperature range. Acharya et al. [37] observed similar trends at temperature range of 600-670°C for white fir steam gasification in presence of CaO.

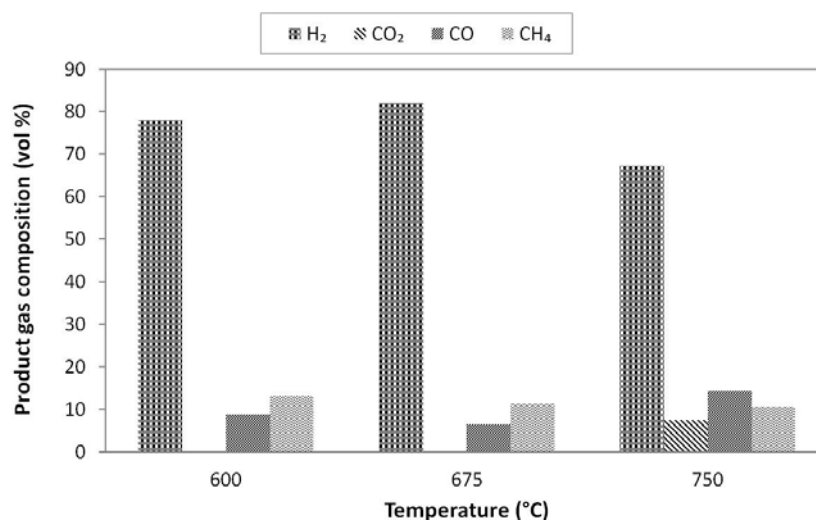


Figure 4.16: Effect of temperature on product gas composition

Additionally, no CO<sub>2</sub> is found at 600°C and 675°C which shows high activity of adsorption reaction ( $\text{CaO} + \text{CO}_2 \rightleftharpoons \text{CaCO}_3$ ). Methane composition in the product gas gradually decreases from 600°C to 750°C. Low CH<sub>4</sub> composition at 750°C shows that the methane steam reforming reaction ( $\text{CH}_4 + \text{H}_2\text{O} \rightleftharpoons \text{CO} + 3\text{H}_2$ ) which is an endothermic reaction and shows less activity at gasification temperature of 600°C and 675°C. At 750°C, hydrogen and methane content decreases while CO and CO<sub>2</sub> increases. High CO<sub>2</sub> composition is due to reversible carbonation reaction that enhances formation of CO<sub>2</sub> ( $\text{CaCO}_3 \rightleftharpoons \text{CO}_2 + \text{CaO}$ ) at high temperature. Xu et al. [56] and Pfeifer et al. [28] observed the onset of calcinations reaction temperatures higher than 727°C and 675°C, respectively. With high CO<sub>2</sub> composition, the CO content in the product gas may increase due to water gas shift reaction. Overall, this increase of CO and CO<sub>2</sub> composition decreases hydrogen content at high temperature. Low activity of water gas shift reaction at high temperature also contributes to decrease in hydrogen content in the product gas. This low activity of exothermic water gas shift reaction is supported by the literature [37]. In the present study, water gas shift reaction is dominant as temperature increases from 600°C to 675°C. The amount of CO increases at high temperature (750°C) due to high reactivity of steam

methane reforming in the presence of Ni catalyst which was not considered in the previous study of in-situ CO<sub>2</sub> adsorbent steam gasification [64].

Figure 4.17 shows the comparison of product gas composition with the literature. Study performed by Han et al. [86] operated at high temperature of 740°C in fluidized bed gasifier and showed similar CH<sub>4</sub> content as observed in the current study operated at relatively lower temperature of 675°C. Li et al. [15] reported the catalytic steam gasification in fixed bed reactor at 800°C utilizing oil palm waste. Lv et al. [126] used air steam gasification in fluidized bed reactor with presence of fixed bed reactor at the downstream operated at 820°C. This study showed lowest CH<sub>4</sub> content in product gas. It can be seen clearly that the present study produces maximum H<sub>2</sub> of 82.11 vol% with no CO<sub>2</sub> in the product gas at relatively low temperature of 675°C.

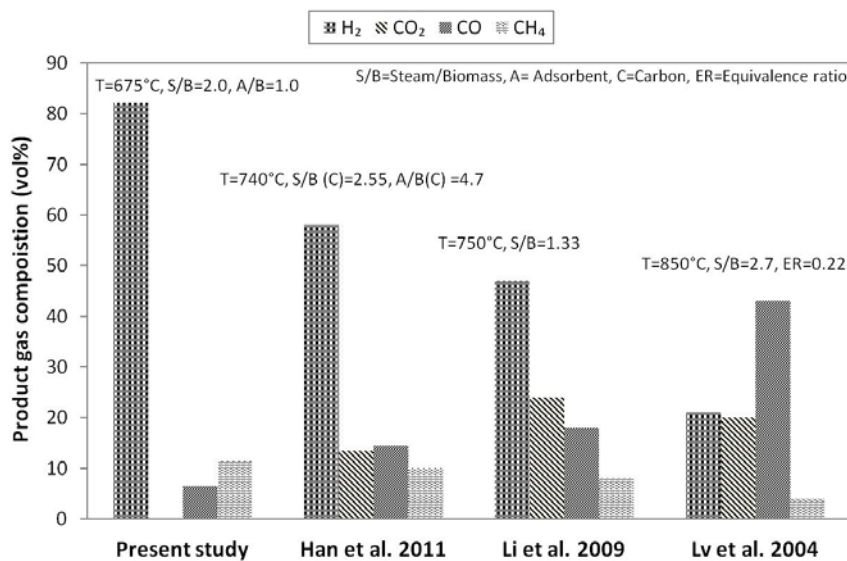


Figure 4.17: Comparative study of product gas composition

These results inferred that the CO<sub>2</sub> capturing favors low reactor temperature of 600-675°C in the presence of catalyst for hydrogen production. This shows that the presence of adsorbent material is found to be more effective at 600-675°C in ICA steam gasification. This low gasification temperature can save additional cost of external energy compare to conventional system operated at high temperature (>800°C). In addition, the present ICA steam gasification system should be operated at lower temperature (<700°C) to avoid reverse carbonation reaction which not only reduces hydrogen gas quality but also produces measurable CO<sub>2</sub> in the product gas.

#### 4.5.1.4 Gasification and Carbon Conversion Efficiency

The values obtained for gasification efficiencies are 12.41%, 25.66% and 111.98% at temperatures of 600°C, 675°C and 750°C, respectively, as shown in Figure 4.18. Similar trend is observed for carbon conversion efficiency but at lower values of 10.73%, 20.96% and 84.41% at the said temperature range. Very low carbon conversion efficiency at 600°C and 675°C is observed due to zero content of CO<sub>2</sub> in the product gas. Low gasification efficiencies associated with palm kernel shell gasification are due to the absence of CO<sub>2</sub> content at temperature of 600°C and 675°C. High gasification and carbon conversion efficiency at 750°C shows high reactivity of endothermic gasification/reforming reactions in ICA steam gasification. Similar observation related to carbon conversion efficiency are reported by Weerachanchai et al. [106] using steam gasification with in-situ CO<sub>2</sub> adsorbent in fluidized bed gasifier in the temperature range of 650-750°C. The trend of gasification efficiency in the present study is also observed by others researchers at temperature range of 700-900°C [91].

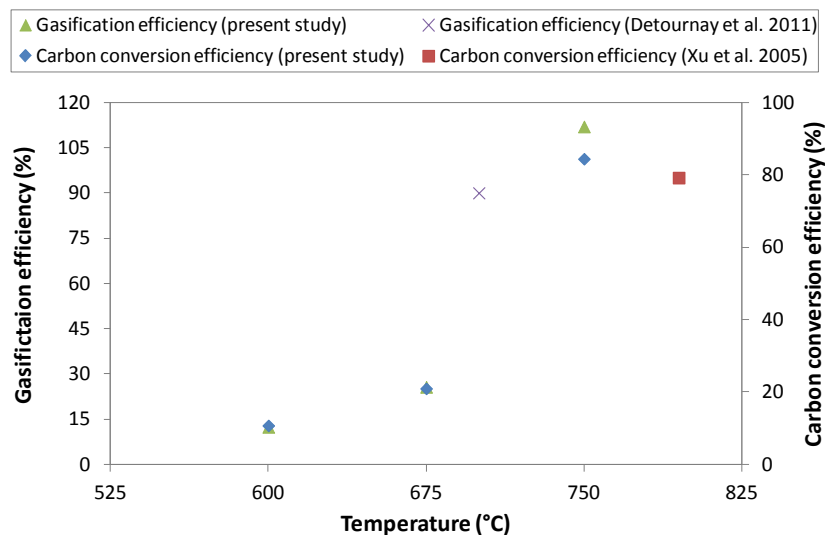


Figure 4.18: Effect of temperature on gasification and carbon conversion efficiency

Figure 4.18 compares the gasification and carbon conversion efficiency produced in present study with works reported by other researchers. Gasification efficiency is rarely reported in the literature for biomass gasification processes. The present study produces gasification efficiency of 112% which is comparable with 108% reported by

Detournay et al. [91] for steam catalytic gasification in fluidized bed gasifier operated with downstream cyclone and water condensation units at temperature of 750°C. Xu et al. [56] reported carbon conversion efficiency of 79.2% at temperature of 795°C in steam gasification with CO<sub>2</sub> adsorbent in the fluidized bed gasifier utilizing cyclone and water condensers in the downstream.

#### 4.5.1.5 Selectivity

Figure 4.19 describes overall selectivity of hydrogen production. The selectivity represents mole flow rate of hydrogen (desired product) over moles flow rates of CO, CO<sub>2</sub>, CH<sub>4</sub> and char (undesired product). Selectivity of 2.19, 3.63 and 2.04 at temperature of 600°C, 675°C and 750°C, respectively, is observed at steam to biomass ratio (S/B) of 2.0, adsorbent to biomass ratio of 1.0 and catalyst to biomass ratio of 0.1. The maximum selectivity of 3.63 is produced at 675°C which is due to the absence of CO<sub>2</sub> content in the product gas. Although, high mole flow rates of H<sub>2</sub> is observed at high temperature of 750°C but production of considerable mole flow rates of CO<sub>2</sub> (10.91 mol/hr) due to the reverse carbonation reaction and high mole flow rates of CO (20.51 mol/hr) decreases overall selectivity to 2.04.

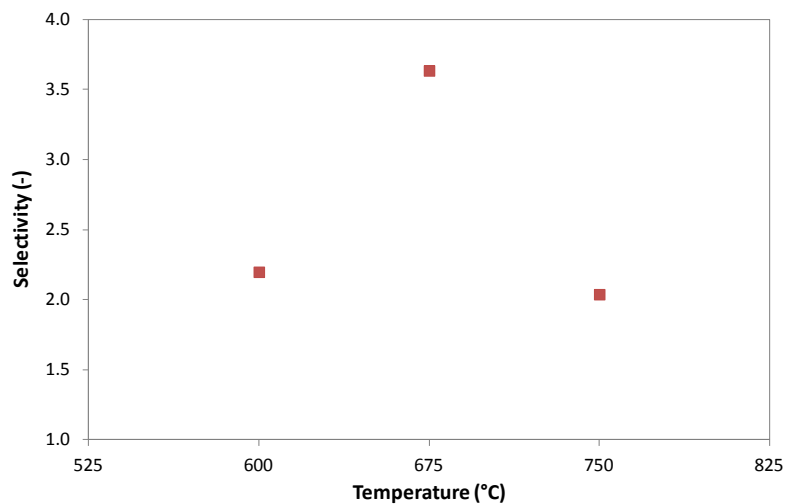


Figure 4.19: Effect of temperature on selectivity

#### 4.5.1.6 Product Gas Heating Values

Figure 4.20 shows the lower heating value ( $LHV_{gas}$ ) and higher heating value ( $HHV_{gas}$ ) of product gas at three different temperatures of 600°C, 675°C, 750°C. The  $LHV_{gas}$  varies from 12.88 MJ/Nm<sup>3</sup> to 14.27 MJ/Nm<sup>3</sup> while  $HHV_{gas}$  is observed in the range of 14.57 MJ/Nm<sup>3</sup> to 16.23 MJ/Nm<sup>3</sup>, respectively. It is observed that the  $LHV_{gas}$  and  $HHV_{gas}$  decrease with increasing temperature from 600-750°C. The maximum values are found at temperature of 600°C. The product gas heating values depend on the composition of hydrogen, carbon monoxide and methane proportions in the product gas. With increasing temperature from 600°C to 675°C, hydrogen composition increases while methane and carbon monoxide content decreases. Similarly, from 675°C to 750°C, hydrogen and methane content decreases while that of CO increases. These different trends of hydrogen, carbon monoxide and methane collectively produce lower values of  $LHV_{gas}$  and  $HHV_{gas}$  at high temperature of 750°C. CH<sub>4</sub> contributes a slightly larger heating values compared to the other two gases based on its higher proportion in Equations 3.25 and 3.26 in Section 3.8.

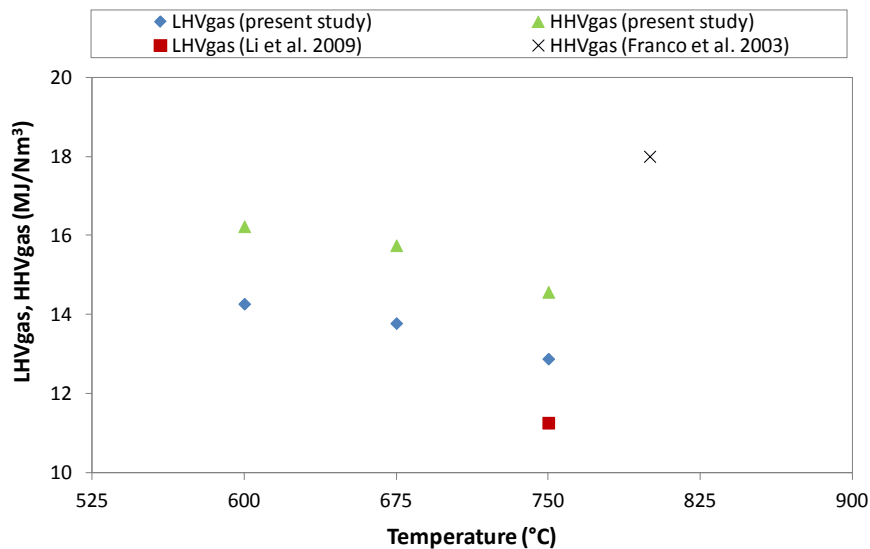


Figure 4.20: Effect of temperature on product gas heating values

As CH<sub>4</sub> content decreases with increasing temperature,  $LHV_{gas}$  and  $HHV_{gas}$  decrease with an increase in temperature. Lower  $LHV_{gas}$  is due to increase in hydrogen composition. The energy content of 10.78 MJ/Nm<sup>3</sup> of hydrogen is lower compared to 35.88 MJ/Nm<sup>3</sup> for CH<sub>4</sub> [204]. This reduces the heating value of the

product gas at 600-675°C. Similar trends for product gas heating values are reported in the literature [204]. In the present study, product gas heating values observed are in medium range of 12-18 MJ/Nm<sup>3</sup>.

Figure 4.20 also shows the comparative study of the LHV<sub>gas</sub>, and HHV<sub>gas</sub> of present work with the literature. The analysis shows that the present study provides good performance of the system in terms of LHV<sub>gas</sub> (14.27 MJ/Nm<sup>3</sup> at 600°C) and HHV<sub>gas</sub> (16.27 MJ/Nm<sup>3</sup> at 600°C) as compared to other studies. Study by Li et al. [15] showed very low LHV<sub>gas</sub> (11 MJ/Nm<sup>3</sup>) was due to the catalytic steam gasification system which produced high CO<sub>2</sub> (24 vol%) and low CH<sub>4</sub> (8 vol%) content in the product gas in the fixed bed gasifier. On the other hand, Franco et al. [83] reported higher values of 18 MJ/Nm<sup>3</sup> at 850°C with only steam gasification in fluidized bed gasifier with cyclone and water condenser in the downstream.

#### 4.5.1.7 Energy Balance

The energy balance over gasifier is carried out at 600°C and 750°C as shown in Figure 4.21 and Figure 4.22. As indicated in Figure 4.21, energy required for gasification process is found to be 3.64 kW which shows that the steam gasification is an endothermic process. Energy associated with PKS is 4.34 kW which makes up maximum proportion of the input energy. On the other hand, energy associated with steam generation is 0.72 kW. This represents only the portion of the energy which has been utilized in the boiler and superheater to rise up the steam temperature to 250°C prior injection to the fluidized bed gasifier. At the outlet of the gasifier, the product gas contributes about 0.21 kW of energy. Major part of energy is released as an unreacted steam in the process which can be optimized through heat integration.

Figure 4.22 illustrates the energy balance at 750°C. The results indicate that gasification energy increased up to 4.74 kW. All other input energy associated with PKS and steam generation is similar in the case of 600°C due to same mass flow rates. The input energy associated with PKS is evaluated based on its heat of formation (based on LHV) and number of moles entering the reactor. The energy release with product gas increases to 2.35 kW. This increase is due to the endothermic

nature of the gasification process which produces higher composition of gaseous product at high temperature. This argument can be justified with energy portion of 7.45 kW leaving as an unreacted steam.

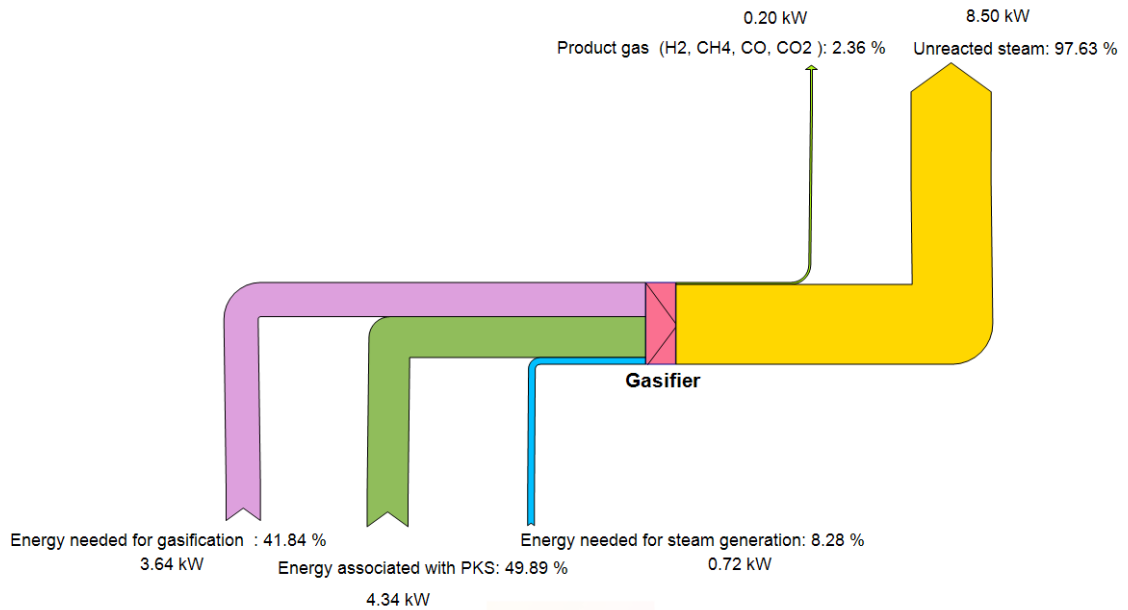


Figure 4.21: Energy balance over gasifier at 600°C

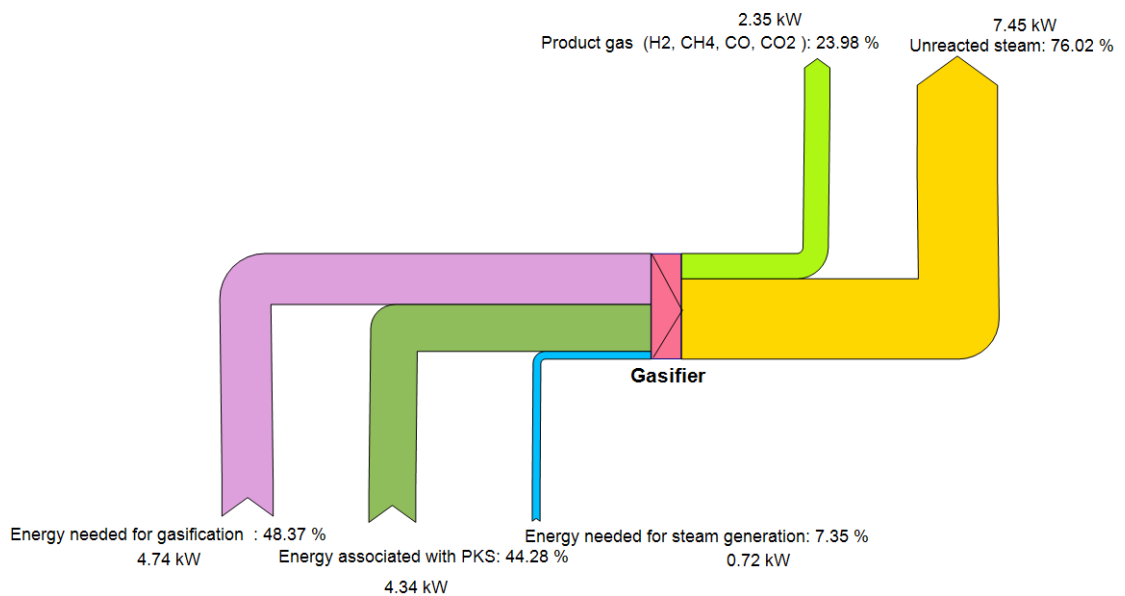


Figure 4.22: Energy balance over gasifier at 750°C

Table 4.20 shows gasification energy required with respect to the reactor temperature. The energy required for gasification increase from 3.64 kW to 4.74 kW by increasing gasifier temperature from 600°C to 750°C. The analysis clearly

indicates that the required energy increases due to endothermic nature of the process. Generally, this energy is utilized to heat up the injected steam to the desired reactor temperature, biomass decomposition and associated endothermic reactions i.e. char gasification and methane reforming. As the temperature of the gasifier increases, energy requirement increases inside the reactor. This increasing energy consumption enhances the product gas yield via endothermic reactions which corresponds to higher energy released in the outlet stream as shown in Figure 4.22. Similarly, high activity of endothermic reactions increase the steam consumption inside the reactor which reduces the energy associated with unreacted steam at the exit of the fluidized bed gasifier. The increase of external energy requirement with increasing gasification temperature is also observed by Franco et al. [83] for biomass steam gasification in fluidized bed gasifier.

Table 4.20: Gasification energy requirement with respect to reactor temperature

Gasification energy require (kW)	Reactor temperature (°C)
3.64	600
4.74	750

#### 4.5.2 Effect of Steam to Biomass Ratio

The amount of steam content in the biomass steam gasification is an important variable not only as the reactant but also as the fluidizing agent. The effect of steam to biomass ratio (wt/wt) was tested at three different levels i.e. 1.5, 2.0 and 2.5.

##### 4.5.2.1 Gas and Char Yield

Figure 4.23 and Figure 4.24 show the effect of S/B ratio on total gas (H<sub>2</sub>, CO, CO<sub>2</sub> and CH<sub>4</sub>) and char yield at temperature of 675°C, adsorbent to biomass ratio of 1.0 and catalyst to biomass ratio of 0.1. Total gas yield is increased from 0.43 m<sup>3</sup>/kg biomass to 1.44 m<sup>3</sup>/kg biomass by varying S/B ratio from 1.5 to 2.5. The subsequent decrease in char yield in the said S/B ratio is observed. The increase in gaseous

product and decrease in solid char with increasing steam content in the gasifier is due to the shift/reforming and char gasification reactions which moves the forward reaction with excess reactant (steam). Similar observation is reported by Herguido et al. [101] and Karmaker et al. [79] for steam gasification in fluidized bed gasifier.

A comparative study is carried out for char and gas yield generated in the present study as shown in Figure 4.23 and Figure 4.24. Acharya et al. [37] observed low gaseous product of  $0.35 \text{ m}^3/\text{kg}$  in steam gasification with in-situ  $\text{CO}_2$  adsorbent at S/B ratio of 1.58 and temperature of  $670^\circ\text{C}$  in fixed bed gasifier. This value is closed to  $0.43 \text{ m}^3/\text{kg}$  observed in the present study at S/B ratio of 1.5 and  $600^\circ\text{C}$ . The difference may be due to the presence of catalyst with  $\text{CO}_2$  adsorption in present study. Li et al. [15] reported  $2.39 \text{ m}^3/\text{kg}$  biomass gas yield at 2.0 S/B ratio and at  $900^\circ\text{C}$  in the catalytic steam gasification in fixed bed gasifier. In spite of similar S/B ratio, higher temperature in the study produced higher gas yield. In the present study, gas yield of  $1.19 \text{ m}^3/\text{kg}$  biomass is produced at S/B ratio of 2.0 which is close to the gas yield of  $1.21 \text{ m}^3/\text{kg}$  biomass reported by Karmaker et al. [79] at 2.0 S/B ratio for steam gasification operating at  $750^\circ\text{C}$  in fluidized bed gasifier. From the discussion, it is concluded that the temperature is more significant variable as compared to the S/B ratio for conversion of biomass into gaseous product. The comparative study of char yield is also carried out. Wei et al. [43] reported char yield of  $30 \text{ g}/\text{kg}$  biomass at S/B ratio of 0.6 and temperature of  $750^\circ\text{C}$  utilizing only steam in a free fall reactor. In spite of low residence time in the reactor and S/B ratio, relatively high temperature was able to produce low char yield. Char yield reported in the present study is closed to a value of  $32.5 \text{ g}/\text{kg}$  biomass at S/B ratio of 1.5 and  $675^\circ\text{C}$  reported by Wei et al. [43]. For higher S/B ratio of 2.5, Herguido et al. [101] reported  $40 \text{ g}/\text{kg}$  biomass char yield at  $750^\circ\text{C}$  in steam gasification operated in fluidized bed gasifier. Relatively high char yield produced by the study [101] was due to biomass steam gasification process. For same S/B ratio, the present study generates lower char yield of  $26 \text{ g}/\text{kg}$  biomass.

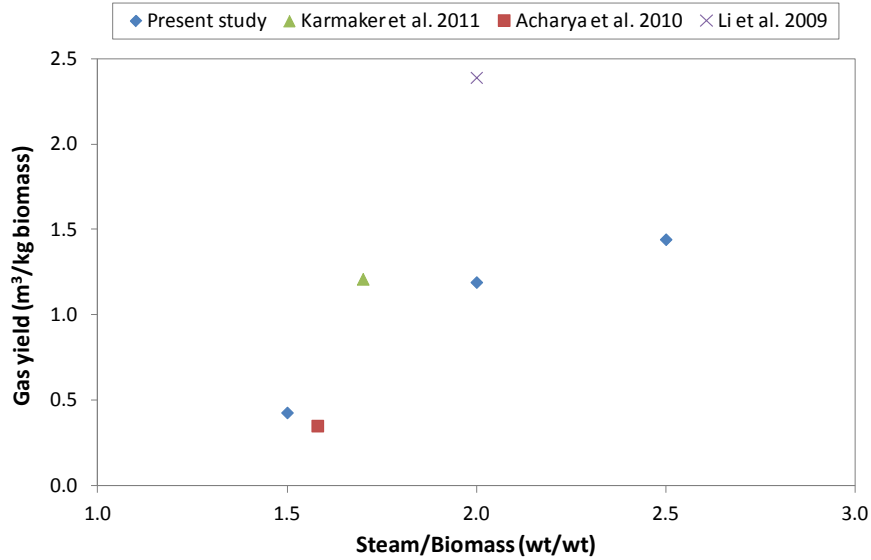


Figure 4.23: Effect of steam to biomass ratio on gas yield

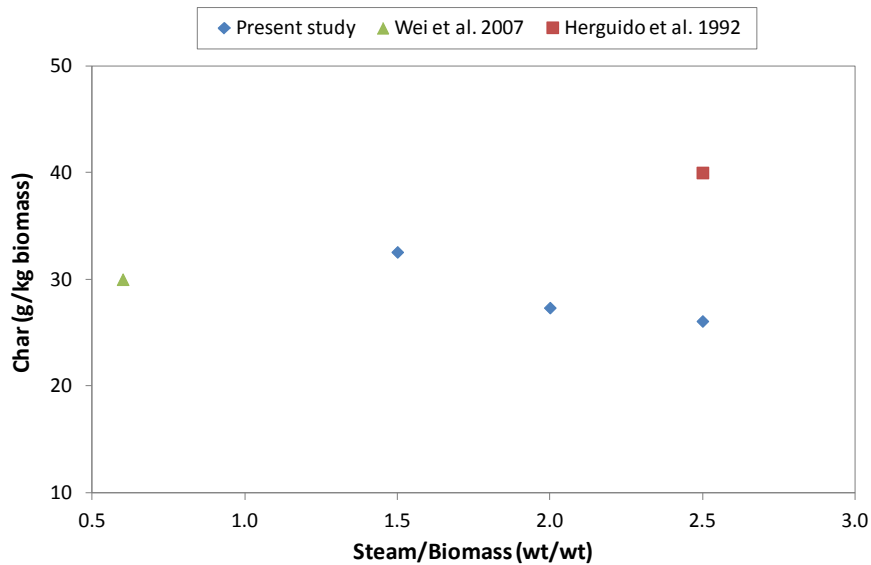


Figure 4.24: Effect of steam to biomass ratio on char yield

#### 4.5.2.2 Hydrogen Yield

Figure 4.25 shows the effect of S/B ratio on H<sub>2</sub> yield. The yield produced at 1.5, 2.0 and 2.5 is 28.69 g/kg biomass, 80.39 g/kg biomass and 97.93 g/kg biomass, respectively. As S/B ratio increases, H<sub>2</sub> yield increases. From S/B ratio of 1.5 to 2.0, H<sub>2</sub> yield increases 2.8 times. However, increase of H<sub>2</sub> yield from 2.0 to 2.5 S/B ratio is only 1.22 fold. This speculation can be made due to the enhance activity of char

gasification, water gas shift and methane reforming reactions with increasing amount of steam in the process. The yield profiles with respect to S/B ratio is well supported by the results reported by Han et al. [86] in fluidized bed gasifier for saw dust steam gasification with CO<sub>2</sub> adsorbent. However, the results provided by another study [37] showed that the H<sub>2</sub> yield decreased with increasing S/B from 0.83 to 1.58. They observed decrease in H<sub>2</sub> yield due to decreased in reactor temperature in the presence of excessive steam in fixed bed reactor. However, in the present study, the temperature inside the fluidized bed gasifier is almost constant (Figures 4.8 and 4.9). The use of fluidized bed reactor keeps the temperature homogeneous due to high heat transfer in fluidizing bed condition.

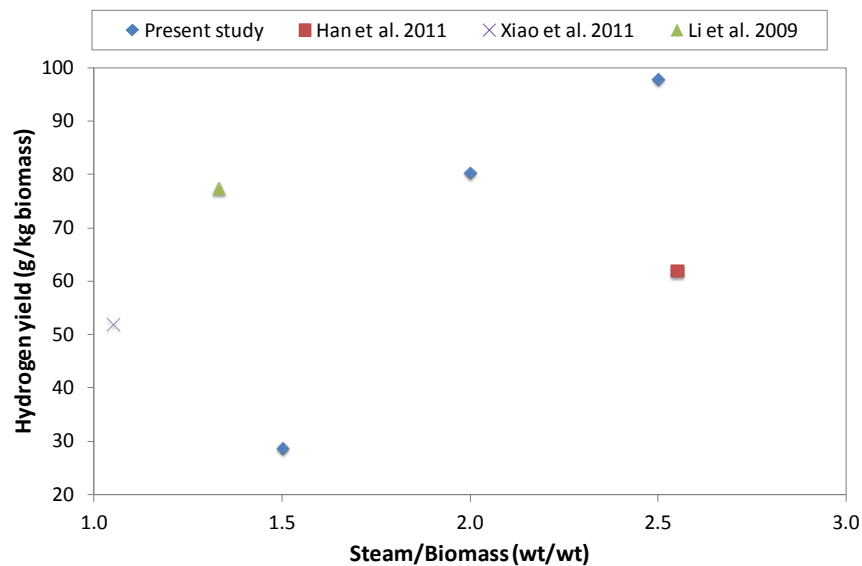


Figure 4.25: Effect of steam to biomass ratio on hydrogen yield

Figure 4.25 also provides comparative study of hydrogen yield with literature. The comparison clearly shows that the ICA steam gasification produces high yield of 97.93 g/kg biomass at 675°C, S/B ratio of 2.5, adsorbent to biomass ratio of 1.0 and catalyst to biomass ratio of 0.1. At similar S/B (carbon) ratio, Han et al. [86] carried out steam gasification with CO<sub>2</sub> adsorbent in fluidized bed gasifier and observed hydrogen yield of 62 g/kg biomass at 740°C with adsorbent/biomass (carbon) ratio of 4.67 (wt/wt). On the other hand, catalytic steam gasification studies reported by Xiao et al. [44] in two stage fluidized bed gasifier and Li et al. [15] in fixed bed gasifier

produced hydrogen yield of 52 g/kg biomass and 77.49 g/kg biomass at S/B ratio of 1.05 and 1.33, and temperature of 630-648°C and 750°C, respectively.

It is found that the hydrogen yield is proportional to S/B ratio. Higher ratio provides better hydrogen yield in the product gas. However, higher ratio carries additional steam into the reactor which needs external energy to be provided at the reactor temperature. It can be seen from the results that the increase of hydrogen yield is not significant from 2.0-2.5 of S/B ratio. Therefore, for hydrogen yield, the optimum S/B ratio is found to be 2.0 in ICA steam gasification utilizing PKS as the feedstock.

#### *4.5.2.3 Product Gas Composition*

In Figure 4.26, product gas compositions are plotted at three different S/B ratios. By increasing S/B ratio from 1.5 to 2.5, H<sub>2</sub> composition in the product gas increases from 80.87 vol% to 82.61 vol%. The overall increase of H<sub>2</sub> composition with increasing S/B ratio shows the activity of char gasification reaction, water gas shift reaction and steam methane reforming. This evidence is supported by several studies related to biomass catalytic steam gasification [44, 119] and biomass steam gasification in the presence of CO<sub>2</sub> adsorbent [21, 86]. In the present study, no significant increase in H<sub>2</sub> composition at S/B ratio of 2.0 to 2.5 is observed. Similar observation is found by several other researchers [21, 86]. The CO<sub>2</sub> composition increases from 0 to 8 vol% at S/B ratio of 2.0 to 2.5. This increase is due to the high activity of water gas shift reaction in the presence of high amount of steam in the process. This can be justified by increase in H<sub>2</sub> and decrease in CO composition in the product gas. Similar trends are observed by Acharya et al. [37]. CO composition is gradually decreased from 10.49 vol% to 5.45 vol% at 1.5 to 2.5 of S/B ratio. This decrease eventually shows the increase in H<sub>2</sub> composition which gives the high activity of water gas shift reaction. However, no significant rise in CO composition (6.45 vol% to 5.45 vol%) is observed at S/B ratio of 2.0 to 2.5. No CO<sub>2</sub> is detected at S/B ratio of 1.5 to 2.0 which apparently shows the presence of strong adsorption activity of CaO in spite of high CO<sub>2</sub> composition present in the stream due to water gas shift reaction. On the other hand, CH<sub>4</sub> composition increases from 8.63 vol% to

11.43 vol% within S/B ratio of 1.5 to 2.0, and then decreases to 3.95 vol% at 2.5. Lowest CH<sub>4</sub> composition at higher S/B ratio shows the effectiveness of methane reforming reaction in the presence of excess steam.

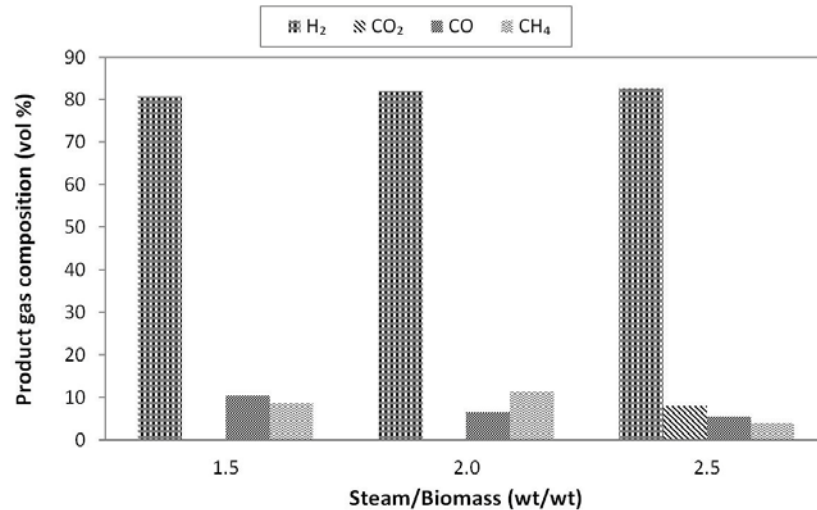


Figure 4.26: Effect of steam to biomass ratio on product gas composition

Based on the results, S/B ratio is an important parameter for enhance H<sub>2</sub> composition in the product gas. Higher the ratio, higher is the H<sub>2</sub> concentration in the product gas. However, high S/B ratio resulted in energy penalty in the system by generating large amount of steam which is not likely to be recovered if the steam condensation occurred. Based on this argument, S/B ratio must be optimized for steam gasification system to produce H<sub>2</sub> rich gas for economical operation of the gasification system. Based on the results, the optimum value of S/B ratio identified is 2.0.

Figure 4.27 illustrates the comparison of hydrogen composition of present study with other researchers. In the present study, hydrogen composition of 82.61 vol% is observed at temperature of 675°C, S/B ratio of 2.5, adsorbent to biomass ratio of 1.0 and catalyst to biomass ratio of 0.1. The study reported by Salleh et al. [205] observed hydrogen composition of 69 vol% at relatively higher temperature of 850°C utilizing air gasification in fluidized bed gasifier. Work reported by Xiao et al. [44] carried out steam gasification in fluidized bed gasifier at S/B ratio of 0.7 and 630-648°C. The hydrogen content in the product gas reported was 60 vol%. Han et al. [86] produced hydrogen composition of 58 vol% at S/B (carbon) of 2.55 in steam gasification with

CO<sub>2</sub> adsorbent in fluidized bed gasifier. Overall, air gasification in fluidized bed gasifier produced good hydrogen composition in the product gas but at the expense of higher temperature operation (850°C). On the other hand, steam gasification produced relatively good hydrogen composition at lower temperature (630-675°C).

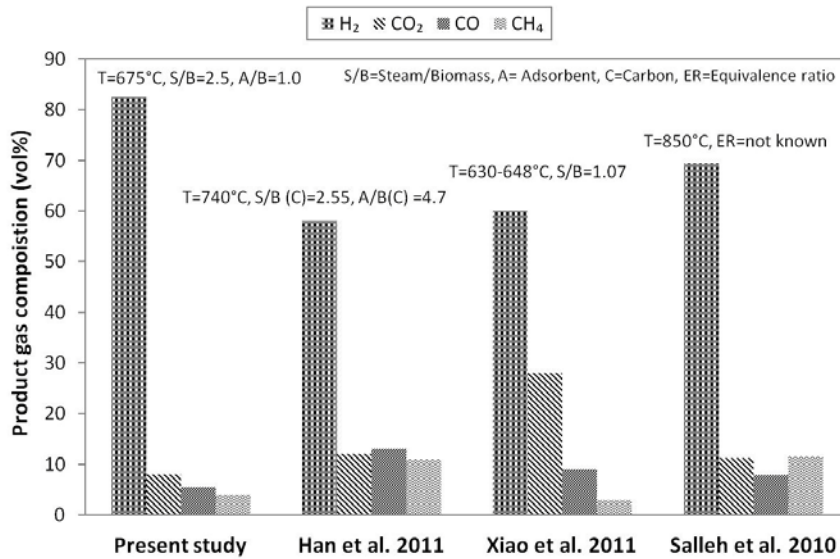


Figure 4.27: comparative study of product gas composition

The comparative study shows that the combination of adsorbent and catalyst in steam gasification of PKS increases hydrogen content to a better extent at high S/B ratio (2.50-2.55) as compared to steam catalytic [44] and steam gasification with in-situ CO<sub>2</sub> adsorbent [86].

#### 4.5.2.4 Gasification and Carbon Conversion Efficiency

Gasification and carbon conversion efficiencies are plotted against S/B ratio of 1.5, 2.0 and 2.5 in Figure 4.28. As shown, S/B ratio has proportional effect on both efficiencies. Gasification efficiency depicted is 10.34%, 25.66% and 43.08% at three S/B ratios. Similarly, carbon conversion efficiency increases while increasing S/B ratio. The values reported are 8.03%, 20.96% and 24.66% at S/B ratio of 1.5, 2.0 and 2.5, respectively. However, rise in carbon conversion efficiency is not significant when S/B values are increased from 2.0 to 2.5. This may be due to the decrease in composition of CH<sub>4</sub> and CO. Slightly increase in efficiency comes from considerable CO<sub>2</sub> content which appears at S/B ratio of 2.5. Meanwhile, gasification efficiency

depicted is 10.34%, 25.66% and 43.08% at S/B ratio of 1.5 to 2.5. This shows gradual increase in gasification efficiency as the amount of steam increases. Unlike carbon conversion efficiency, gasification efficiency increases at S/B ratio of 2.0 to 2.5. This may be due to the compensation of total moles of the product gas by the number of moles of CO<sub>2</sub>. Conversely, number of moles of CO and CH<sub>4</sub> decreased by varying S/B ratio from 2.0 to 2.5 while number of moles of H<sub>2</sub> are almost constant. This difference comes from the fact that the gasification efficiency was calculated based on the number of moles of the product gas where as conversion efficiency was calculated based on mass of the product gas. Similar trends are reported for gasification efficiency at variable S/B ratio from 0.5 to 2.0 [91], and carbon conversion efficiency at variable range of 0.5 to 4.2 [206] and 0.73 to 2.10 [112].

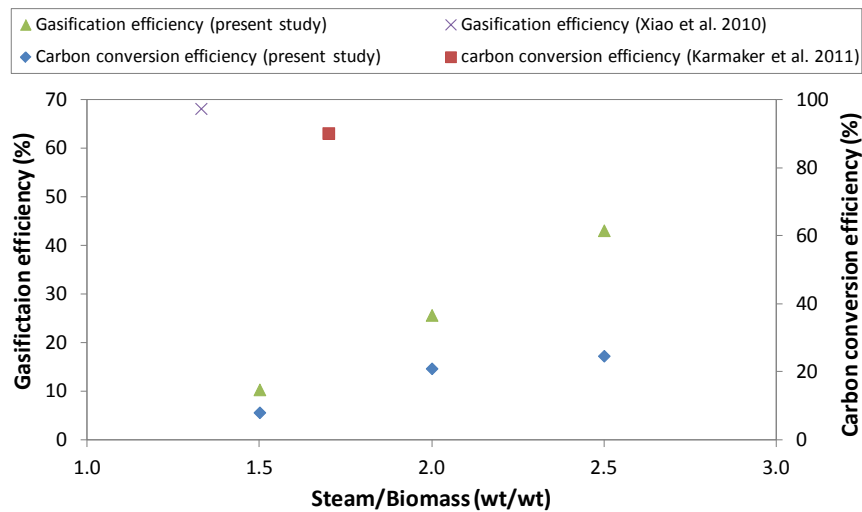


Figure 4.28: Effect of steam to biomass ratio on gasification and carbon conversion efficiency

As mentioned, gasification and carbon conversion efficiency observed are 43.08% and 24.66%, respectively. The gasification and carbon conversion efficiencies are compared with other researcher's findings as shown in Figure 4.28. The gasification and carbon conversion efficiencies reported by Karmaker et al. [79] in steam gasification and Xiao et al. [121] in catalytic steam gasification are higher compared to the present study. They reported gasification efficiency of 68.14% at S/B ratio of 1.3, temperature of 639°C, and carbon conversion efficiency of 90.11% at S/B ratio of 1.7, and temperature of 750°C, respectively. This is due to the lower CO<sub>2</sub> composition

of 7.9 vol% at S/B ratio of 2.5 in present study while Karmaker et al. [79] and Xiao et al. [121] found CO<sub>2</sub> composition of 24.81 vol% and 30.77 vol% in the product gas, respectively. Moreover, lower CO content of 5.45 vol% in the present study contributes to low gasification and carbon conversion efficiencies while concentration of CO reported by Karmaker et al. [79] and Xiao et al. [121] were 17.38 vol% and 10.07 vol%, respectively.

#### 4.5.2.5 Selectivity

Figure 4.29 illustrates the effect of steam to biomass ratio on the overall selectivity. The results show that the selectivity increases with increasing steam to biomass ratio in ICA steam gasification. The excess steam in the gasification process drives the water gas shift, methane reforming and char gasification reactions toward H<sub>2</sub> production. The increase in selectivity from 2.23 to 3.63 is observed at S/B ratio of 1.5 to 2.0. However, the increase of selectivity from 3.63 to 3.93 at S/B ratio of 2.0 to 2.5 is not significant. This is due to excess steam (2700 g/h) available at low feed rate of biomass (1100 g/h). This shows that the S/B ratio of 2.0 is suitable to obtain good selectivity values of 3.63 in ICA steam gasification.

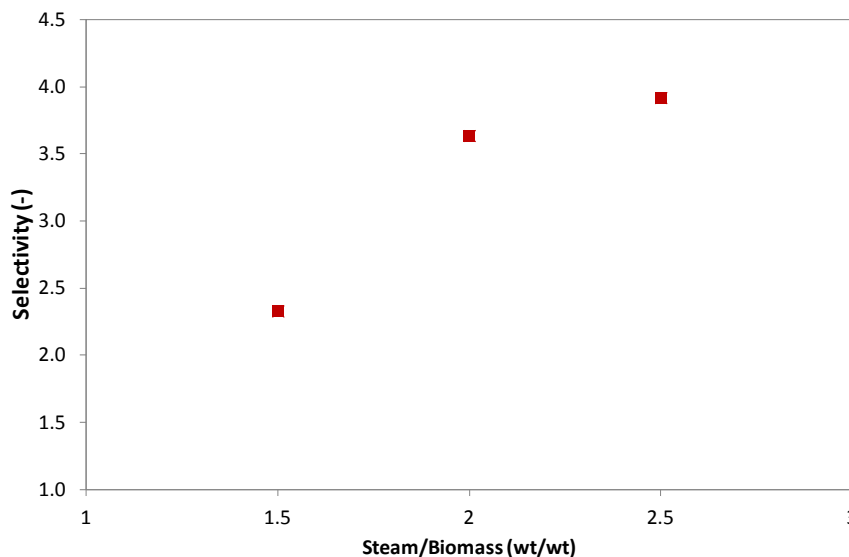


Figure 4.29: Effect of steam to biomass ratio on selectivity

#### 4.5.2.6 Product Gas Heating Values

Figure 4.30 shows the lower heating values ( $LHV_{gas}$ ) and higher heating values ( $HHV_{gas}$ ) of product gas by varying ratio of 1.5 to 2.5 of S/B. The values reported for  $LHV_{gas}$  are  $13.14 \text{ MJ/Nm}^3$ ,  $13.78 \text{ MJ/Nm}^3$  and  $11.02 \text{ MJ/Nm}^3$  while  $HHV_{gas}$  values produced are  $14.99 \text{ MJ/Nm}^3$ ,  $15.75 \text{ MJ/Nm}^3$  and  $12.71 \text{ MJ/Nm}^3$ . The results show that the  $LHV_{gas}$  and  $HHV_{gas}$  increases with S/B ratio of 1.5 to 2.0 and then decreases at S/B ratio of 2.5. The product gas heating values are contributed largely by the composition of  $H_2$ ,  $CO$  and  $CH_4$ . At S/B ratio of 2.5,  $CH_4$  and  $CO$  content decreases while  $H_2$  content slightly increases thus lowers the heating values of the product gas. This decreasing trend of product gas heating values is observed in other studies by Li et al. [15], Pfeifer et al. [204] and Kinoshita et al. [207]. The  $LHV_{gas}$  and  $HHV_{gas}$  reported by Li et al. [15] in biomass catalytic gasification and Karmaker et al. [79] in biomass steam gasification were  $8.73 \text{ MJ/Nm}^3$  and  $11.18 \text{ MJ/Nm}^3$ , respectively. The  $LHV_{gas}$  and  $HHV_{gas}$  observed under current study are in the range of  $11.02 \text{ MJ/Nm}^3$ - $13.14 \text{ MJ/Nm}^3$  and  $12.71 \text{ MJ/Nm}^3$ - $15.75 \text{ MJ/Nm}^3$ , respectively, which are higher than that reported values in the literature at S/B ratio of 2.5.

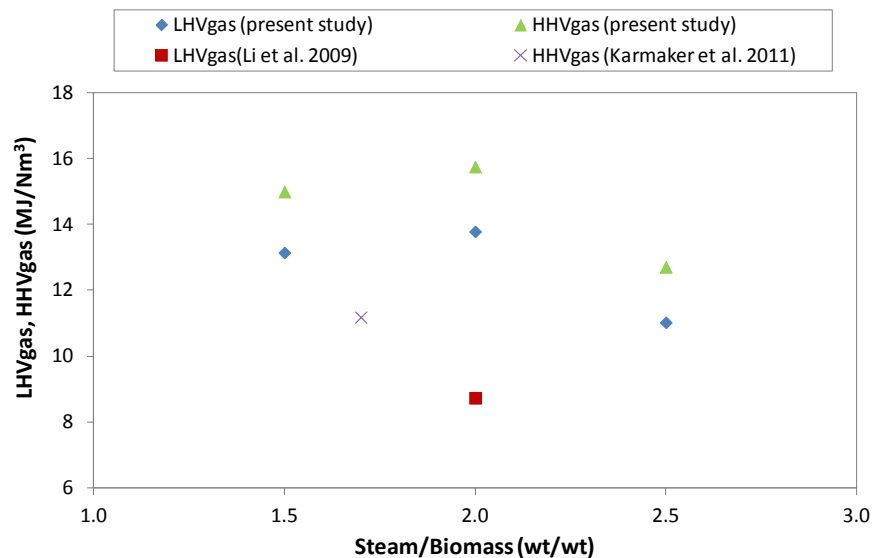


Figure 4.30: Effect of steam to biomass ratio on product gas heating values

#### 4.5.2.7 Energy Balance

The energy balance is performed on the gasifier by varying S/B ratio from 1.5 to 2.5 as shown in Figure 4.31 and Figure 4.32, respectively. In the present study, biomass flow rate is varied from 1100 g/h to 1800 g/h with constant flow rate of steam at 2700 g/h. By keeping constant steam flow rate, the fluidization velocity is constant even though the S/B ratio is changing from 1.5 to 2.5. At S/B ratio of 1.5 (Figure 4.31), the energy required for gasification process is 1.81 kW. At biomass flow rate of 1800 g/h, energy associated with PKS contributes about 5.79 kW. Steam generation consumes about 0.72 kW of energy. At the outlet of the gasifier, major part of the energy is released as an unreacted steam and contributes about 8.08 kW of energy.

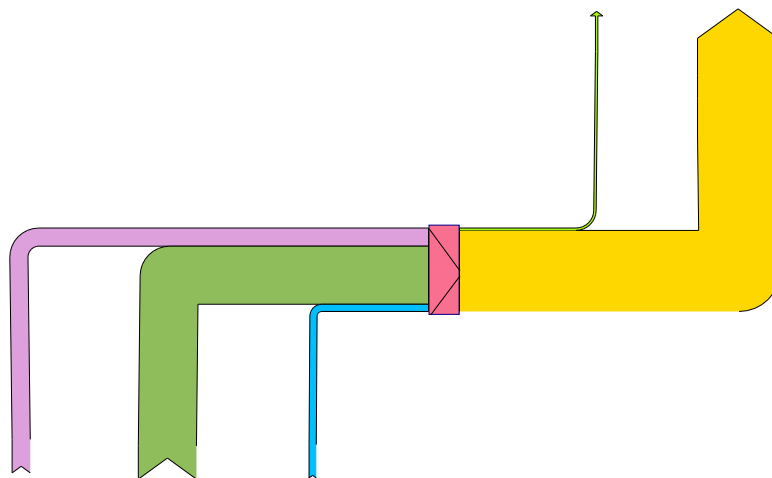


Figure 4.31: Energy balance over gasifier at steam to biomass ratio of 1.5

The energy balance at inlet and outlet streams at S/B ratio of 2.5 for ICA is shown in Figure 4.32. The results show that the energy required for gasification reactions is increased to 5.14 kW. But energy input associated with PKS (1100 g/h) decreases when S/B ratio is 1.5 at constant flow rate of steam. Total product gas is increased (Appendix A) and thus energy released with the gas is also increased to 0.91 kW. This increase is due to the excess steam (2700 g/h) available for gasification/ reforming reactions in the presence of catalyst and CO<sub>2</sub> adsorbent in the system.

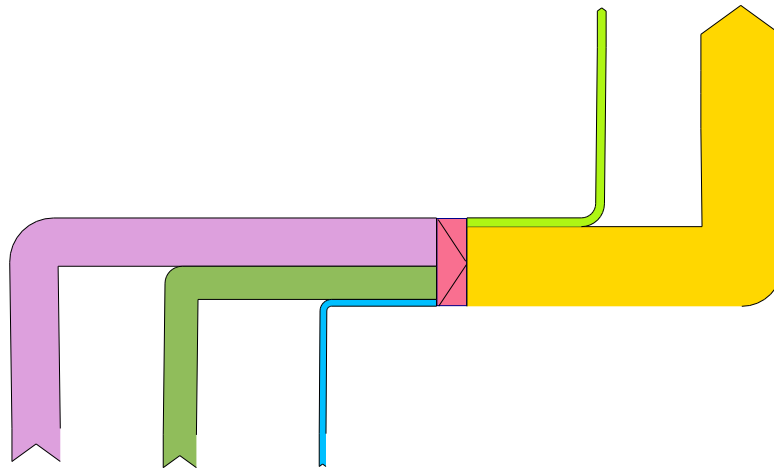


Figure 4.32: Energy balance over gasifier at steam to biomass ratio of 2.5

Table 4.21 shows the relationship of gasification energy required with respect to the S/B ratio. The required energy increases from 1.81 kW to 5.14 kW by varying S/B ratio from 1.5 to 2.5. High steam content relates to more energy requires to maintain the desired reactor temperature. This high steam content (S/B=2.5) enhances the gasification and reforming reaction in the reactor and collectively produce high gas yield compared to lower steam content (S/B=1.5). This can be justified with high energy associated with product gas. The findings are similar to that reported by other researchers at S/B ratio of 0.5-0.8 (wt/wt) and temperature of 800°C [83].

Table 4.21: Gasification energy requirement with respect to steam to biomass ratio

Gasification energy require (kW)	Steam to biomass ratio (wt/wt)
1.81	1.5
5.14	2.5

### 4.5.3 Effect of Adsorbent to Biomass Ratio

The effect of adsorbent (CaO) to biomass (A/B) ratio on performance parameters such as char and gas yield, hydrogen yield, product gas composition, gasification and carbon conversion efficiency, gas heating values and selectivity is carried out at temperature of 675°C, S/B ratio of 2.0 and catalyst to biomass ratio of 0.1. The adsorbent to biomass ratio tested in the present study is 0.5, 1.0 and 1.5.

#### 4.5.3.1 Gas and Char Yield

Figures 4.33 and 4.34 show the effect of A/B ratio on the gas (H<sub>2</sub>, CO, CO<sub>2</sub>, and CH<sub>4</sub>) and char yield. The rate of gas and char yield is represented as m<sup>3</sup>/kg biomass and g/kg biomass, respectively. Overall, the gas yield varies from 0.63 m<sup>3</sup>/kg biomass to 1.31 m<sup>3</sup>/kg biomass at A/B ratio of 0.5-1.5. The increase in product gas yield is about 1.9 times by varying A/B ratio of 0.5 to 1.0. By varying A/B ratio from 1.0 to 1.5, the total gas yield increases in parallel with an increase of 60 vol% to 82.11 vol% of hydrogen composition. The char yield continues to decrease from 62.98 g/kg biomass to 23.62 g/kg biomass at A/B ratio of 0.5 to 1.5.

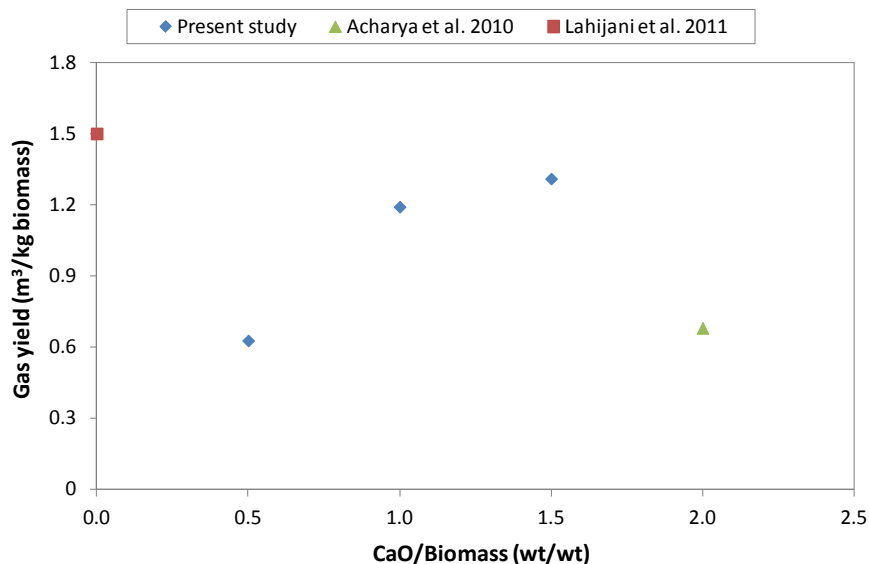


Figure 4.33: Effect of adsorbent to biomass ratio on gas yield

Since the A/B ratio from 1.0 to 1.5 does not show significant effect on gas and char yield, an optimum value of A/B ratio of 1.0 is sufficient for good performance of the fluidized bed gasifier.

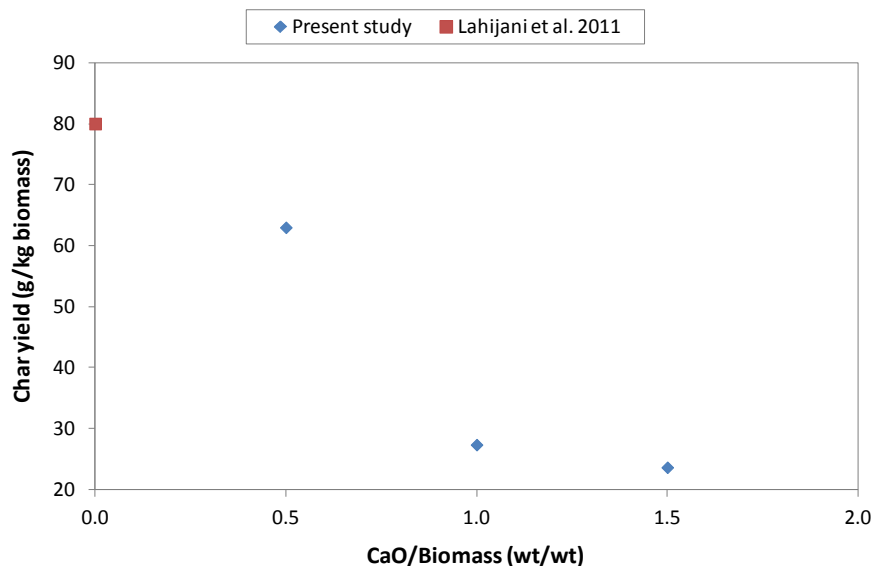


Figure 4.34: Effect of adsorbent to biomass ratio on char yield

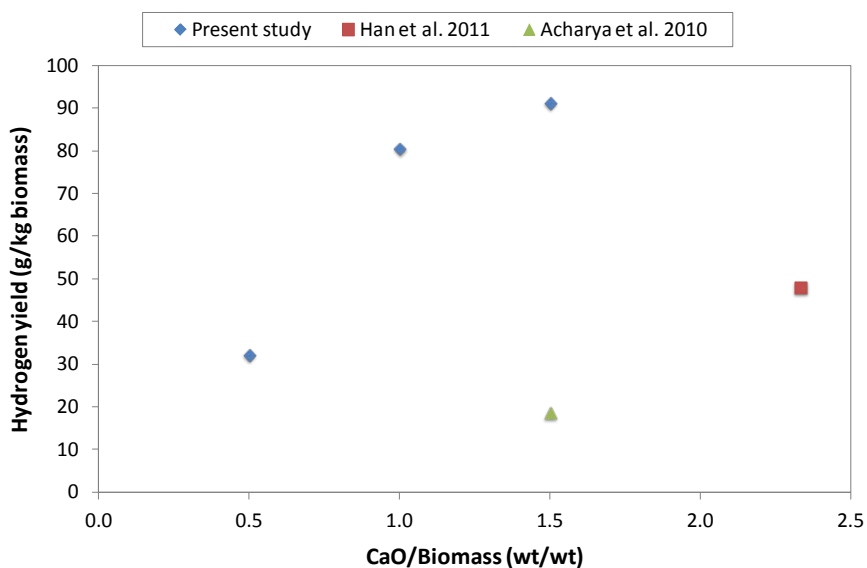


Figure 4.35: Effect of adsorbent to biomass ratio on hydrogen yield

#### 4.5.3.2 Hydrogen Yield

Figure 4.35 shows the effect of A/B ratio on H<sub>2</sub> yield. The yields produced at 0.5, 1.0 and 1.5 are 32.89 g/kg of biomass, 80.39 g/kg biomass and 91.11 g/kg of biomass, respectively. As A/B increases, H<sub>2</sub> yield increases. H<sub>2</sub> yield increases about 2.5 times at varying A/B ratio of 0.5 to 1.0. However, the increase of H<sub>2</sub> yield from 1.0 to 1.5 is only 1.33 times due to the enhance activity of water gas shift and methane reforming

reactions. The profiles of H<sub>2</sub> yield with respect to A/B are also observed in other studies [37, 208]. Han et al. [86] and Acharya et al. [37] reported 48 g/kg of biomass and 18 g/kg biomass of hydrogen yield in fluidized bed and fixed bed gasifier at A/B ratio of 2.33 and 1.5, respectively.

#### *4.5.3.3 Product Gas Composition*

Figure 4.36 compares the product gas composition at different adsorbent to A/B ratio. The results show that the addition of CaO gradual increases H<sub>2</sub> content in the product gas. For A/B ratio of 0.5 to 1.0, the composition of H<sub>2</sub> increases from 62.52-82.11 vol%. This composition is further increased from 82.11 to 84.86 vol% at A/B ratio of 1.0 to 1.5. The increase of adsorbent (CaO) in the system facilitates more CO<sub>2</sub> adsorption and lowers its partial pressure in the system via water gas shift reaction. This shifts the reaction in forward direction and produces more hydrogen. This speculation can be justified by observing the decrease of CO concentration from A/B ratio of 0.5 to 1.5. The presence of CaO enhances the activity of steam methane reforming which causes an increase of H<sub>2</sub> fraction in product gas [57]. CH<sub>4</sub> composition in the product gas decreases with increasing A/B ratio from 0.5 to 1.5. CO<sub>2</sub> composition is highest at A/B ratio of 0.5 which reduces to negligible value at 1.0 ratio of A/B and slightly increases to 1.1 vol% at A/B ratio of 1.5. The increase in CO<sub>2</sub> composition in the presence of excess CaO (A/B=1.5) is due to water gas shift reaction. H<sub>2</sub> is found to be increased while CO to be decreased. The increase of H<sub>2</sub> composition with increasing A/B ratio is also observed by other researchers [37, 86].

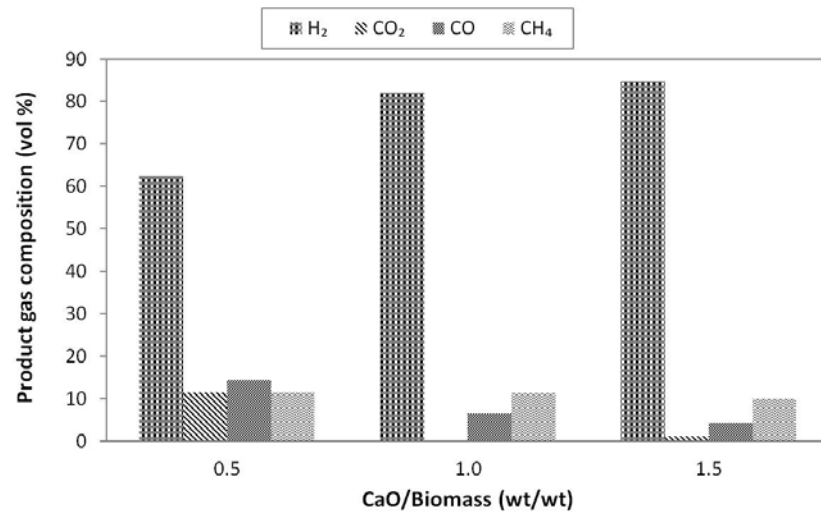


Figure 4.36: Effect of adsorbent to biomass ratio on product gas composition

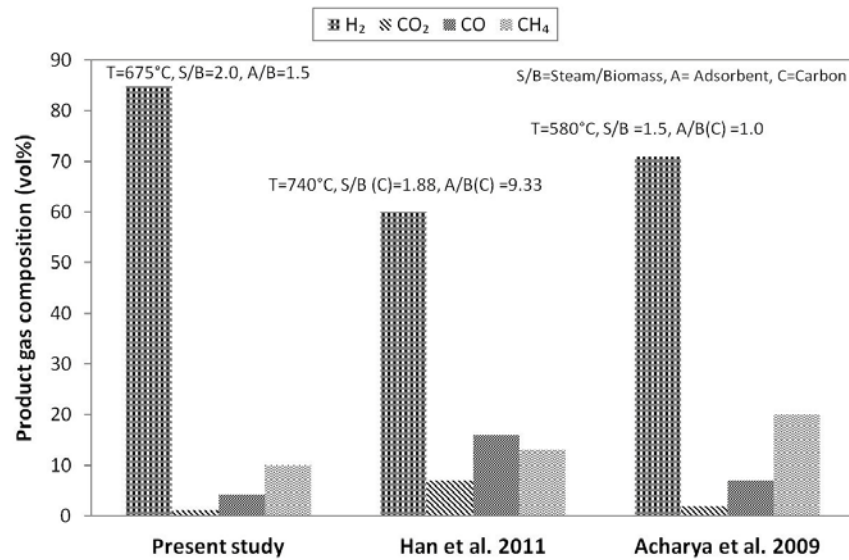


Figure 4.37: Comparative study of product gas composition

Figure 4.37 shows the comparative study of the gas composition with the literature findings. In the present study, highest H<sub>2</sub> composition of 84.11 vol% is observed at A/B ratio of 1.5, S/B ratio of 2.0, catalyst/biomass ratio of 0.1 and temperature of 675°C. Acharya et al. [197] studied the steam gasification with presence of CO<sub>2</sub> adsorbent at A/B ratio of 1.0, S/B ratio of 1.5 and temperature of 580°C in a fluidized bed reactor with adsorbent regenerator. The hydrogen content of 71 vol% was observed. In addition, low CO<sub>2</sub> concentration of 1.1 vol% is also

observed in the present work. The value observed is negligible to 2 vol% and 7 vol% reported by Acharya et al. [197] and Han et al. [86], respectively.

#### 4.5.3.4 Gasification and Carbon Conversion Efficiency

Gasification and carbon conversion efficiencies with respect to A/B ratio of 0.5, 1.0 and 1.5 are given in Figure 4.38. Initially, carbon conversion efficiency decreases from 23.12% to 20.60% at varying A/B ratio of 0.5 to 1.5. This is due to the reduction of CO<sub>2</sub> and CO composition in the product gas at A/B ratio of 0.5 to 1.5. The gasification efficiency is decreased from 31.15% to 25.66% by varying A/B ratio from 0.5 to 1.0. The efficiency increases slightly from 25.66% to 27.21% at 1.0-1.5 of ratio A/B. The decrease is due to the combine effect of reduction in CO<sub>2</sub> and CO composition. The increase in gasification efficiency from 1.0 to 1.5 of A/B ratio can be explained based on the slight increase of CO<sub>2</sub> and H<sub>2</sub> content in the product gas.

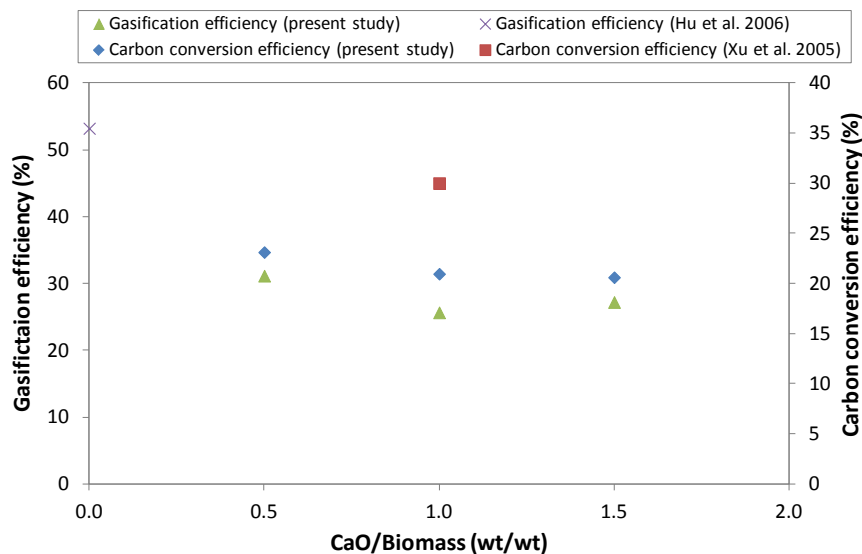


Figure 4.38: Effect of adsorbent to biomass ratio on gasification and carbon conversion efficiency

Figure 4.38 compares the gasification and carbon conversion efficiency produced in the present study with similar works reported by other researchers. In the present study, the maximum gasification and carbon conversion efficiencies observed are 31.15% and 23.12% at A/B ratio of 0.5 and temperature of 675°C, respectively. Xu et

al. [56] observed carbon conversion efficiency of 24% at A/B ratio of 1.0 and temperature of 722°C in fluidized bed gasifier. For gasification efficiency of catalytic steam gasification, Hu et al. [25] reported a value of 50.3% at 800°C using fluidized bed gasifier.

#### 4.5.3.5 Selectivity

Figure 4.39 describes the effect of adsorbent to biomass ratio on overall selectivity of hydrogen. The selectivity of 1.07, 3.63 and 4.43 is observed at adsorbent to biomass ratio of 0.5, 1.0 and 2.5, respectively, at temperature of 675°C, S/B ratio of 2.0 and catalyst to biomass ratio of 0.1. Maximum selectivity of 4.43 is produced at higher A/B ratio of 1.5. The CaO presence captures CO<sub>2</sub> and enhances activity of shift, reforming and gasification reactions towards hydrogen production.

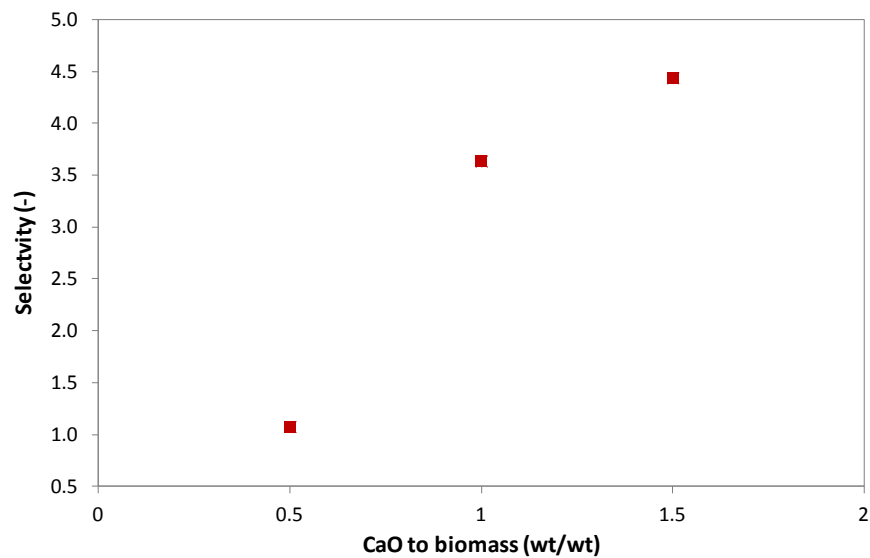


Figure 4.39: Effect of adsorbent to biomass ratio on selectivity

#### 4.5.3.6 Product Gas Heating Values

Figure 4.40 shows the lower values heating values (LHV<sub>gas</sub>) and higher heating values (HHV<sub>gas</sub>) of product gas at varying A/B ratio of 0.5 to 1.5. The values reported for LHV<sub>gas</sub> are 12.72 MJ/Nm<sup>3</sup>, 13.78 MJ/Nm<sup>3</sup>, and 13.34 MJ/Nm<sup>3</sup> at A/B ratios of 0.5,

1.0 and 1.5 respectively. The  $\text{HHV}_{\text{gas}}$  generated are  $14.35 \text{ MJ/Nm}^3$ ,  $15.75 \text{ MJ/Nm}^3$  and  $15.32 \text{ MJ/Nm}^3$  for the range of A/B ratio studied. The  $\text{LHV}_{\text{gas}}$  value is not affected by varying A/B ratio. Similar results are also observed for  $\text{HHV}_{\text{gas}}$ . The A/B ratio of 1.0 to 1.5 only increases  $0.44 \text{ MJ/Nm}^3$  and  $0.43 \text{ MJ/Nm}^3$  in  $\text{LHV}_{\text{gas}}$  and  $\text{HHV}_{\text{gas}}$ , respectively. This is due to small variation in the composition of  $\text{CH}_4$ ,  $\text{H}_2$  and  $\text{CO}$  at varying A/B ratio of 1.0 to 1.5. The high  $\text{HHV}_{\text{gas}}$  value of  $20.51 \text{ MJ/Nm}^3$  is reported by Xu et al. [56] utilizing steam- $\text{O}_2$  mixture as gasifying agent with in-situ  $\text{CO}_2$  adsorption in fluidized bed gasifier. Conversely,  $\text{LHV}_{\text{gas}}$  value of  $11.26 \text{ MJ/Nm}^3$  is observed by Li et al. [15] in catalytic steam gasification due to steam methane reforming reaction that lowered the  $\text{CH}_4$  composition in the product gas. This value is close to  $\text{LHV}_{\text{gas}}$  value of  $12.72\text{-}13.34 \text{ MJ/Nm}^3$  observed in the present study.

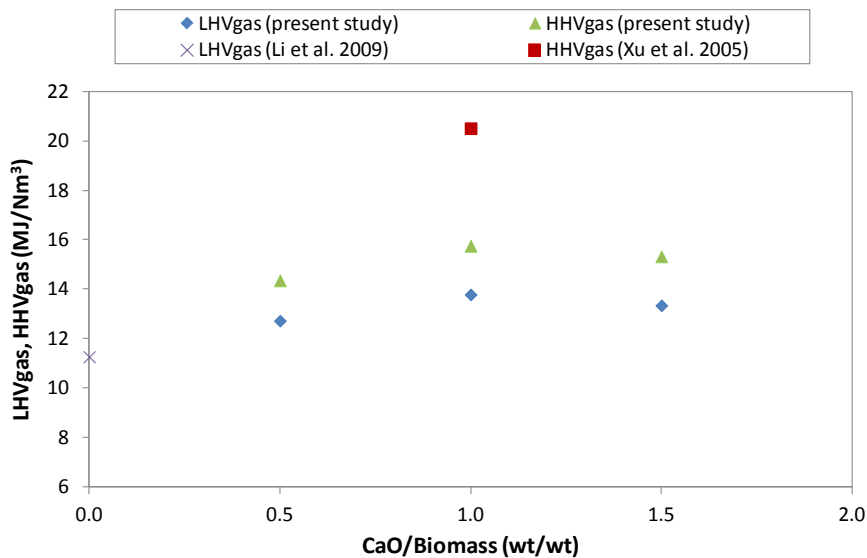


Figure 4.40: Effect of adsorbent to biomass ratio on product gas heating values

#### 4.5.3.7 Energy Balance

The energy balance is conducted for the gasifier system by varying the ratio of A/B from 0.5 to 1.5. The biomass flow rate is constant at  $1350 \text{ g/h}$  with constant steam flow rate of  $2700 \text{ g/h}$ . At A/B ratio of 0.5 (Figure 4.41), the required energy for gasification process is found to be  $3.95 \text{ kW}$ . Energy input associated with PKS at the inlet stream contributes to about  $4.34 \text{ kW}$  which corresponds to maximum portion of energy at the input stream. Energy consumed for steam generation is  $0.72 \text{ kW}$ . At the

outlet of the gasifier, major part of the energy is released as an unreacted steam and contributes to about 8.17 kW. The mixture of the product gas which consists of  $H_2$ ,  $CO$ ,  $CO_2$  and  $CH_4$  provides 0.84 kW of energy.

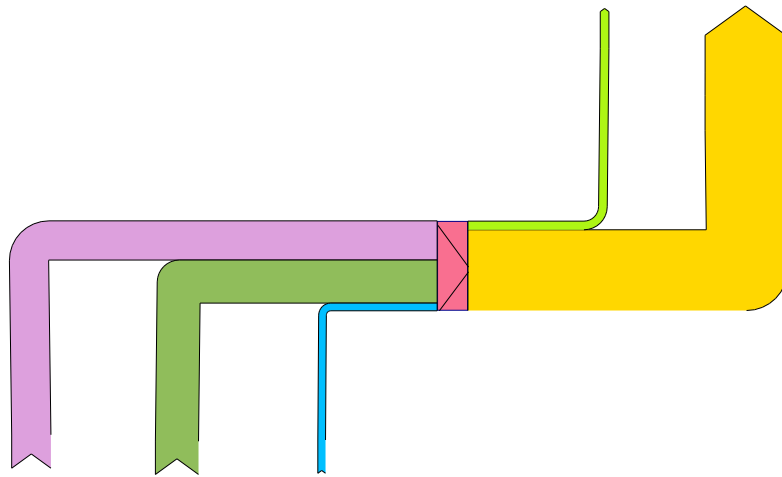


Figure 4.41: Energy balance over gasifier at adsorbent to biomass ratio of 0.5

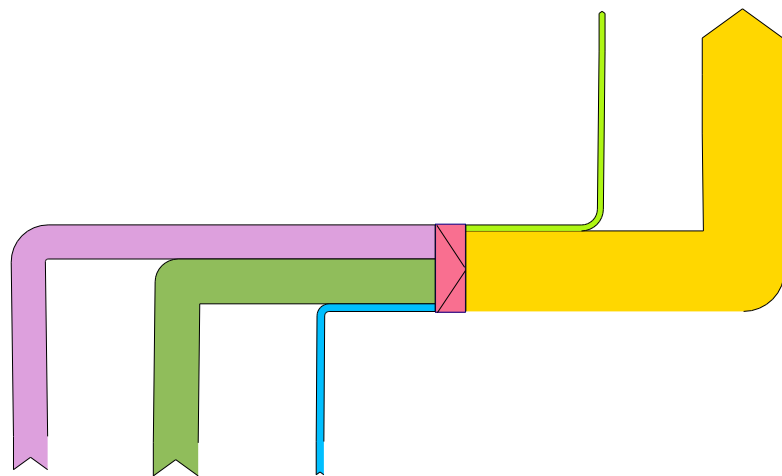


Figure 4.42: Energy balance over gasifier at adsorbent to biomass ratio of 1.5

Figure 4.42 demonstrates the energy balance at inlet and outlet streams at A/B ratio of 1.5. The results show that the energy required for gasification reactions decrease from 3.95 kW to 3.31 kW while increasing A/B ratio of 0.5 to 1.5. The energy input associated with PKS and steam generation is similar at A/B ratio of 1.5.

It appears that the energy of the product gas decreases from 0.84 to 0.54 kW while increasing A/B ratio. This decrease is due to capturing of CO<sub>2</sub> by the large amount of adsorbent available in ICA steam gasification process.

Table 4.22 depicts the gasification energy required with respect to A/B ratio. It decreases from 3.95 kW to 3.31 kW by varying the A/B ratio from 0.5 to 1.5. This decrease is due to the high activity of CO<sub>2</sub> adsorption reaction in the presence of excess amount of adsorbent. The CO<sub>2</sub> adsorption reaction is an exothermic reaction and hence reduces the overall energy requirement in the process. Similar findings is observed by Pfeifer et al. [96] in dual fluidized bed gasification system. In their case study, the energy requirement for absorption enhanced reforming (AER) of steam gasification was lower than the conventional dual fluidized bed steam gasification process. It can be concluded that the CO<sub>2</sub> adsorption reaction is not only enhanced H<sub>2</sub> content but also reduced the external energy requirement of the ICA steam gasification system.

Table 4.22: Gasification energy requirement with respect to adsorbent to biomass ratio

Gasification energy require (kW)	Absorbent to biomass ratio (wt/wt)
3.95	0.5
3.31	1.5

#### 4.5.4 Effect of Fluidization Velocity

Fluidized bed gasifier operates in bubbling fluidizing region in the current study. The fluidization velocities ( $U$ ) vary in the range of 3-5 times of minimum fluidization velocity ( $U_{mf}$ ). The effect of  $U$  is tested for  $3U_{mf}$ ,  $4U_{mf}$  and  $5U_{mf}$  which give 0.15 m/s, 0.21 m/s and 0.26 m/s of steam velocities acting as the gasifying agent. For constant steam to biomass ratio of 2.0, biomass flow rate is varied from 1000 g/h to 1700 g/h. The temperature of the gasifier is kept at 675°C. In addition, the adsorbent to biomass ratio of 1.0 and catalyst to biomass ratio of 0.1 are set for all the experimental runs at different fluidization velocity.

#### 4.5.4.1 Gas and Char Yield

Figures 4.43 and 4.44 show the effect of fluidization velocity on gas yield and char yield. Overall, the gas yield varies from 0.76 m<sup>3</sup>/kg biomass to 0.44 m<sup>3</sup>/kg biomass while varying fluidization velocity from 0.15 m/s to 0.21 m/s. The total gas yield increase to 1.0 m<sup>3</sup>/kg biomass by varying fluidization velocity from 0.21 m/s to 0.26 m/s. The gas yield is the lowest at 0.21 m/s due to the complete CO<sub>2</sub> adsorption in the process.

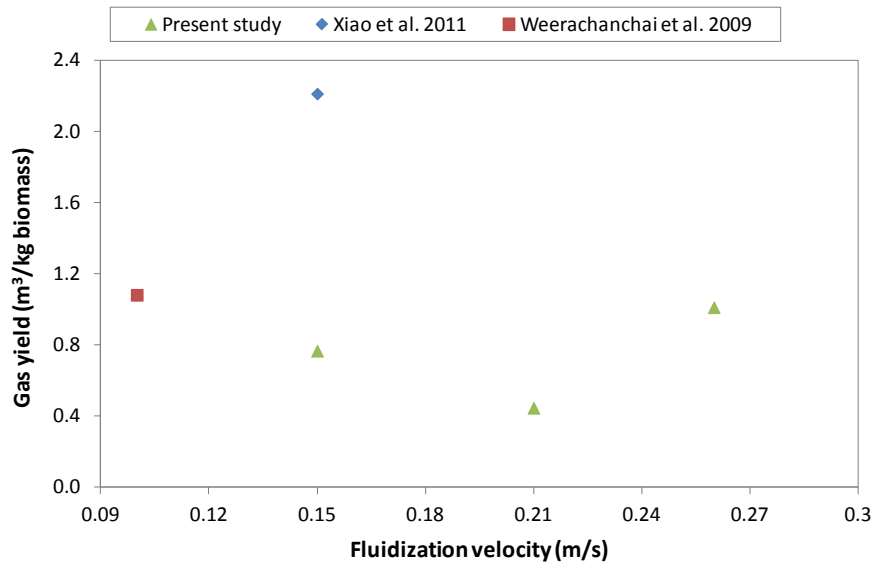


Figure 4.43: Effect of fluidization velocity on gas yield

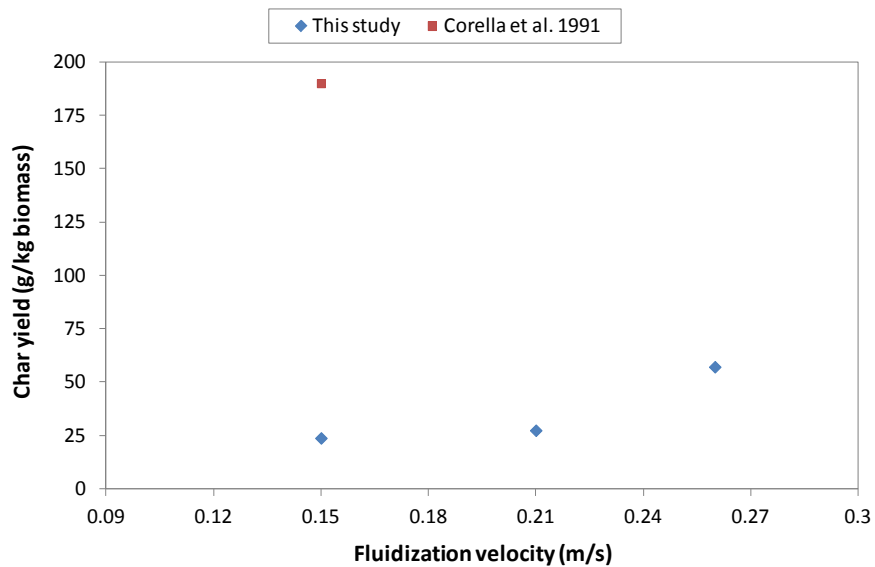


Figure 4.44: Effect of fluidization velocity on char yield

The char yield increases from 23.73 g/kg biomass to 57.09 kg/biomass as shown in Figure 4.44. The increase of char yield with respect to fluidization velocity is due to decrease in residence time of steam in the reactor with increasing fluidization velocity. Higher biomass flow rates resulted in higher char yield in the system whereas low residence time of steam resulted in containing observation.

Figure 4.43 shows that the high gas yield of 2.21 m<sup>3</sup>/kg biomass reported by Xiao et al. [44] was based on the two stage catalytic steam gasification process in fluidized bed gasifier at fluidization velocity of 0.15 m/s ( $3U_{mf}$ ) and 700°C. The study produced significant amount of CO<sub>2</sub> (25 vol%) in the product gas as compared to the findings of the present study (9.48 vol%). On the other hand, previous study reported by Weerachanchai et al. [106] produced gas yield of 1.08 m<sup>3</sup>/kg biomass in steam gasification with CO<sub>2</sub> adsorption at fluidization velocity of 0.1 m/s ( $5U_{mf}$ ) and 650°C, which is closed to the gas yield of 0.76 m<sup>3</sup>/kg biomass produced in present study. Higher char yield of 190 g/kg biomass is reported by Corella et al. [125] at fluidization velocity of 0.15 m/s ( $3U_{mf}$ ) and 760°C in biomass steam gasification process in fluidized bed gasifier. The possible reason for high char yield in the study was due to low steam to biomass ratio of 0.89 (wt/wt) and feeding biomass from the top of fluidized bed reactor which offered less residence time to solid char particles in the reactor.

#### 4.5.4.2 Hydrogen Yield

Figure 4.45 shows the effect of fluidization velocity on H<sub>2</sub> yield. The yields generated are 42.32 g/kg of biomass, 80.39 g/kg biomass and 47.96 g/kg of biomass at fluidization velocities of 0.15 m/s, 0.21 m/s and 0.26 m/s, respectively. All experiments are operated at 675°C, S/B ratio of 2.0, adsorbent to biomass ratio of 1.0 and catalyst to biomass ratio of 0.1. The results indicate that the H<sub>2</sub> yield increases initially from 42.32 g/kg biomass to 80.39 g/kg biomass by varying fluidization velocity from 0.15 m/s to 0.21 m/s and then drops to 47.96 g/kg of biomass at fluidization velocity of 0.26 m/s. Maximum yield is produced at 0.21 m/s which shows highest activity of CaO (adsorbent). The CO<sub>2</sub> adsorption process derives the water gas shift and gasification/reforming reactions towards hydrogen rich gas

production. The higher is the adsorbent activity, the better is the yield and higher the composition of H<sub>2</sub> in the product gas.

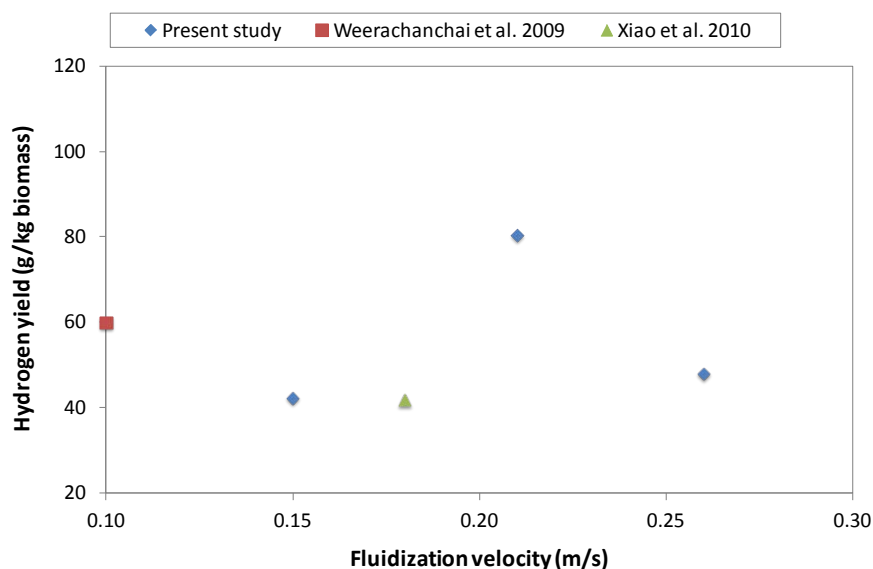


Figure 4.45: Effect of fluidization velocity on hydrogen yield

For steam gasification with CO<sub>2</sub> adsorbent, hydrogen yield of 60 g/kg biomass is reported by Weerachanchai et al. [106] in the fluidized bed gasifier which does lie in the range of hydrogen yield observed at fluidization velocity of 0.15 to 0.21 m/s in the present study (Figure 4.45). On the other hand, Xiao et al. [121] carried out two stage catalytic steam gasification in fluidized bed gasifier and claimed hydrogen yield of 41.8 g/kg of biomass at a fluidization velocity of 0.18 m/s and temperature of 639°C. At similar fluidization conditions, lesser hydrogen yield observed by the study [121] may be due to low reactor temperature of 639°C.

#### 4.5.4.3 Product Gas Composition

Figure 4.46 compares the product gas composition at different fluidization velocity. The H<sub>2</sub> content in the product gas is 67.24 vol%, 82.11 vol% and 57 vol% at 0.15 m/s, 0.21 m/s and 0.26 m/s, respectively. The results show that the maximum H<sub>2</sub> content is observed at medium velocity (0.21 m/s) which is equal to 4 times the minimum fluidization velocity. At velocity lower and higher than the medium velocity produce lower H<sub>2</sub> composition in the product gas. The similar statement is

also true for CO and CH<sub>4</sub> content in the product gas. For CO<sub>2</sub> content, optimal fluidization velocity is 0.21 m/s (medium), followed by the fluidization velocity of 0.26 m/s which results in CO<sub>2</sub> composition of 4 vol% in the product gas. On the other hand, the highest CO<sub>2</sub> content of 9.48 vol% is observed at lower velocity of 0.15 m/s. The fluidization velocity of steam from 0.21 to 0.26 m/s increases the CO<sub>2</sub> content due to less residence time for CO<sub>2</sub> to react with CaO adsorbent in the gasifier. Similar observation is reported by Han et al. [86] for biomass steam gasification with the presence of CO<sub>2</sub> adsorbent in fluidized bed gasifier. This can be justified by the large amount of CO present in the product gas. High CO<sub>2</sub> concentration at low fluidization velocity of 0.15 m/s is due to low fluidizing conditions which results ineffective mixing between the adsorbent (bed material), upcoming steam and gaseous product in the bed.

Based on the discussion, it can be concluded that the steam fluidization velocity ranging from 3-4 $U_{mf}$  which is equal to 0.15 m/s to 0.21 m/s velocity produce better H<sub>2</sub> content in the product gas.

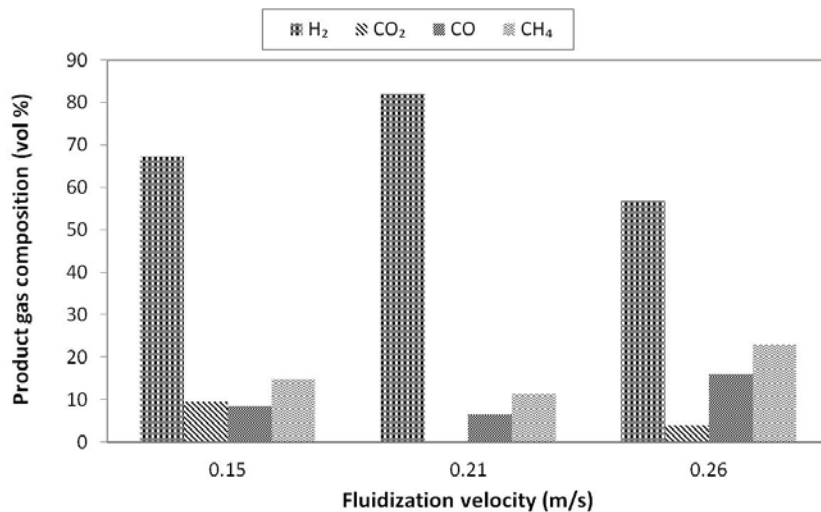


Figure 4.46: Effect of fluidization velocity on product gas composition

Figure 4.47 describes the comparative study with other researcher's findings. In the present study, hydrogen composition of 67.24 vol% is achieved at fluidization velocity of 0.15 m/s (3 $U_{mf}$ ), temperature of 675°C, S/B ratio of 2.0, and adsorbent to biomass ratio of 1.0 and catalyst to biomass ratio of 0.1. In previous studies reported by Weerachanchai et al. [106] and Xiao et al. [121], they observed hydrogen

composition of 63.57 vol% and 54.7 vol% at fluidization velocity of 0.1 m/s ( $5U_{mf}$ ) and 0.15 ( $2U_{mf}$ ) m/s, respectively. Similar hydrogen composition observed by Weerachanchai et al. [106] in steam gasification with  $\text{CO}_2$  adsorbent which was due to the same bed particles (calcined limestone,  $\text{CaO}$ ) and temperature ( $650^\circ\text{C}$ ). Xiao et al. [121] used steam catalytic gasification with different bed material ( $\text{Ni-Al}_2\text{O}_3$ ) and lower temperature of  $639^\circ\text{C}$ .

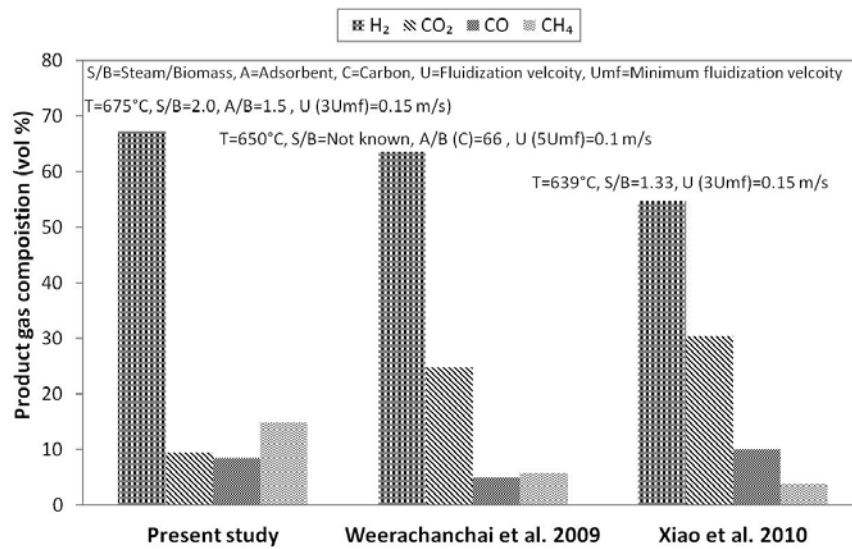


Figure 4.47: Comparative study of product gas composition

#### 4.5.4.4 Gasification and Carbon Conversion Efficiency

Figure 4.48 shows the effect of fluidization velocities i.e. 0.15 m/s, 0.21 m/s and 0.26 m/s on gasification and carbon conversion efficiencies. Initially, carbon conversion efficiency decreases from 24.67% to 20.60% while varying velocity from 0.15 m/s to 0.21 m/s. This is due to the reduction of  $\text{CO}_2$  composition in the product gas. Reduction in carbon conversion efficiency is due to the decrease in  $\text{CO}$  content at 0.15 m/s to 0.21 m/s. At higher fluidization velocity of 0.26 m/s, the conversion increased to 41.95%. This increase is mainly due to high  $\text{CH}_4$ ,  $\text{CO}$  and sufficient  $\text{CO}_2$  content in the product gas at 0.26 m/s (Figure 4.46).

Based on the results, highest conversion efficiency is observed at highest fluidization velocity. Similar trend is also observed for gasification efficiency. The gasification efficiency obtained is 31.99%, 25.66% and 42.95% at 0.15 m/s, 0.21 m/s

and 0.26 m/s, respectively. Similar gasification efficiencies are observed by Weerachanchai et al. [106] for steam gasification with CO<sub>2</sub> adsorbent.

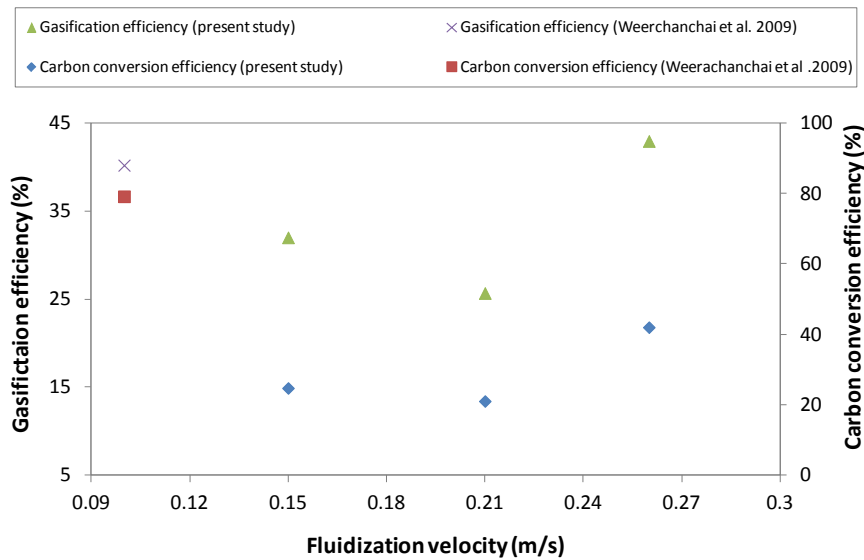


Figure 4.48: Effect of fluidization velocity on gasification and carbon conversion efficiency

#### 4.5.4.5 Selectivity

Figure 4.49 shows the overall selectivity of hydrogen production with respect to fluidization velocity. The selectivity of 1.72, 3.63 and 1.07 is generated at fluidization velocities of 0.15 m/s, 0.21 m/s and 0.26 m/s, respectively. Maximum selectivity of 3.63 is produced at 0.21 m/s ( $4U_{mf}$ ) which represents the intermediate value of the fluidization velocity. The lower value of 1.07 of selectivity is observed at higher fluidization velocity of 0.26 m/s. Low residence time of gasifying agent and product gas at higher fluidization velocity resulted in less hydrogen production. The CO<sub>2</sub> capturing process is inefficient while char gasification and steam methane reforming reactions are dominant.

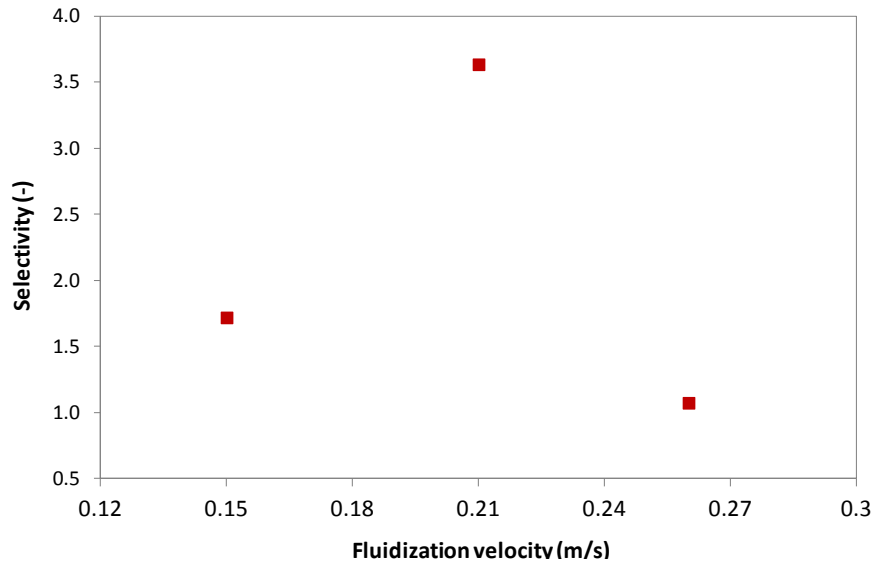


Figure 4.49: Effect of fluidization velocity on selectivity

#### 4.5.4.6 Product Gas Heating Values

Figure 4.50 shows the lower heating values ( $LHV_{\text{gas}}$ ) and higher heating values ( $HHV_{\text{gas}}$ ) at varying fluidization velocity of 0.15 ( $3U_{mf}$ ), 0.21 m/s ( $4U_{mf}$ ) and 0.26 m/s ( $5U_{mf}$ ). The  $LHV_{\text{gas}}$  reported are  $13.64 \text{ MJ/Nm}^3$ ,  $13.78 \text{ MJ/Nm}^3$ , and  $17.02 \text{ MJ/Nm}^3$  at the defined fluidization velocities. The  $HHV_{\text{gas}}$  values generated are  $15.47 \text{ MJ/Nm}^3$ ,  $15.75 \text{ MJ/Nm}^3$  and  $19.04 \text{ MJ/Nm}^3$ . The  $LHV_{\text{gas}}$  and  $HHV_{\text{gas}}$  are in a narrow range at 0.15 m/s and 0.21 m/s. This is due to similar composition of  $\text{CH}_4$  and  $\text{CO}$  present in the product gas at both fluidization velocities as shown in Figure 4.46. Conversely, from 0.21 m/s to 0.26 m/s,  $LHV_{\text{gas}}$  and  $HHV_{\text{gas}}$  drastically increase to  $17.02 \text{ MJ/Nm}^3$  and  $19.04 \text{ MJ/Nm}^3$ , respectively. This is due to highest  $\text{CH}_4$  and  $\text{CO}$  composition generated in the product gas at highest fluidization velocity compared to that at lower fluidization velocity. High  $\text{CH}_4$  content in the product is due to less residence time of steam in the reactor.

The heating values of product gases are compared with that of other researchers for steam gasification with  $\text{CO}_2$  adsorbent process. Almost similar  $LHV_{\text{gas}}$  is reported by Weerachanchai et al. [106] at fluidization velocity of  $5U_{mf}$  (0.1 m/s) as compared to the present study. On the other hand, for fluidization velocity of 0.21 m/s,  $HHV_{\text{gas}}$  of  $13.39 \text{ MJ/Nm}^3$  was observed by Xu et al. [56] compared to  $15.75 \text{ MJ/Nm}^3$  in the

present study. The lower  $HHV_{gas}$  values observed due to higher operating temperature of  $795^{\circ}\text{C}$  which promoted reverse carbonation reaction that produced more  $\text{CO}_2$  in the product gas.

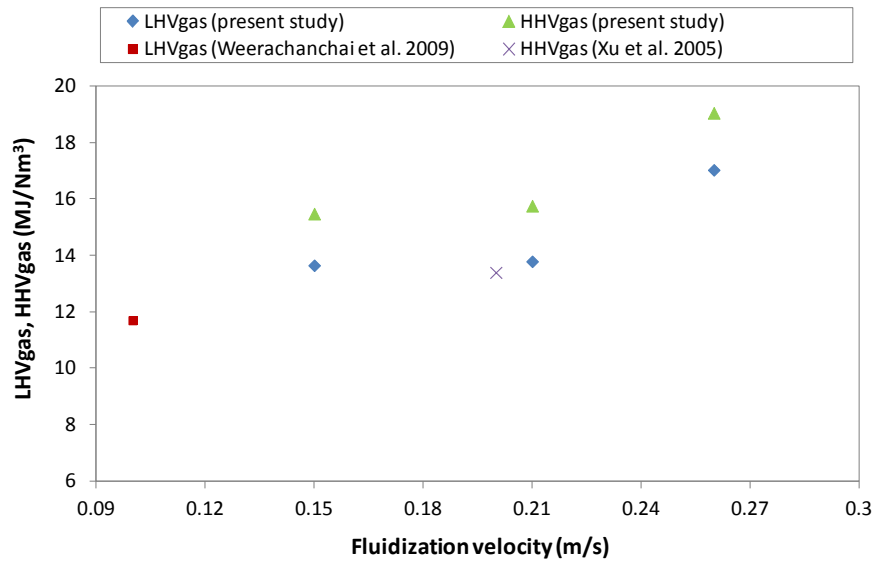


Figure 4.50: Effect of fluidization velocity on product gas heating values

#### 4.5.4.7 Energy Balance

Energy balance was carried out for the adopted process by varying fluidization velocities from 0.15 m/s to 0.26 m/s. The biomass flow rate was varied from 1000 g/h to 1700 g/h at varying steam flow rates of 2000 g/h to 3400 g/h.

Figure 4.51 predicts the input and output energy stream for the gasifier at fluidization velocity of 0.15 m/s. Initially, the energy required for gasification process is found to be 2.82 kW. The energy input associated with PKS at the inlet stream contributes about 3.22 kW. The amount of energy utilized by steam is 0.53 kW. At the outlet stream, major part of the energy is released as an unreacted steam, and contributes to 6.23 kW of energy. The product gas carries energy of 0.37 kW at the exit of the gasifier.

Figure 4.52 illustrates the energy balance at fluidization velocity of 0.26 m/s. It can be seen that the energy associated with steam generation increases from 0.53 kW to 0.91 kW by changing fluidization velocity from 0.15 m/s to 0.26 m/s. High amount

of steam in the system increases the required gasification energy from 2.82 kW to 5.02 kW. Energy content of PKS increases to 5.47 kW at the biomass flow rates of 1700 g/h. At the exit of gasifier, energy possessed by unreacted steam reaches to the highest value of 10.61 kW. Meanwhile, product gas carries 0.79 kW which is higher than that at lower fluidization velocity.

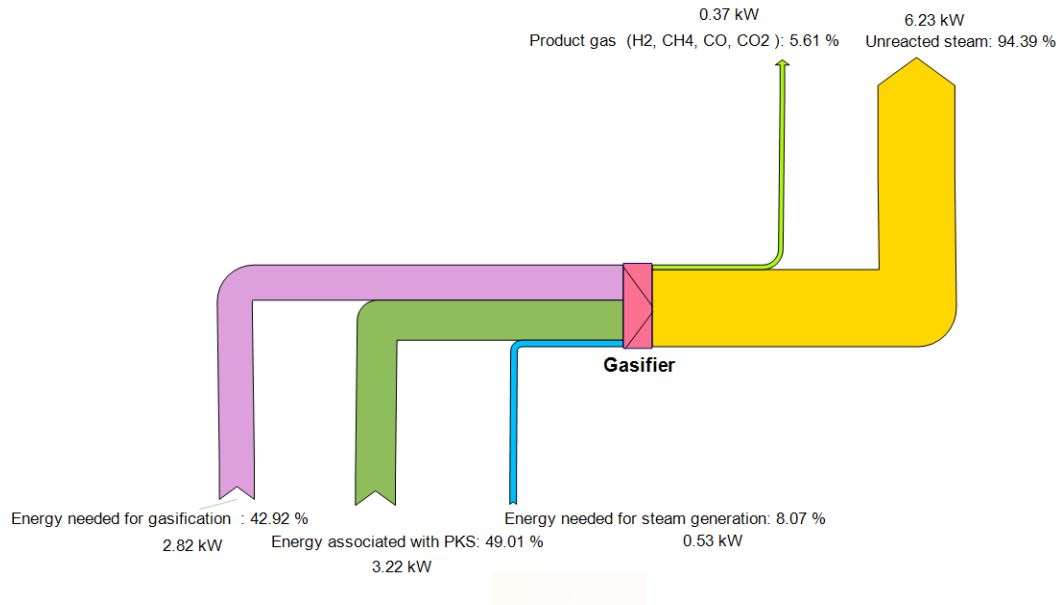


Figure 4.51: Energy balance over gasifier at fluidization velocity of 0.15 m/s

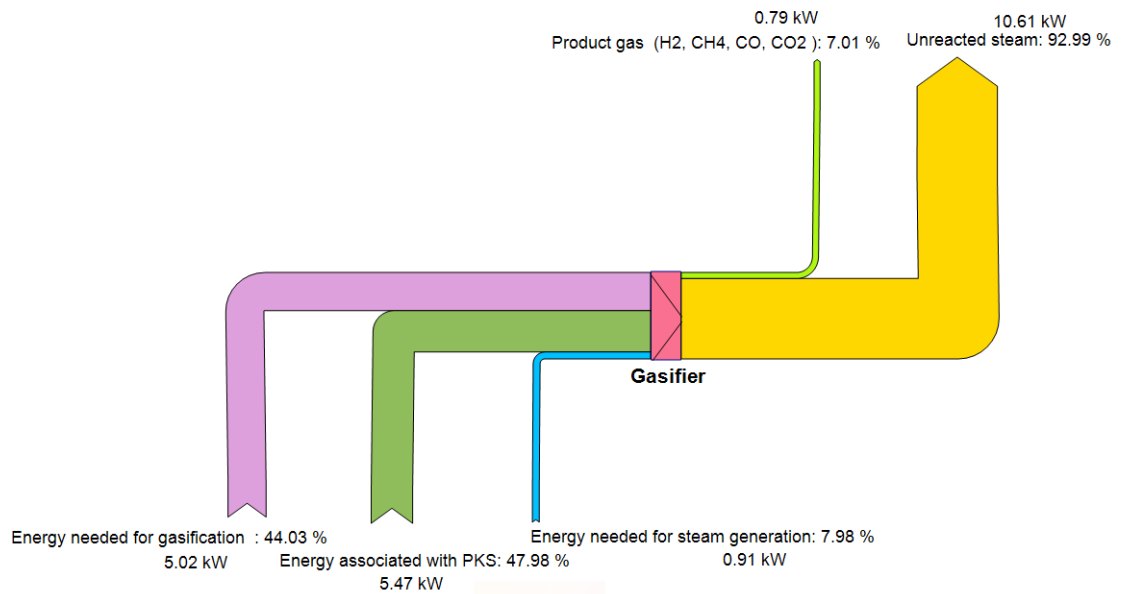


Figure 4.52: Energy balance over gasifier at fluidization velocity of 0.26 m/s

Table 4.23 describes the effect of fluidization velocity on gasification energy required. The required gasification energy increases from 2.82 kW to 5.02 kW by varying velocity from 0.15 to 0.26 m/s. Furthermore, high fluidization velocity increases the product gas flow rates and associated energy with the product gas. At high steam flow rates, more energy is released with the unreacted steam.

Table 4.23: Gasification energy requirement with respect to fluidization velocity

Gasification energy require (kW)	Fluidization velocity (m/s)
2.82	0.15
5.02	0.26

#### 4.5.5 Effect of Biomass Particle Size

The effect of biomass particle size within the range of 0.355-0.500 mm and 1.0-2.0 mm on product gas composition, char and total gas yield, hydrogen yield, gasification and carbon conversion efficiency, selectivity and product gas heating values was studied at temperature of 675°C, S/B ratio of 2.0, A/B ratio of 1.0 and catalyst to biomass ratio of 0.1. The biomass flow rate was set at 1350 g/h.

##### 4.5.5.1 Gas and Char Yield

Gas and char yield with respect to different feedstock particle sizes are shown in Table 4.24. The product gas comprises of H<sub>2</sub>, CO, CO<sub>2</sub> and CH<sub>4</sub> (dry free N<sub>2</sub>). Significant variation is observed in total gas yield by varying biomass particle size from 0.355-0.500 mm to 1.0-2.0 mm. On the other hand, char yield increases slightly with increasing particle size. Char produced in the system is 25.19 g/kg biomass and 27.33 g/kg biomass when the particle size for the feedstock is 0.355-0.500 mm and 1.0-2.0 mm, respectively. Smaller the particle size, lower the heat transfer resistance and high the temperature inside the particle which enhances the gaseous product and reduces the amount of solid char in the product gas. Similar observations are reported by other researchers [102, 113, 209]. For biomass particle size close to 0.3-0.5 mm,

Salleh et al. [205] and Rapagna et al. [102] reported low gas yield of 0.75 m<sup>3</sup>/kg biomass and 0.16 m<sup>3</sup>/kg biomass as compared to the total gas yield of 1.6 m<sup>3</sup>/kg biomass obtained in present study. Very low gas yield observed by the study [205] was due to only char gasification reaction in fluidized bed reactor. High gas yield of 2.33 m<sup>3</sup>/kg biomass is reported by Goa et al. [81] which was due to very high temperature of 850°C in updraft fixed bed gasifier.

Table 4.24: Effect of biomass particle size on gas and char yield

Parameter	Value	Biomass particle size (mm)	Reference
Gas yield (m <sup>3</sup> /kg biomass)	1.600	0.355-0.500	Present study
	1.590	1.000-2.000	
	0.160	0.500	[205]
	0.750	0.600	[102]
	2.330	0.400	[81]
Char yield (g/kg biomass)	25.190	0.355-0.500	Present study
	27.130	1.000-2.000	
	80.000	0.500	[113]

#### 4.5.5.2 Hydrogen Yield

The effect of biomass particle size on hydrogen yield (g/kg biomass) is shown in Table 4.25. The yields are 81.94 g/kg biomass and 80.39 g/kg biomass using feedstock particle size of 0.355-0.500 mm and 1.0-2.0 mm, respectively. The results indicate that the H<sub>2</sub> yield slightly improves using small particle size. However, the increase in H<sub>2</sub> yield is 1.55 g/kg biomass by varying biomass particle size from 1.0-2.0 mm to 0.355-0.500 mm. Similar observation is reported in previous study using particle size range between 0.15-2.0 mm [15]. The comparison of hydrogen yield in the present study with other researchers is shown in Table 4.25. For particle size of 1.0-2.0 mm, Li et al. [15] produced high hydrogen yield of 115 g/kg biomass using catalytic steam gasification at high temperature of 850°C. On the other hand, Xiao et

al. [121] reported hydrogen yield of 48.48 g/kg biomass in catalytic steam gasification at temperature of 656°C for particle size of 0.3-0.5 mm. Very low hydrogen yield of 30.50 g/kg biomass is reported by Guoxin et al. [57] in steam gasification of wet biomass with CO<sub>2</sub> adsorbent in fixed bed reactor with downstream water condensation system. This may due to the high moisture content of 90 wt% in biomass feed which needs measurable amount of energy to remove the moisture content and hence reduce possibility of converting efficiently biomass into useful gaseous product such as H<sub>2</sub>, CO, CH<sub>4</sub>, and CO<sub>2</sub>.

Table 4.25: Effect of biomass particle size on hydrogen yield

Hydrogen yield (g/kg biomass)	Biomass particle size (mm)	Reference
81.940	0.355-0.500	Present study
80.390	1.000-2.000	
48.480	0.500	[121]
30.500	0.600	[57]
115.000	1.000-2.000	[15]

#### 4.5.5.3 Product Gas Composition

Figure 4.53 compares the product gas composition at different biomass particle sizes. The H<sub>2</sub> content in the product gas is 82.42 vol% and 82.11 vol% at biomass particle size of 0.355-0.500 mm and 1.0-2.0 mm, respectively. There is no significant variation of H<sub>2</sub> content for both particle sizes. At lower biomass particle size, H<sub>2</sub> content is increased by 0.31 vol%. However, for CH<sub>4</sub>, there is considerable increase from 1.3 vol% to 11.43 vol%. CO content drastically decreases from 12.37 vol% to 6.45 vol% with increasing biomass particle size. Moreover, for larger particle size, CO<sub>2</sub> content decreases from 3.91 vol% to 0. The obtained gas profiles are similar with those reported by other researchers using almond shell team gasification in fluidized bed gasifier [102].

Based on the analysis presented, it can be concluded that the biomass particle size ranging from 0.355-0.500 mm to 1.0-2.0 mm has no significant effect on H<sub>2</sub> composition in the product gas at the set experimental conditions. This may be due to narrow particle size of biomass studied in the present work.

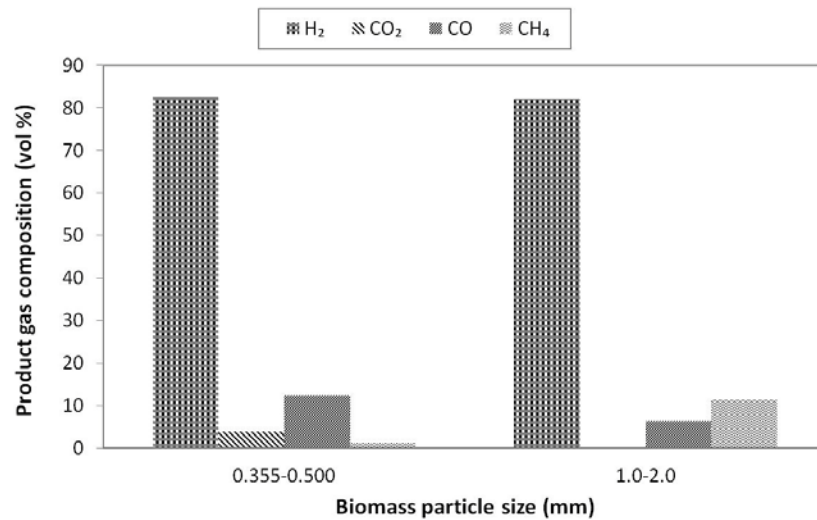


Figure 4.53: Effect of biomass particle size on product gas composition

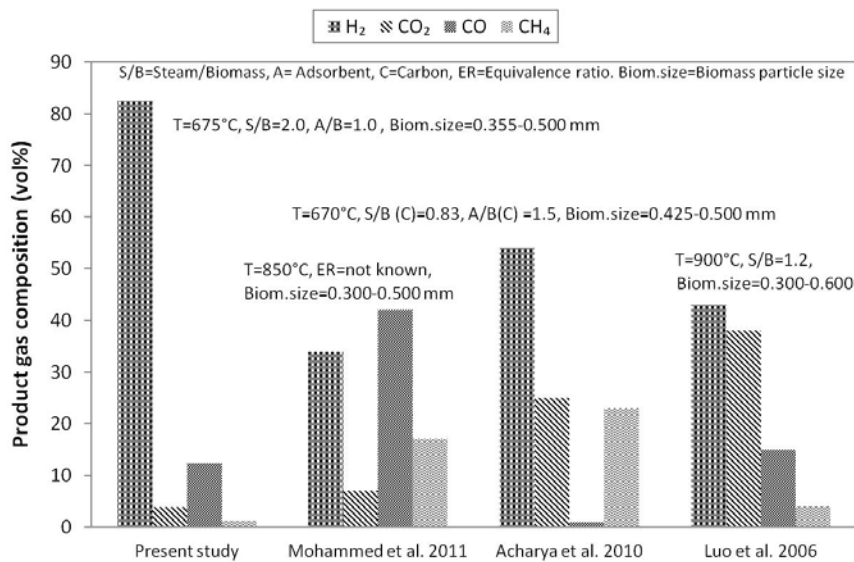


Figure 4.54: Comparative study of product gas composition

Figure 4.54 shows the comparative study of product gas composition. PKS with particle size of 0.355-0.500 mm produces hydrogen composition of 82.42 vol%. The study reported by Luo et al. [119] in catalytic steam gasification and Mohammad et al. [113] investigated air gasification at similar range of biomass particle size (0.3-

0.6 mm) observed hydrogen composition of 43 vol% and 34 vol%, respectively. Low hydrogen composition observed by Mohammad et al. [113] was due to the utilization of air gasification in fluidized bed gasifier at high temperature of 850°C which contributed high CO content (42 vol%) in the product gas.

#### *4.5.5.4 Gasification and Carbon Conversion Efficiency*

Gasification and carbon conversion efficiency are plotted with respect to biomass particle size i.e. 0.350-0.500 mm and 1.0-2.0 mm at temperature of 675°C, S/B ratio of 2.0, adsorbent to biomass ratio of 1.0 and catalyst to biomass ratio of 0.1 as listed in Table 4.26. The values reported for carbon conversion efficiency are 20.76% and 20.96% at 0.350-0.500 mm and 1.0-2.0 mm, respectively. The results indicate that carbon conversion efficiency has no significant variation while decreasing biomass particle size. The number of moles of product gases i.e. CO, CO<sub>2</sub> and CH<sub>4</sub> influence the conversion efficiency of the system. CO and CO<sub>2</sub> decrease while CH<sub>4</sub> increases in product gas by reducing biomass particle size as shown in Figure 4.53. The sum of molar flow rate of CO, CO<sub>2</sub> and CH<sub>4</sub> produces at 0.355-0.500 mm and 1.0-2.0 mm is 11.59 and 11.62 mol, respectively, with no significant variations.

The gasification efficiency increases from 25.66% to 34.53% by decreasing biomass particle size. The total mass flow rate of H<sub>2</sub>, CO, CO<sub>2</sub> and CH<sub>4</sub> are 466.16 g/h and 346.90 g/h at 0.355-0.500 mm and 1.0-2.0 mm, respectively (Appendix A). High gasification efficiency of 89% is reported by Detournay et al. [91] at particle size of 0.3-0.4 mm for biomass steam gasification as compared to gasification efficiency of 34.53% in the present study. The wide difference is due to high temperature of 850°C in the said work and utilization of CO<sub>2</sub> adsorbent in present study which reduces considerable CO<sub>2</sub> concentration (3.9 vol%) via carbonation reaction in the product gas. Hanaoka et al. [90] observed more than double carbon conversion efficiency of 46% compared to that observed in the present study which may be attributed to relatively smaller particle size of 0.1-0.25 mm and higher pressure of 3 bar in biomass gasification process with CO<sub>2</sub> adsorbent.

Table 4.26: Effect of biomass particle size on gasification and carbon conversion efficiency

Parameter	Value	Biomass particle size (mm)	Reference
Gasification efficiency (%)	25.66	0.355-0.500	Present study
	34.53	1.000-2.000	
	89.000	0.300-0.400	[102]
Carbon conversion efficiency (%)	20.760	0.355-0.500	Present study
	20.960	1.000-2.000	
	46.000	0.100-0.250	[90]

#### 4.5.5.5 Selectivity

The effect of biomass particle size on overall selectivity of hydrogen production is illustrated in Table 4.27. The selectivity of 3.77 and 3.63 is observed at biomass particle size range of 0.355-0.50 mm and 1.0-2.0 mm at 675°C, S/B ratio of 2.0, adsorbent to biomass ratio of 1.0 and catalyst to biomass ratio of 0.1. The results show that the selectivity is decreased from 3.77 to 3.63 in the range of biomass particle size studied. In conclusion, biomass particle size from 0.355-0.50 mm to 1.0 to 2.0 mm has no significance effect on the selectivity of H<sub>2</sub> in ICA steam gasification utilizing PKS as the feedstock.

Table 4.27: Effect of biomass particle size on selectivity

Selectivity	Biomass particle size (mm)
3.770	0.355-0.500
3.630	1.000-2.000

#### 4.5.5.6 Product Gas Heating Values

Table 4.28 shows the lower heating values ( $LHV_{gas}$ ) and higher heating values ( $HHV_{gas}$ ) at varying biomass particle size of 0.355-0.500 mm and 1.0-2.0 mm, respectively. The values reported for  $LHV_{gas}$  are 10.92 MJ/Nm<sup>3</sup> and 13.78 MJ/Nm<sup>3</sup> at 0.355-0.500 mm and 1.0-2.0, respectively. The higher  $LHV_{gas}$  values at larger particle size are due to the presence of high CH<sub>4</sub> content in product gas (Figure 4.53). Similarly,  $HHV_{gas}$  has similar trends with value of 12.59 MJ/Nm<sup>3</sup> and 15.75 MJ/Nm<sup>3</sup> at varying particle size from 0.355-0.500 mm to 1.0-2.0 mm. Based on the previous work reported on air-steam biomass gasification [15], high product gas heating value at lower biomass particle size was due to different product gas profiles as compared to the present study in ICA steam gasification in the fluidized bed gasifier. Lower  $LHV_{gas}$  of 8.5 MJ/Nm<sup>3</sup> was observed by Lv et al. [209] at 850°C in air-steam gasification process. A combination of air-steam gasification provides lower product gas heating values compared to steam alone [97]. For  $HHV_{gas}$  values, Franco et al. [83] produced similar values of 15 MJ/Nm<sup>3</sup> in steam gasification at 800°C in fluidized bed gasifier.

Table 4.28: Effect of biomass particle size on product gas heating values

Parameter	Value	Biomass particle size (mm)	Reference
$LHV_{gas}$ (MJ/Nm <sup>3</sup> )	10.920	0.355-0.500	Present study
	13.780	1.000-2.000	
	8.5	0.500	[209]
$HHV_{gas}$ (MJ/Nm <sup>3</sup> )	12.590	0.355-0.500	Present study
	15.750	1.000-2.000	
	15.000	1.200-2.000	[83]

#### 4.5.5.7 Energy Balance

The energy balance of the gasifier was carried out by varying biomass particle size from 0.355-0.500 mm to 1.0-2.0 mm at temperature of 675°C, S/B ratio of 2.0,

adsorbent to biomass ratio of 1.0 and catalyst to biomass ratio of 0.1. The biomass flow rate is constant at 1350 g/h with steam flow rate of 2700 g/h. Figure 4.55 shows input and output energy stream of gasifier system for biomass particle size of 0.355-0.500 mm. The energy required for gasification process is found to be 3.38 kW. Energy associated with PKS at the inlet stream contributes 4.34 kW. Amount of energy consumed by the steam is 0.72 kW. At the outlet stream, major part of the energy is released as an unreacted steam, and contributes 7.93 kW. The product gas contributes 0.77 kW at the exit of the gasifier.

Figure 4.56 shows the energy balance over gasifier by considering large biomass particle size i.e. 1.0-2.0 mm. The result shows no significant increase in energy requirement at large biomass particle size. Furthermore, the input energy with steam and PKS are similar as observed for small particle sizes. Similar biomass flow rates of 1350 g/h were used for both cases. At the outlet, the energy associated with unreacted steam is similar in both cases i.e. 8 kW. However, energy of the product gas is slightly higher than the case of smaller particle size. This effect is due to high heat transfer for small particle compared to larger particle size. Higher product gas flow rates are observed for smaller particle size which accounts for more energy to be associated with product gas at the exit of the gasifier.

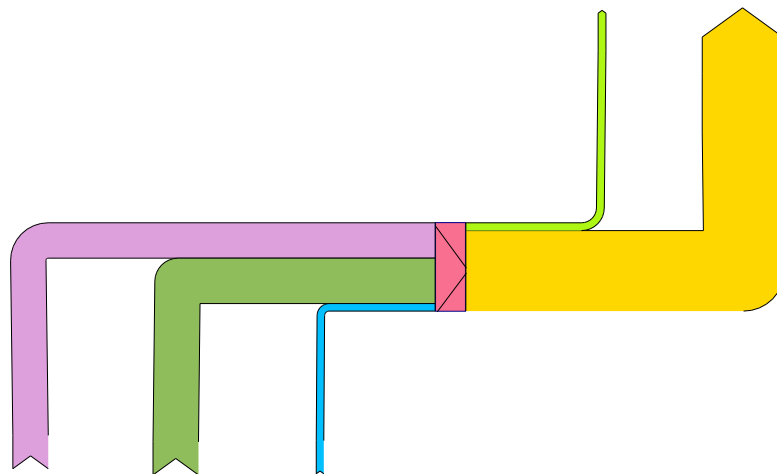


Figure 4.55: Energy balance over gasifier for biomass particle size of 0.355-0.50 mm

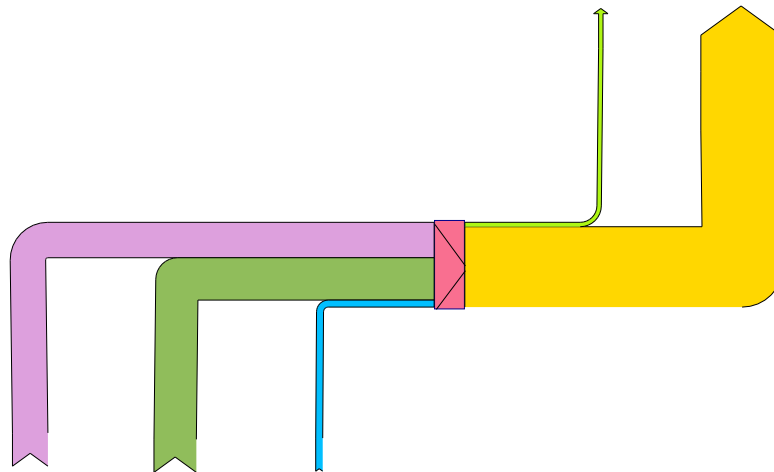


Figure 4.56: Energy balance over gasifier for biomass particle size of 1.0-2.0 mm

Table 4.29 describes the effect of biomass particle size on gasification energy requirement. The results indicate that gasification energy required has not significant variation for both particle sizes. The values decrease from 3.63 kW to 3.38 kW by decreasing particle size from 0.355-0.500 to 1.0-2.0 mm.

Table 4.29: Gasification energy requirement with respect to biomass particle size

Gasification energy require (kW)	Biomass particle size (mm)
3.38	0.355-0.500
3.63	1.000-2.000

#### 4.6 Optimization Study of Parameter Influence on ICA Steam Gasification

Present study used response surface methodology (RSM) approach to assess the effect of five variables i.e. temperature, steam to biomass ratio (S/B), adsorption to biomass ratio (A/B), fluidization velocity (U) and biomass particle size ( $D_{bio}$ ) on hydrogen composition and yield in product gas. Hydrogen composition and yield are known as the output responses. As discussed in Section 3.17, there are 26 experiments designed by the Expert Design-8 software using central composite rotatable design

(CCRD) under RSM approach. Once the experiments are designed, the ICA steam gasification system is operated following the set process conditions. Hydrogen composition and yield are then evaluated for each run. The operating conditions of all the experiments and their associated output responses i.e. hydrogen composition ( $Y_1$ ) and yield ( $Y_2$ ) are give in Table 4.30. As observed, the hydrogen yield varies from 10.9 g/kg biomass to 150.99 g/kg biomass. The minimum yield of 10.9 kg/kg biomass is achieved at 634°C, S/B ratio of 1.73, A/B ratio of 0.73, C/B ratio of 0.1 and U of 0.17 m/s while maximum yield is obtained at 750°C, S/B ratio 2.0, A/B ratio 1.0, C/B ratio of 0.1, U of 0.21 m/s. For hydrogen, minimum composition of 57.77 vol% is observed at 675°C, S/B ratio of 2.0, A/B ratio of 1.0, C/B ratio of 0.1, U of 0.26 m/s, while maximum composition of 84.62 vol% is obtained at 675°C, S/B ratio of 2.0, A/B ratio of 1.5, C/B ratio of 0.1 and U of 0.21 m/s.

#### 4.6.1 Analysis of Variance (ANOVA)

In present study, output responses are hydrogen composition ( $Y_1$ ) and hydrogen yield ( $Y_2$ ) which are connected with process variables through regression analysis. This regression analysis produces response surface model equations for each output responses i.e.  $Y_1$  and  $Y_2$ . These equations represent second order polynomial regression model:

$$H_2 (\text{vol}\%) = 75.53 - 2.70 \times T + 6.07 \times (A/B) - 3.35 \times D_{\text{bio}} + 6.94 \times T \times U - 6.33 \times T \times (A/B) - 8.51 \times (S/B) \times (A/B) + 8.72 \times U \times D_{\text{bio}} \quad (4.1)$$

$$H_2 (\text{g/kg biomass}) = 73.31 - 32.72 \times T + 19.01 \times (S/B) + 16.17 \times (A/B) + 8.35 \times D_{\text{bio}} + 11.88 \times T \times U + 9.59 \times T \times D_{\text{bio}} - 8.25 \times (S/B) \times (A/B) + 12.71 \times U \times D_{\text{bio}} \quad (4.2)$$

To assess statistical significance of the influence of the variables to the output responses, test for individual model coefficient and lack of fit are performed. This statistical analysis is called Analysis of variance (ANOVA). Table 4.31 depicts the results produced from the ANOVA for hydrogen composition ( $Y_1$ ) as the output response. The analysis introduced probability value (p-value) and F-value to define the significance of the model.

Table 4.30: Experimental operating conditions and associated output responses

Run.	Temperature (T)	Biomass (B)	Steam (S)	CaO (A)	Catalyst (C)	Steam/Biomass (S/B)	Fluidization velocity (U)	CaO/Biomass (A/B)	Biomass particle dia. (D <sub>bio</sub> )	H <sub>2</sub> (Y <sub>1</sub> )	H <sub>2</sub> (Y <sub>2</sub> )
	°C	kg/h				-	m/s	-	mm	Vol%	g/kg biomass
1	716	1.320	2.280	1.680	0.135	1.730	0.170	1.270	1.000-2.000	66.510	95.510
2	675	1.350	2.670	1.350	0.135	2.000	0.210	1.000	1.000-2.000	82.110	80.390
3	634	1.320	2.280	0.960	0.135	1.730	0.170	0.730	0.710-1.000	72.670	10.900
4	675	0.980	1.960	0.980	0.100	2.000	0.150	1.000	1.000-2.000	67.240	42.320
5	634	1.350	3.070	0.980	0.135	2.270	0.240	0.730	1.000-2.000	75.000	37.710
6	675	1.350	2.670	1.350	0.135	2.000	0.210	1.000	1.000-2.000	75.130	80.610
7	600	1.350	2.670	1.350	0.135	2.000	0.210	1.000	1.000-2.000	78.010	31.800
8	750	1.350	2.670	1.350	0.135	2.000	0.210	1.000	1.000-2.000	68.160	150.990
9	716	1.780	3.070	1.290	0.180	1.730	0.240	0.730	1.000-2.000	78.310	98.750
10	716	1.000	2.280	1.280	0.100	2.270	0.170	1.270	0.700-1.000	70.240	89.770
11	675	1.350	2.670	1.350	0.135	2.000	0.210	1.000	1.000-2.000	70.230	84.530
12	675	1.350	2.670	1.350	0.135	2.000	0.210	1.000	1.000-2.000	73.000	71.560
13	716	1.780	3.070	2.260	0.180	1.730	0.240	1.270	0.710-1.000	72.070	85.070
14	675	1.690	3.390	1.690	0.170	2.000	0.260	1.000	1.000-2.000	57.770	47.960
15	675	1.350	2.670	1.350	0.135	2.000	0.210	1.000	1.000-2.000	74.740	69.970
16	675	1.350	2.670	2.000	0.135	2.000	0.210	1.500	1.000-2.000	84.620	91.110
17	675	1.350	2.670	0.670	0.135	2.000	0.210	0.500	1.000-2.000	62.500	32.210
18	716	1.000	2.280	0.730	0.100	2.270	0.170	0.730	1.000-2.000	62.060	97.860
19	675	1.350	2.670	1.350	0.135	2.000	0.210	1.000	0.355-0.500	82.420	54.110
20	675	1.780	2.670	1.780	0.180	1.500	0.210	1.000	1.000-2.000	80.870	28.690
21	634	1.000	2.280	1.280	0.100	2.270	0.170	1.270	1.000-2.000	73.330	55.050
22	634	1.350	3.070	1.720	0.135	2.270	0.240	1.270	1.000-2.000	69.260	52.360
23	634	1.780	3.070	2.260	0.180	1.730	0.240	1.270	1.000-2.000	78.430	43.450
24	675	1.070	2.670	1.070	0.110	2.500	0.210	1.000	1.000-2.000	82.610	97.930
25	675	1.350	2.670	1.350	0.135	2.000	0.210	1.000	1.000-2.000	72.500	66.260
26	716	1.350	3.070	0.98	0.135	2.270	0.240	0.730	0.710-1.000	76.830	90.250

Table 4.31: Analysis of variance (ANOVA) on hydrogen composition

	Source	F- value	p-value
Process variables	Model	4.60	0.0490
Temperature	T	4.06	0.0995
Steam/biomass	S/B	0.13	0.74
Fluidization velocity	U	3.76	0.11
Adsorbent/ biomass	A/B	20.49	0.01
Biomass particle size	D <sub>bio</sub>	6.22	0.05
Temperature×steam/biomass	T(S/B)	0.11	0.75
Temperature×fluidization velocity	T(U)	12.35	0.02
Temperature×adsorbent/biomass	T(A/B)	10.24	0.02
Temperature×biomass particle size	T(D <sub>bio</sub> )	1.74	0.24
Steam/biomass×fluidization velocity	S/B(U)	1.28	0.31
Steam/biomass×adsorbent/biomass	S/B(A/B)	18.52	0.01
Steam/biomass×biomass particle size	S/B(D <sub>bio</sub> )	0.02	0.88
Fluidization velocity×adsorbent/biomass	U(A/B)	3.50	0.12
Fluidization velocity×biomass particle size	U(D <sub>bio</sub> )	19.46	0.01
Adsorbent/biomass×biomass particle size	A/B(D <sub>bio</sub> )	2.82	0.15
Model check	Lack of fit	0.00	0.96

Initially, the significance of the quadratic model is tested for 95% confidence level, which is shown by p-value < 0.050 with high model F-value indicates [164] the reliability of the fitted model for response of hydrogen composition ( $Y_1$ ). The “lack of fit” is then calculated and is found to be “not significant” based on its p-value of 0.96 for the quadratic model. This shows that the model do not show “lack of fit” to the experimental data based on hydrogen composition ( $Y_1$ ). ANOVA is also able to predict the significance of individual process input variables and their interactions. The smaller the p-value, more significant is the process parameter in influencing the output response. Amongst the five process variables; adsorption to biomass ratio (A/B) has a p-value of 0.01 and is a significant variables that influence the hydrogen composition in ICA steam gasification utilizing PKS as the feedstock. For temperature (T) and biomass particle size (D<sub>bio</sub>), the p-values are 0.05 and 0.0995, respectively, which are marginal significant (0.05<p-value<0.1). Similarly, the

significant model interactive terms are; temperature and fluidization velocity (TU), temperature and adsorbent to biomass ratio (TA/B), steam to biomass and adsorbent to biomass ratios (S/BA/B), and fluidization velocity and biomass particle size ( $UD_{bio}$ ) with p-values of 0.02, 0.02, 0.01 and 0.01, respectively. These interactions of two process variables on the out response will be discussed in the following section.

Determination coefficient,  $R^2$ , is shown in Table 4.32. In this case, high value of 0.95 for the  $R^2$  is obtained which shows that the model can be used for the prediction of output response with acceptable precision. However, previous researchers reported that the value of  $R^2$  increases with increasing number of process variables in the proposed model [155]. To avoid any misleading conclusion, Adj- $R^2$  is evaluated as extra variables to the model. The value of Adj- $R^2$  is 0.74 which is in agreement with  $R^2$ .

Table 4.32: Coefficient of determination on hydrogen composition response ( $Y_1$ )

Coefficients	Values
Determination coefficient, $R^2$	0.95
Adjusted determination coefficient, Adj- $R^2$	0.74

Table 4.33 shows the ANOVA results of the hydrogen yield as the second output response, ( $Y_1$ ). The p-value of 0.0005 with high F-value of 33.37 confirms that the quadratic model is significant to predict the hydrogen yield as the output response. Similar to hydrogen composition ( $Y_1$ ), lack of fit is found to be non significant which can be seen by its p-value of 0.697. This further confirms the reliability of fitting the experimental data to the regression model for  $Y_2$ . Additionally, amongst the five processes variables, temperature (T) is the most significant due to lowest p-value of <0.0001 with highest F-value of 204.57. This is followed by S/B, A/B and  $D_{bio}$  with p-value of 0.0004, 0.0009 and 0.0147 representing the associated F-value of 69.04, 49.96 and 13.30, respectively. This means that the three process variables; T, S/B and A/B are the most important variables that influence the hydrogen yield in ICA steam gasification. On the effects of two combined process variables, the order of the most significant to less significant combinations are; fluidization velocity  $\times$  biomass particle size > temperature  $\times$  fluidization velocity > temperature  $\times$  biomass particle size and > steam/biomass  $\times$  adsorbent/biomass.

Table 4.33: Analysis of variance (ANOVA) on hydrogen yield

	Source	F- value	p-value
Process variables	Model	33.37	0.0005
Temperature	T	204.57	< 0.0001
Steam/biomass	S/B	69.04	0.0004
Fluidization velocity	U	0.46	0.5286
Adsorbent/ biomass	A/B	49.96	0.0009
Biomass particle size	D <sub>bio</sub>	13.33	0.0147
Temperature×steam/biomass	T(S/B)	1.89	0.2278
Temperature×fluidization velocity	T(U)	12.42	0.0169
Temperature×adsorbent/biomass	T(A/B)	1.19	0.3253
Temperature×biomass particle size	T(D <sub>bio</sub> )	8.09	0.0361
Steam/biomass×fluidization velocity	S/B(U)	0.41	0.5510
Steam/biomass×adsorbent/biomass	S/B(A/B)	6.00	0.0580
Steam/biomass×biomass particle size	S/B(D <sub>bio</sub> )	0.38	0.5651
Fluidization velocity×adsorbent/biomass	U(A/B)	2.32	0.1883
Fluidization velocity×biomass particle size	U(D <sub>bio</sub> )	14.22	0.0130
Adsorbent/biomass×biomass particle size	A/B(D <sub>bio</sub> )	0.23	0.6527
Model check	Lack of fit	0.17	0.6972

The coefficient of determination,  $R^2$ , is given in Table 4.34. In this case, high value of 0.99 for  $R^2$  is obtained which shows that the model can be used to predict hydrogen yield with acceptable precision. Additionally, the value of  $Adj-R^2$  predicted is 0.96 and is in a good agreement with  $R^2$ .

Table 4.34: Coefficient of determination on hydrogen yield response ( $Y_2$ )

Coefficients	Values
Determination coefficient, $R^2$	0.99
Adjusted determination coefficient, $Adj-R^2$	0.96

#### 4.6.2 Predicted versus Actual Response

Once the developed model is generated through ANOVA, it can be used to predict the theoretical values of the responses i.e. hydrogen composition ( $Y_1$ ) and hydrogen yield ( $Y_2$ ). Figure 4.57 shows the graph between the predicted values of hydrogen composition ( $Y_1$ ) versus actual values of hydrogen composition generated experimentally in ICA steam gasification system. As indicated by the graph, the model fits well with the experimental values. Only fewer experimental points in the range of 75 vol% yield are shifted from the central line. Moreover, most of the points are located in the range of 65 vol% to 77 vol% which is considered to be the most populated area. The full range exists between maximum and minimum values of 57.77 vol% and 84.62 vol%, respectively.

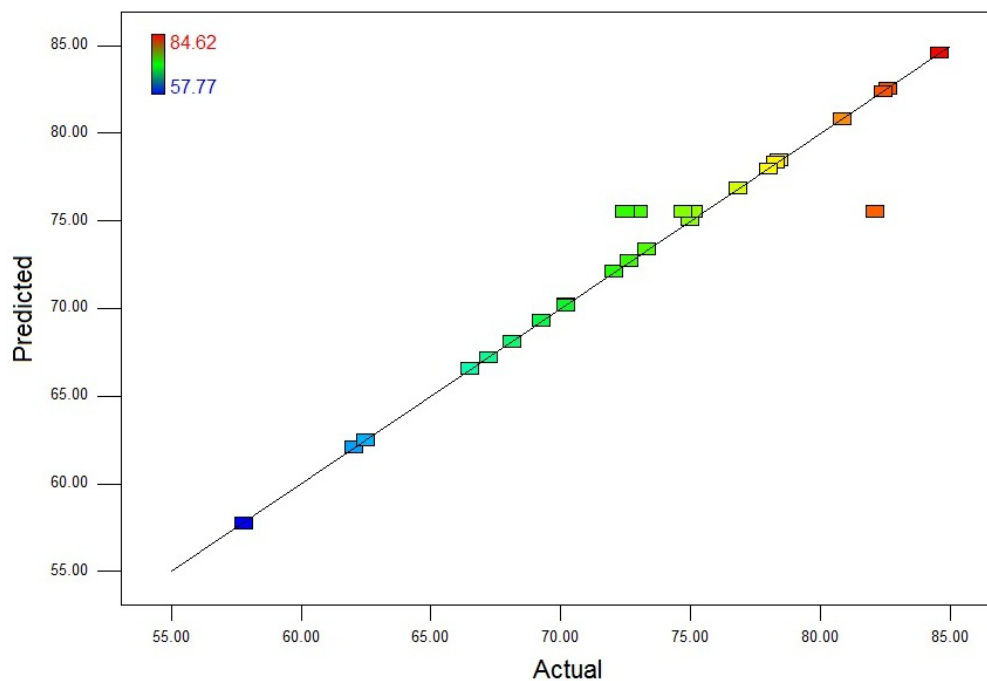


Figure 4.57: Predicted versus actual hydrogen composition ( $Y_1$ )

Figure 4.58 demonstrates the predicted versus actual hydrogen yield ( $Y_2$ ) in ICA steam gasification. Contrary from the results presented in Figure 4.57, points are closer and two groups of points are identified in two narrow regions. The first populated region exists between 28-55 g/kg biomass of hydrogen yield predicted by the model. The second region varies from 73-99 g/kg biomass. Apart from some scattered points in the region, this region is in good agreement with the experimental

values. The maximum point is only observed at high temperature of 750°C. Minimum hydrogen yield is observed at temperature of 634°C. The full range lies between maximum and minimum value of 150 g/kg biomass and 10.9 g/kg biomass, respectively.

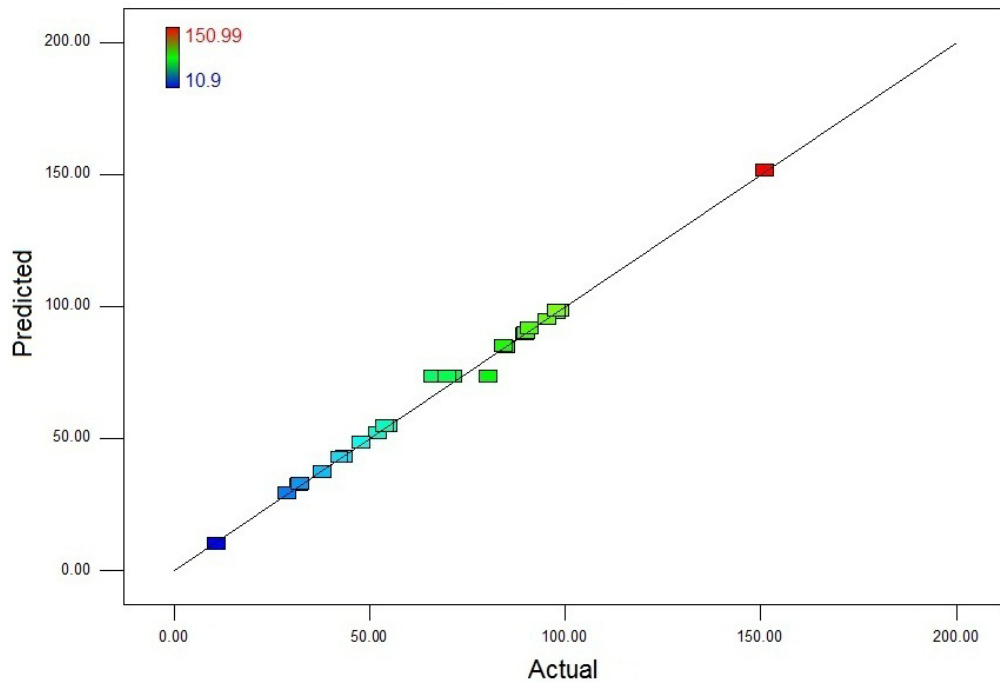


Figure 4.58: Predicted versus actual hydrogen yield ( $Y_2$ )

#### 4.6.3 Three Dimensional (3D) Surface Plots

Three dimensional (3D) surface plots are used to study the combine effects of two process variables towards the output response. These combine effects of the process variables are presented in the form of surface response. As shown in the ANOVA analysis of Table 4.31 and 4.33, there are 10 combined process effects in which some are significant and some are not significant based on their p-values and F-values. Moreover, the 3D surface plots not only give the combine effects at the experimental values but also interpolate these effects to the intermediate points. The 3D surface plots for hydrogen composition and hydrogen yield are discussed in the following sections.

#### 4.6.3.1 Hydrogen Composition

Table 4.31 provides the combine variables effects on hydrogen composition generated in the ANOVA analysis. The effect of temperature (T) and steam to biomass ratio (S/B) is shown in Figure 4.59. The results indicates that H<sub>2</sub> composition (vol%) decreases by 3.8% when the temperature increases from 600°C to 750°C at S/B ratio of 1.5. At constant temperature of 600°C, H<sub>2</sub> composition increased by 10.3% with varying S/B ratio from 1.5 to 2.5. This shows that increasing steam is relatively more significant at lowest temperature of 600°C as compared to increasing temperature from 600°C to 750°C at low S/B ratio of 1.5. The possible reason is that the activity of the reverse carbonation reaction is dominant at temperature higher than 700°C which reduces the overall H<sub>2</sub> content in the product gas.

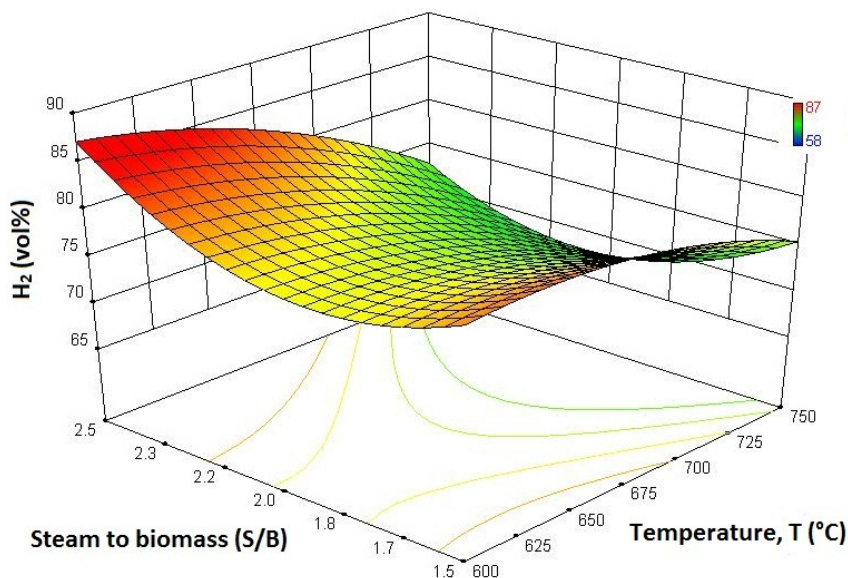


Figure 4.59: Effect of temperature and steam to biomass ratio on hydrogen composition based on adsorbent to biomass ratio of 1.0 wt/wt, biomass particle size of 1000-2000  $\mu\text{m}$  and fluidization velocity of 0.21 m/s

By increasing the S/B ratio at low temperature of 600°C, most gasification and reforming reactions proceed in the forward direction with high activity of CO<sub>2</sub> adsorption reaction collectively produce more H<sub>2</sub> in the product gas. Nevertheless, varying steam to biomass ratio at high temperature has no impact and H<sub>2</sub> content in

the product gas decreases by 2.7%. Similarly, increasing temperature to 750°C at high S/B ratio reduces H<sub>2</sub> content by 17.2%.

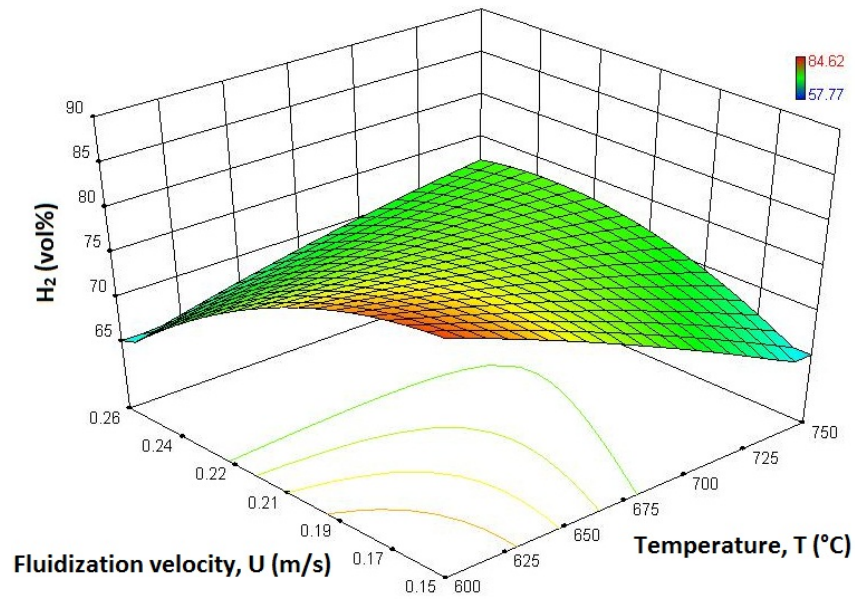


Figure 4.60: Effect of temperature and fluidization velocity on hydrogen composition based on steam to biomass ratio of 2.0 wt/wt, adsorbent to biomass ratio of 1.0 wt/wt, catalyst to biomass ratio of 0.1 wt/wt and biomass particle size of 1000-2000  $\mu\text{m}$

The effect of temperature (T) and fluidization velocity (U) on H<sub>2</sub> composition is shown in Figure 4.60. It is observed that the H<sub>2</sub> composition (vol%) decreases by 16.7% by increasing temperature from 600°C to 750°C at 0.15 m/s. Similarly, by keeping the temperature constant at 600°C, H<sub>2</sub> composition gradual decreases by 16.7% at varying fluidization velocity from 0.15 m/s to 0.26 m/s. This gives the equal effect on H<sub>2</sub> composition by increasing temperature from 600°C to 750°C at low fluidization velocity or increasing the fluidization velocity from 0.15 m/s to 0.26 m/s at low temperature of 600°C. Conversely, at high temperature of 750°C, increasing fluidization velocity from 0.15 m/s to 0.26 m/s increase H<sub>2</sub> content by 8.4% in the product gas. Similar result is also observed at high fluidization velocity of 0.26 m/s by varying temperature from 600°C to 750°C. This may be due to the high temperature which helps to improve H<sub>2</sub> composition in the product gas.

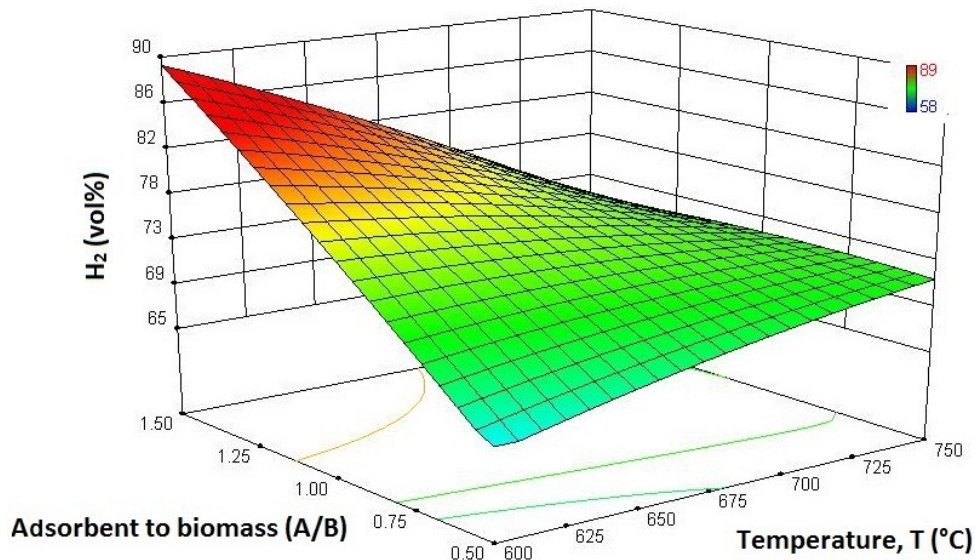


Figure 4.61: Effect of temperature and adsorbent to biomass ratio on hydrogen composition at steam to biomass ratio of 2.0 wt/wt, fluidization velocity of 0.21 m/s, catalyst to biomass ratio of 0.1 wt/wt and biomass particle size of 1000-2000  $\mu\text{m}$

The effect of temperature (T) and adsorption to biomass ratio (A/B) is illustrated in Figure 4.61. The results shows that  $\text{H}_2$  composition (vol%) increased by 15.5 % when temperature is increased from 600°C to 750°C at adsorbent to biomass ratio of 0.5. At constant temperature of 600°C,  $\text{H}_2$  composition increases to about 32.6% in the range of 0.50 to 1.50 adsorbent to biomass ratio. This can be justified by excess amount of adsorbent available that enhanced  $\text{CO}_2$  adsorption in the produce gas at low temperature of 600°C. However, effect of this excess adsorbent at high temperature of 750°C does not influence the  $\text{H}_2$  content. Similarly, a decrease by 20.2% is observed in  $\text{H}_2$  composition while varying temperature from 600°C to 750°C. This concluded that the presence of excess adsorbent at high temperature in the system is not promoting  $\text{H}_2$  composition in the product gas due to active reverse carbonation reaction in the system.

Figure 4.62 shows the effect of temperature (T) and biomass particle size ( $D_{\text{bio}}$ ) on hydrogen gas composition. The results indicated that  $\text{H}_2$  content decreases by 9.75% by increasing the temperature from 600°C to 750°C at biomass particle size of 355-500  $\mu\text{m}$ . The effect of increasing biomass particle size at low temperature of 600°C, decrease  $\text{H}_2$  concentration by 11.25% in the range of 355-500  $\mu\text{m}$  to 1000-2000  $\mu\text{m}$

due to heat transfer limitation for large biomass particle which inhibits the release of gaseous product during the gasification process. However, no significant decrease in  $H_2$  content is observed with increasing biomass particle size at high temperature  $750^\circ\text{C}$ . This indicates that the high heat transfer limitation is not effective at high temperature of  $750^\circ\text{C}$  as compared to low temperature of  $600^\circ\text{C}$ . Other researchers found that the larger particle ( $\sim 1000\ \mu\text{m}$ ) was not affected by the heat resistant limitation at high temperature ( $800^\circ\text{C}$ ) [102].

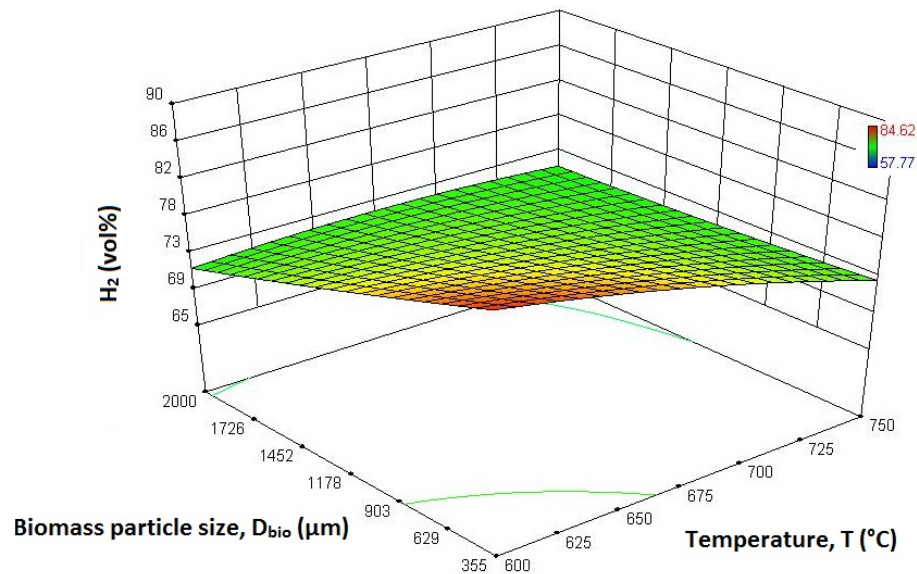


Figure 4.62: Effect of temperature and biomass particle size on hydrogen composition based on steam to biomass ratio of 2.0 wt/wt, adsorbent to biomass ratio of 1.0 wt/wt, catalyst to biomass ratio of 0.1 wt/wt and fluidization velocity of 0.21 m/s

The effect of steam to biomass ratio (S/B) and fluidization velocity (U) is illustrated in Figure 4.63. The results shows that the  $H_2$  composition (vol%) decrease by 6.4% at S/B ratio of 1.5 to 2.5 at low fluidization velocity of 0.15 m/s. Conversely, at high fluidization velocity of 0.26 m/s,  $H_2$  composition increases by 6.8% which due is to the presence of excess steam. No significant variation is observed at high S/B ratio of 2.5 by increasing fluidization velocity from 0.15 m/s to 0.26 m/s. The overall results show that the low fluidization velocity prefers low S/B ratio to produce high  $H_2$  content in the product gas. However, high S/B ratio of 2.5 produces maximum  $H_2$  content of 78 vol% at medium fluidization velocity of 0.21 m/s which indicates the optimum residence time of the reacting gases in the reactor.

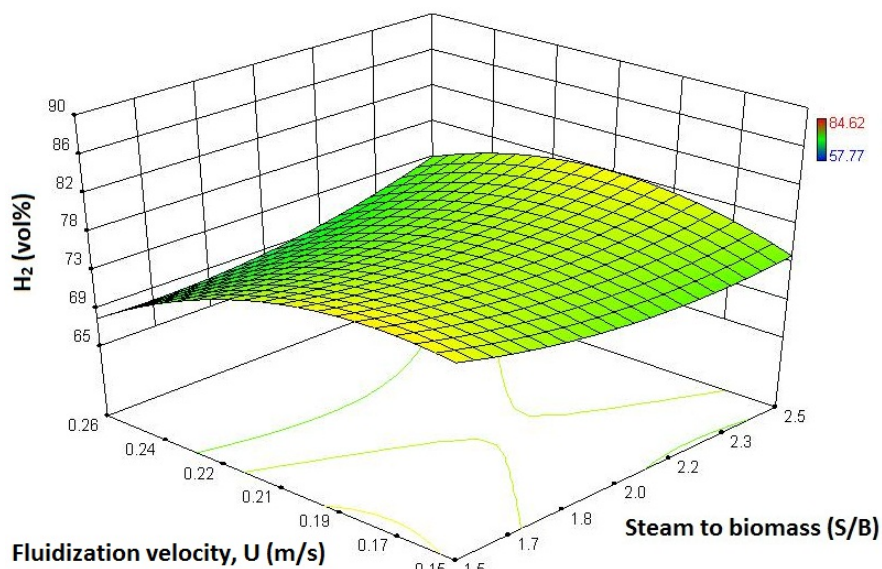


Figure 4.63: Effect of steam to biomass ratio and fluidization velocity on hydrogen composition at 675°C, adsorbent to biomass of 1.0 wt/wt, catalyst to biomass ratio of 0.1 wt/wt and biomass particle size of 1000-2000  $\mu\text{m}$

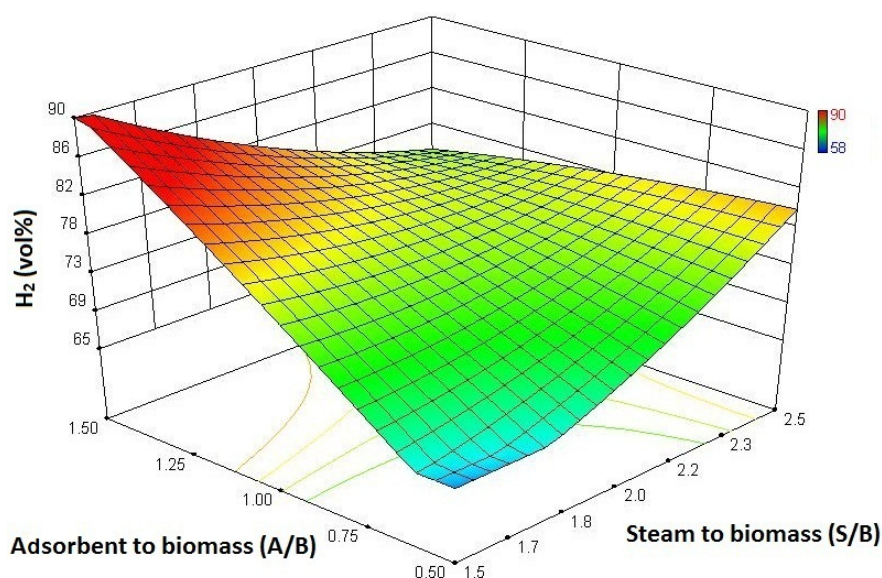


Figure 4.64: Effect of steam to biomass ratio and adsorbent to biomass ratio on hydrogen composition at 675°C, fluidization velocity of 0.21 m/s, catalyst to biomass ratio of 0.10 wt/wt, and biomass particle size of 1000-2000  $\mu\text{m}$

The effect of steam to biomass ratio (S/B) and adsorbent to biomass (A/B) is shown in Figure 4.64. The results show that the  $\text{H}_2$  composition increases by 24% at

varying S/B ratio of 1.5 to 2.5 at adsorbent to biomass ratio of 0.5. Now by lowering S/B ratio to 1.50, H<sub>2</sub> composition increases by an increment of 33.3 % by varying adsorbent to biomass ratio from 0.5 to 1.5. However, varying adsorbent to biomass from 0.5 to 1.5 at high S/B ratio of 2.5 decreased the H<sub>2</sub> content by 7.6%. At high adsorbent to biomass ratio of 1.50, H<sub>2</sub> content decreases to 18.9% in the product gas. It can be concluded that varying adsorbent to biomass ratios at lower S/B is more significant as compared to varying S/B ratios at low adsorbent to biomass ratio. Moreover, it can be observed that the activity of adsorbent in the excess amount of steam decreases which influences the gasification and reforming reactions towards H<sub>2</sub> production.

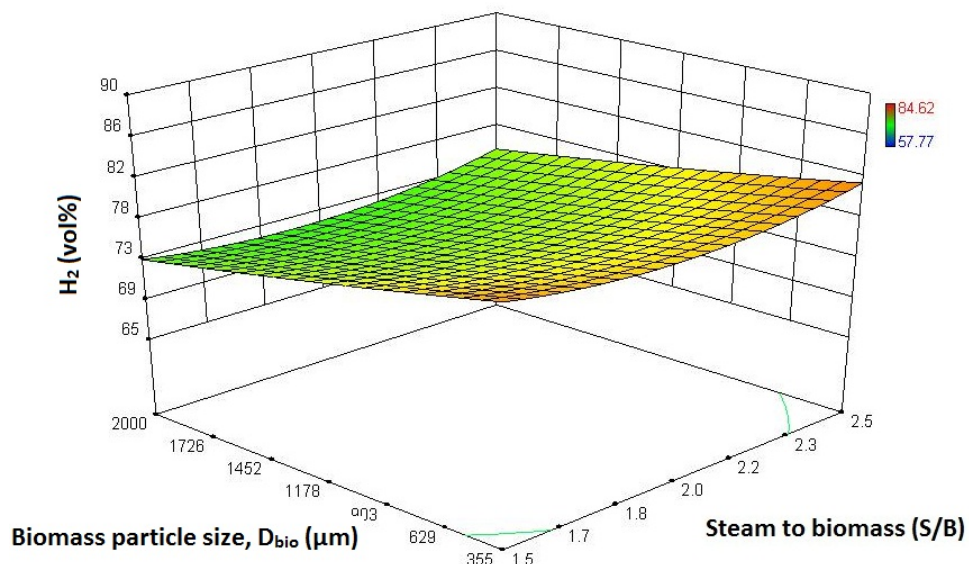


Figure 4.65: Effect of steam to biomass ratio and biomass particle size on hydrogen composition at 675°C, adsorbent to biomass ratio of 0.1 wt/wt, catalyst to biomass ratio of 0.1 wt/wt and fluidization velocity of 0.21 m/s

Figure 4.65 illustrates the effect of steam to biomass ratio (S/B) and biomass particle size ( $D_{bio}$ ) on hydrogen content (vol%) in the product gas. The results indicate that no significant effect is observed for H<sub>2</sub> content by increasing S/B from 1.5 to 2.5 at particle size of 355-500 μm. By increasing biomass particle size from 355-500 mm to 1000-2000 μm decreases the H<sub>2</sub> content by an increment of 9.9% at S/B ratio of 1.5. However, H<sub>2</sub> content decreases by 8.6% at high S/B ratio of 2.5 at similar biomass particle size range. This result concluded that the decrease in H<sub>2</sub> content at high S/B is compensated by excess steam and produces 1.3% more H<sub>2</sub> as compared to low S/B at the same biomass particle size variation. No significant effect of increasing

steam on H<sub>2</sub> content is observed at larger biomass particle (1000-2000 μm). This negligible variation is due to the heat transfer limitation which inhibits the release of gaseous product and gives low product gas.

The effect of fluidization velocity (U) and adsorbent to biomass (A/B) is shown in Figure 4.66. The results show that H<sub>2</sub> content increases by 26.5% while varying adsorbent to biomass ratio from 0.5 to 1.5 at fluidization velocity of 0.15 m/s. Meanwhile, no significant effect is observed on H<sub>2</sub> composition at adsorbent to biomass ratio of 0.50 while increasing fluidization velocity from 0.15 m/s to 0.26 m/s. H<sub>2</sub> content decreases by 16.7% at high adsorbent to biomass ratio when the fluidization velocity is increased from 0.15 m/s to 0.26 m/s. This effect is due to the high adsorbent activity towards CO<sub>2</sub> at lower fluidization velocity under high residence time of the product gases in the reactor.

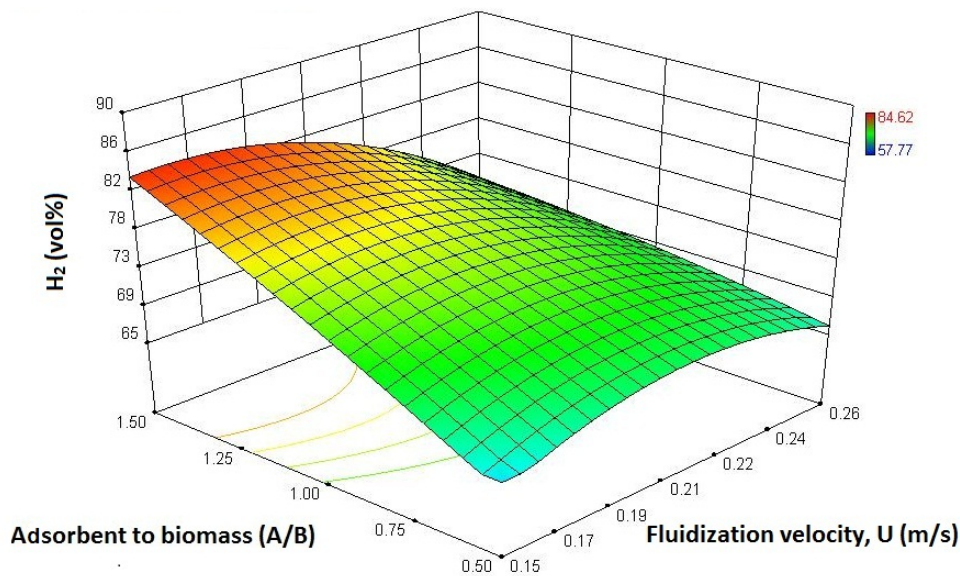


Figure 4.66: Effect of fluidization velocity and adsorbent to biomass ratio on hydrogen composition at 675°C, steam to biomass ratio of 2.0 wt/wt, catalyst to biomass ratio of 0.1 wt/wt and biomass particle size of 1000-2000 μm

The effect of fluidization velocity (U) and biomass particle size ( $D_{\text{bio}}$ ) on H<sub>2</sub> composition is shown in Figure 4.67. The graphical results show similar effect of fluidization velocity and biomass particle size on H<sub>2</sub> content. Both parameters reduce the H<sub>2</sub> content in the product. The increase of H<sub>2</sub> content in the product gas at high fluidization velocity of 0.26 m/s by varying biomass particle size from 355-500 μm to

1000-2000  $\mu\text{m}$  is observed. This may be due to the reduction of heat and mass transfer limitations under high fluidization conditions (0.26 m/s). This statement can also be justified by observing a rise in the  $\text{H}_2$  content at high biomass particle size of 1000-2000  $\mu\text{m}$  at varying fluidization velocity of 0.15 m/s to 0.26 m/s.

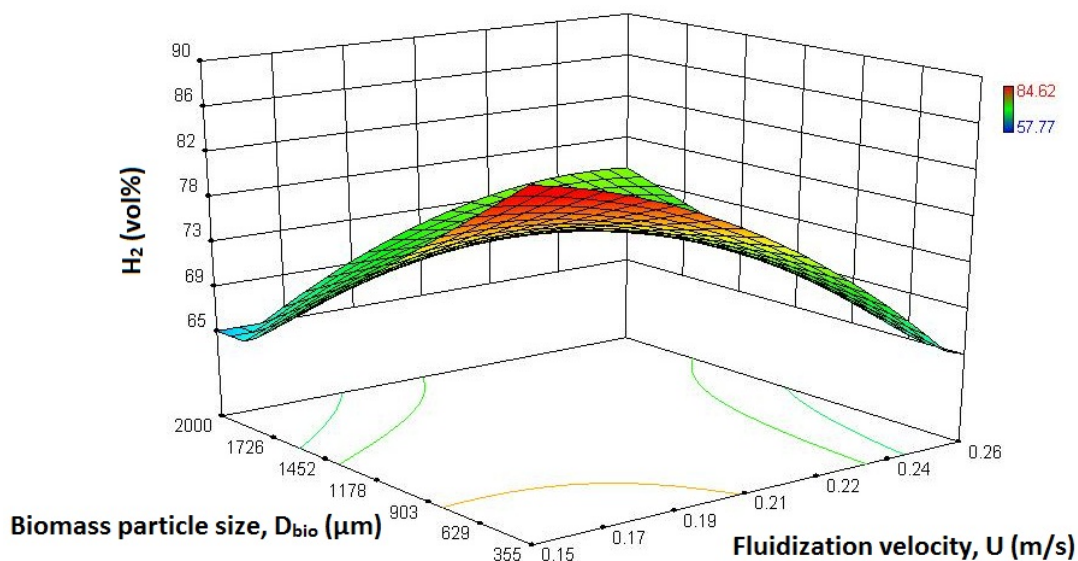


Figure 4.67: Effect of fluidization velocity and biomass particle size on hydrogen composition at  $675^\circ\text{C}$ , steam to biomass ratio 2.0 wt/wt, catalyst to biomass ratio of 0.1 wt/wt and adsorbent to biomass ratio of 1.0 wt/wt

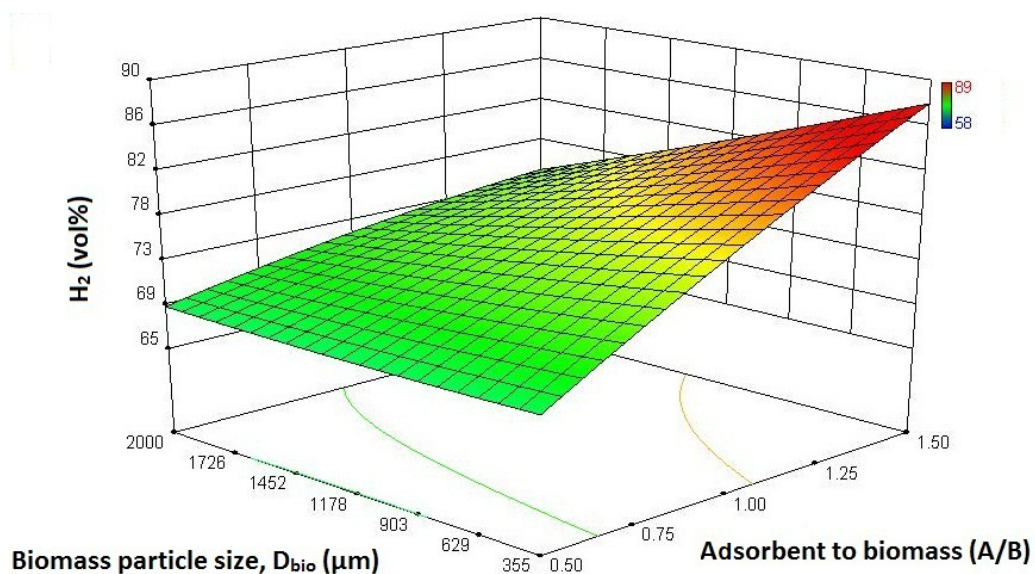


Figure 4.68: Effect of adsorbent to biomass ratio and biomass particle size on hydrogen composition based on temperature of  $675^\circ\text{C}$ , steam to biomass ratio 2.0 wt/wt, catalyst to biomass ratio of 0.1 wt/wt and fluidization velocity of 0.21 m/s

Figure 4.68 illustrates the effect of adsorbent to biomass ratio (A/B) and biomass particle size ( $D_{\text{bio}}$ ) on  $\text{H}_2$  content (vol%) in the product gas. The results indicate no significant effect on  $\text{H}_2$  content by increasing biomass particle size from 355-500  $\mu\text{m}$  to 1000-2000  $\mu\text{m}$  at adsorbent to biomass ratio of 0.5. However, increase in  $\text{H}_2$  content by 21.6% is observed at the smaller biomass particle size of 355-500  $\mu\text{m}$  by varying adsorbent to biomass from 0.5 to 1.5. At high biomass particle size of 1000-2000  $\mu\text{m}$ , increase in  $\text{H}_2$  content in product gas is reported to be 6.7%. At higher adsorbent to biomass ratio, the effect of increasing biomass particle size is more dominant, and decrease of  $\text{H}_2$  content by 15.9% is depicted.

#### 4.6.3.2 Hydrogen Yield

The 3D surface plots for hydrogen yield based on the combine effect of process variables; temperature (T), steam to biomass (S/B), adsorbent to biomass (A/B), fluidization velocity (U) and biomass particle size ( $D_{\text{bio}}$ ) are presented in the current section. The different combination of process variables generated by ANOVA is listed in the Table 4.33.

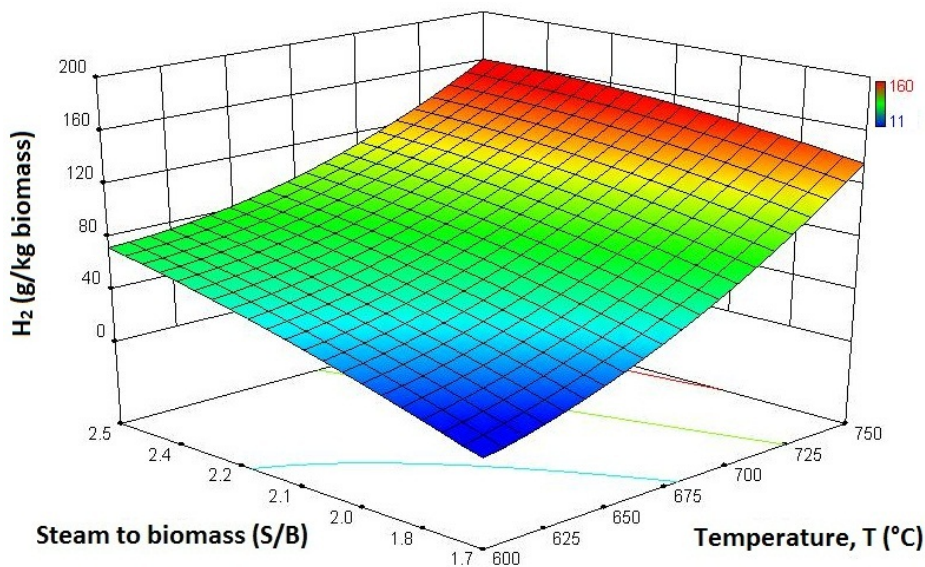


Figure 4.69: Effect of temperature and steam to biomass ratio on hydrogen yield based on fluidization velocity of 0.21 m/s, adsorbent to biomass ratio of 1.0 wt/wt, catalyst to biomass ratio of 0.1 wt/wt and biomass particle size of 1000-2000  $\mu\text{m}$

The effect of temperature (T) and steam to biomass ratio (S/B) on H<sub>2</sub> yield is illustrated in Figure 4.69. The graphical results show that the H<sub>2</sub> yield increases by increasing T and S/B ratio. The H<sub>2</sub> yield increases by 91.7% when temperature varies from 600°C to 750°C at lower S/B ratio of 1.5. On the other hand, at the lower temperature of 600°C, the rise in H<sub>2</sub> concentration is almost 83% by varying 1.5 to 2.5 of S/B ratio. For high temperature of 750°C, H<sub>2</sub> yield is increased by an increment of 25% when S/B increases from 1.5 to 2.5. It can be concluded that the increasing of S/B ratio at lower temperature of 600°C is more effective as compared to the higher temperature of 750°C. By keeping the S/B ratio at 2.5, the increment added in the H<sub>2</sub> yield is 56.2% by changing the temperature from 600°C to 750°C. This gives an important indication of using high temperature at relatively lower S/B ratio. Amongst temperature (T) and steam to biomass ratio (S/B), temperature is the most significant process parameter that enhance H<sub>2</sub> yield. At high T, endothermic reaction i.e. chars gasification, steam methane reforming, and tar cracking reactions are enhanced which increased H<sub>2</sub> content in the product gas. The significant increase in H<sub>2</sub> yield with temperature in biomass steam gasification with CO<sub>2</sub> adsorbent is reported by number of researchers [57, 86]. The increasing steam content also enhances the H<sub>2</sub> yield at lower and high temperature whereas lower temperature is more effective. The increase of H<sub>2</sub> yield with increasing S/B ratio (1.8-3.3 wt/wt) is also observed by Han et al. [86].

The effect of temperature (T) and fluidization velocity (U) on H<sub>2</sub> composition is shown in the Figure 4.70. It is observed that the H<sub>2</sub> yield increases by an increment of 48% by increasing the temperature from 600°C to 750°C at fluidization velocity of 0.15 m/s. Similarly, at constant temperature of 600°C, H<sub>2</sub> yield decreases by 76% by varying fluidization velocity of 0.15 m/s to 0.24 m/s. At high temperature of 750°C, increasing fluidization velocity from 0.21 m/s to 0.24 m/s give a rise in H<sub>2</sub> content by 53% in the product gas. H<sub>2</sub> yield increases by 94% at fluidization velocity of 0.24 m/s at temperature of 600°C to 750°C. This is due to high steam flow rates provided at high fluidization velocity, and high temperature that improves H<sub>2</sub> yield in product gas.

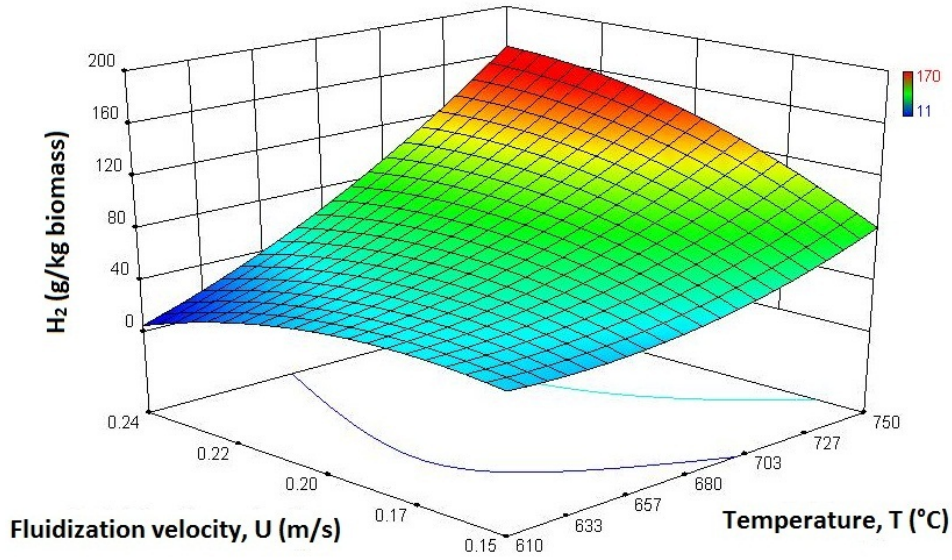


Figure 4.70: Effect of temperature and fluidization velocity on hydrogen yield based on steam to biomass ratio of 2.0 wt/wt, adsorbent to biomass ratio of 1.0 wt/wt, catalyst to biomass ratio of 0.1 wt/wt and biomass particle size of 1000-2000  $\mu\text{m}$

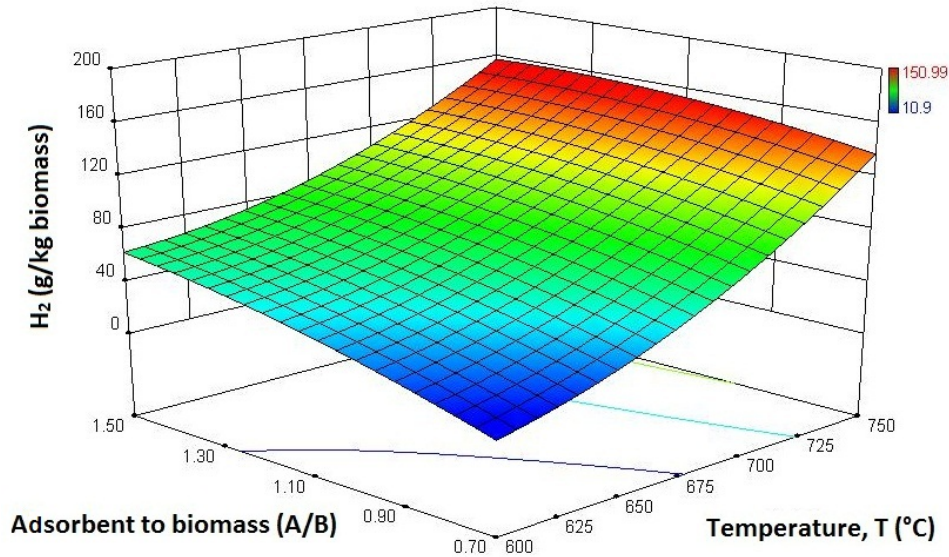


Figure 4.71: Effect of temperature and adsorbent to biomass ratio on hydrogen yield at steam to biomass ratio of 2.0 wt/wt, fluidization velocity of 0.21 m/s, catalyst to biomass ratio of 0.1 wt/wt and biomass particle size of 1000-2000  $\mu\text{m}$

The effect of temperature (T) and adsorbent to biomass (A/B) is shown in Figure 4.71. It can be observed that  $\text{H}_2$  yield increases by 92.3% by increasing temperature from 600°C to 750°C at adsorption to biomass ratio of 0.7. At constant temperature of

600°C, H<sub>2</sub> yield increases by 86.3% in the range of 0.70 to 1.50 A/B ratios. At high A/B ratio of 1.50, the yield increases by 56.9% when the temperature varies from 600°C to 750°C. However, no significant increase in H<sub>2</sub> yield is observed at 750°C by varying A/B from 0.70 to 1.50.

Figure 4.72 shows the effect of temperature (T) and biomass particle size (D<sub>bio</sub>) on hydrogen yield. H<sub>2</sub> yield increases by an increment of 58% as temperature increases from 600°C to 750°C at biomass particle size of 355-500 μm. The effect of increasing biomass particle size at low temperature of 600°C decrease H<sub>2</sub> yield by 76% at particle size of 355-500 μm to 1000-2000 μm. Heat transfer limitation in larger particle size inhibits the release of gas in biomass gasification. At high temperature of 750°C, H<sub>2</sub> yield increases by an increment of 44% when biomass particle size increased.

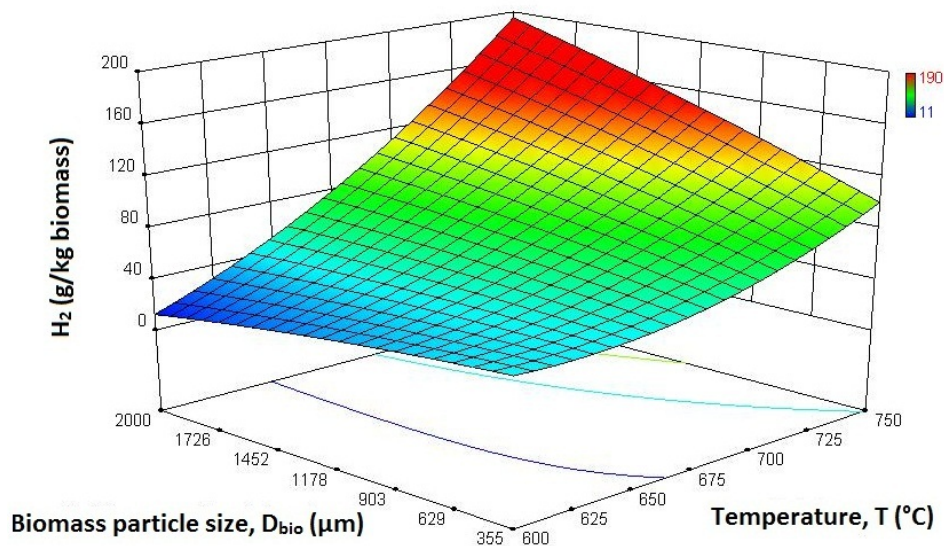


Figure 4.72: Effect of temperature and biomass particle size on hydrogen composition based on steam to biomass ratio of 2.0 wt/wt, adsorbent to biomass ratio of 1.0 wt/wt, catalyst to biomass ratio of 0.1 wt/wt and fluidization velocity of 0.21 m/s

Figure 4.73 explains the effect of steam to biomass ratio (S/B) and fluidization velocity (A/B) on hydrogen yield. At S/B ratio of 1.5, no significant variation is observed in H<sub>2</sub> yield. The results further show that the increase of H<sub>2</sub> yield by 44% is reported with respect to S/B ratio at fluidization velocity of 0.15 m/s. On the other

hand, at high fluidization velocity of 0.26 m/s, the yield of H<sub>2</sub> increases by 55.5% in the product gas. However, at high S/B ratio of 2.5, H<sub>2</sub> yield increases by 16.7% at varying fluidization velocity from 0.15 m/s to 0.26 m/s. High fluidization velocity and high S/B ratio favors H<sub>2</sub> yield.

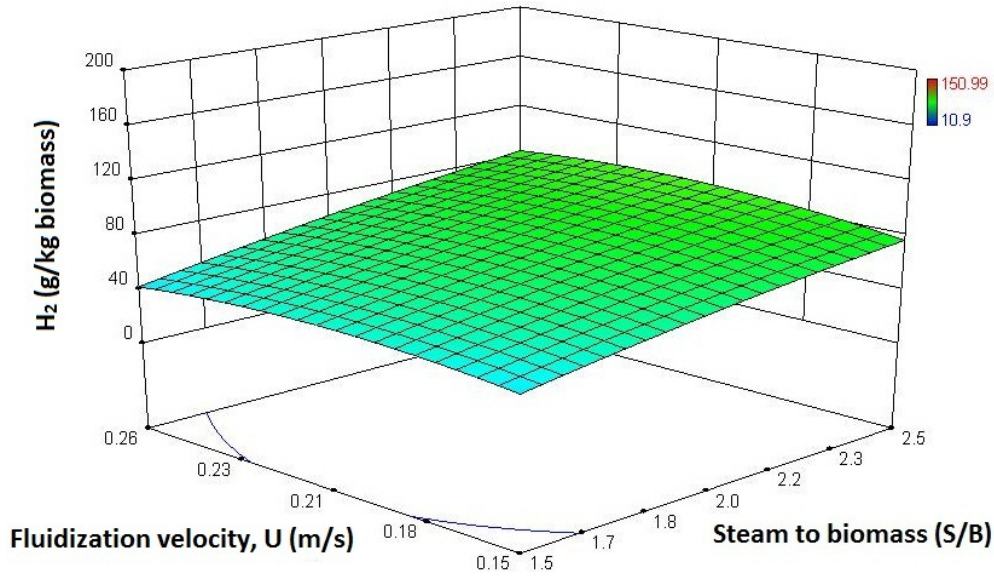


Figure 4.73: Effect of steam to biomass ratio and fluidization velocity on hydrogen yield at 675°C, adsorbent to biomass ratio of 1.0 wt/wt, catalyst to biomass ratio of 0.1 wt/wt and biomass particle size of 1000-2000 μm

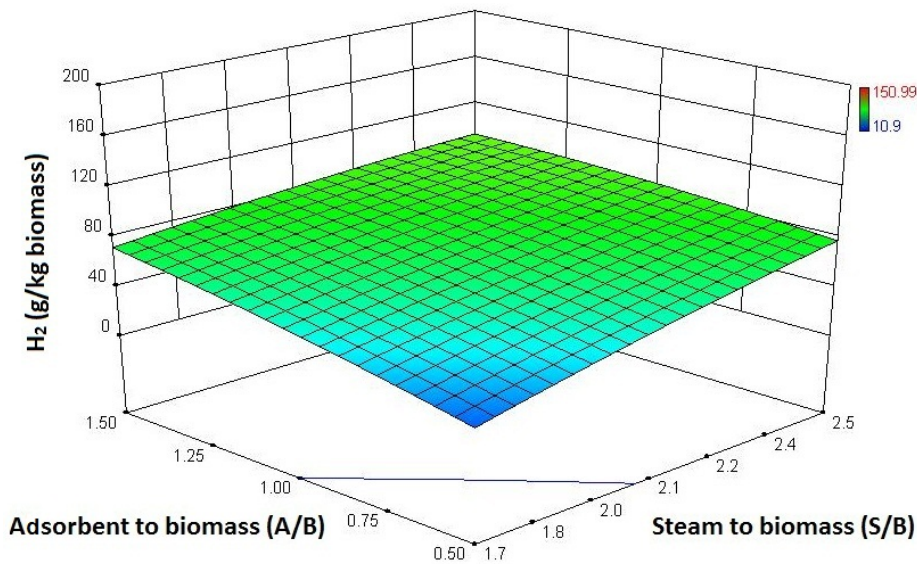


Figure 4.74: Effect of steam to biomass ratio and adsorbent to biomass ratio on hydrogen yield at 675°C, fluidization velocity of 0.21 m/s, catalyst to biomass ratio of 0.1 wt/wt and biomass particle size of 1000-2000 μm

The effect of steam to biomass ratio (S/B) and adsorbent to biomass (A/B) is shown in Figure 4.74. At S/B ratio of 1.7, H<sub>2</sub> yield increases by 52% by varying adsorbent to biomass ratio from 0.5 to 1.5. By keeping the adsorbent to biomass ratio at lowest value of 0.5, H<sub>2</sub> yield increases by an increment of 50% by increasing S/B ratio from 1.7 to 2.5. At 2.5 S/B ratios, increase of 13.3% is observed in H<sub>2</sub> yield by changing adsorbent to biomass from 0.5 to 1.5. On the other hand, at 1.5 adsorbent to biomass ratio, H<sub>2</sub> content increases by 18.9%. Based on the analysis, higher steam to biomass and adsorbent to biomass ratios increase the H<sub>2</sub> yield.

Figure 4.75 shows the effect of steam to biomass ratio (S/B) and biomass particle size ( $D_{bio}$ ) on H<sub>2</sub> yield in product gas. The results indicated that no significant effect is observed on H<sub>2</sub> content by increasing biomass particle size from 355-500  $\mu\text{m}$  to 1000-2000  $\mu\text{m}$  at lower S/B ratio of 1.5. Similar result is also observed in the case of high S/B ratio of 2.5. It can be concluded that no significant variation in H<sub>2</sub> yield is observed with respect to biomass particle size by varying S/B ratio. On the other hand, addition of steam doubles the H<sub>2</sub> yield in product gas at lower biomass particle size of 355-500  $\mu\text{m}$ . At larger particle size of 1000-2000  $\mu\text{m}$ , H<sub>2</sub> yield increases by 16%.

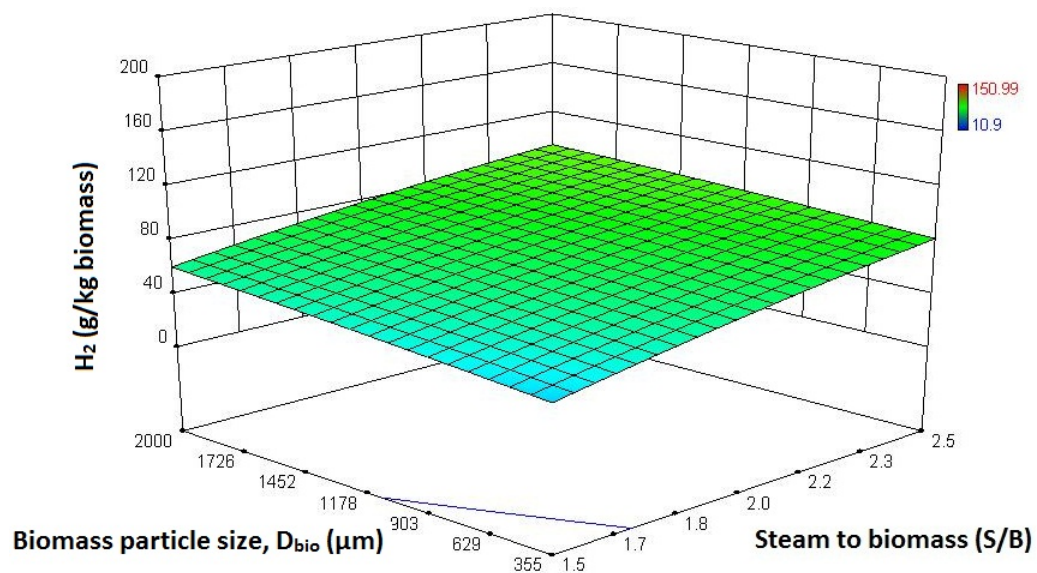


Figure 4.75: Effect of steam to biomass ratio and biomass particle size on hydrogen composition at 675°C, adsorbent to biomass ratio of 1.0 wt/wt, catalyst to biomass ratio of 0.1 wt/wt and fluidization velocity of 0.21 m/s

As shown in Figure 4.76, the effect of adsorbent to biomass ratio (A/B) and fluidization velocity on H<sub>2</sub> yield in ICA steam gasification is illustrated. The analysis shows that no considerable effect is observed on the H<sub>2</sub> yield by increasing fluidization velocity from 0.15 m/s to 0.26 m/s at 0.5 adsorbent to biomass ratio. However, an increment of 12.5% is observed at high value of adsorbent to biomass ratio of 1.50 by varying fluidization velocity within the similar range. H<sub>2</sub> yield increases by 45% by changing adsorbent to biomass ratio in the range of 0.50 to 1.50 at 0.15 m/s. Based on the results presented, it can be concluded that the adsorbent to biomass ratio is more significant as compared to the fluidization velocity.

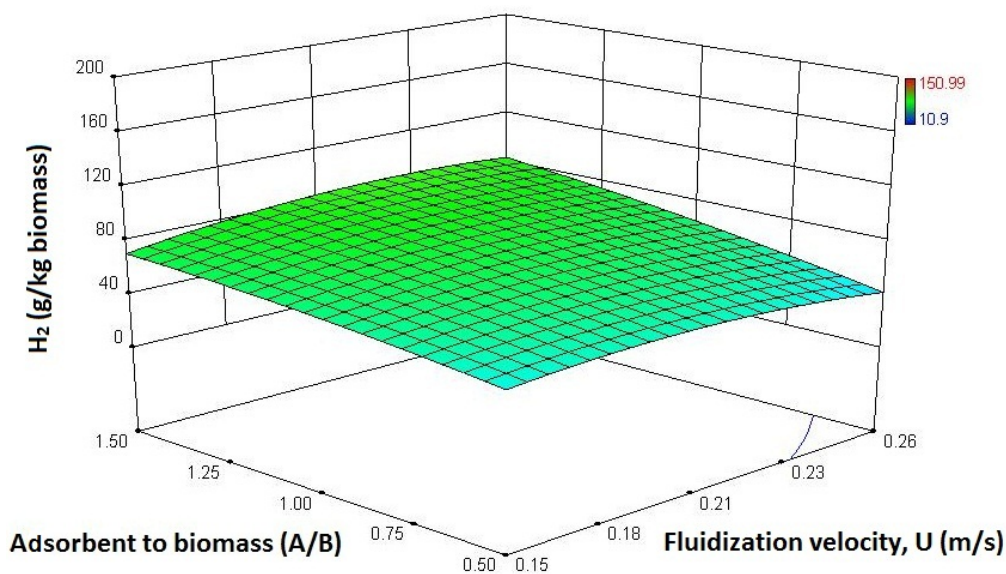


Figure 4.76: Effect of adsorbent to biomass ratio and fluidization velocity on hydrogen yield based on 675°C, steam to biomass ratio of 2.0 wt/wt, catalyst to biomass ratio of 0.1 wt/wt and biomass particle size of 1000-2000  $\mu\text{m}$

The effect of fluidization velocity (U) and biomass particle size ( $D_{\text{bio}}$ ) on H<sub>2</sub> yield in product gas is shown in Figure 4.77. In general, no significant variation is observed at 0.15 m/s at varying biomass particle size from 355-500  $\mu\text{m}$  to 1000-2000  $\mu\text{m}$  and at 355-500  $\mu\text{m}$  by changing the fluidization velocity from 0.15 m/s to 0.26 m/s. However, significant variation is observed at high U by changing biomass particle size from 355-500  $\mu\text{m}$  to 1000-2000  $\mu\text{m}$  while changing U from 0.15 to 0.26 m/s. In the present study, fluidization velocity and biomass particle size do not have significant increase in H<sub>2</sub> yield. Therefore, the combine effect of these two process

variables is not significant as compared to the other variables combinations in the process such as temperature and steam to biomass ratio.

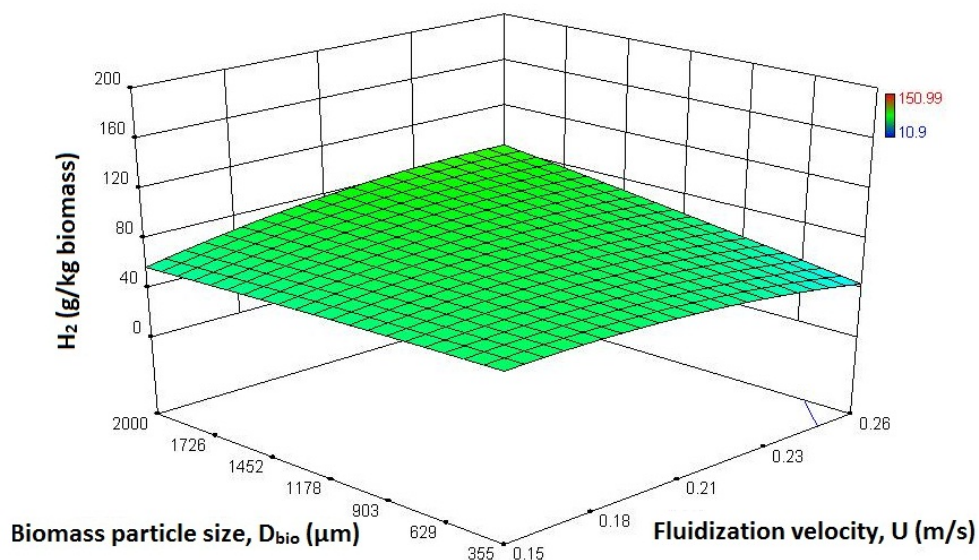


Figure 4.77: Effect of biomass particle size and fluidization velocity on hydrogen yield at 675°C, steam to biomass ratio of 2.0 wt/wt, catalyst to biomass ratio of 0.1 wt/wt and adsorbent to biomass ratio of 1.0 wt/wt

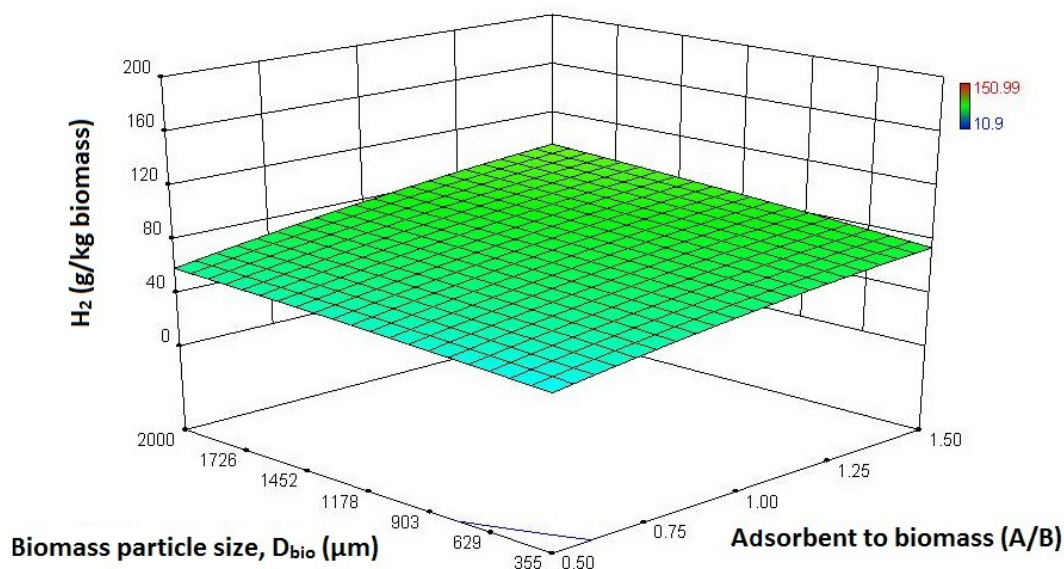


Figure 4.78: Effect of biomass particle size and adsorbent to biomass ratio on hydrogen yield at 675°C, steam to biomass ratio of 2.0 wt/wt, catalyst to biomass ratio of 0.1 wt/wt and fluidization velocity of 0.21 m/s

Figure 4.78 describes the effect of adsorbent to biomass ( $A/B$ ) ratio and biomass particle size ( $D_{bio}$ ) on  $H_2$  yield in product gas. The results show that no significant is

observed in hydrogen yield by varying fluidization velocity and/or adsorbent to biomass ratio.

#### 4.6.4 Optimization of Hydrogen Composition and Yield

RSM was applied to assess the effect of process variables on output response that includes hydrogen composition and yield. A regression analysis was used to check the fitting of experimental results via analysis of variance (ANOVA). Based on the ANOVA analysis, a quadratic model is fitted to the experimental results based on p-value, F-value and lack of fit as regression coefficients. It is concluded from experimental results, and the effect of combine variables analysis that composition and yield are at their maximum values at different conditions. Temperature is the most influential variable. The optimization study is carried out following the design of experiments using the Expert Design 8 software. The optimum process conditions produced are listed in Table 4.35.

Table 4.35: The optimum parameter selected to maximize H<sub>2</sub> composition and yield

Parameter	Optimum process variables
Temperature (°C)	675
Steam to biomass (wt/wt)	2.0
Fluidization velocity (m/s)	0.21
Adsorbent (CaO) /biomass (wt/wt)	1.0
Biomass particle size (µm)	1000-2000

#### 4.6.5 Reproducibility of Experimental Results

Four confirmation experiments are carried out to reproduce the experimental results of hydrogen composition and yield. The reproducibility results are compared with optimized values of hydrogen composition and yield predicted by the model.

The results from the confirmation experiments are presented in Table 4.36. It can be concluded that the results are reproducible with acceptable accuracy as shown in Table 4.37. The results from confirmation experiments are compared with optimized

model predicted values. The hydrogen composition observed is  $82.11 \pm 4.77$  vol%. For hydrogen yield, the value of  $80.39 \pm 6.45$  g/kg biomass is observed. On the other hand, hydrogen composition and yield predicted by the model are  $75.53 \pm 3.46$  vol% and  $73.31 \pm 5.89$  g/kg biomass, respectively. The comparison shows that the model prediction values are in good agreement with the experimental values.

Table 4.36: Results of confirmation runs for hydrogen composition and yield

Parameter	Experimental run				
	First run	Confirmation runs			
		1	2	3	4
H <sub>2</sub> (vol%)	82.11	74.74	69.36	72.50	75.13
H <sub>2</sub> (g/kg biomass)	80.39	80.61	71.56	69.94	66.26

Table 4.37: Comparison of experimental values with modeling for hydrogen composition and yield

Parameter	Experimental	Model prediction
H <sub>2</sub> (vol%)	$82.11 \pm 4.77$	$75.53 \pm 3.46$
H <sub>2</sub> (g/kg biomass)	$80.39 \pm 6.45$	$73.31 \pm 5.89$

#### 4.7 Determination of Kinetic and Thermodynamic Parameters

The present section consists of two parts. The first part considers the kinetic parameters determination for the main reactions involved in ICA steam gasification and second part deals with estimation of product gas composition using reaction kinetic parameters.

The kinetic parameter evaluation was carried out using product gas composition. The study was conducted for the gas composition at different temperature. The kinetic parameters were evaluated by minimizing the residual between the experimental data and theoretical data. Table 4.38 summarizes all the kinetic parameters for the main reactions occurring in ICA steam gasification process.

Table 4.38: Evaluated kinetic parameters

No	Reaction	Frequency factor, A (1/s)	Activation energy, E (kJ/mol)	Kinetic constant, k (1/s)
1	Char gasification	$3.32 \times 10^4$	999.95	$3.32 \times 10^4 \exp(-999.95/RT)$
2	Methanation	$3.19 \times 10^4$	0.98	$3.19 \times 10^4 \exp(-0.98/RT)$
3	Boudouard	$1.7 \times 10^3$	16.84	$1.7 \times 10^3 \exp(-16.84/RT)$
4	Methane reforming	$3.19 \times 10^4$	21.57	$3.19 \times 10^4 \exp(-21.57/RT)$
5	Water gas shift	$0.4 \times 10^1$	22.38	$0.4 \times 10^1 \exp(-22.38/RT)$
6	Carbonation	$2.81 \times 10^2$	17.57	$2.81 \times 10^2 \exp(-17.57/RT)$

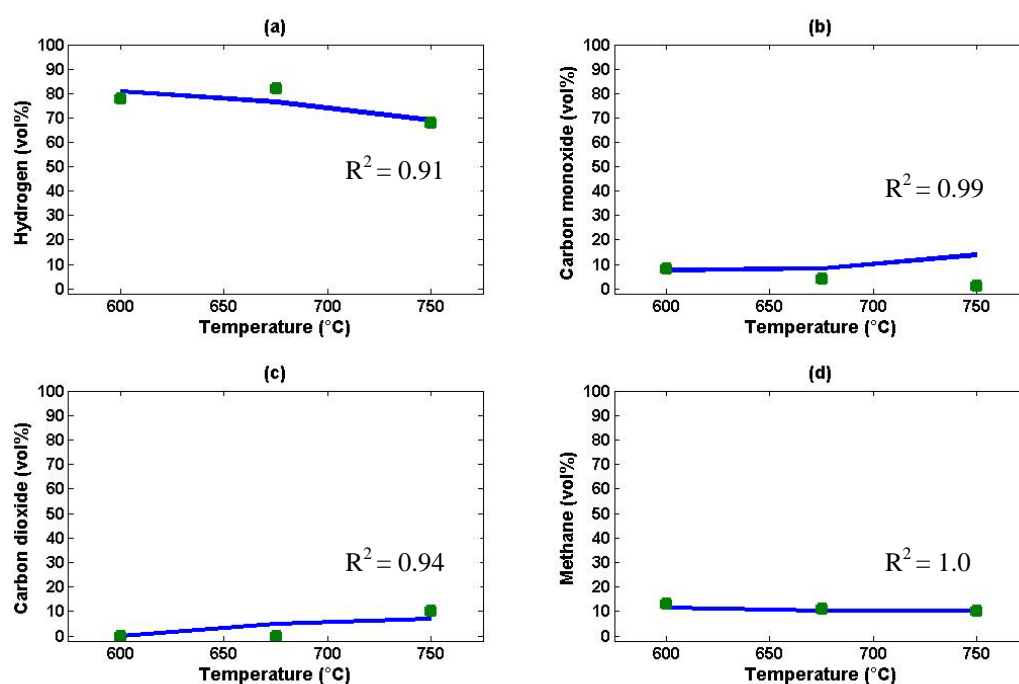


Figure 4.79: Effect of temperature on product gas composition; modeling (—) and experiment (■)

Figure 4.79 shows the effect of temperature at 600°C, 675°C and 750°C on product gas composition of H<sub>2</sub>, CO, CO<sub>2</sub> and CH<sub>4</sub>. As observed, the model predicts the product gas composition in a good agreement with the experimental results. The coefficient of determination ( $R^2$ ) is found to be higher than 0.91. Overall, high

temperature reduces H<sub>2</sub> content in the product gas due to the reverse carbonation reaction that promotes high concentration of CO<sub>2</sub> in the product gas. High CO content is observed at high temperature due to reverse carbonation reaction. Similar trends are also reported by the previous researchers [104].

Table 4.39 provides the mean error calculated for each product gas. The results show that the low mean error shows good fit of modeling results to the experimental values.

Table 4.39: Mean error of product gas composition with temperature

Product gas	Mean error
H <sub>2</sub>	0.004
CO <sub>2</sub>	0.325
CO	0.002
CH <sub>4</sub>	0.030

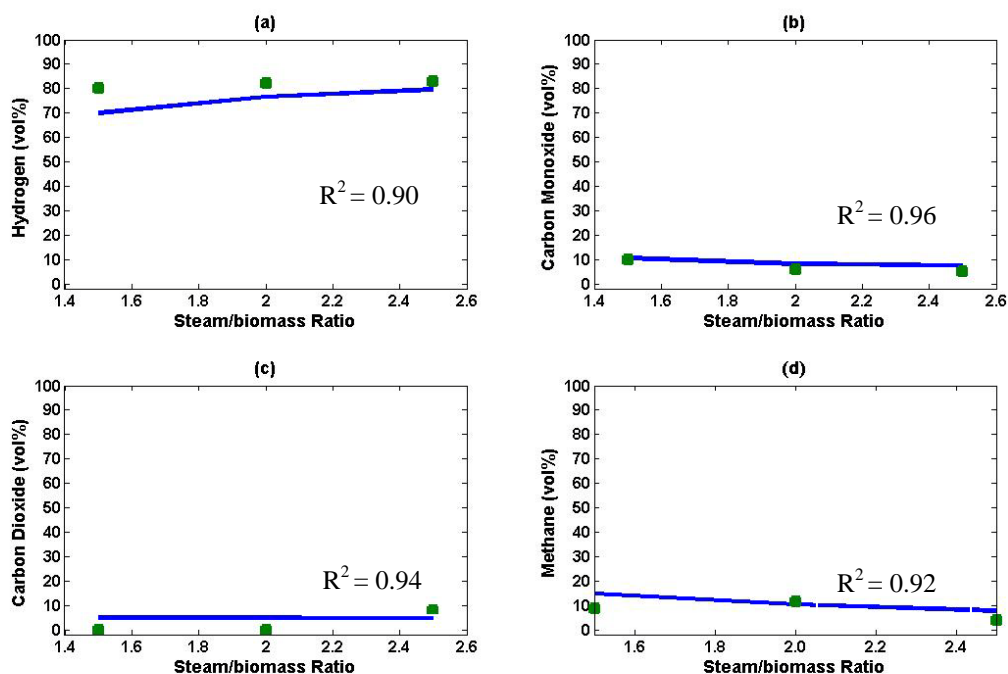


Figure 4.80: Effect of steam to biomass ratio on product gas composition; modelling (—) and experiment (■)

Figure 4.80 illustrates the effect of steam to biomass (S/B) ratio on product gas composition for experiments and model. The results are in good agreement with experimental values that is observed at 675°C, A/B ratio of 1.0 and catalyst to

biomass ratio of 0.1 at varying S/B ratio from 1.5 to 2.5. The coefficient of determination ( $R^2$ ) is found to be higher than 0.90. The addition of steam increases the  $H_2$  content in the product gas and promotes methane reforming, water gas shift and char gasification reactions in the forward direction to produce more  $H_2$ . This increase in  $H_2$  content is due to decreases in CO and  $CH_4$  and increase in  $CO_2$  content in product gas. Similar trends are reported by Mahishi et al. [104] for steam gasification with in-suit  $CO_2$  adsorbent in fluidized bed reactor. Table 4.40 indicates mean error calculated between the experimental and models results. Based on the mean error values, the results provide good agreement between experimental and model data.

Table 4.40: Mean error of product gas composition with steam to biomass ratio

Product gas	Mean error
$H_2$	0.044
$CO_2$	0.48
CO	0.14
$CH_4$	0.21

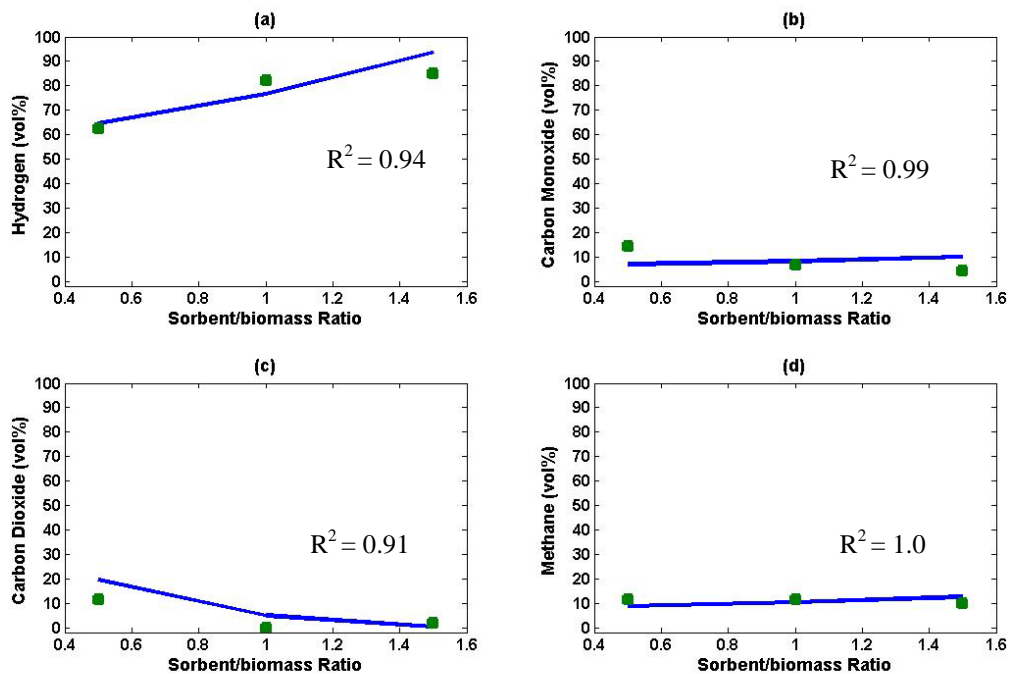


Figure 4.81: Effect of adsorbent to biomass ratio on product gas composition; modeling (—) and experiment (■)

The adsorbent to biomass ratio is tested for product gas distribution as shown in the Figure 4.81. The model results fitted well to the experimental values generated at

process conditions of 675°C, S/B ratio of 2.0, and catalyst to biomass ratio of 0.1 by varying A/B ratio from 0.5 to 1.5. The coefficient of determination ( $R^2$ ) is found to be higher than 0.91. The product gases i.e. H<sub>2</sub>, CO, CO<sub>2</sub> and CH<sub>4</sub> show similar trends as observed from the experimental data.

The addition of adsorbent increases the H<sub>2</sub> content in the product gas. The excess amount of adsorbent (CaO) captured CO<sub>2</sub> in the process which subsequently enhances the activity of water gas shift and drives all the gasification and reforming reactions towards H<sub>2</sub> generation. The mean error for the gas component is listed in Table 4.41. Low mean errors are observed for all the gases.

Table 4.41: Mean error of product gas composition with adsorbent to biomass ratio

Product gas	Mean error
H <sub>2</sub>	0.013
CO <sub>2</sub>	0.49
CO	0.002
CH <sub>4</sub>	0.023

Thermodynamic parameters such as equilibrium constant and Gibbs free energy are calculated for water gas shift reaction in the present study. Several studies [101, 128] found that the water gas shift seems to reach the equilibrium, and control the gas phase kinetics in biomass steam gasification in fluidized bed reactor. Equilibrium constants and Gibbs free energy are evaluated based on the concentration of product gas at three different temperatures of 600°C, 675°C, 750°C at steam to biomass ratio of 2.0, adsorbent to biomass ratio of 1.0 and catalyst to biomass ratio of 0.1. Water gas shift reaction can be written as:



Equilibrium constant for the reaction is calculated as [210]:

$$K_e = \frac{[\text{CO}_2][\text{H}_2]}{[\text{CO}][\text{H}_2\text{O}]} \quad (4.4)$$

The quantity in the bracket shows the concentration (mol/m<sup>3</sup>) of product i.e. CO<sub>2</sub>, H<sub>2</sub> and reactant i.e. CO, H<sub>2</sub>O. Once  $K_e$  is determined, change in Gibbs free energy is

calculated [211] to check spontaneous and nonspontaneous nature of the reaction at given operating conditions:

$$\Delta G^\circ = -RT \ln K_e \quad (4.5)$$

$R$  and  $T$  represent universal gas constant (mol/k) and temperature (K), respectively.

Equilibrium constants and Gibbs free energy evaluated are listed in Table 4.42. The result shows that the equilibrium constant increases with increasing temperature. These results infer that the concentration of product gas i.e.  $H_2$  and  $CO_2$  is increasing with increasing temperature. This can be justified under the effect of temperature on individual gas composition as shown in Figure 4.37. In the present study,  $H_2$  composition increases at temperature range of 600-675°C while no  $CO_2$  composition depicted at this temperature. At 750°C,  $H_2$  composition decreases but  $CO_2$  increases due to reverse carbonation reaction. The positive Gibbs free energy shows that the water gas shift reaction is nonspontaneous at given experimental conditions (Table 4.42).

Table 4.42: Effect of temperature on equilibrium constant and Gibbs free energy

Parameter	Temperature (°C)		
	600	675	750
Equilibrium constant (-)	0.04	0.14	0.40
Gibbs free energy (KJ/mol)	23.50	15.77	8.81

To assess the results further, equilibrium constant evaluated are plotted along with theoretical equilibrium constant [212] and experimental equilibrium constant observed by Herguido et al. [101] at 600°C, 700°C and 750°C for steam gasification in fluidized bed reactor as shown in Figure 4.82. The equilibrium constants observed in the present study increases with increasing temperature which is in a good agreement with Herguido et al. [101]. Similar observation is also observed by other researchers [43]. Comparative study shows that the lower equilibrium constant values observed in the present study may be due to the presence of  $CO_2$  adsorbent which captures most of the  $CO_2$  in the product gas thus reduces overall equilibrium constant values for water gas shift reaction.

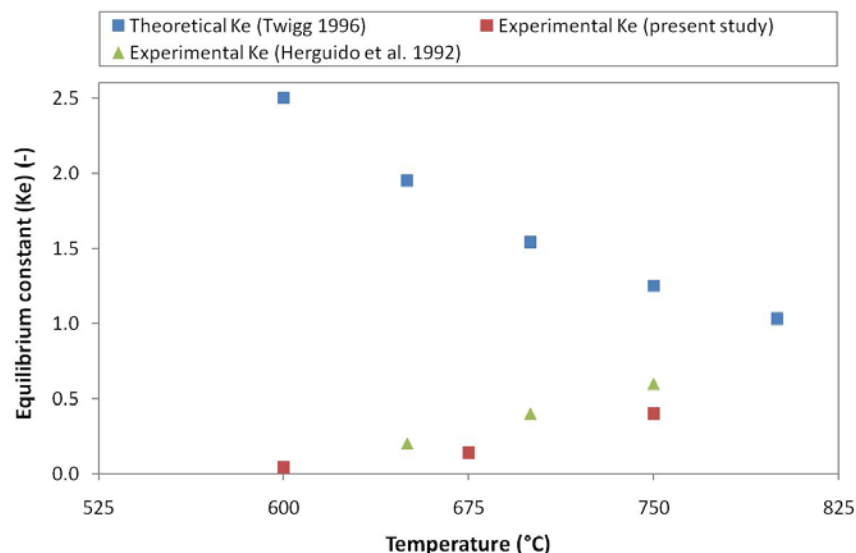


Figure 4.82: Effect of reactor temperature on the equilibrium of water gas shift reaction

#### 4.8 Chapter Summary

Material characterization of commercial Quicklime and Ni catalyst are carried out using XRD, XRF, SEM, and physisorption analysis. The chemical composition of the samples indicated that Quicklime sample contained 93 wt% CaO, 4.24 wt% MgO, 0.95 wt% SiO<sub>2</sub>, 0.2 wt% Fe<sub>2</sub>O<sub>3</sub>, 0.18 wt% Al<sub>2</sub>O<sub>3</sub> and 1 wt% metal oxides (MnO, CuO, SrO and ZnO). The Ni catalyst contained 97 wt% Ni, 2.2 wt% P<sub>2</sub>O<sub>5</sub> and 0.38 wt% Fe<sub>2</sub>O<sub>3</sub>. Based on pore size, volume, and BET surface area, both samples are classified as mesoporous solid. This is further supported by the adsorption isotherm plots for Quicklime and Ni catalyst.

The effect of process parameters i.e. temperature, steam to biomass ratio (A/B), adsorbent to biomass ratio (A/B), fluidization velocity and biomass particle size on hydrogen composition and yield are studied for ICA steam gasification system. By studying the temperature effect, maximum H<sub>2</sub> composition i.e. 82.11 vol% is observed at 675°C while no CO<sub>2</sub> content is found in product gas. By increasing the temperature, H<sub>2</sub> composition decreases with considerable amount of CO<sub>2</sub> present in the product gas. This is due to the existence of reverse carbonation reaction at temperature higher than 675°C. Conversely, H<sub>2</sub> yield increases with temperature and

maximum yield of 150 g/kg biomass is produced at 750°C. Furthermore, by increasing S/B and A/B ratios, H<sub>2</sub> composition and yield is gradual increased. However, optimum fluidization velocity is found at 0.21 m/s which is 4 time of the minimum fluidization velocity. By further increasing the velocity to 0.26 m/s (5 times of fluidization velocity), H<sub>2</sub> composition and yield is decreased. In addition, performance parameters such as gasification efficiency, carbon conversion efficiency, product gas heating values selectivity are studied for each process variables. Energy required for the gasification process increases with temperature, S/B ratio and fluidization velocity, and decreases with increasing A/B ratio. Biomass particle size has no significance effect on the energy required for gasification.

The optimization study is carried out to investigate the optimum process conditions for H<sub>2</sub> composition and yield. The experimental results are best fitted to the quadratic model through ANOVA analysis. Apart from the model significance prediction, ANOVA is also able to predict the significance of individual process input variables as well as their interactions. As observed, amongst the five process variables, adsorption to biomass ratio is a significant variable that influenced hydrogen composition in ICA steam gasification. For hydrogen yield, the significance process parameters are temperature, steam to biomass ratio and adsorbent to biomass ratio. Finally, the optimization conditions are found to be at temperature of 675°C, S/B ratio of 2.0, biomass particle size of 1.0-2.0 mm and adsorbent to biomass ratio of 1.0. Further confirmation experimental runs are performed in the gasification system to obtained hydrogen composition and yield at the optimum conditions. Experimental values of hydrogen composition and yield are found to be in good agreement with values predicted by the model.

The kinetic parameters are evaluated through kinetic model for the main reactions involved in biomass gasification i.e. char gasification, boudouard, methanation, steam methane reforming and water gasification reactions. The activation energy and frequency factor are found to be in the range of 0.98-999.95 kJ/mol and  $0.41 \times 10^1$ - $3.32 \times 10^4$  s<sup>-1</sup>, respectively, for first order kinetic model. These kinetic parameters are used to predict the product gas composition at varying temperature, steam to biomass

ratio and adsorbent to biomass ratio. The results are in good agreement with experimental values.



## CHAPTER 5

### CONCLUSIONS AND RECOMMENDATIONS

#### 5.1 Conclusions

Integrated catalytic adsorption (ICA) steam gasification process for hydrogen production utilizing palm kernel shell as the feedstock is investigated in fluidized bed gasifier. The ultimate aim is to enhance the hydrogen content in the product gas. Overall, the main objectives of the study were; development of the main process design utilizing in-situ catalytic and adsorption process, design of main fluidized bed gasifier, performance evaluation of in-situ catalytic and adsorption process under the effect of reactor temperature, steam to biomass ratio, adsorbent to biomass ratio, fluidization velocity and biomass particle size, and kinetic parameter evaluation through kinetic modelling of simultaneous reactions in in-situ catalytic and adsorption process.

The overall process design is evaluated through hierarchical approach. The overall process divides into gasification and downstream gas cleaning systems. Gasification involves main fluidized bed reactor associated with biomass feeding system and steam generation unit. The downstream gas cleaning system is divided into solid separator, and water cooling and separation units.

The fluidized bed reactor configuration is evaluated based on the hydrodynamics parameter i.e. minimum fluidization velocity and total steam requirement for the reactions involved in the ICA steam gasification process. The minimum fluidization velocity is calculated based on the physical properties of the bed material and steam as gasifying agent. The diameter and height of the fluidized bed gasifier calculated are 0.15 m and 2.0 m, respectively. The orifice type of distributor is used and designed based on the ratio of pressure drop across the distributor plate to the bed. The

performance of the designed fluidized bed reactor has eliminated the needs of downstream processing reactor thus reduce production and operating cost.

The performance of the ICA gasification system is evaluated through hydrogen composition and yield under the effect of different parameters. It is shown that the hydrogen yield (g/kg biomass) increases with increasing temperature, steam to biomass ratio and adsorbent to biomass ratio while biomass particle size has no significant effect on hydrogen yield. It is found that the system has a potential to produce maximum hydrogen yield of 150 g/kg biomass at 750°C, steam/biomass ratio of 2.0, adsorbent to biomass ratio of 1.0, and catalyst to biomass ratio of 0.1. Maximum hydrogen composition of 84 vol% is depicted at 675°C, steam/biomass ratio of 2.0, adsorbent to biomass ratio of 1.5 and catalyst to biomass ratio of 0.1. It is further demonstrated that the water gas shift and methane steam reforming are the dominant reactions for hydrogen production. Moreover, carbonation reaction is dominant at temperature range of 600-675°C while high temperature of 750°C favors the reverse carbonation reaction, and reduces hydrogen content and increases CO<sub>2</sub> in product gas. Medium fluidization velocity (0.21 m/s) which is 4 times of minimum fluidization velocity favors high hydrogen yield and composition. Furthermore, hydrogen composition (vol%) increases by increasing steam to biomass ratio and adsorbent to biomass ratio while medium temperature (675°C) produces maximum composition of 82.11 vol% with no CO<sub>2</sub> content in the product gas. The comparison shows that the present study improved the hydrogen composition and yield in the product gas from 58 vol% [86] to 82 vol% (present study) and 67 g/kg biomass [86] to 150 g/kg biomass (present study). It is found that the endothermic reactions i.e. char gasification; steam methane reforming and tar cracking reactions are mainly responsible for increase in total gas yield at high temperature. Excess steam and adsorbent (CaO) also contributes to high gas yield and lower char yield. No significant effect of biomass particle size is observed on total gas and char yield.

The study of kinetic parameter shows that the activation energy and frequency factor are found to be in the range of 0.98 kJ/mol-999.95 kJ/mol and  $0.41 \times 10^1 \text{ s}^{-1}$ - $3.32 \times 10^4 \text{ s}^{-1}$ , respectively, for first order kinetic model. These kinetic parameters are then used to predict the product gas composition by varying temperature, steam to

biomass ratio and adsorbent to biomass ratio. The results are in good agreement with experimental findings. Thermodynamic parametric study shows that the equilibrium constant of water gas shift reaction increases with increasing reactor temperature from 600-750°C. It is found that the presence of CO<sub>2</sub> adsorbent in the system produce lower values of equilibrium constant as compared to steam gasification process reported in the literature. Continues capturing of CO<sub>2</sub> in water gas shift keeps the reaction away from the equilibrium point. The change in Gibbs free energy shows that the water gas shift reaction is nonspontaneous in ICA steam gasification utilizing palm kernel shell as the feedstock.

## **5.2 Recommendations**

- The integrated catalytic adsorption (ICA) steam gasification study can be extended to tar production under the influence of process variables i.e. temperature, steam to biomass ratio, adsorbent to biomass ratio, fluidization velocity, type of catalysts and bed materials.
- An integrated design from heat integration prospective needs to be considered utilizing the amount of energy associated with unreacted steam at the exit of fluidized bed gasifier for improved economical aspect of the developed technology.
- Future study can also be attributed towards utilization of catalyst in downstream unit to compare the efficiency of the developed system.

## REFERENCES

- [1] Energy Information Administration, "World energy outlook 2010."
- [2] International Energy Agency, "Key world energy statistics 2010."
- [3] Energy Information Administration, "World energy outlook 1998."
- [4] T. L. Kelly-Yong, K. T. Lee, A. R. Mohamed, and S. Bhatia, "Potential of hydrogen from oil palm biomass as a source of renewable energy worldwide", *Energy Policy*. vol. 35, 2007, pp. 5692-5701.
- [5] S. Mekhilef, R. Saidur, A. Safari, and W. E. S. B. Mustaffa, "Biomass energy in Malaysia: Current state and prospects", *Renewable and Sustainable Energy Reviews*. vol. 15, 2011, pp. 3360-3370.
- [6] Z. Khan, S. Yusup, M. M. Ahmad, V. S. Chok, Y. Uemura, and K. M. Sabil, "Review on hydrogen production technologies in Malaysia", *International Journal of Engineering & Technology*. vol. 10, 2010, pp. 111-118.
- [7] A. Rahman Mohamed and K. T. Lee, "Energy for sustainable development in Malaysia: Energy policy and alternative energy", *Energy Policy*. vol. 34, 2006, pp. 2388-2397.
- [8] H. Hashim and W. S. Ho, "Renewable energy policies and initiatives for a sustainable energy future in Malaysia", *Renewable and Sustainable Energy Reviews*. vol. 15, 2011, pp. 4780-4787.
- [9] J. D. Holladay, J. Hu, D. L. King, and Y. Wang, "An overview of hydrogen production technologies", *Catalysis Today*. vol. 139, 2009, pp. 244-260.
- [10] H. Balat and E. Kırtay, "Hydrogen from biomass – present scenario and future prospects", *International Journal of Hydrogen Energy*. vol. 35, 2010, pp. 7416-7426.
- [11] N. Florin and A. Harris, "Hydrogen production from biomass", *The Environmentalist*. vol. 27, 2007, pp. 207-215.
- [12] Y. Kalinci, A. Hepbasli, and I. Dincer, "Biomass-based hydrogen production: A review and analysis", *International Journal of Hydrogen Energy*. vol. 34, 2009, pp. 8799-8817.

- [13] M. Balat and M. Balat, "Political, economic and environmental impacts of biomass-based hydrogen", *International Journal of Hydrogen Energy*. vol. 34, 2009, pp. 3589-3603.
- [14] S. Babu, "Biomass gasification for hydrogen production – process description and research needs," Gas Technology Institute, Des Plaines, Illinois, 2002.
- [15] J. Li, Y. Yin, X. Zhang, J. Liu, and R. Yan, "Hydrogen-rich gas production by steam gasification of palm oil wastes over supported tri-metallic catalyst", *International Journal of Hydrogen Energy*. vol. 34, 2009, pp. 9108-9115.
- [16] S. Rapagnà, N. Jand, and P. U. Foscolo, "Catalytic gasification of biomass to produce hydrogen rich gas", *International Journal of Hydrogen Energy*. vol. 23, 1998, pp. 551-557.
- [17] J. Corella, M. P. Aznar, M. A. Caballero, G. Molina, and J. M. Toledo, "140 g H<sub>2</sub>/kg biomass d.a.f. By a CO-shift reactor downstream from a FB biomass gasifier and a catalytic steam reformer", *International Journal of Hydrogen Energy*. vol. 33, 2008, pp. 1820-1826.
- [18] International Network for Sustainable Energy, " Biomass energy", 2006.
- [19] S. H. Shuit, K. T. Tan, K. T. Lee, and A. H. Kamaruddin, "Oil palm biomass as a sustainable energy source: A Malaysian case study", *Energy*. vol. 34, 2009, pp. 1225-1235.
- [20] S. Yusup, M. T. Arpin, Y. Uemura, A. Ramli, L. Ismail, S. H. Shuit, K. T. Tan, and K. T. Lee, "Review on agricultural biomass utilization as energy source in Malaysia," in *Proceedings of 16th Asean Regional Symposium on Chemical Engineering*, Manila, Philippines, 2009.
- [21] N. H. Florin and A. T. Harris, "Enhanced hydrogen production from biomass with in situ carbon dioxide capture using calcium oxide sorbents", *Chemical Engineering Science*. vol. 63, 2008, pp. 287-316.
- [22] C. Pfeifer and H. Hofbauer, "Development of catalytic tar decomposition downstream from a dual fluidized bed biomass steam gasifier", *Powder Technology*. vol. 180, 2008, pp. 9-16.
- [23] R. Warnecke, "Gasification of biomass: Comparison of fixed bed and fluidized bed gasifier", *Biomass and Bioenergy*. vol. 18, 2000, pp. 489-497.

- [24] E. Gusta, A. K. Dalai, M. A. Uddin, and E. Sasaoka, "Catalytic decomposition of biomass tars with dolomites", *Energy & Fuels*. vol. 23, 2009, pp. 2264-2272.
- [25] G. Hu, S. Xu, S. Li, C. Xiao, and S. Liu, "Steam gasification of apricot stones with olivine and dolomite as downstream catalysts", *Fuel Processing Technology*. vol. 87, 2006, pp. 375-382.
- [26] D. Sutton, B. Kelleher, and J. R. H. Ross, "Review of literature on catalysts for biomass gasification", *Fuel Processing Technology*. vol. 73, 2001, pp. 155-173.
- [27] T. Marquard-Möllenstedt, P. Sichler, M. Specht, M. Michel, R. Berger, K. R. G. Hein, E. Höftberger, R. Rauch, and H. Hofbauer, "New approach for biomass gasification to hydrogen " in *2nd World Conference and Technology Exhibition on Biomass for Energy, Industry and Climate Protection*, Rome, Italy, 2004.
- [28] C. Pfeifer, B. Puchner, and H. Hofbauer, "In-situ CO<sub>2</sub>-absorption in a dual fluidized bed biomass steam gasifier to produce a hydrogen rich syngas", *International Journal of Chemical Reactor Engineering*. vol. 5, A9, 2008, pp. 1-13.
- [29] M. Ni, D. Y. C. Leung, M. K. H. Leung, and K. Sumathy, "An overview of hydrogen production from biomass", *Fuel Processing Technology*. vol. 87, 2006, pp. 461-472.
- [30] A. Demirbas, "Gaseous products from biomass by pyrolysis and gasification: Effects of catalyst on hydrogen yield", *Energy Conversion and Management*. vol. 43, 2002, pp. 897-909.
- [31] H. Yang, R. Yan, H. Chen, D. H. Lee, D. T. Liang, and C. Zheng, "Pyrolysis of palm oil wastes for enhanced production of hydrogen rich gases", *Fuel Processing Technology*. vol. 87, 2006, pp. 935-942.
- [32] A. Çağlar and A. Demirbas, "Conversion of cotton cocoon shell to liquid products by pyrolysis", *Energy Conversion and Management*. vol. 41, 2000, pp. 1749-1756.
- [33] D. B. Levin, C. R. Carere, N. Cicek, and R. Sparling, "Challenges for biohydrogen production via direct lignocellulose fermentation", *International Journal of Hydrogen Energy*. vol. 34, 2009, pp. 7390-7403.

- [34] P. McKendry, "Energy production from biomass (part 1): Overview of biomass", *Bioresource Technology*. vol. 83, 2002, pp. 37-46.
- [35] H. Yang, R. Yan, H. Chen, D. H. Lee, and C. Zheng, "Characteristics of hemicellulose, cellulose and lignin pyrolysis", *Fuel*. vol. 86, 2007, pp. 1781-1788.
- [36] S.-T. Yang, *Bioprocessing for value-added products from renewable resources: New technologies and applications* Oxford: Elsevier, 2007.
- [37] B. Acharya, A. Dutta, and P. Basu, "An investigation into steam gasification of biomass for hydrogen enriched gas production in presence of CaO", *International Journal of Hydrogen Energy*. vol. 35, 2010, pp. 1582-1589.
- [38] P. Basu, *Biomass gasification and pyrolysis: Practical design and theory*: Academic Press, 2010.
- [39] Richard L. Bain and K. Broer, "Gasification " in *Thermochemical conversion of biomass: Conversion into fuels, chemicals and power*, R. C. Brown, Ed., ed: John Wiley and Sons, 2011.
- [40] M. J. Prins, K. J. Ptasinski, and F. J. J. G. Janssen, "From coal to biomass gasification: Comparison of thermodynamic efficiency", *Energy*. vol. 32, 2007, pp. 1248-1259.
- [41] S. S. Abdullah and S. Yusup, "Method for screening of Malaysian biomass based on aggregated matrix for hydrogen production through gasification", *Journal of Applied Sciences*. vol. 10, 2010, pp. 3301-3306.
- [42] M. P. Aznar, J. Corella, J. Delgado, and J. Lahoz, "Improved steam gasification of lignocellulosic residues in a fluidized bed with commercial steam reforming catalysts", *Industrial & Engineering Chemistry Research*. vol. 32, 1993, pp. 1-10.
- [43] L. Wei, S. Xu, L. Zhang, C. Liu, H. Zhu, and S. Liu, "Steam gasification of biomass for hydrogen-rich gas in a free-fall reactor", *International Journal of Hydrogen Energy*. vol. 32, 2007, pp. 24-31.
- [44] X. Xiao, X. Meng, D. D. Le, and T. Takarada, "Two-stage steam gasification of waste biomass in fluidized bed at low temperature: Parametric investigations and performance optimization", *Bioresource Technology*. vol. 102, 2011, pp. 1975-1981.

- [45] A. Olivares, M. P. Aznar, M. A. Caballero, J. Gil, E. Francés, and J. Corella, "Biomass gasification: Produced gas upgrading by in-bed use of dolomite", *Industrial & Engineering Chemistry Research*. vol. 36, 1997, pp. 5220-5226.
- [46] Z. Abu El-Rub, E. A. Bramer, and G. Brem, "Review of catalysts for tar elimination in biomass gasification processes", *Industrial & Engineering Chemistry Research*. vol. 43, 2004, pp. 6911-6919.
- [47] C. Courson, E. Makaga, C. Petit, and A. Kiennemann, "Development of Ni catalysts for gas production from biomass gasification. Reactivity in steam- and dry-reforming", *Catalysis Today*. vol. 63, 2000, pp. 427-437.
- [48] K. Sato and K. Fujimoto, "Development of new nickel based catalyst for tar reforming with superior resistance to sulfur poisoning and coking in biomass gasification", *Catalysis Communications*. vol. 8, 2007, pp. 1697-1701.
- [49] S. Lee, S. Nam, S. Kim, K. Lee, and C. Choi, "The effect of Na<sub>2</sub>CO<sub>3</sub> on the catalytic gasification of rice straw on the catalytic gasification of rice straw over nickel catalysts supported on kieselguhr", *Korean Journal of Chemical Engineering*. vol. 17, 2000, pp. 174-178.
- [50] S. Choi, J. H. Drese, and C. W. Jones, "Adsorbent materials for carbon dioxide capture from large anthropogenic point sources", *ChemSusChem*. vol. 2, 2009, pp. 796-854.
- [51] R. Xiong, J. Ida, and Y. S. Lin, "Kinetics of carbon dioxide sorption on potassium-doped lithium zirconate", *Chemical Engineering Science*. vol. 58, 2003, pp. 4377-4385.
- [52] A. López-Ortiz, N. G. P. Rivera, A. R. Rojas, and D. L. Gutierrez, "Novel carbon dioxide solid acceptors using sodium containing oxides", *Separation Science and Technology*. vol. 39, 2005, pp. 3559-3572.
- [53] N. H. Florin and A. T. Harris, "Hydrogen production from biomass coupled with carbon dioxide capture: The implications of thermodynamic equilibrium", *International Journal of Hydrogen Energy*. vol. 32, 2007, pp. 4119-4134.
- [54] W.-T. Tsai, K.-J. Hsien, H.-C. Hsu, C.-M. Lin, K.-Y. Lin, and C.-H. Chiu, "Utilization of ground eggshell waste as an adsorbent for the removal of dyes from aqueous solution", *Bioresource Technology*. vol. 99, 2008, pp. 1623-1629.

- [55] M. Muhamed., S. Yusup., and S. Mitra., "Decomposition study of calcium carbonate in cockle shell," in *World Engineering Congress: Conference on Engineering and Technology Education*, Kuching, Sarawak, Malaysia, 2-5 August, 2010, pp. 16-22.
- [56] G. Xu, T. Murakami, T. Suda, S. Kusama, and T. Fujimori, "Distinctive effects of CaO additive on atmospheric gasification of biomass at different temperatures", *Industrial & Engineering Chemistry Research*. vol. 44, 2005, pp. 5864-5868.
- [57] H. Guoxin and H. Hao, "Hydrogen rich fuel gas production by gasification of wet biomass using a CO<sub>2</sub> sorbent", *Biomass and Bioenergy*. vol. 33, 2009, pp. 899-906.
- [58] A. A. Upadhye, W. Qi, and G. W. Huber, "Conceptual process design: A systematic method to evaluate and develop renewable energy technologies", *AIChE Journal*. vol. 57, 2011, pp. 2292-2301.
- [59] G. W. Huber, S. Iborra, and A. Corma, "Synthesis of transportation fuels from biomass: Chemistry, catalysts, and engineering", *Chemical Reviews*. vol. 106, 2006, pp. 4044-4098.
- [60] N. Nisihida, G. Stephanopoulos, and A. W. Westerberg, "A review of process synthesis", *AIChE Journal*. vol. 27, 1981, pp. 321-351.
- [61] J. M. Douglas, "A hierarchical decision procedure for process synthesis", *AIChE Journal*. vol. 31, 1985, pp. 353-362.
- [62] J. M. Douglas, *Conceptual design of chemical processes*. New York: McGraw-Hill, 1988.
- [63] J. S. Luterbacher, M. Fröling, F. Vogel, F. Maréchal, and J. W. Tester, "Hydrothermal gasification of waste biomass: Process design and life cycle assessment", *Environmental Science & Technology*. vol. 43, 2009, pp. 1578-1583.
- [64] L. Han, Q. Wang, Q. Ma, C. Yu, Z. Luo, and K. Cen, "Influence of CaO additives on wheat-straw pyrolysis as determined by TG-FTIR analysis", *Journal of Analytical and Applied Pyrolysis*. vol. 88, 2010, pp. 199-206.
- [65] J. Corella, J.-M. Toledo, and G. Molina, "Biomass gasification with pure steam in fluidised bed: 12 variables that affect the effectiveness of the biomass

- gasifier", *International Journal of Oil, Gas and Coal Technology*. vol. 1, 2008, pp. 194-207.
- [66] R. Smith, *Chemical process: Design and integration*. West Sussex, England: John Wiley & Sons, 2005.
- [67] P. Lv, Z. Yuan, C. Wu, L. Ma, Y. Chen, and N. Tsubaki, "Bio-syngas production from biomass catalytic gasification", *Energy Conversion and Management*. vol. 48, 2007, pp. 1132-1139.
- [68] T.A. Milne and R.J. Evans, "Biomass gasification "tars": Their nature, formation and conversion," National Renewable Energy Laboratory, Colorado, USA, 1998.
- [69] J. Corella, A. Orío, and P. Aznar, "Biomass gasification with air in fluidized bed: Reforming of the gas composition with commercial steam reforming catalysts", *Industrial & Engineering Chemistry Research*. vol. 37, 1998/12/01 1998, pp. 4617-4624.
- [70] R. Zhang, R. C. Brown, and A. Suby, "Thermochemical generation of hydrogen from switchgrass", *Energy & Fuels*. vol. 18, 2003, pp. 251-256.
- [71] V. S. A. Zabaniotou, G. Koufodimos and Z. Samaras, "Conceptual design and preliminary hydrodynamic study of an agro biomass bench gasification fluidized bed reactor", *International Journal of Chemical Reactor Engineering*. vol. 6, A14, 2008, pp. 1-17.
- [72] A. C. Caputo, M. Palumbo, P. M. Pelagagge, and F. Scacchia, "Economics of biomass energy utilization in combustion and gasification plants: Effects of logistic variables", *Biomass and Bioenergy*. vol. 28, 2005, pp. 35-51.
- [73] A. Abuadala and I. Dincer, "Investigation of a multi-generation system using a hybrid steam biomass gasification for hydrogen, power and heat", *International Journal of Hydrogen Energy*. vol. 35, 2010, pp. 13146-13157.
- [74] P. Kalita, G. Mohan, G. P. Kumar, and P. Mahanta, "Determination and comparison of kinetic parameters of low density biomass fuels", *Journal of Renewable and Sustainable Energy*. vol. 1, 2009, pp. 023109-12.
- [75] N. H. Florin and A. T. Harris, "Mechanistic study of enhanced H<sub>2</sub> synthesis in biomass gasifiers with in-situ CO<sub>2</sub> capture using CaO", *AIChE Journal*. vol. 54, 2008, pp. 1096-1109.

- [76] P. Basu and P. Kaushal, "Modeling of pyrolysis and gasification of biomass in fluidized beds: A review", *Chemical Product and Process Modeling*. vol. 4, A 21, 2009, pp. 1-45.
- [77] P. Basu, *Combustion and gasification in fluidized bed*: Taylor and Francis, 2006.
- [78] L. Shen, J. Xiao, F. Niklasson, and F. Johnsson, "Biomass mixing in a fluidized bed biomass gasifier for hydrogen production", *Chemical Engineering Science*. vol. 62, 2007, pp. 636-643.
- [79] M. K. Karmakar and A. B. Datta, "Generation of hydrogen rich gas through fluidized bed gasification of biomass", *Bioresource Technology*. vol. 102, 2011, pp. 1907-1913.
- [80] Z. Khan, S. Yusup, M. M. Ahmad, A. Ramli, M. T. Arpin, S. S. Abdullah, M. F. Mohammad, S. E. E. Mohammad, and A. Inayat, "Effect of steam and catalyst on palm oil wastes thermal decomposition for hydrogen production", *Research Journal of Chemistry and Environment*. vol. 15, 2011, pp. 466-472.
- [81] N. Gao, A. Li, C. Quan, and F. Gao, "Hydrogen-rich gas production from biomass steam gasification in an updraft fixed-bed gasifier combined with a porous ceramic reformer", *International Journal of Hydrogen Energy*. vol. 33, 2008, pp. 5430-5438.
- [82] W. P. Walawender, D. A. Hoveland, and L. T. Fan, "Steam gasification of pure cellulose. 1. Uniform temperature profile", *Industrial & Engineering Chemistry Process Design and Development*. vol. 24, 1985, pp. 813-817.
- [83] C. Franco, F. Pinto, I. Gulyurtlu, and I. Cabrita, "The study of reactions influencing the biomass steam gasification process", *Fuel*. vol. 82, 2003, pp. 835-842.
- [84] D. M. Himmelblau and J. B. Riggs, *Basic principles and calculations in chemical engineering*: Prentice Hall, 2003.
- [85] A. Inayat, M. M. Ahmad, M. I. A. Mutalib, and S. Yusup, "Process modeling for parametric study on oil palm empty fruit bunch steam gasification for hydrogen production", *Fuel Processing Technology*. vol. 93, 2012, pp. 26-34.
- [86] L. Han, Q. Wang, Y. Yang, C. Yu, M. Fang, and Z. Luo, "Hydrogen production via CaO sorption enhanced anaerobic gasification of sawdust in a

- bubbling fluidized bed", *International Journal of Hydrogen Energy*. vol. 36, 2011, pp. 4820-4829.
- [87] T. L. Kelly Yong, "Gasification of oil palm biomass in hot compressed water (HCW) for production of synthesis gas " Master of Science, Chemical Engineering, University Sains Malaysia, Malaysia, 2009.
- [88] N. Nipattumakul, I. I. Ahmed, A. K. Gupta, and S. Kerdsuwan, "Hydrogen and syngas yield from residual branches of oil palm tree using steam gasification", *International Journal of Hydrogen Energy*. vol. 36, 2011, pp. 3835-3843.
- [89] M. R. Mahishi and D. Y. Goswami, "An experimental study of hydrogen production by gasification of biomass in the presence of a CO<sub>2</sub> sorbent", *International Journal of Hydrogen Energy*. vol. 32, 2007, pp. 2803-2808.
- [90] T. Hanaoka, T. Yoshida, S. Fujimoto, K. Kamei, M. Harada, Y. Suzuki, H. Hatano, S.-y. Yokoyama, and T. Minowa, "Hydrogen production from woody biomass by steam gasification using a CO<sub>2</sub> sorbent", *Biomass and Bioenergy*. vol. 28, 2005, pp. 63-68.
- [91] M. Detournay, M. Hemati, and R. Andreux, "Biomass steam gasification in fluidized bed of inert or catalytic particles: Comparison between experimental results and thermodynamic equilibrium predictions", *Powder Technology*. vol. 208, 2011, pp. 558-567.
- [92] M. P. Aznar, M. A. Caballero, J. Corella, G. Molina, and J. M. Toledo, "Hydrogen production by biomass gasification with steam O<sub>2</sub> mixtures followed by a catalytic steam reformer and a CO-shift system", *Energy & Fuels*. vol. 20, 2006, pp. 1305-1309.
- [93] P. Lahijani and Z. A. Zainal, "Gasification of palm empty fruit bunch in a bubbling fluidized bed: A performance and agglomeration study", *Bioresource Technology*. vol. 102, 2011, pp. 2068-2076.
- [94] L. Wei, S. Xu, J. Liu, C. Liu, and S. Liu, "Hydrogen production in steam gasification of biomass with cao as co<sub>2</sub> adsorbent", *Energy & Fuels*. vol. 22, 2008, pp. 1997-2004.
- [95] S. Koppatz, C. Pfeifer, R. Rauch, H. Hofbauer, T. Marquard-Moellenstedt, and M. Specht, "H<sub>2</sub> rich product gas by steam gasification of biomass with in situ

- CO<sub>2</sub> absorption in a dual fluidized bed system of 8 MW fuel input", *Fuel Processing Technology*. vol. 90, 2009, pp. 914-921.
- [96] C. Pfeifer, B. Puchner, and H. Hofbauer, "Comparison of dual fluidized bed steam gasification of biomass with and without selective transport of CO<sub>2</sub>", *Chemical Engineering Science*. vol. 64, 2009, pp. 5073-5083.
- [97] P. McKendry, "Energy production from biomass (part 3): Gasification technologies", *Bioresource Technology*. vol. 83, 2002, pp. 55-63.
- [98] U. Zuberbühler, Specht, M.; Bandi, A., "Gasification of biomass: An overview on available technologies," in *1st European Summer School on Renewable Motor Fuels* Birkemfield, Germany, 2005.
- [99] J. Gil, J. Corella, M. P. Aznar, and M. A. Caballero, "Biomass gasification in atmospheric and bubbling fluidized bed: Effect of the type of gasifying agent on the product distribution", *Biomass and Bioenergy*. vol. 17, 1999, pp. 389-403.
- [100] I. Ahmed and A. K. Gupta, "Syngas yield during pyrolysis and steam gasification of paper", *Applied Energy*. vol. 86, 2009, pp. 1813-1821.
- [101] J. Herguido, J. Corella, and J. Gonzalez-Saiz, "Steam gasification of lignocellulosic residues in a fluidized bed at a small pilot scale. Effect of the type of feedstock", *Industrial & Engineering Chemistry Research*. vol. 31, 1992, pp. 1274-1282.
- [102] S. Rapagnà and A. Latif, "Steam gasification of almond shells in a fluidised bed reactor: The influence of temperature and particle size on product yield and distribution", *Biomass and Bioenergy*. vol. 12, 1997, pp. 281-288.
- [103] J. Delgado, M. P. Aznar, and J. Corella, "Calcined dolomite, magnesite, and calcite for cleaning hot gas from a fluidized bed biomass gasifier with steam: Life and usefulness", *Industrial & Engineering Chemistry Research*. vol. 35, 1996, pp. 3637-3643.
- [104] M. R. Mahishi, M. S. Sadrameli, S. Vijayaraghavan, and D. Y. Goswami, "A novel approach to enhance the hydrogen yield of biomass gasification using CO<sub>2</sub> sorbent", *Journal of Engineering for Gas Turbines and Power*. vol. 130, 2008, pp. 1-8.
- [105] C. P. Pfeifer, Bernhard; and Hofbauer, Hermann "In-situ CO<sub>2</sub>-absorption in a dual fluidized bed biomass steam gasifier to produce a hydrogen rich syngas",

- International Journal of Chemical Reactor Engineering. vol. 5, A9, 2007, pp. 1-13.
- [106] P. Weerachanchai, M. Horio, and C. Tangsathitkulchai, "Effects of gasifying conditions and bed materials on fluidized bed steam gasification of wood biomass", *Bioresource Technology*. vol. 100, 2009, pp. 1419-1427.
- [107] P. Sun, J. R. Grace, C. J. Lim, and E. J. Anthony, "Removal of CO<sub>2</sub> by calcium-based sorbents in the presence of SO<sub>2</sub>", *Energy & Fuels*. vol. 21, 2006, pp. 163-170.
- [108] H. Gupta and L.-S. Fan, "Carbonation–calcination cycle using high reactivity calcium oxide for carbon dioxide separation from flue gas", *Industrial & Engineering Chemistry Research*. vol. 41, 2002, pp. 4035-4042.
- [109] S. Lin, M. Harada, Y. Suzuki, and H. Hatano, "Process analysis for hydrogen production by reaction integrated novel gasification (HYPR-RING)", *Energy Conversion and Management*. vol. 46, 2005, pp. 869-880.
- [110] N. Hildenbrand, J. Readman, I. M. Dahl, and R. Blom, "Sorbent enhanced steam reforming (SESR) of methane using dolomite as internal carbon dioxide absorbent: Limitations due to Ca(OH)<sub>2</sub> formation", *Applied Catalysis A: General*. vol. 303, 2006, pp. 131-137.
- [111] J. B. Lee, T. H. Eom, K. W. Park, J. Ryu, J.-I. Baek, K. Kim, S.-R. Yang, and C. K. Ryu, "CO<sub>2</sub> capture from syngas using solid CO<sub>2</sub> sorbent and wgs catalyst", *Energy Procedia*. vol. 4, 2011, pp. 1133-1138.
- [112] T. Ogi, M. Nakanishi, Y. Fukuda, and K. Matsumoto, "Gasification of oil palm residues (empty fruit bunch) in an entrained-flow gasifier", *Fuel*. vol. 104, 2013, pp. 28-35.
- [113] M. A. A. Mohammed, A. Salmiaton, W. A. K. G. Wan Azlina, M. S. Mohammad Amran, and A. Fakhru'l-Razi, "Air gasification of empty fruit bunch for hydrogen-rich gas production in a fluidized-bed reactor", *Energy Conversion and Management*. vol. 52, 2011, pp. 1555-1561.
- [114] Y. Kalinci, A. Hepbasli, and I. Dincer, "Comparative exergetic performance analysis of hydrogen production from oil palm wastes and some other biomasses", *International Journal of Hydrogen Energy*. vol. 36, 2011, pp. 11399-11407.

- [115] C. Erlich and T. H. Fransson, "Downdraft gasification of pellets made of wood, palm-oil residues respective bagasse: Experimental study", *Applied Energy*. vol. 88, 2011, pp. 899-908.
- [116] W. A. Wan Ab Karim Ghani, M. A. Mohd Salleh, A.B. Alias "Air gasification of agricultural waste in a fluidized bed gasifier: Hydrogen production performance", *Energies*. vol. 2, 2009, pp. 258-268.
- [117] R. M. Esfahani, W. A. Wan Ab Karim Ghani, M. A. Mohd Salleh, and S. Ali, "Hydrogen-rich gas production from palm kernel shell by applying air gasification in fluidized bed reactor", *Energy & Fuels*. vol. 26, 2012/02/16 2011, pp. 1185-1191.
- [118] M.F. Mohamad, A. Ramli, S.E.E Misi, and S. Yusup, "Steam gasification of palm kernel shell (PKS):Effect of Fe/ $\beta$  and Ni/ $\beta$  catalysts and steam to biomass ratio on composition of gaseous products " in *World Academy of Science, Engineering and Technology*, , Kuala Lumpur, 2011, pp. 232-237.
- [119] S. Luo, B. Xiao, X. Guo, Z. Hu, S. Liu, and M. He, "Hydrogen-rich gas from catalytic steam gasification of biomass in a fixed bed reactor: Influence of particle size on gasification performance", *International Journal of Hydrogen Energy*. vol. 34, 2009, pp. 1260-1264.
- [120] A. A. Boateng, W. P. Walawender, L. T. Fan, and C. S. Chee, "Fluidized-bed steam gasification of rice hull", *Bioresource Technology*. vol. 40, 1992, pp. 235-239.
- [121] X. Xiao, D. D. Le, L. Li, X. Meng, J. Cao, K. Morishita, and T. Takarada, "Catalytic steam gasification of biomass in fluidized bed at low temperature: Conversion from livestock manure compost to hydrogen-rich syngas", *Biomass and Bioenergy*. vol. 34, 2010, pp. 1505-1512.
- [122] S. Turn, C. Kinoshita, Z. Zhang, D. Ishimura, and J. Zhou, "An experimental investigation of hydrogen production from biomass gasification", *International Journal of Hydrogen Energy*. vol. 23, 1998, pp. 641-648.
- [123] L. García, M. L. Salvador, J. Arauzo, and R. Bilbao, "Catalytic steam gasification of pine sawdust. Effect of catalyst weight/biomass flow rate and steam/biomass ratios on gas production and composition", *Energy & Fuels*. vol. 13, 1999, pp. 851-859.

- [124] P. Raman, W. P. Walawender, L. T. Fan, and C. C. Chang, "Mathematical model for the fluid-bed gasification of biomass materials. Application to feedlot manure", *Industrial & Engineering Chemistry Process Design and Development*. vol. 20, 1981, pp. 686-692.
- [125] J. Corella, M. P. Aznar, J. Delgado, and E. Aldea, "Steam gasification of cellulosic wastes in a fluidized bed with downstream vessels", *Industrial & Engineering Chemistry Research*. vol. 30, 1991, pp. 2252-2262.
- [126] P. M. Lv, Z. H. Xiong, J. Chang, C. Z. Wu, Y. Chen, and J. X. Zhu, "An experimental study on biomass air-steam gasification in a fluidized bed", *Bioresource Technology*. vol. 95, 2004, pp. 95-101.
- [127] J. Guo and A. Lua, "Kinetic study on pyrolysis of extracted oil palm fiber. Isothermal and non-isothermal conditions", *Journal of Thermal Analysis and Calorimetry*. vol. 59, 2000, pp. 763-774.
- [128] E. D. Gordillo and A. Belghit, "A two phase model of high temperature steam-only gasification of biomass char in bubbling fluidized bed reactors using nuclear heat", *International Journal of Hydrogen Energy*. vol. 36, 2011, pp. 374-381.
- [129] J. Corella and A. Sanz, "Modeling circulating fluidized bed biomass gasifiers. A pseudo-rigorous model for stationary state", *Fuel Processing Technology*. vol. 86, 2005, pp. 1021-1053.
- [130] J. Gonzalez-Saiz, "Advances in biomass gasification in fluidized bed," PhD Thesis, Department of Chemical Engineering, University of Saragossa, Spain, 1988.
- [131] P. A. Simell, E. K. Hirvensalo, V. T. Smolander, and A. O. I. Krause, "Steam reforming of gasification gas tar over dolomite with benzene as a model compound", *Industrial & Engineering Chemistry Research*. vol. 38, 1999, pp. 1250-1257.
- [132] M. L. de Souza-Santos, "Comprehensive modelling and simulation of fluidized bed boilers and gasifiers", *Fuel*. vol. 68, 1989, pp. 1507-1521.
- [133] P. Lü, X. Kong, C. Wu, Z. Yuan, L. Ma, and J. Chang, "Modeling and simulation of biomass air-steam gasification in a fluidized bed", *Frontiers of Chemical Engineering in China*. vol. 2, 2008, pp. 209-213.

- [134] W. L. Fu, *Coal combustion theory and its macro universal law*: Tsinghua University Press, 2003.
- [135] V. Biba, J. Malecha, J. Macak, and E. Klose, "Mathematical model for the gasification of coal under pressure", *Industrial & Engineering Chemistry Process Design and Development*. vol. 17, 1978, pp. 92-98.
- [136] I. Petersen and J. Werther, "Experimental investigation and modeling of gasification of sewage sludge in the circulating fluidized bed", *Chemical Engineering and Processing*. vol. 44, 2005, pp. 717-736.
- [137] K. Matsumoto, K. Takeno, T. Ichinose, T. Ogi, and M. Nakanishi, "Gasification reaction kinetics on biomass char obtained as a by-product of gasification in an entrained-flow gasifier with steam and oxygen at 900-1000 °C", *Fuel*. vol. 88, 2009, pp. 519-527.
- [138] J. C. Wurzenberger, S. Wallner, H. Raupenstrauch, and J. G. Khinast, "Thermal conversion of biomass: Comprehensive reactor and particle modeling", *AIChE Journal*. vol. 48, 2002, pp. 2398-2411.
- [139] A. Jess, "Reaktionskinetische untersuchungen zur thermischen zersetzung von modellkohlenwasserstoffen", *Erdöl Erdgas Kohle*. vol. 111, 1995, pp. 479-489.
- [140] E. Salaices, "Catalytic steam gasification of biomass surrogates: A thermodynamic and kinetic approach," PhD, Chemical and Biochemical Engineering, The University of Western Ontario, Ontario, Canada, 2010.
- [141] L. Shen, Y. Gao, and J. Xiao, "Simulation of hydrogen production from biomass gasification in interconnected fluidized beds", *Biomass and Bioenergy*. vol. 32, 2008, pp. 120-127.
- [142] C. Li and K. Suzuki, "Process design and simulation of H<sub>2</sub>-rich gases production from biomass pyrolysis process", *Bioresource Technology*. vol. 101, 2010, pp. 86-90.
- [143] T. Pröll and H. Hofbauer, "H<sub>2</sub> rich syngas by selective CO<sub>2</sub> removal from biomass gasification in a dual fluidized bed system -- process modelling approach", *Fuel Processing Technology*. vol. 89, 2008, pp. 1207-1217.
- [144] H. Liu and B. M. Gibbs, "Modeling NH<sub>3</sub> and HCN emissions from biomass circulating fluidized bed gasifiers", *Fuel*. vol. 82, 2003, pp. 1591-1604.

- [145] P. Sun, J. R. Grace, C. J. Lim, and E. J. Anthony, "Determination of intrinsic rate constants of the CaO-CO<sub>2</sub> reaction", *Chemical Engineering Science*. vol. 63, 2008, pp. 47-56.
- [146] M. Puig-Arnavat, J. C. Bruno, and A. Coronas, "Review and analysis of biomass gasification models", *Renewable and Sustainable Energy Reviews*. vol. 14, 2010, pp. 2841-2851.
- [147] A. K. Sharma, "Equilibrium and kinetic modeling of char reduction reactions in a downdraft biomass gasifier: A comparison", *Solar Energy*. vol. 82, 2008, pp. 918-928.
- [148] C. R. Altafini, P. R. Wander, and R. M. Barreto, "Prediction of the working parameters of a wood waste gasifier through an equilibrium model", *Energy Conversion and Management*. vol. 44, 2003, pp. 2763-2777.
- [149] A. Inayat, M. M. Ahmad, M. I. A. Mutalib, and S. Yusup, "Optimization approach for kinetics parameters determination for oil palm waste steam gasification with in-situ CO<sub>2</sub> capture for hydrogen production," in *National Postgraduate Conference (NPC), 2011*, 2011, pp. 1-6.
- [150] Y. Wang and C. M. Kinoshita, "Kinetic model of biomass gasification", *Solar Energy*. vol. 51, 1993, pp. 19-25.
- [151] Y. Wang and C. M. Kinoshita, "Experimental analysis of biomass gasification with steam and oxygen", *Solar Energy*. vol. 49, 1992, pp. 153-158.
- [152] J. M. Monteagudo, L. Rodríguez, J. Rincón, and J. Fuertes, "Optimization of the conditions of the fermentation of beet molasses to lactic acid by *Lactobacillus delbrueckii*", *Acta Biotechnologica*. vol. 14, 1994, pp. 251-260.
- [153] A. L. Larentis, N. S. de Resende, V. M. M. Salim, and J. C. Pinto, "Modeling and optimization of the combined carbon dioxide reforming and partial oxidation of natural gas", *Applied Catalysis A: General*. vol. 215, 2001, pp. 211-224.
- [154] T.D. Kusworo, A.R. Songip, and N. A. S. Amin, "Optimization of partial oxidation of methane for hydrogen production on NiO-CoO/MgO catalyst using design of experiment", *International Journal of Engineering & Technology IJET-IJENS* vol. 10, 2010, pp. 1-8.
- [155] J. Feroso, M. V. Gil, B. Arias, M. G. Plaza, C. Pevida, J. J. Pis, and F. Rubiera, "Application of response surface methodology to assess the

- combined effect of operating variables on high-pressure coal gasification for H<sub>2</sub>-rich gas production", *International Journal of Hydrogen Energy*. vol. 35, 2010, pp. 1191-1204.
- [156] P. W. Bo, X. H. Zhen, and R. Tommi, "A novel response surface method for design optimization of electronic packages," in *6th International Conference on Thermal Mechanical and Multiphysics Simulation and Experiments in Micro-Electronics and Micro-Systems*, 2005, pp. 175-181.
- [157] R. O. Kuehl, *Design of experiments: Statistical principles of research design and analysis*, 2nd ed. California Brooks/Cole, 2000.
- [158] J. N. Sahu, J. Acharya, and B. C. Meikap, "Optimization of production conditions for activated carbons from tamarind wood by zinc chloride using response surface methodology", *Bioresource Technology*. vol. 101, 2010, pp. 1974-1982.
- [159] T. R. J. Satonsaowapak, T. Kulworawaichpong, P.Pao-La-Or., B. Maeungsri., and A. Oonsivilai, "Gasifier system identification for biomass power plants using response surface method " in *4th IASME / WSEAS International Conference on Energy and Environment* Cambridge, UK, February 24-26, , 2009
- [160] D. P. Obeng, S. Morrell, and T. J. Napier-Munn, "Application of central composite rotatable design to modelling the effect of some operating variables on the performance of the three-product cyclone", *International Journal of Mineral Processing*. vol. 76, 2005, pp. 181-192.
- [161] R. D. Crozier, *Flotation theory, reagents and ore testing*. New York: Pergamon Press, 1992.
- [162] S. Yi, Y. Su, B. Qi, Z. Su, and Y. Wan, "Application of response surface methodology and central composite rotatable design in optimizing the preparation conditions of vinyltriethoxysilane modified silicalite/polydimethylsiloxane hybrid pervaporation membranes", *Separation and Purification Technology*. vol. 71, 2010, pp. 252-262.
- [163] S. Ghafari, H. A. Aziz, M. H. Isa, and A. A. Zinatizadeh, "Application of response surface methodology (RSM) to optimize coagulation–flocculation treatment of leachate using poly-aluminum chloride (PAC) and alum", *Journal of Hazardous Materials*. vol. 163, 2009, pp. 650-656.

- [164] U. Rashid, H. A. Rehman, I. Hussain, M. Ibrahim, and M. S. Haider, "Muskmelon (*cucumis melo*) seed oil: A potential non-food oil source for biodiesel production", *Energy*. vol. 36, 2011, pp. 5632-5639.
- [165] Q. Liu, X. Zhang, Y. Zhou, A. Zhao, S. Chen, G. Qian, and Z. P. Xu, "Optimization of fermentative biohydrogen production by response surface methodology using fresh leachate as nutrient supplement", *Bioresource Technology*. vol. 102, 2011, pp. 8661-8668.
- [166] Q. Liu, X. L. Zhang, Z. Jun, A. H. Zhao, S. P. Chen, F. Liu, J. Tai, J. Y. Liu, and G. R. Qian, "Effect of carbonate on anaerobic acidogenesis and fermentative hydrogen production from glucose using leachate as supplementary culture under alkaline conditions", *Bioresource Technology*. vol. 113, 2012, pp. 37-43.
- [167] J. Guo and A. C. Lua, "Kinetic study on pyrolytic process of oil-palm solid waste using two-step consecutive reaction model", *Biomass and Bioenergy*. vol. 20, 2001, pp. 223-233.
- [168] P. Luangkiattikhun, C. Tangsathitkulchai, and M. Tangsathitkulchai, "Non-isothermal thermogravimetric analysis of oil-palm solid wastes", *Bioresource Technology*. vol. 99, 2008, pp. 986-997.
- [169] L. Núñez-Regueira, Rodríguez-Añón, J. A. Proupín, J. n-Castiñeiras, A. Vilanova-Diz, and N. Montero-Santoveña, "Determination of calorific values of forest waste biomass by static bomb calorimetry", *Thermochimica Acta*. vol. 371, 2001, pp. 23-31.
- [170] L. Núñez-Regueira, J. A. Rodríguez-Añón, and J. Proupín-Castiñeiras, "Using calorimetry for determining the risk indices to prevent and fight forest fires", *Thermochimica Acta*. vol. 422, 2004, pp. 81-87.
- [171] D. Kunii and O. Levenspiel, *Fluidization engineering* 2nd ed.: Butterworth-Heinemann, 1992.
- [172] M. Rhodes, *Introduction to particle technology* John Wiley and Sons, 1998.
- [173] J. R. Cooper. (2007, 10-06-2011). *The international association for the properties of water and steam, also see <http://twf.Mpei.Ac.Ru/mcs/worksheets/wsp/denspt.Xmcd>*.

- [174] P. Kaushal, J. Abedi, and N. Mahinpey, "A comprehensive mathematical model for biomass gasification in a bubbling fluidized bed reactor", *Fuel*. vol. 89, 2010, pp. 3650-3661.
- [175] M. B. Nikoo and N. Mahinpey, "Simulation of biomass gasification in fluidized bed reactor using ASPEN PLUS", *Biomass and Bioenergy*. vol. 32, 2008, pp. 1245-1254.
- [176] M. Horio and A. Nonaka, "A generalized bubble diameter correlation for gas-solid fluidized beds", *AIChE Journal*. vol. 33, 1987, pp. 1865-1872.
- [177] K. Krishnaiah, Janaun, J., and Prabhakar, A., "Fluidized bed reactor as solid state fermenter", *Malaysian Journal of Microbiology*. vol. 1, 2005, pp. 7-11.
- [178] A. E. Qureshi and D. E. Creasy, "Fluidised bed gas distributors", *Powder Technology*. vol. 22, 1979, pp. 113-119.
- [179] R. H. Perry and D. W. Green, "Perry's chemical engineering's handbook," McGraw Hill: 1999, pp. 2-309.
- [180] P. J. van den Enden and E. S. Lora, "Design approach for a biomass fed fluidized bed gasifier using the simulation software CSFB", *Biomass and Bioenergy*. vol. 26, 2004, pp. 281-287.
- [181] L.T. Kelly-Yong, S. Lim, and K. T. Lee, "Gasification of oil palm empty fruit bunch fibers in hot compressed water for synthesis gas production ", *Journal of Applied Science*. vol. 11, 2009, pp. 3563-3570.
- [182] M. A. A. A. Mohammed, A. Salmiaton, W. A. Wan ab Karim Ghani, and M. S. M. Amran, "Gasification of empty fruit bunch for hydrogen rich fuel gas production," in *International Conference on Chemical & Bioprocess Engineering*, Universiti Malaysia Sabah, Kota Kinabalu, Sabah, 2009, pp. 1292-1297.
- [183] V. Skoulou, A. Swiderski, W. Yang, and A. Zabaniotou, "Process characteristics and products of olive kernel high temperature steam gasification (HTSG)", *Bioresource Technology*. vol. 100, 2009, pp. 2444-2451.
- [184] M. K. Cohce, I. Dincer, and M. A. Rosen, "Thermodynamic analysis of hydrogen production from biomass gasification", *International Journal of Hydrogen Energy*. vol. 35, 2010, pp. 4970-4980.

- [185] W.-C. Yang, *Handbook of fluidization and fluid-particle systems*, New York: Marcel Dekker Inc., 2003.
- [186] S. S. Sadaka, A. E. Ghaly, and M. A. Sabbah, "Two phase biomass air-steam gasification model for fluidized bed reactors: Part i--model development", *Biomass and Bioenergy*. vol. 22, 2002, pp. 439-462.
- [187] W. M. Rohsenow, J. P. Hartnett, and Y. I. Cho, *Handbook of heat transfer*, 3rd ed. New York: McGraw-Hill, 1998.
- [188] M. Avriel, *Nonlinear programming analysis and methods*, New York: Dover Publishing, 2003.
- [189] S. Nasrazadani and E. Eureste, "Application of FTIR for quantitative lime analysis " University of North Texas, 2008.
- [190] S. Inc, *Basics of x-ray diffraction manual*: Scintag Inc Curptino USA, 1999.
- [191] M. Muhamed, "Synthesis of calcium oxide from waste cockle shell for CO<sub>2</sub> adsorption," MS, Department of Chemical Engineering Universiti Teknologi PETRONAS, Bandar Seri Iskandar, Malaysia 2011.
- [192] S. Therdthianwong, C. Siangchin, and A. Therdthianwong, "Improvement of coke resistance of Ni/Al<sub>2</sub>O<sub>3</sub> catalyst in CH<sub>4</sub>/CO<sub>2</sub> reforming by ZrO<sub>2</sub> addition", *Fuel Processing Technology*. vol. 89, 2008, pp. 160-168.
- [193] P. A. Webb and C. Orr, *Analytical methods in fine particle technology* Micromeritics Instrument corporation, USA 1997.
- [194] S. Ramkumar, M. Iyer, D. Wong, H. Gupta, and B. S. L.-S. Fan, "Enhanced hydrogen production integrated with CO<sub>2</sub> separation in a single-stage reactor " Department of Chemical and Biomolecular Engineering, The Ohio State University, , Final Technical Project Report, 2008.
- [195] K. Katsumi, "Determination of pore size and pore size distribution: 1. Adsorbents and catalysts", *Journal of Membrane Science*. vol. 96, 1994, pp. 59-89.
- [196] S. Rakass, H. Oudghiri-Hassani, P. Rowntree, and N. Abatzoglou, "Steam reforming of methane over unsupported nickel catalysts", *Journal of Power Sources*. vol. 158, 2006, pp. 485-496.
- [197] B. Acharya, A. Dutta, and P. Basu, "Chemical-looping gasification of biomass for hydrogen-enriched gas production with in-process carbon dioxide capture", *Energy & Fuels*. vol. 23, 2009, pp. 5077-5083.

- [198] B. Chalermsoonsin, P. Piumsomboon, and D. Gidaspow, "Kinetic theory based computation of PSRI riser: Part ii—computation of mass transfer coefficient with chemical reaction", *Chemical Engineering Science*. vol. 64, 2009, pp. 1212-1222.
- [199] W. Wu and P. K. Agarwal, "The effect of bed temperature on mass transfer between the bubble and emulsion phases in a fluidized bed", *The Canadian Journal of Chemical Engineering*,. vol. 81, 2003, pp. 940-948.
- [200] W. Wu and P. K. Agarwal, "Heat transfer to an isolated bubble rising in a high-temperature incipiently fluidized bed", *The Canadian Journal of Chemical Engineering*,. vol. 82, 2004, pp. 399-405.
- [201] D. Kunii and O. Levenspiel, "Bubbling bed model for kinetic processes in fluidized beds. Gas-solid mass and heat transfer and catalytic reactions", *Industrial & Engineering Chemistry Process Design and Development*. vol. 7, 1968, pp. 481-492.
- [202] C. Dupont, G. Boissonnet, J.-M. Seiler, P. Gauthier, and D. Schweich, "Study about the kinetic processes of biomass steam gasification", *Fuel*. vol. 86, 2007, pp. 32-40.
- [203] N. Gao, A. Li, and C. Quan, "A novel reforming method for hydrogen production from biomass steam gasification", *Bioresource Technology*. vol. 100, 2009, pp. 4271-4277.
- [204] C. Pfeifer, R. Rauch, and H. Hofbauer, "In-bed catalytic tar reduction in a dual fluidized bed biomass steam gasifier", *Industrial & Engineering Chemistry Research*. vol. 43, 2004, pp. 1634-1640.
- [205] M. A. Mohd Salleh, N. H. Kisiki, H. M. Yusuf, and W. A. W. Ab Karim Ghani, "Gasification of biochar from empty fruit bunch in a fluidized bed reactor", *Energies*. vol. 3, 2010, pp. 1344-1352.
- [206] S. Luo, B. Xiao, Z. Hu, S. Liu, X. Guo, and M. He, "Hydrogen-rich gas from catalytic steam gasification of biomass in a fixed bed reactor: Influence of temperature and steam on gasification performance", *International Journal of Hydrogen Energy*. vol. 34, 2009, pp. 2191-2194.
- [207] C. M. Kinoshita, Y. Wang, and J. Zhou, "Effect of reformer conditions on catalytic reforming of biomass-gasification tars", *Industrial & Engineering Chemistry Research*. vol. 34, 1995, pp. 2949-2954.

- [208] J. Han and H. Kim, "The reduction and control technology of tar during biomass gasification/pyrolysis: An overview", *Renewable and Sustainable Energy Reviews*. vol. 12, 2008, pp. 397-416.
- [209] P. M. Lv, Z. H. Xiong, J. Chang, C. Z. Wu, Y. Chen, and J. X. Zhu, "An experimental study on biomass air–steam gasification in a fluidized bed", *Bioresource Technology*. vol. 95, 2004, pp. 95-101.
- [210] A. Mountouris, E. Voutsas, and D. Tassios, "Solid waste plasma gasification: Equilibrium model development and exergy analysis", *Energy Conversion and Management*. vol. 47, 2006, pp. 1723-1737.
- [211] C. Loha, P. K. Chatterjee, and H. Chattopadhyay, "Performance of fluidized bed steam gasification of biomass – modeling and experiment", *Energy Conversion and Management*. vol. 52, 2011, pp. 1583-1588.
- [212] M. V. Twigg, *Catalyst handbook*, 2nd ed. London: Manson Publisher 1996.

## LIST OF PUBLICATION

### A. Journal Publication

1. **Zakir Khan**, Suzana Yusup, Murni M Ahmad, Anita Ramli, Mohammad T Arpin, Sharifah S Abdullah, Mas F Muhamad, Siti E Misi and Abrar Inayat, "Effect of steam and catalyst on palm oil wastes thermal decomposition for hydrogen production", Research journal of Chemistry and Environment. vol. 15, 2011, pp. 466-472.

*Indexing: ISI Web of Science (Impact factor=0.379)*

2. Tigabwa Y Ahmed, Murni M Ahmad, Suzana Yusup, Abrar Inayat and **Zakir Khan**, "Mathematical and computational approaches for design of biomass gasification for hydrogen production: A review", Renewable and Sustainable Energy Reviews. vol. 16, 2012, pp. 2304-2315.

*Indexing: ISI Web of Science (Impact factor=6.0)*

3. **Zakir Khan**, Suzana Yusup and Murni M Ahmad, "Thermogravimetric analysis of palm oil wastes decomposition", International Journal of Renewable Energy Research. vol. 1, 2011, pp. 7-10.

*Indexing: google scholar*

4. **Zakir Khan**, Suzana Yusup, Murni M Ahmad, Calvin C Vui, Yushimitso Uemura, and Khalik M Sabil, "Review on hydrogen production technologies in Malaysia ", International Journal of Engineering & Technology. vol. 10, 2010, pp. 111-118.

*Indexing: google scholar*

## B. Conference Publications

1. **Zakir Khan**, Suzana Yusup and Murni M. Ahmad, "Hydrogen production technologies-A Malaysian prospect," in *The 15 Asian Chemical Congress*, Singapore, Aug 19-23, 2013 (accepted).  
*Indexing: Google Scholar*
2. **Zakir Khan**, Suzana Yusup and Murni M Ahmad, "Effect of temperature and steam to biomass ratio on NO and SO<sub>2</sub> formation in palm kernel shell catalytic steam gasification with in-situ CO<sub>2</sub> adsorption," in *2nd World Sustainability Forum*, , 1-30 November 2012, Sciforum Electronic Conferences Series, 2102.  
*Indexing: Google Scholar*
3. Suzana Yusup, Anita Ramli, Murni M Ahmad, **Zakir Khan**, Mas F Mohamad, Sharifah S Abdullah, Abrar Inayat, Mohammad T Arpin and Calvin C Vui, "Potential of hydrogen production in in-situ catalytic adsorption gasification system" in International Conference on Biofuels and Biomass for Value-Added Products 2012 (ICBBVAP 2012), 23-24 October, Kuala Lumpur.  
*Indexing: Google Scholar*
4. **Zakir Khan**, Suzana Yusup and Murni M Ahmad, "Study of surface morphology of Quicklime and Ni for enhanced hydrogen production from biomass steam gasification". *The 2<sup>nd</sup> International Conference on Process Engineering and Advance Material (ICPEAM)*, 12-14 June 2012, Kuala Lumpur, Malaysia.  
*Indexing: Google Scholar*
5. **Zakir Khan**, Suzana Yusup and Murni M Ahmad, "Thermogravimetric analysis of palm oil wastes decomposition" in *proceeding of First Conference on Clean Energy and Technology (CET)*, 27-29 June, 2011, Kuala Lumpur, Malaysia.  
*Indexing: Scopus*
6. **Zakir Khan**, Suzana Yusup and Murni M Ahmad, Anita Ramli, Mohammad T Arpin, Sharifah S Abdullah, Mas F Mohamad, Siti E Misi and Abrar Inayat "Effect of steam and catalyst on palm oil wastes thermal decomposition for

hydrogen production" in *proceeding of 5th International Conference of Congress and Environment* (ICCE 2011), 27-29 May, 2011, Port Dickson, Malaysia.

*Indexing: Google Scholar*

C. Book

1. Suzana Yusup and **Zakir Khan**. "Enhancement of bioH<sub>2</sub> production via in-situ catalytic adsorption (ICA): Optimization and kinetic studies", Lambert Academic Publishing, Germany, 2013 (ISBN: 978-3-659-40782-6).

D. Book Sections

1. **Zakir Khan**, Suzana Yusup, Murni M Ahmad, Yushimitso Uemura, Voi S Chok, Umer Rashid and Abrar Inayat. "Kinetic study on palm oil waste decomposition", in *Biofuels*, Vol 4, InTech Open Access Publishers, Croatia, 2011 (ISBN 978-953-307-480-1).

*Indexing: Google Scholar*

2. Suzana Yusup, Reza A. Moghadam, Ahmed Al Shoaibi, Murni M Melati, **Zakir Khan**, Lim M. Tzeng, and Wan Ab K. Ghani." Hydrogen production from catalytic steam co-gasification of waste tyre and palm kernel shell in pilot scale fluidized bed gasifier", in *Biomass Processing, Conversion and Refinery*, Vol. 4, Nova Science Publishers, New York, 2013 (ISBN: 978-1-62808-126-8).

*Indexing: Google Scholar*

E. List of Awards

1. **Gold Medal**. *International invention, innovation and Technology Exhibition*. 17-19 May, 2012 Kuala Lumpur, "Integrated Catalytic Adsorption (ICA) Steam Gasification for Biohydrogen Production from Biomass".
2. **Silver Medal**. *Malaysian Technology Expo*, 16-18 February 2012, Kuala Lumpur, "Integrated Catalytic Adsorption (ICA) Steam Gasification for Biohydrogen Production from Biomass".
3. **Gold Medal**. *The Belgian and International Trade Fair for Technological Innovation (60<sup>th</sup> INNOVA 2011)*, 19 November 2011, Brussels, Belgium.

“Integrated Catalytic Adsorption (ICA) Steam Gasification for Biohydrogen Production from Biomass”.

4. **Special Sustainable Development Award.** *The Belgian and International Trade Fair for Technological Innovation (60<sup>th</sup> INNOVA 2011)*, 19 November 2011, Brussels, Belgium. “Integrated Catalytic Adsorption (ICA) Steam Gasification for Biohydrogen Production from Biomass”.

#### F. Submitted Articles

1. **Zakir Khan**, Suzana Yusup and Murni M Ahmad, "Integrated catalytic adsorption (ICA) steam gasification system for enhanced hydrogen production using palm kernel shell", *International Journal of Hydrogen Energy*. 2013, Under review (Manuscript ID: HE-D-13-01181).

*Indexing: ISI Web of Science (Impact factor = 4.054)*

2. **Zakir Khan**, Suzana Yusup and Murni M Ahmad, "Optimization of hydrogen production in integrated catalytic adsorption (ICA) steam gasification based on response surface methodology ", *Biomass and Bioenergy*. 2013, Under review (Manuscript ID: JBB-13-00400).

*Indexing: ISI Web of Science (Impact factor = 3.646)*

3. **Zakir Khan**, Suzana Yusup and Murni M Ahmad, "Performance study of Ni catalyst with quicklime (CaO) as CO<sub>2</sub> adsorbent in palm kernel shell steam gasification for hydrogen production ", *International Journal of Material engineering Innovation*, 2012, Under review.

*Indexing: ISI Web of Knowledge*

#### G. Patent

1. “Development of Integrated Biomass Catalytic Gasification System for Hydrogen Production” (**PI2012002104**)

## Effect of Steam and Catalyst on Palm Oil Wastes Thermal Decomposition for Hydrogen Production

Khan Zakir, Yusup Suzana \*, Murni Melati A., Ramlı Anita, Mohammad Taufiq A., Sharifah Shahidah A., Mas Fatiha M., Siti Eda E.M. and Inayat Abrar

Department of Chemical Engineering, Universiti Teknologi PETRONAS, Bandar Seri Iskandar, 31750 Tronoh, Perak Darul Ridzuan, Malaysia

\*drsuzana\_yusuf@petronas.com.my

### Abstract

The thermal decomposition of palm oil wastes in the form of palm shell and palm oil fronds in the presence of steam and catalyst was experimentally investigated using thermogravimetric analyzer-gas chromatography (TGA-GC). The hydrogen gas composition was observed for palm oil wastes thermal decomposition i) under inert atmosphere (no steam), ii) in steam gasification and iii) in catalytic steam gasification using a newly developed bi-metallic catalyst. Detailed discussion has been made for product gas composition profiles at steam-to-biomass ratio of 1 and biomass-to-catalyst ratio of 3. Maximum H<sub>2</sub> content up to 64 mol% and 50 mol% in product gas was observed for palm shell and palm oil fronds, respectively, in the catalytic steam gasification. The usage of steam has almost increased H<sub>2</sub> content by 28% for both palm oil wastes. The catalyst usage in the steam gasification increased H<sub>2</sub> content by 12.5% and 6% for palm shell and palm oil fronds, respectively. Moreover, CO<sub>2</sub> concentration in the product gas was reduced in steam gasification where CO concentration was decreased in catalytic steam gasification. This decrease in CO concentration is due to the bi-metallic catalyst activity on water gas shift reaction.

**Key words:** Palm oil wastes, Thermogravimetric analyzer (TGA), Hydrogen production.

### Introduction

There is growing interest in hydrogen as an energy carrier due to serious environmental issues and green houses emissions caused by conventional fossil fuel. Presently, almost 98% hydrogen comes from fossil fuels<sup>1</sup>. However, fast depleting rate and other competing usage of fossil fuel have serious concerns, and search for alternative feed stock has been intensified.

Biomass is one of most promising source among renewable resources to produce abundant, clean and renewable hydrogen. Among thermal conversion processes, biomass gasification is the one, shows great potential for renewable hydrogen production<sup>2</sup>. Biomass gasification produces gaseous mixture that mainly contains H<sub>2</sub>, CH<sub>4</sub>, CO and CO<sub>2</sub> (by using air, oxygen and steam or in combination as the gasifying agent). Steam as a sole gasifying agent has numerous advantages over air which dilutes the final product due to excess nitrogen, and pure oxygen is considered costly for small scale operation<sup>3</sup>. Steam as a gasifying agent avoids product gas dilution due to the absence of N<sub>2</sub> and can be easily separated from

product gas by condensation, hence producing more and pure hydrogen<sup>4</sup>.

The use of catalyst in biomass steam gasification has gained a lot of interest in order to enhance reaction rate, lower reaction temperature and improve gas quality by reducing tar content in product gas<sup>5</sup>. Tar in the product gas is one of the main problems associated with biomass gasification because it does create problems to the equipment and deactivate the downstream catalyst<sup>6</sup>. The catalyst activity in biomass steam gasification increased the H<sub>2</sub> content up to more than 60 vol% in product gas<sup>7</sup>. Typical catalysts used in biomass steam gasification are alkali metal, dolomites and Ni based catalysts<sup>8</sup>.

Palm oil is the main resource for Southeast Asia particularly Malaysia and Indonesia which collectively produced 87% of world wide<sup>9</sup>. In 2006, Malaysia was the largest producer of palm oil and contributed 51.2 million tons of palm oil wastes including empty fruit bunch (EFB), palm oil fronds (POF), mesocarp fiber (MF), palm oil trunks (POT) and palm shell (PS)<sup>10</sup>. This tremendous amount of palm oil wastes can contribute significantly to renewable hydrogen.

Thermogravimetric analyzer (TGA) is one of the promising systems to produce in-depth thermal decomposition and reaction kinetics information to develop the basis for biomass thermal conversion processes. This technique is based on sample mass loss with respect to time or temperature at a desired heating rate. TGA provides fast data collection along with excellent repeatability under well defined kinetics control environment. Beside thermal decomposition and reaction kinetics information, recent researches showed the possibility of capturing gas evaluation data for each decomposition step using Gas Chromatography (GC)<sup>12</sup> and Fourier-Transformation Infrared (FTIR)<sup>13</sup> under inert conditions and Mass spectrometer (MS) in steam gasification of pure components (cellulose and lignin)<sup>4</sup>. Moreover, a few works have been reported utilizing TGA for real biomass gasification using air<sup>15</sup>, steam<sup>16</sup> and pure oxygen<sup>17</sup>. However, these reported works have been done only to study the biomass thermal decomposition and reaction kinetics, and give no information about gas evaluation from real biomass gasification.

Some limited work has been reported for gaseous product evaluation using palm oil wastes under inert conditions in TGA. Yang et al<sup>11</sup> studied the main gaseous product evaluation from palm oil fiber (POF) pyrolysis in



## Mathematical and computational approaches for design of biomass gasification for hydrogen production: A review

Tigabwa Y. Ahmed<sup>1</sup>, Murni M. Ahmad\*, Suzana Yusup<sup>2</sup>, Abrar Inayat<sup>3</sup>, Zakir Khan<sup>4</sup>

Department of Chemical Engineering, Universiti Teknologi PETRONAS, Bandar Seri Iskandar, Tronoh 31750, Malaysia

### ARTICLE INFO

#### Article history:

Received 30 May 2011

Accepted 9 January 2012

Available online 21 February 2012

#### Keywords:

Hydrogen

Biomass

Gasification

Modeling

Heat integration

Cogeneration

### ABSTRACT

The ever growing environmental concern caused by excessive use of fossil fuels in energy and transportation systems triggered considerable investigations on alternative energy sources such as biomass. Furthermore, the availability and security of fossil fuels to meet future global energy need are also subjected to uncertainty. For these reasons, the world's current focus is shifted towards hydrogen-based future economy. Gasification is a proven technology to produce satisfactory yield of hydrogen. Many studies have been performed to increase the production yield. Due to the extensive range of investigations, mathematical and computational approaches have been applied to conduct these studies. Thus, this paper aims to update and broaden the review coverage by incorporating works done to materialize the investigations on the potential of producing hydrogen from biomass via gasification encompassing mathematical modeling, simulation, optimization, process heat integration and cogeneration. Each of these subjects is reviewed and analyzed which helped to identify their respective strength and areas which require further research effort.

© 2012 Elsevier Ltd. All rights reserved.

### Contents

1. Introduction .....	2305
2. Biomass conversion into hydrogen .....	2305
2.1. Gasification of biomass into hydrogen .....	2305
2.2. Gasifying agents .....	2305
2.3. Types of biomass gasifier .....	2306
3. Development of mathematical models .....	2306
3.1. Equilibrium models .....	2306
3.2. Kinetics models .....	2307
3.2.1. Fluidized bed gasifiers .....	2308
3.2.2. Fixed bed gasifiers .....	2308
3.2.3. Entrained flow gasifiers .....	2308
3.3. Artificial neural networks models .....	2308
4. Development of simulation models .....	2309
4.1. Process simulation models .....	2310
4.2. Computational fluid dynamics simulation models .....	2311
5. Process optimization .....	2311
6. Heat integration .....	2312

Abbreviations: BFBG, bubbling fluidized bed gasifier; CFBG, circulating fluidized bed gasifier; TFBFG, twin-bed fluidized bed gasifier; D, dimension.

\* Corresponding author. Tel.: +6053688215; fax: +6053688204.

E-mail addresses: [tigabwa@gmail.com](mailto:tigabwa@gmail.com) (T.Y. Ahmed), [murnim@petronas.com.my](mailto:murnim@petronas.com.my) (M.M. Ahmad), [drsuzana.yusuf@petronas.com.my](mailto:drsuzana.yusuf@petronas.com.my) (S. Yusup), [abrar\\_g00931@utp.edu.my](mailto:abrar_g00931@utp.edu.my) (A. Inayat), [zakirkhan\\_g00915@utp.edu.my](mailto:zakirkhan_g00915@utp.edu.my) (Z. Khan).

<sup>1</sup> Tel.: +6053688208; fax: +6053688204.

<sup>2</sup> Tel.: +60536887642; fax: +6053688204.

<sup>3</sup> Tel.: +6053688208; fax: +6053688204.

<sup>4</sup> Tel.: +6053688208; fax: +6053688204.

1364-0321/\$ – see front matter © 2012 Elsevier Ltd. All rights reserved.  
doi:10.1016/j.rser.2012.01.035

## THERMOGRAVIMETRIC ANALYSIS OF PALM OIL WASTES DECOMPOSITION

Z. Khan, S. Yusup and M.M. Ahmad

Department of Chemical Engineering, Universiti Teknologi PETRONAS  
Bandar Seri Iskandar, Tronoh 31750, Malaysia  
Email: drsuzana\_yusuf@petronas.com.my

### ABSTRACT

Thermal decomposition of palm oil wastes i.e. palm kernel shell (PKS) and palm oil fronds (POF) was studied using thermogravimetric analysis (TGA) under non-isothermal conditions. Thermogravimetric (TG) and its first derivative profiles were depicted to show different breakdown regions for PKS and POF. The decomposition region of hemicellulose, cellulose and lignin was identified. Kinetic parameters i.e. activation energy, pre-exponential factor and order of reaction were then evaluated from the weight loss profiles for the temperature range of 50-900 °C at a heating rate of 20 °C/min. Nearly 60 wt% of palm oil wastes decomposed at the temperature less than 400 °C. The thermal decomposition of palm oil wastes fitted well as first order kinetics with correlation coefficient of  $R^2 > 0.99$ . The activation energy of PKS and POF was 35 kJ/mol and 41 kJ/mol, respectively. This fundamental study provides the basic information on palm oil wastes decomposition which can benefit our current development work on palm oil wastes steam gasification unit.

**Keywords:** Palm oil wastes, Thermogravimetric analysis, Biomass, thermal decomposition, kinetic study

### 1. INTRODUCTION

Biomass has been upgraded as an alternative source of chemical feedstock and fuels in the last two decades due to serious environmental issues and fast depleting rate associated with conventional fossil fuel. It has been accepted as renewable, abundant and CO<sub>2</sub> neutral by the society. The efficient use of biomass depends on its conversion into clean and valuable energy. Thermal decomposition of biomass is an important step in its thermochemical conversion processes. The detail understanding of the biomass decomposition process and associated kinetic parameters are valuable information for the design of equipment and process operation for biomass thermal conversion processes (Guo and Lua 2001). Palm oil is the main resource for Southeast Asia particularly Malaysia and Indonesia which contributed 43% and 44% of global production in 2006, respectively (Shuit et al. 2009). In the same year, Malaysia generated 51.2 million tons of palm oil wastes including empty fruit bunch (EFB), palm oil fronds (POF), mesocarp fiber (MF), palm oil trunks (POT) and palm kernel shell

(PKS) (Sumathi et al. 2008). The distribution of the wastes is given in Figure 1. Several techniques are available to understand the (in-depth) processes and reaction kinetics for biomass decomposition. Among these, thermogravimetric analysis (TGA) which is based on the observation of sample mass loss with respect to time or temperature at a specific heating rate is the most popular and simplest technique (Luangkiattikhun et al. 2008). Moreover, TGA provides high precision (Várhegyi et al. 2009), a fast rate data collection and high repeatability (Yang et al. 2004) under well-defined kinetic control region. Very few attempts have been carried out to study the thermal decomposition of palm oil wastes using TGA. Guo et al. (2001) reported the effect of heating rate on the thermal decomposition and kinetic parameters for PKS. They found a lateral shift in derivative thermograms (DTG) when the heating rate was increased.

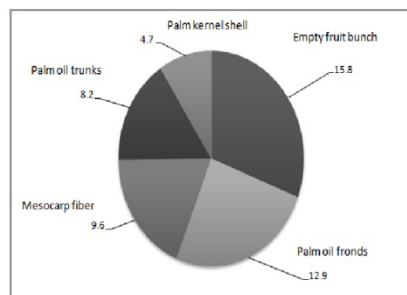


Figure 1 Palm oil wastes distribution (million tons) in Malaysia in 2006 (Sumathi et al. 2008)

Yang et al. (2004) studied hemicellulose and cellulose decompositions in PKS and EFB. They proposed the decomposition temperatures in the range of 220-300°C and 300-340°C for hemicellulose and cellulose, respectively. Hooi et al. (2009) (Hooi et al. 2009) observed the thermal decomposition of palm oil pressed fruit fibres (PFF) at temperature zones of 220-300 °C, 300-400°C and 400-700°C, and determined the kinetic parameters. Recently, Khan et al. (2011) studied the thermal decomposition of PKS and EFB and reported kinetic parameters at three different

# Review on Hydrogen Production Technologies in Malaysia

Z. Khan, S. Yusup, M.M. Ahmad, V.S. Chok, Y. Ucmura, K. M. Sabil

**Abstract-** Hydrogen has wide applications in petroleum, chemical synthesis and has been successfully demonstrated as a potentially zero emission fuel for transportations. As a country that is rich with natural resources and with the aims to be a developed country in 2020, Malaysia is currently intensified its renewable energy activities. The present work reviews all the resources and technologies related to hydrogen production in Malaysia. These technologies include non-renewable e.g. steam methane reforming (SMR) and renewable resources related to biomass processes e.g. gasification, pyrolysis, supercritical water gasification, biological water gas shift reaction, fermentation and water electrolysis e.g. using solar and wind energy. The techno-economic review is then presented for all these technologies to highlight the potential of present and future hydrogen production technologies in Malaysia.

**Keywords-** Review, hydrogen production technologies, hydrogen production in Malaysia

## I. INTRODUCTION

HYDROGEN economy has been promoted due to large number of hydrogen applications in petroleum and chemical sectors such as upgrading crude oil and synthesizing of methanol and ammonia. Besides this, hydrogen has been upgraded as an alternative to fossil fuel products due to its environmental friendly, high energy capacity and potentially gives high efficient processes such as in fuel cell application. Currently, about 98% of hydrogen comes from fossil fuel [1]. However, fast depleting rate and

other competing usage of fossil fuels has becoming a serious concern and the search for alternative feedstock for hydrogen production has been intensified.

Hydrogen as an energy carriers comprised numerous advantages over other conventional energy carriers. Hydrogen combustion provides energy based on mass basis with lower heating value (LHV), which is 2.4, 2.8 and 4 times more than that of methane, gasoline and coal respectively [2]. In addition, it is a clean fuel as the combustion of hydrogen produced only water as by-product.

Malaysia is a country of vast renewable and non-renewable sources of energy. The country energy demand mainly depended on non-renewable sources comprising of oil and gas. Up to 2005, non-renewable sources contributed about 87.9% of country energy demand while renewable sources shared 12.1% [3]. Due to fast growing economy, it is expected that the country energy demand will go up to 18000 MW by the year 2010 [4]. Moreover, unwanted green house gases emission and other serious environmental issues associated with the transportation sector have become a great concern to the future of the country development. As part of the UN Convention on Climate Change and Kyoto Protocol, Malaysia has to take steps to reduce green house gases emissions. More recently, in Copenhagen Climate Change Summit 2009, Malaysian Prime Minister has showed commitment to reduce carbon emission. The Prime Minister has also announced RM 1.5 billion in the 2010 national budget for green technology development in the country [5]. In the present scenario, the country needs to have abundant clean energy to maintain its journey towards a developed country.

The present work provides a brief summary of current and developing technologies available for the hydrogen production in Malaysia. The hydrogen production technologies are divided into two categories: non-renewable (fossil fuel) and renewable resources. Non-renewable hydrogen production technologies includes SMR while renewable hydrogen production technologies related to biomass utilization including gasification, pyrolysis, supercritical water gasification, biological water gas shift reaction, biological fermentation and hydrogen production from water, which includes electrolysis using solar and wind energy. The techno-economical comparison of available technologies is then made to evaluate the processes that can be used for future hydrogen production.

Manuscript received March 10, 2010. This work is supported by Petroleum Research Fund of PETRONAS.

Zakir Khan is a PhD student in the Department of Chemical Engineering, Universiti Teknologi PETRONAS, Bandar Seri Iskandar, Tronoh 31750, Perak, Malaysia (e-mail: [khan.zakir@gmail.com](mailto:khan.zakir@gmail.com)).

Suzana Yusup is working as a Associate Professor in the Department of Chemical Engineering, Universiti Teknologi PETRONAS, Bandar Seri Iskandar, Tronoh 31750, Perak, Malaysia (Ph:+605-3687642, fax: +605-3656176, e-mail: [drsuzana\\_yusuf@petronas.com.my](mailto:drsuzana_yusuf@petronas.com.my)).

Murni Melati Ahmad is working as a Lecturer in the Department of Chemical Engineering, Universiti Teknologi PETRONAS, Bandar Seri Iskandar, Tronoh 31750, Perak, Malaysia (e-mail: [murnim@petronas.com.my](mailto:murnim@petronas.com.my)).

Vui Soon Chok is working as a Research Officer in the Department of Chemical Engineering, Universiti Teknologi PETRONAS, Bandar Seri Iskandar, Tronoh 31750, Perak, Malaysia (e-mail: [chokvuisoon@yahoo.com.sg](mailto:chokvuisoon@yahoo.com.sg)).

Yoshimitsu Uemura is working as Professor, Mitsubishi Chair in Green Technology, in the Department of Chemical Engineering, Universiti Teknologi PETRONAS, Bandar Seri Iskandar, Tronoh 31750, Perak, Malaysia (e-mail: [yoshimitsu\\_uemura@petronas.com.my](mailto:yoshimitsu_uemura@petronas.com.my)).

Khalik Muhammad Sabil is working as a Lecturer in the Department of Chemical Engineering, Universiti Teknologi PETRONAS, Bandar Seri Iskandar, Tronoh 31750, Perak, Malaysia (e-mail: [khalik\\_msabil@petronas.com.my](mailto:khalik_msabil@petronas.com.my)).

## APPENDIX A

## Mass Balance over Gasifier

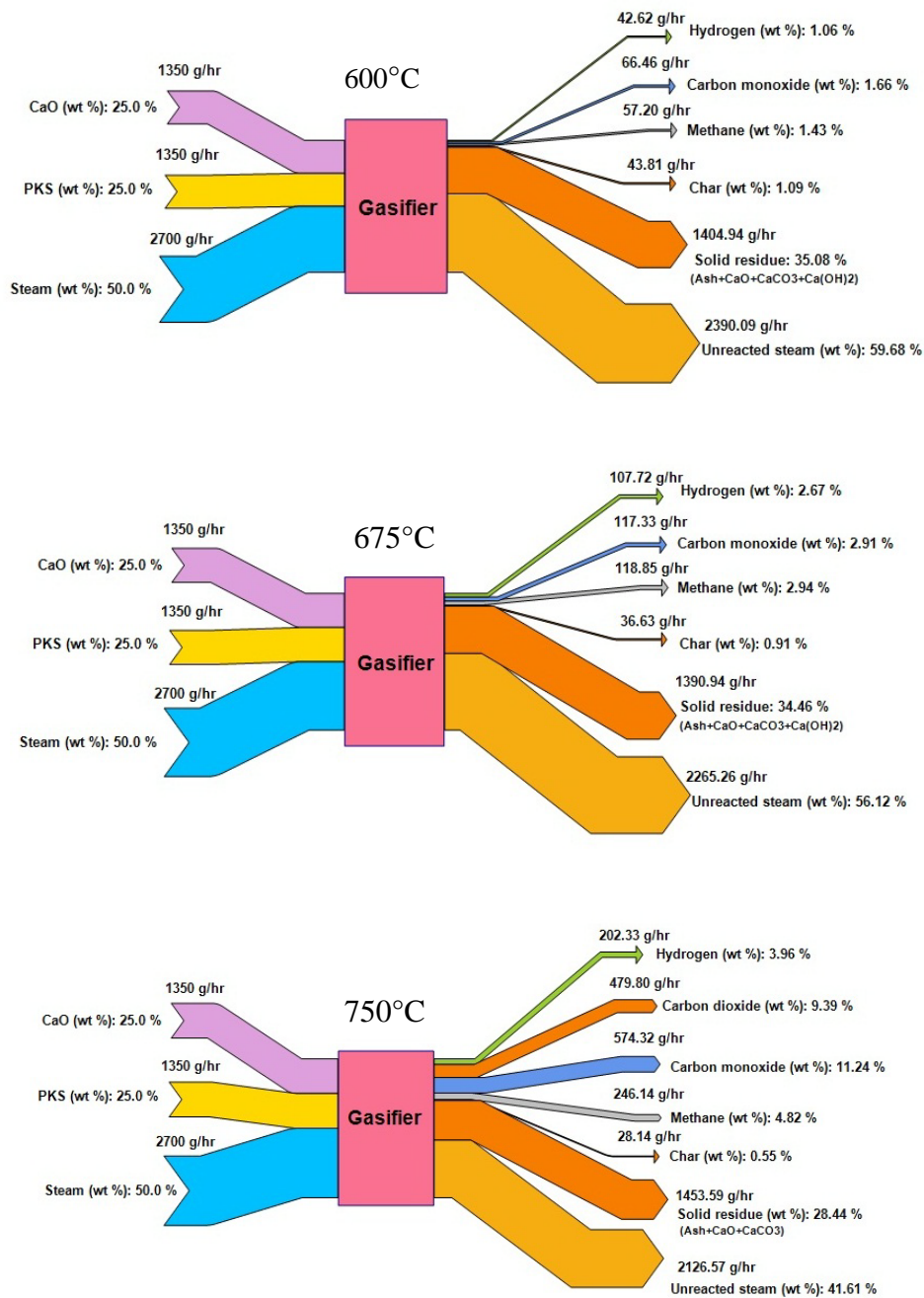


Figure A.2: Mass balance over gasifier at 600°C, 675°C and 750°C with steam to biomass, adsorbent to biomass of 1.0, catalyst to biomass ratio of 0.1, fluidization velocity of 0.21 m/s and biomass particle size of 1.0-2.0 mm

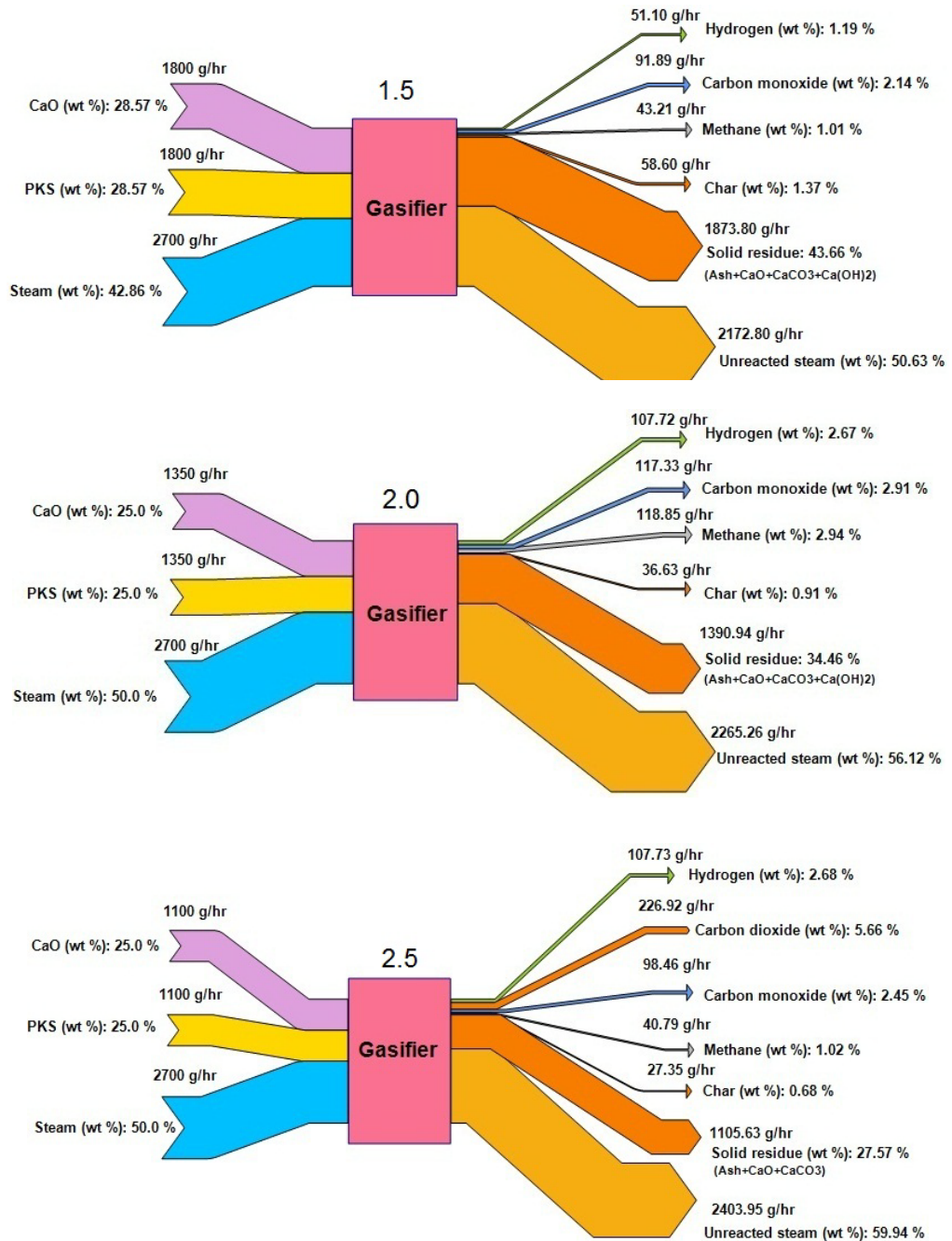


Figure A.2: Mass balance over gasifier at steam to biomass ratio of 1.5, 2.0 and 2.5 with temperature of 675°C, adsorbent to biomass ratio of 1.0, catalyst to biomass ratio of 0.1, fluidization velocity of 0.21 m/s and particle size of 1.0-2.0 mm

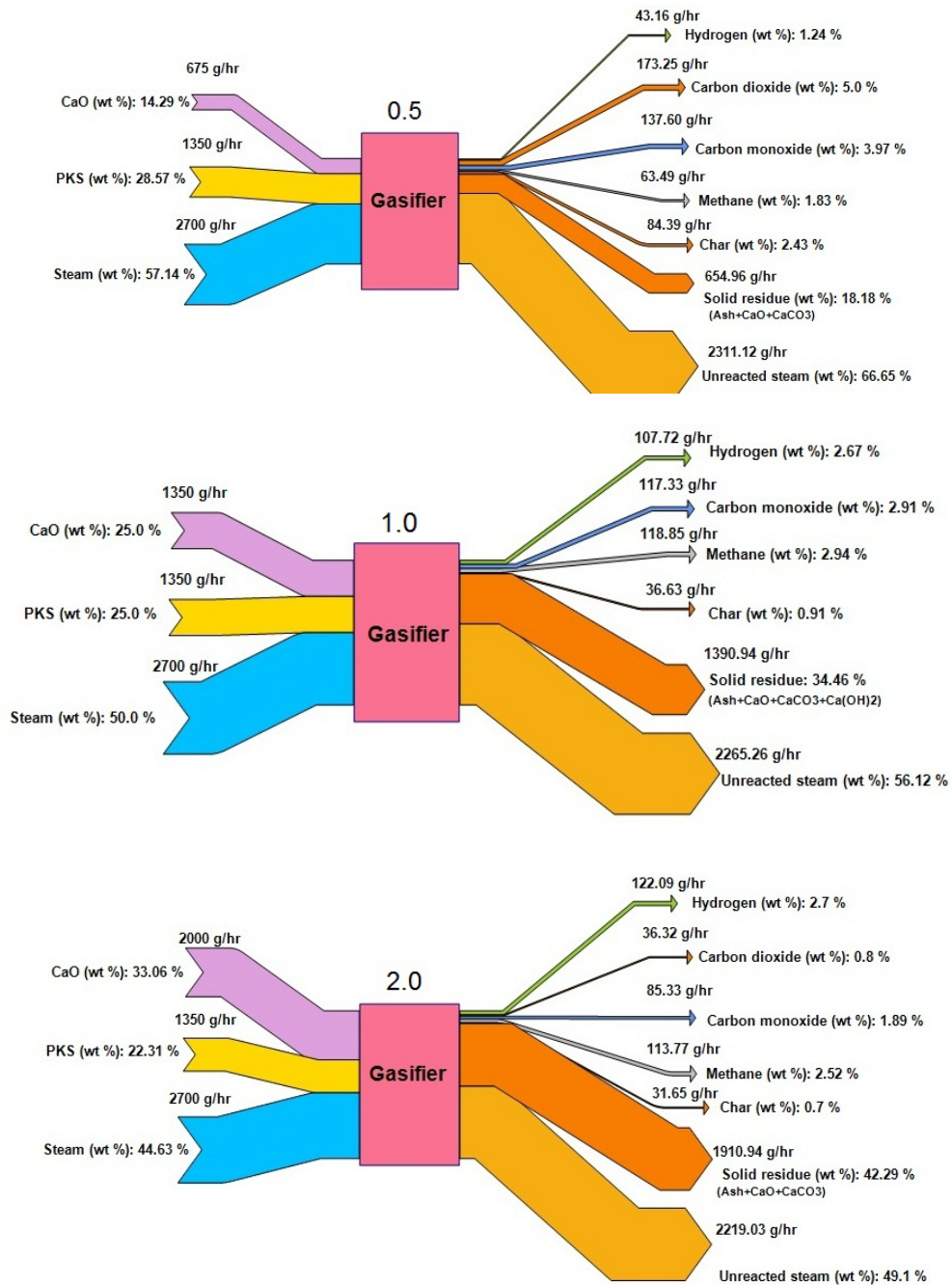


Figure A 1: Mass balance over gasifier at adsorbent to biomass ratio of 0.5, 1.0 and 1.5 with temperature of 675°C, steam to biomass ratio of 2.0, catalyst to biomass ratio of 0.1, fluidization velocity of 0.21 m/s and particle size of 1.0-2.0 mm

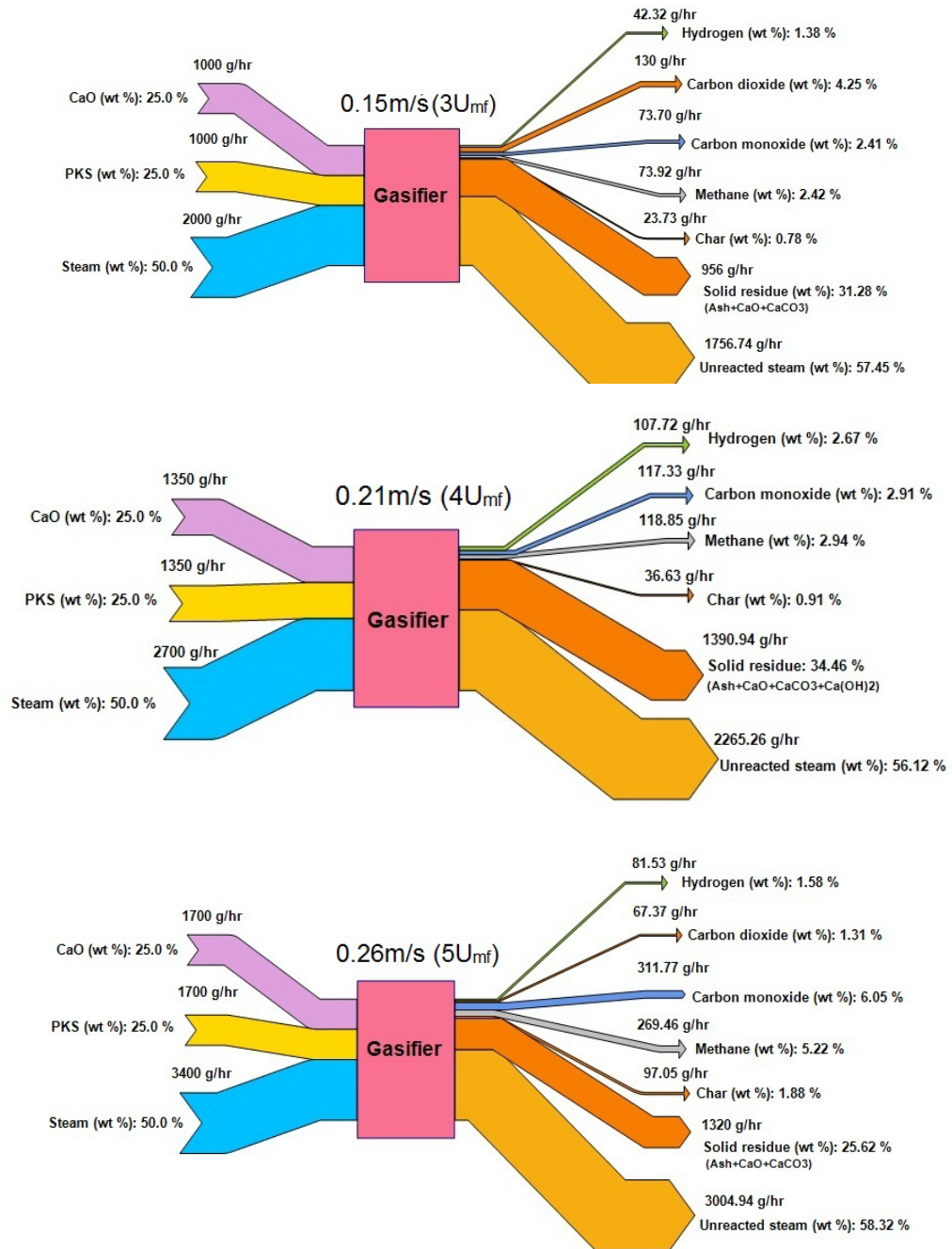


Figure A 2: Mass balance over gasifier at fluidization velocity of 0.15 m/s ( $3U_{mf}$ ), 0.21 m/s ( $4U_{mf}$ ) and 0.26 m/s ( $5U_{mf}$ ) with temperature of 675°C, steam to biomass ratio of 2.0, adsorbent to biomass ratio of 1.0, catalyst to biomass ratio of 0.1, and particle size of 1.0-2.0 mm

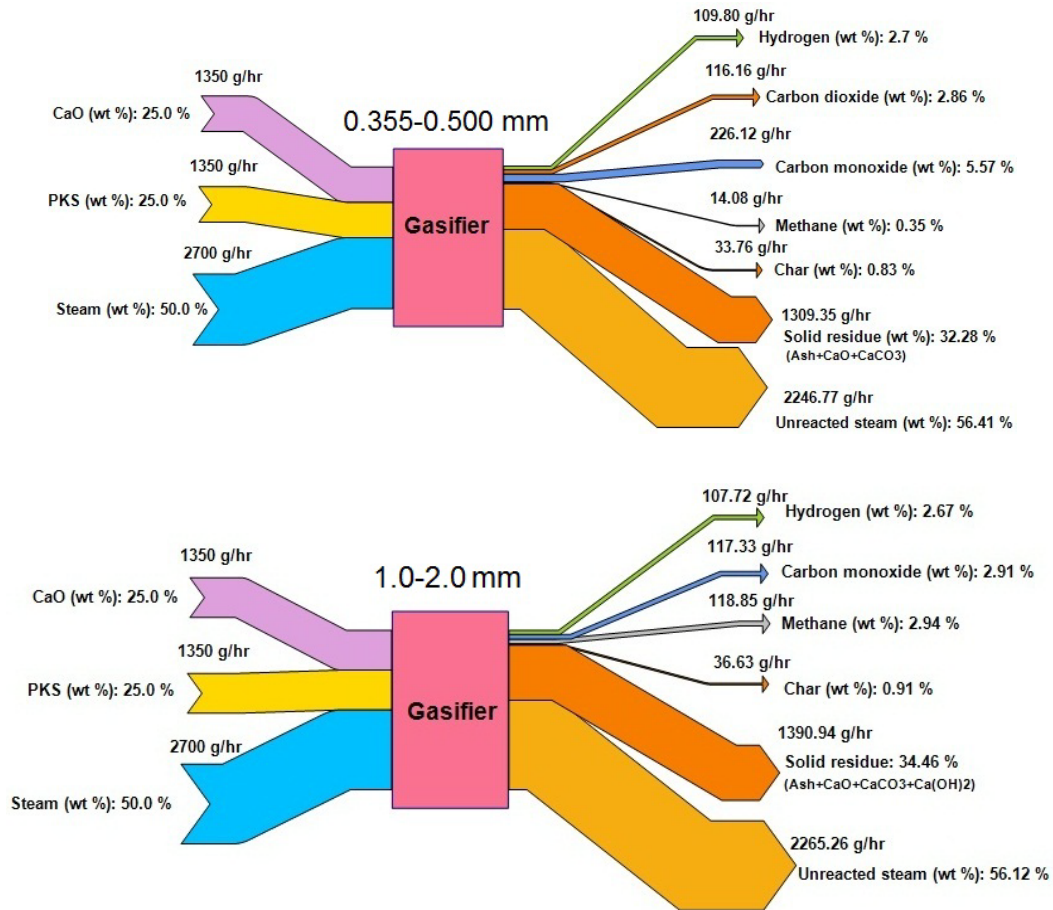


Figure A 3: Mass balance over gasifier at biomass particle size of 0.355-0.500 mm with temperature of 675°C, steam to biomass ratio of 2.0, adsorbent to biomass ratio of 1.0, catalyst to biomass ratio of 0.1 and fluidization velocity of 0.21 m/s

## APPENDIX B

## A.2 Data from Figures

Table A.1: Product gas composition (vol%) profiles at 600°C

Minute	H <sub>2</sub>	CO <sub>2</sub>	CO	CH <sub>4</sub>	NO	SO <sub>2</sub>
6	92.88	0.00	1.27	5.85	0.000	0.003
12	83.42	0.00	5.24	11.34	0.004	0.014
18	77.81	0.00	8.65	13.54	0.007	0.020
24	76.92	0.00	9.15	13.92	0.007	0.004
30	78.01	0.00	8.78	13.22	0.003	0.010
36	78.37	0.00	8.83	12.80	0.004	0.012
42	76.06	0.00	10.14	13.80	0.004	0.011
48	73.67	0.00	11.52	14.82	0.003	0.011
54	72.74	0.00	11.99	15.27	0.003	0.011
60	70.68	0.00	13.23	16.09	0.003	0.010

Table A.2: Product gas composition (vol%) profiles at 675°C

Minute	H <sub>2</sub>	CO <sub>2</sub>	CO	CH <sub>4</sub>	NO	SO <sub>2</sub>
6	93.24	0.00	0.00	6.76	0.003	0.013
12	76.02	0.00	9.17	14.81	0.005	0.022
18	83.46	0.00	7.57	8.96	0.005	0.024
24	92.04	0.00	2.49	5.47	0.006	0.027
30	78.95	0.00	7.66	13.40	0.005	0.025
36	81.08	0.00	6.49	12.43	0.005	0.024
42	82.11	0.00	6.45	11.44	0.006	0.028
48	83.09	0.00	7.45	9.46	0.007	0.031
54	81.76	0.00	6.60	11.64	0.008	0.033
60	83.06	0.00	6.31	10.63	0.009	0.036

Table A.3: Product gas composition (vol%) profiles at 750°C

Minute	H <sub>2</sub>	CO <sub>2</sub>	CO	CH <sub>4</sub>	NO	SO <sub>2</sub>
6	99.10	0.00	0.00	0.90	0.000	0.003
12	68.29	0.00	9.60	22.10	0.004	0.004
18	67.48	0.00	11.49	21.03	0.031	0.109
24	65.60	0.18	12.40	21.82	0.147	0.126
30	69.47	0.03	11.35	19.15	0.147	0.140
36	68.86	0.98	11.44	18.71	0.147	0.114
42	64.52	2.26	14.08	19.14	0.147	0.126
48	62.51	6.81	16.63	14.05	0.147	0.133
54	68.16	7.42	13.96	10.47	0.037	0.147
60	63.67	7.16	15.99	13.19	0.039	0.098

Table A.4: Product gas concentration (mol/m<sup>3</sup>) profiles at 600°C

Minute	H <sub>2</sub>	CO <sub>2</sub>	CO	CH <sub>4</sub>
6	37.80	0.00	0.52	2.38
12	33.95	0.00	2.13	4.61
18	31.67	0.00	3.52	5.51
24	31.31	0.00	3.72	5.67
30	31.75	0.00	3.57	5.38
36	31.89	0.00	3.59	5.21
42	30.95	0.00	4.13	5.62
48	29.98	0.00	4.69	6.03
54	29.60	0.00	4.88	6.21
60	28.76	0.00	5.39	6.55

Table A.5: Product gas concentration (mol/m<sup>3</sup>) profiles at 675°C

Minute	H <sub>2</sub>	CO <sub>2</sub>	CO	CH <sub>4</sub>
6	37.95	0.00	0.00	2.75
12	30.94	0.00	3.73	6.03
18	33.97	0.00	3.08	3.65
24	37.46	0.00	1.01	2.23
30	32.13	0.00	3.12	5.45
36	33.00	0.00	2.64	5.06
42	33.42	0.00	2.63	4.65
48	33.82	0.00	3.03	3.85
54	33.27	0.00	2.69	4.74
60	33.80	0.00	2.57	4.33

Table A.6: Product gas concentration (mol/m<sup>3</sup>) profiles at 750°C

Minute	H <sub>2</sub>	CO <sub>2</sub>	CO	CH <sub>4</sub>
6	40.33	0.00	0.00	0.37
12	27.79	0.00	3.91	9.00
18	27.46	0.00	4.68	8.56
24	26.70	0.07	5.05	8.88
30	28.27	0.01	4.62	7.79
36	28.03	0.40	4.66	7.62
42	26.26	0.92	5.73	7.79
48	25.44	2.77	6.77	5.72
54	27.74	3.02	5.68	4.26
60	25.91	2.91	6.51	5.37

Table A.7: Product gas composition (vol%) profiles at steam to biomass ratio of 1.5

Minute	H <sub>2</sub>	CO <sub>2</sub>	CO	CH <sub>4</sub>	NO	SO <sub>2</sub>
6	64.29	0.00	19.23	16.48	0.009	0.002
12	55.84	0.00	22.34	21.82	0.012	0.026
18	68.43	0.00	15.83	15.74	0.010	0.034
24	67.36	0.00	16.96	15.68	0.010	0.029
30	77.95	0.00	9.99	12.06	0.007	0.030
36	83.72	0.00	8.06	8.22	0.004	0.021
42	80.87	0.00	10.49	8.63	0.005	0.016
48	83.09	0.00	10.32	6.59	0.004	0.016
54	82.81	0.00	10.16	7.03	0.003	0.013
60	83.82	0.00	10.29	5.88	0.012	0.013

Table A.8: Product gas composition (vol%) profiles at steam to biomass ratio of 2.0

Minute	H <sub>2</sub>	CO <sub>2</sub>	CO	CH <sub>4</sub>	NO	SO <sub>2</sub>
6	93.24	0.00	0.00	6.76	0.003	0.013
12	76.02	0.00	9.17	14.81	0.005	0.022
18	83.46	0.00	7.57	8.96	0.005	0.024
24	92.04	0.00	2.49	5.47	0.006	0.027
30	78.95	0.00	7.66	13.40	0.005	0.025
36	81.08	0.00	6.49	12.43	0.005	0.024
42	82.11	0.00	6.45	11.44	0.006	0.028
48	83.09	0.00	7.45	9.46	0.007	0.031
54	81.76	0.00	6.60	11.64	0.008	0.033
60	83.06	0.00	6.31	10.63	0.009	0.036

Table A.9: Product gas composition (vol%) profiles at steam to biomass ratio of 2.5

Minute	H <sub>2</sub>	CO <sub>2</sub>	CO	CH <sub>4</sub>	NO	SO <sub>2</sub>
6	80.33	5.72	4.20	9.74	0.001	0.013
12	80.58	5.80	4.52	9.10	0.001	0.017
18	92.99	3.07	2.93	1.01	0.001	0.004
24	83.33	11.54	4.52	0.60	0.002	0.011
30	79.23	10.88	5.83	4.06	0.004	0.014
36	82.61	7.99	5.45	3.95	0.004	0.014
42	82.13	7.31	6.09	4.47	0.003	0.010
48	82.56	8.90	4.80	3.75	0.002	0.009
54	81.05	10.83	4.47	3.65	0.003	0.012
60	79.03	10.21	5.90	4.86	0.002	0.012

Table A.10: Product gas concentration (mol/m<sup>3</sup>) profiles at steam to biomass ratio of 1.5

Minute	H <sub>2</sub>	CO <sub>2</sub>	CO	CH <sub>4</sub>
6	26.16	0.00	7.83	6.71
12	22.73	0.00	9.09	8.88
18	27.85	0.00	6.44	6.41
24	27.41	0.00	6.90	6.38
30	31.73	0.00	4.06	4.91
36	34.07	0.00	3.28	3.34
42	32.91	0.00	4.27	3.51
48	33.82	0.00	4.20	2.68
54	33.70	0.00	4.13	2.86
60	34.11	0.00	4.19	2.39

Table A.11: Product gas concentration (mol/m<sup>3</sup>) profiles at steam to biomass ratio of 2.0

Minute	H <sub>2</sub>	CO <sub>2</sub>	CO	CH <sub>4</sub>
6	37.95	0.00	0.00	2.75
12	30.94	0.00	3.73	6.03
18	33.97	0.00	3.08	3.65
24	37.46	0.00	1.01	2.23
30	32.13	0.00	3.12	5.45
36	33.00	0.00	2.64	5.06
42	33.42	0.00	2.63	4.65
48	33.82	0.00	3.03	3.85
54	33.27	0.00	2.69	4.74
60	33.80	0.00	2.57	4.33

Table A.12: Product gas concentration (mol/m<sup>3</sup>) profiles at steam to biomass ratio of 2.5

Minute	H <sub>2</sub>	CO <sub>2</sub>	CO	CH <sub>4</sub>
6	32.69	2.33	1.71	3.96
12	32.79	2.36	1.84	3.70
18	37.84	1.25	1.19	0.41
24	33.91	4.70	1.84	0.25
30	32.24	4.43	2.37	1.65
36	33.62	3.25	2.22	1.61
42	33.42	2.98	2.48	1.82
48	33.60	3.62	1.95	1.52
54	32.98	4.41	1.82	1.49
60	32.16	4.16	2.40	1.98

Table A.13: Product gas composition (vol%) profiles at adsorbent to biomass ratio of 0.5

Minute	H <sub>2</sub>	CO <sub>2</sub>	CO	CH <sub>4</sub>	NO	SO <sub>2</sub>
6	46.95	19.01	24.65	9.39	0.001	0.005
12	51.70	14.86	19.55	13.89	0.001	0.011
18	50.49	15.15	19.54	14.82	0.004	0.016
24	56.18	12.92	17.28	13.62	0.004	0.016
30	57.67	12.88	16.20	13.25	0.004	0.015
36	58.35	12.17	15.29	14.19	0.004	0.018
42	61.94	11.67	15.35	11.04	0.006	0.018
48	62.50	11.52	14.38	11.61	0.007	0.016
54	63.69	11.57	14.44	10.30	0.007	0.015
60	62.81	12.94	15.83	8.42	0.003	0.013

Table A.14: Product gas composition (vol%) profiles at adsorbent to biomass ratio of 1.0

Minute	H <sub>2</sub>	CO <sub>2</sub>	CO	CH <sub>4</sub>	NO	SO <sub>2</sub>
6	93.24	0.00	0.00	6.76	0.003	0.013
12	76.02	0.00	9.17	14.81	0.005	0.022
18	83.46	0.00	7.57	8.96	0.005	0.024
24	92.04	0.00	2.49	5.47	0.006	0.027
30	78.95	0.00	7.66	13.40	0.005	0.025
36	81.08	0.00	6.49	12.43	0.005	0.024
42	82.11	0.00	6.45	11.44	0.006	0.028
48	83.09	0.00	7.45	9.46	0.007	0.031
54	81.76	0.00	6.60	11.64	0.008	0.033
60	83.06	0.00	6.31	10.63	0.009	0.036

Table A.15: Product gas composition (vol%) profiles at adsorbent to biomass ratio of 1.5

Minute	H <sub>2</sub>	CO <sub>2</sub>	CO	CH <sub>4</sub>	NO	SO <sub>2</sub>
6	40.71	0.83	18.48	39.98	0.001	0.004
12	48.28	1.38	15.34	35.00	0.001	0.005
18	62.81	1.18	10.39	25.62	0.001	0.005
24	75.14	1.19	6.71	16.96	0.001	0.005
30	76.41	1.22	6.54	15.83	0.001	0.005
36	82.91	1.00	4.67	11.42	0.002	0.005
42	83.35	1.07	4.51	11.07	0.002	0.005
48	84.62	1.16	4.27	9.96	0.003	0.005
54	84.94	0.70	4.04	10.31	0.003	0.006
60	83.84	0.91	3.74	11.50	0.002	0.007

Table A.16: Product gas concentration (mol/m<sup>3</sup>) profiles at adsorbent to biomass ratio of 0.5

Minute	H <sub>2</sub>	CO <sub>2</sub>	CO	CH <sub>4</sub>
6	19.11	7.74	10.03	3.82
12	21.04	6.05	7.96	5.65
18	20.55	6.16	7.95	6.03
24	22.86	5.26	7.03	5.54
30	23.47	5.24	6.59	5.39
36	23.75	4.95	6.22	5.77
42	25.21	4.75	6.25	4.49
48	25.44	4.69	5.85	4.72
54	25.92	4.71	5.88	4.19
60	25.56	5.27	6.44	3.43

Table A. 17: Product gas concentration (mol/m<sup>3</sup>) profiles at adsorbent to biomass ratio of 1.0

Minute	H <sub>2</sub>	CO <sub>2</sub>	CO	CH <sub>4</sub>
6	37.95	0.00	0.00	2.75
12	30.94	0.00	3.73	6.03
18	33.97	0.00	3.08	3.65
24	37.46	0.00	1.01	2.23
30	32.13	0.00	3.12	5.45
36	33.00	0.00	2.64	5.06
42	33.42	0.00	2.63	4.65
48	33.82	0.00	3.03	3.85
54	33.27	0.00	2.69	4.74
60	33.80	0.00	2.57	4.33

Table A.18: Product gas concentration (mol/m<sup>3</sup>) profiles at adsorbent to biomass ratio of 1.5

Minute	H <sub>2</sub>	CO <sub>2</sub>	CO	CH <sub>4</sub>
6	16.57	0.34	7.52	16.27
12	19.65	0.56	6.24	14.24
18	25.56	0.48	4.23	10.43
24	30.58	0.49	2.73	6.90
30	31.10	0.50	2.66	6.44
36	33.74	0.41	1.90	4.65
42	33.92	0.44	1.84	4.51
48	34.44	0.47	1.74	4.05
54	34.57	0.29	1.65	4.20
60	34.12	0.37	1.52	4.68

Table A.19: Product gas composition (vol%) profiles at fluidization velocity of  
0.15 m/s ( $3U_{mf}$ )

Minute	H <sub>2</sub>	CO <sub>2</sub>	CO	CH <sub>4</sub>	NO	SO <sub>2</sub>
6	70.87	9.06	3.54	16.54	0.002	0.008
12	66.67	10.26	5.13	17.95	0.003	0.011
18	69.00	7.60	7.90	15.50	0.005	0.016
24	68.97	8.05	8.05	14.94	0.005	0.016
30	69.03	8.63	7.57	14.77	0.005	0.015
36	66.20	9.71	9.09	15.00	0.006	0.018
42	67.24	9.48	8.45	14.83	0.006	0.018
48	65.74	10.06	8.47	15.74	0.005	0.016
54	63.69	11.06	8.94	16.31	0.004	0.015
60	67.94	10.25	6.91	14.90	0.003	0.013

Table A.20: Product gas composition (vol%) profiles at fluidization velocity of  
0.21 m/s ( $4U_{mf}$ )

Minute	H <sub>2</sub>	CO <sub>2</sub>	CO	CH <sub>4</sub>	NO	SO <sub>2</sub>
6	93.24	0.00	0.00	6.76	0.003	0.013
12	76.02	0.00	9.17	14.81	0.005	0.022
18	83.46	0.00	7.57	8.96	0.005	0.024
24	92.04	0.00	2.49	5.47	0.006	0.027
30	78.95	0.00	7.66	13.40	0.005	0.025
36	81.08	0.00	6.49	12.43	0.005	0.024
42	82.11	0.00	6.45	11.44	0.006	0.028
48	83.09	0.00	7.45	9.46	0.007	0.031
54	81.76	0.00	6.60	11.64	0.008	0.033
60	83.06	0.00	6.31	10.63	0.009	0.036

Table A.21: Product gas composition (vol%) profiles at fluidization velocity of  
0.26 m/s ( $5U_{mf}$ )

Minute	H <sub>2</sub>	CO <sub>2</sub>	CO	CH <sub>4</sub>	NO	SO <sub>2</sub>
6	87.30	0.79	3.97	7.94	0.002	0.007
12	65.15	0.00	12.16	22.69	0.007	0.018
18	65.58	0.24	14.31	19.87	0.010	0.027
24	58.68	0.98	16.36	23.99	0.013	0.033
30	57.97	1.67	16.01	24.35	0.015	0.038
36	57.77	2.19	15.94	24.10	0.017	0.041
42	56.56	3.31	16.06	24.07	0.018	0.045
48	55.56	4.40	16.15	23.90	0.018	0.045
54	54.45	5.15	16.57	23.83	0.017	0.045
60	55.56	4.89	16.49	23.07	0.017	0.044

Table A.22: Product gas concentration (mol/m<sup>3</sup>) profiles at fluidization velocity of  
0.15 m/s (3U<sub>mf</sub>)

Minute	H <sub>2</sub>	CO <sub>2</sub>	CO	CH <sub>4</sub>
6	28.84	3.69	1.44	6.73
12	27.13	4.17	2.09	7.30
18	28.08	3.09	3.22	6.31
24	28.07	3.27	3.27	6.08
30	28.09	3.51	3.08	6.01
36	26.94	3.95	3.70	6.11
42	27.37	3.86	3.44	6.03
48	26.75	4.09	3.45	6.40
54	25.92	4.50	3.64	6.64
60	27.65	4.17	2.81	6.06

Table A.23: Product gas concentration (mol/m<sup>3</sup>) profiles at fluidization velocity of  
0.21 m/s (4U<sub>mf</sub>)

Minute	H <sub>2</sub>	CO <sub>2</sub>	CO	CH <sub>4</sub>
6	37.95	0.00	0.00	2.75
12	30.94	0.00	3.73	6.03
18	33.97	0.00	3.08	3.65
24	37.46	0.00	1.01	2.23
30	32.13	0.00	3.12	5.45
36	33.00	0.00	2.64	5.06
42	33.42	0.00	2.63	4.65
48	33.82	0.00	3.03	3.85
54	33.27	0.00	2.69	4.74
60	33.80	0.00	2.57	4.33

Table A.24: Product gas concentration (mol/m<sup>3</sup>) profiles at fluidization velocity of  
0.26 m/s (5U<sub>mf</sub>)

Minute	H <sub>2</sub>	CO <sub>2</sub>	CO	CH <sub>4</sub>
6	35.53	0.32	1.61	3.23
12	26.51	0.00	4.95	9.24
18	26.69	0.10	5.82	8.09
24	23.88	0.40	6.66	9.76
30	23.59	0.68	6.52	9.91
36	23.51	0.89	6.49	9.81
42	23.02	1.35	6.54	9.79
48	22.61	1.79	6.57	9.73
54	22.16	2.10	6.74	9.70
60	22.61	1.99	6.71	9.39

Table A.25: Product gas composition (vol%) profiles biomass particle size of 0.355-0.500 mm

Minute	H <sub>2</sub>	CO <sub>2</sub>	CO	CH <sub>4</sub>	NO	SO <sub>2</sub>
6	91.41	2.82	1.36	4.41	0.009	0.030
12	93.50	2.25	0.85	3.40	0.008	0.028
18	92.58	2.61	0.77	4.04	0.007	0.026
24	94.26	2.11	0.53	3.11	0.007	0.025
30	94.87	2.09	0.36	2.68	0.007	0.024
36	83.13	3.82	12.39	0.67	0.006	0.018
42	82.42	4.00	12.24	1.33	0.005	0.019
48	81.94	4.10	12.14	1.82	0.005	0.019
54	81.37	4.18	12.55	1.90	0.006	0.020
60	80.84	4.37	12.77	2.02	0.006	0.019

Table A.26: Product gas composition (vol%) profiles at biomass particle size of 1.0-2.0 mm

Minute	H <sub>2</sub>	CO <sub>2</sub>	CO	CH <sub>4</sub>	NO	SO <sub>2</sub>
6	93.24	0.00	0.00	6.76	0.003	0.013
12	76.02	0.00	9.17	14.81	0.005	0.022
18	83.46	0.00	7.57	8.96	0.005	0.024
24	92.04	0.00	2.49	5.47	0.006	0.027
30	78.95	0.00	7.66	13.40	0.005	0.025
36	81.08	0.00	6.49	12.43	0.005	0.024
42	82.11	0.00	6.45	11.44	0.006	0.028
48	83.09	0.00	7.45	9.46	0.007	0.031
54	81.76	0.00	6.60	11.64	0.008	0.033
60	83.06	0.00	6.31	10.63	0.009	0.036

Table A.27: Product gas concentration (mol/m<sup>3</sup>) profiles at particle size of 0.355-0.500 mm

Minute	H <sub>2</sub>	CO <sub>2</sub>	CO	CH <sub>4</sub>
6	37.20	1.15	0.56	1.80
12	38.05	0.92	0.35	1.38
18	37.68	1.06	0.31	1.64
24	38.36	0.86	0.21	1.26
30	38.61	0.85	0.15	1.09
36	33.83	1.56	5.04	0.27
42	33.54	1.63	4.98	0.54
48	33.35	1.67	4.94	0.74
54	33.12	1.70	5.11	0.77
60	32.90	1.78	5.20	0.82

Table A.28: Product gas concentration (mol/m<sup>3</sup>) profiles at biomass particle size of  
1.0-2.0 mm

Minute	H <sub>2</sub>	CO <sub>2</sub>	CO	CH <sub>4</sub>
6	37.95	0.00	0.00	2.75
12	30.94	0.00	3.73	6.03
18	33.97	0.00	3.08	3.65
24	37.46	0.00	1.01	2.23
30	32.13	0.00	3.12	5.45
36	33.00	0.00	2.64	5.06
42	33.42	0.00	2.63	4.65
48	33.82	0.00	3.03	3.85
54	33.27	0.00	2.69	4.74
60	33.80	0.00	2.57	4.33

### B.1 XRD Analysis of Solid Residual Samples in Fluidized Bed gasifier and cyclone Separator

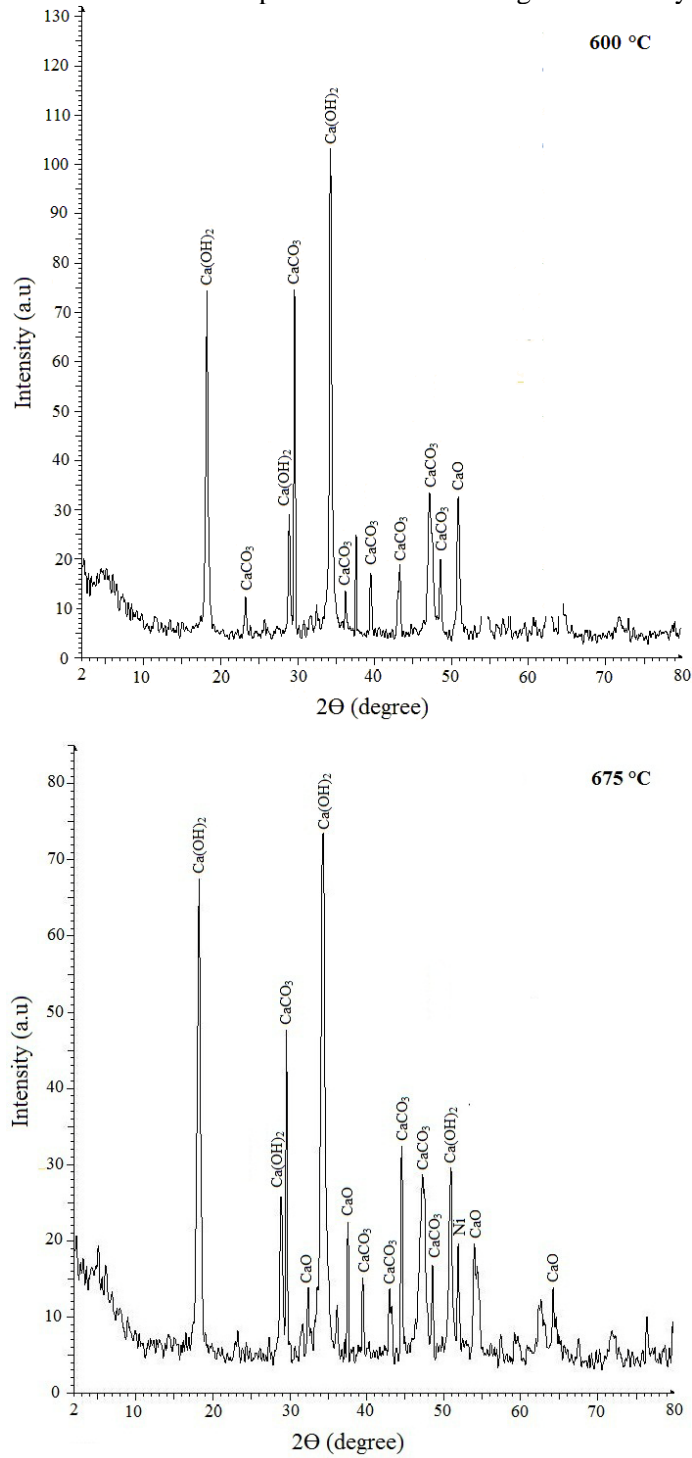


Figure B 1: XRD analysis of solid residue samples (after experiment) in fluidized bed gasifier at 600°C and 675°C

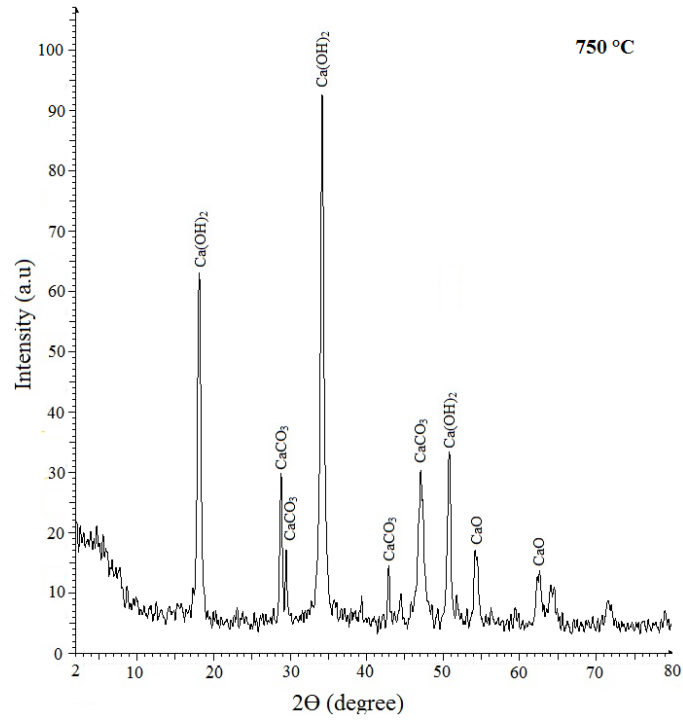


Figure B 2: Solid residual samples (after experiments) in fluidized bed gasifier at 750°C

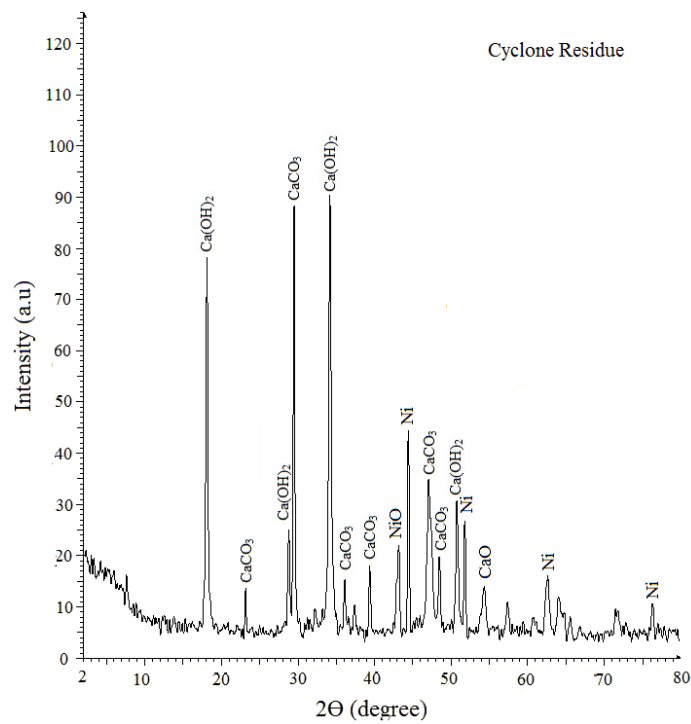


Figure B 3: XRD analysis of cyclone solid residual samples (after experiments) at 675°C

## B 2. Tar Analysis

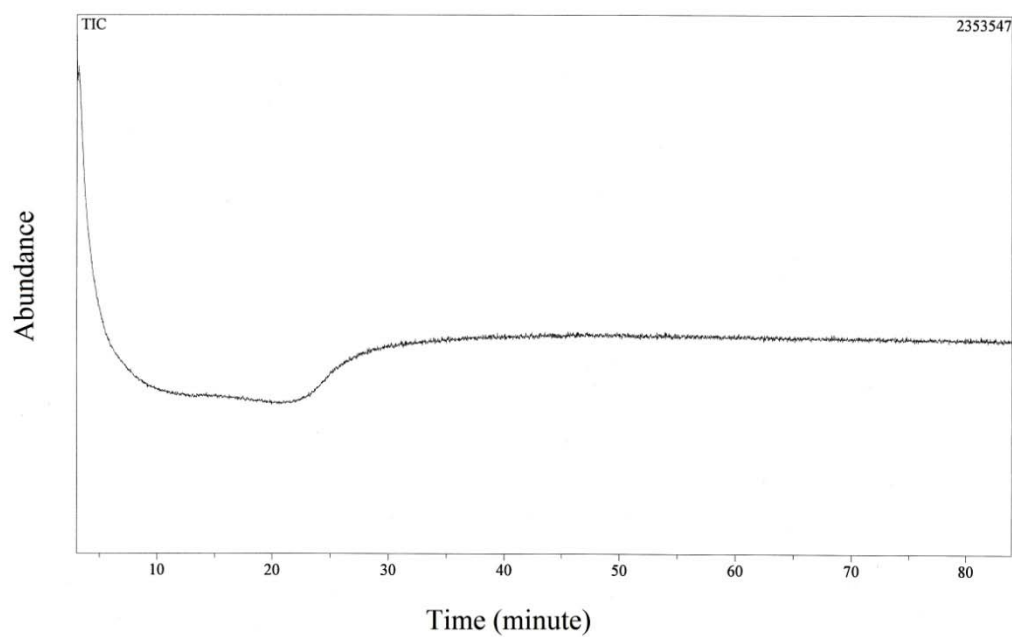


Figure B 4: Analysis of tar produced at 675°C, steam to biomass ratio of 2.0, adsorbent to biomass ratio of 1.0 and catalyst to biomass ratio of 0.1, fluidization velocity of 0.21 m/s and biomass particle size of 1.0-2.0 mm

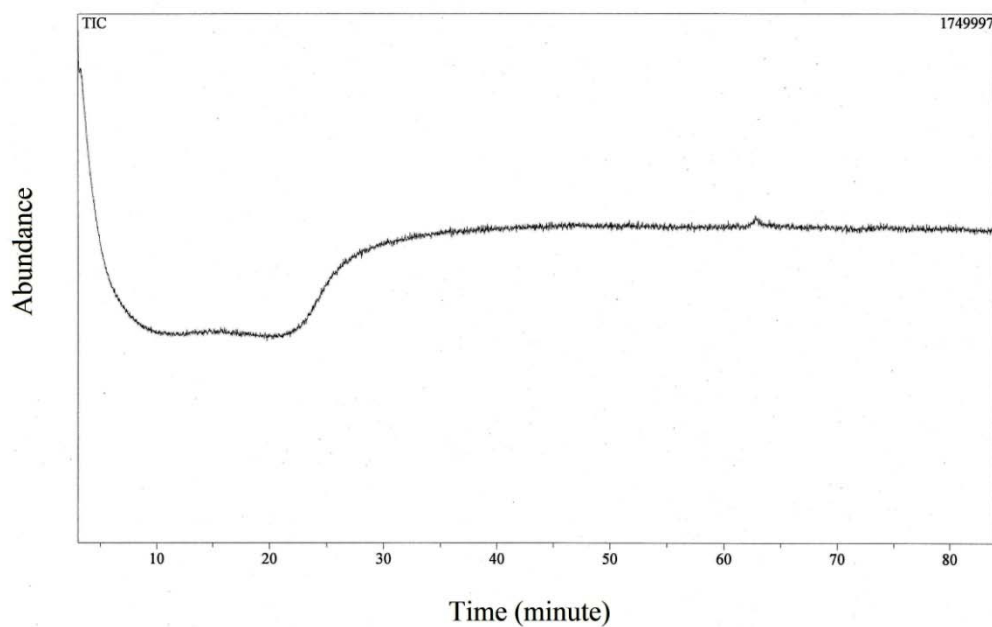


Figure B 5: Water analysis (reference)

## **Commissioning and Operating Procedure of ICA Gasifier System**

### *Commissioning*

Commissioning of pilot scale integrated catalytic adsorption (ICA) steam gasification system was initiated by ensuring sufficient electricity supply to the system. The electricity for the system was supplied by 150 ampere (A). Exhaust system is installed to assure safe operation. Different types of valves i.e. solenoid were used to control and regulate flow rates, pressure in the reactors, water treatment and water circulation systems. The gas analyzing points i.e. at the exit of fluidized bed gasifier and water separator were then attached to the main gas analyzer system. The analyzer system is placed in the control room.

### *Supervisory Control and Data Acquisition (SCADA)*

The operating system, SCADA, was used to operate the pilot scale gasification plant. SCADA system was operated via Personal computer (PC) in the control room. The pilot scale gasification system can be operated in automatic or manual modes. The process parameters i.e. temperature, pressure and flow rates were controlled from control room. Lower and upper bounds of alarms are specified manually to the system to assure safe operation.

### *Start up Procedure*

Initially, start up procedures was initiated by turning on the main electric supply line to the pilot scale gasification system. The compressed air supply was then switched on. The system is then monitored and operated through SCADA. This executed all the control valves and pumps associated with the gasification system. Meanwhile, external heaters of the fluidized bed gasifier were switched on and the set point of temperature was adjusted through the panel mounted on the system. Boiler was manually switched on from local panel controller, and its manual steam outlet valve needs to be closed until steam reaches the desired pressure of 6 bar<sub>g</sub>. Superheater, gas supply, gas analyzing system and heating system at the exit of fluidized bed gasifier were then switched on. Gas analyzing system took approximately 20 minutes to stabilize. Palm kernel shell was prepared and fed into the biomass hopper.

### *Experimental Operation*

The catalytic steam gasification with CO<sub>2</sub> adsorption experiment utilized palm kernel shell as a feedstock were performed in the gasification system as shown in Figure 3.3. Palm kernel shell was selected due to its physical properties i.e. high fixed carbon (49.74 wt%) and volatiles matter (80.92 wt%), good calorific value (17.42 MJ/kg based on lower heating value) which was suitable for catalytic steam gasification with CO<sub>2</sub> adsorption process to produce hydrogen rich gas. The main reactor system consisted of externally heated fluidized bed gasifier which was continuously feeding 1000-1800 g/h of feed from biomass feeding system. The cooling water jacket was provided to the feeding system to reduce biomass decomposition in the feeding line prior injection to the gasifier. N<sub>2</sub> was used to transfer the biomass into the gasifier to avoid any back flow.

Quicklime as bed material was first introduced into fluidized bed gasifier which was then heated up to the desired temperature. Simultaneously, the heating tape was switch on which was used to avoid tar condensation in the product gas at the exit of fluidized bed gasifier. This heater tape was wrapped and insulated all the way to the cyclone. The tape is knitted and braided by fiberglass. The temperature range of heating tape was 300-400°C which is controlled through controller. At this stage, N<sub>2</sub> gas was purged into the system to remove entrapped gases. Then saturated steam was introduced by the boiler system which is further heated to 250-300°C in superheater prior injection to the gasifier. After steam injection to the system, the temperature inside fluidized bed gasifier decreased and stabilized after certain period of time (0.5-1.0 hr). Catalyst (100-180 g/h, based on catalyst to biomass ratio of 0.1) was mixed with the biomass for all experimental runs and is loaded to biomass feeding system. Before starting the biomass feeding system, gas analyzer was checked for any presence of moisture in the unit due to continuous flow of the steam throughout the process. N<sub>2</sub> was introduced to the unit to remove moisture content from the tubing system, sample flow meter and bypass flow meter in the gas analyzing system. Continuous biomass feeding was started when the temperature of the system was reached the desired reactor temperature. After the gasifier, product gas was passed through the cyclone to separate solid particles from the product gas. The product gas

was then passed through the scrubber to reduce its temperature to less than 40°C, followed by a separator to remove any final traces of water in the product gas stream. Two gas sampling points were provided which are located after the exit of fluidized bed gasifier and water separator. At the exit of water separator, gas flow was then passed through the flow meter to measure the volumetric flow rate. Product gas was analyzed at the exit of the separator. All experiments were run for 60 min duration. This duration was chosen due to the achievement of steady state gasification operation and attainment of equilibrium for at least 50 min of operation time. At the end of the experiment, the biomass supply was stopped and air was purged into the system. The amount of char was then determined by the amount of CO<sub>2</sub> formed when combusting residual solid sample in the fluidized bed gasifier and downstream piping network. The purging was performed at gasification temperature.

#### *Shutdown Procedure*

The entire pilot scale ICA gasification system was shutdown through SCADA. Boiler and heaters were then switch off manually from local panel. Boiler drain valve was opened to drain off residual water/steam gradually. The main water supply was then switched off.

#### *Cleaning Procedure*

At the end of experiment, the system was first purged by compressed air which was used to combust residual char and tar content. The purged air is gone through all the way to the gas cleaning system. Additionally, N<sub>2</sub> purging was utilized after air combustion for further cleaning. Solids particulates were removed from the cyclone once the system was cooled down. Finally, gas analyzer system was purged with N<sub>2</sub> to remove entrapped moisture content, tar and particulate solids.